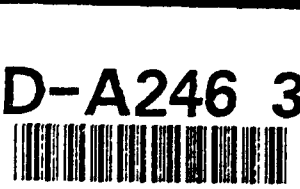

McDonnell Aircraft Company

MCDONNELL DOUGLAS

GENERAL DYNAMICS
Fort Worth Division

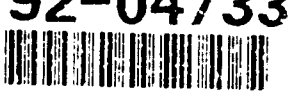

31 Dec 91 Final Report

Early Risk Reduction Phase I
FLIR/Laser Designator Window

C-N00019-88-6-0051
Order 0012

Robert J. Lord
Alfred Rosenfeld

McDonnell Aircraft Company
P.O. Box 516
St Louis MO 63166-0516

86PR0869

ASD/SDA
Wright-Patterson AFB OH 45433-6503

None

DOD-A

This program evaluated and tested materials and coatings for use as a common aperture for a Laser Target Designator (LTD) and a Forward Looking Infrared (FLIR). Desired characteristics include: transmission at 1.06 microns for laser and 8 to 11.5 microns for FLIR, radar frequency attenuation for low observability, and durability in tactical aircraft environments. The designs were a zinc sulfide/zinc selenide design produced by Hughes Danbury Optical Systems, Inc and zinc selenide and gallium arsenide designs from Litton Itek Optical Systems. This report summarizes the McDonnell portion of a joint McDonnell/General Dynamics effort.

Zinc Sulfide
Zinc Selenide
Gallium Arsenide

FLIR Window
Laser Window
E-O Window

174

UNCLASSIFIED UNCLASSIFIED UNCLASSIFIED UL

Doc No.: 86PR0869
Date: 30 Sept 1991
Revision A
31 December 1991
Copy No. 52

Early Risk Reduction Phase I
FLIR/Laser Designator Window

Prepared by:

Robert J. Lord (MCAIR)

Alfred Rosenfeld (MCAIR)

Reviewed by:

William H. Miltenberger (MCAIR)

Daniel T. Hislop (GDFW)

Brian S. Clinch (MCAIR)

John P. Browning (GDFW)

McDonnell Aircraft Company
P.O. Box 516, Saint Louis, MO 63166-0516 (314) 232-0232 TELEX 44-857

MCDONNELL DOUGLAS

GENERAL DYNAMICS
Fort Worth Division

INDEX OF PAGE CHANGES						
REVISION DATE AND LETTER	PAGES AFFECTED			REMARKS	REVISED BY	APPROVED
	REVISED	ADDED	REMOVED			
31 DEC 91 Rev. A	 iii- xiv 1-2 2-2 2-3 2-4 2-5 2-6 3-4 4-1 4-3 4-4 4-5 4-6 5-25 5-26 5-35 5-38 5-43 5-46 5-49 5-50 5-51 5-52 5-53 5-70	i ii			A. Rosenfeld	

ABSTRACT

This program evaluated and tested materials and coatings for use as a common aperture for a laser target designator (LTD) and a Forward Looking Infrared (FLIR). Desired characteristics include: transmission at 1.06 um for laser and 8 to 11.5 um for FLIR, radar frequency attenuation for low observability, and durability in tactical aircraft environments. The designs were a zinc sulfide/zinc selenide design produced by Hughes Danbury Optical Systems, Inc. and zinc selenide and gallium arsenide designs from Litton Itek Optical Systems.

All three designs had some degree of success in meeting optical transmission and RF attenuation goals, but all were damaged by sand and rain erosion. A large performance variability of the gallium arsenide used in this program indicated immaturity in the substrate manufacturing expertise.

Our evaluation showed that substrate cost is high and the industrial base for the production of large window panels is small. Production cost ranges from $190 per cubic inch for zinc selenide to $500 per cubic inch for gallium arsenide.
Multi-paned windows for large field of regard operation could cost as much as $500,000. Currently, Morton International (formerly CVD) has the only production experience for large window substrates of zinc selenide and zinc sulfide/zinc selenide. Gallium arsenide is unavailable in large desired sizes, and moving this technology into production will require substantial capital investment.

FOREWORD

This report contains a summary of material development and assessment for a broadband window system suitable for use in a high performance aircraft.

It was prepared by McDonnell Aircraft Company (MCAIR) and General Dynamics-Fort Worth (GDFW) for the United States Air Force Systems Command. Capt. Michael Kondas is the Air Force Program Manager and Mr. David Guthridge is the Air Force Engineering Manager. The effort documented in this report was accomplished by a team which included personnel in material and process development, avionics strike and defensive systems, high energy laser and optics laboratory, electronic systems technology, avionics optical systems laboratory, materials laboratory and electromagnetics laboratory. Contributors to this effort include the following people: S. C. Buckner, T. L. Clark, J. H. Gruss, M. W. Howarth, D. J. Tyberend, R. J. Albers, J. Kelly, M. J. Lahm for MCAIR and D. T. Hislop, M. I. Jones, and K. G. Sewell for GDFW. Authors of this report are J. A. Maynard, R. J. Lord, A. Rosenfeld, P. Feit, T. Fiala, W. H. Miltenberger, D. J. Wolters, and L. A. Scruggs of MCAIR and K. Osmer, R. Torti, and E. Wong of GDFW.

Special thanks go to Dr. Wasimul Hasan of Hughes Danbury Corporation and Mr. Stephen Kendrick of Litton/Itek Corporation for their advise and enthusiastic support of this program.

A

TABLE OF CONTENTS

TABLE OF CONTENTS
(Continued)

LIST OF FIGURES

LIST OF FIGURES
(continued)

LIST OF FIGURES
(continued)

LIST OF FIGURES
(continued)

LIST OF FIGURES
(continued)

LIST OF FIGURES
(continued)

LIST OF EFFECTIVE PAGES

Title Page
Signature Page
i - xiv
1-1 - 1-2
2-1 - 2-6
3-1 - 3-4
4-1 - 4-6
5-1 - 5-85
6-1 - 6-6
7-1 - 7-3
A-1 - A-2
B-1 - B-6
C-1 - C-36

REFERENCES

3-1 Wolfe, William L. and Zissis, G. J., "Infrared Handbook, Revised Edition," Environmental Research Institute of Michigan for the Office of Naval Research, Dept. of the Navy, Washington, D.C., 1985.

3-2 "Precision Optics and Components Catalog," JANOS Technology Corp., Townshen, VT, 1989.

3-3 University of Dayton Research Institute Report, "Exploratory Development and Investigation of the Thermal, Electrical, Mechanical, and Physical Properties of Infrared Laser Window and I-R Transmitting Materials," UDRI-TR-76-09, Jan 1976.

3-4 University of Dayton Research Institute Report, "Exploratory Development on Multidisciplinary Characterization of Infrared Transmitting Materials," UDRI-TR-79-75, Oct 1979.

3-5 University of Dayton Research Institute Report, "Multidisciplinary Characterization of Infrared Transmitting Materials," Air Force AFWAL TR-82-4012, Mar 1982.

3-6 Arizona University-Tucson Optical Sciences Center Report, "Scattering Measurements of Raytran Zinc Selenide in Transmission at Wavelengths of 0.6328, 3.39, and 10.6 micrometers," U.S. Army AMMRC TR-81-38, Aug 1981.

3-7 Raytheon Company, Research Div., Report, "ZnS/ZnSe Sandwich-Type FLIR Windows," Air Force AFWAL-TR-83-4122, Nov 1983.

4-1 Hughes Danbury Optical Systems Final Report, "ATA Window Technology Program," PRB11-0324, August 11, 1991.

4-2 Litton, Itek Optical Systems Final Report, "GaAs IR Optical Window Study," 8925, 2 July 1991.

4-3 Litton, Itek Optical Systems Final Report, "ZnSe IR Optical Window Study," 8924, 2 July 1991.

5-1 McDonnell Aircraft Company Technical Memorandum TM 256.91.0054.01, "Early Risk Reduction -- Phase I, Optical Properties Measurement Techniques of Three Wide Band Window Materials," 22 August 1991.

5-2 McDonnell Aircraft Company Technical Memorandum C-1-318-070, "AFATA Wide Band IR Window Material Testing TIS ERR-1-6-004: Optical Tests," 6 Sep 1991.

5-3 Hislop, D. T., et al, "Broadband Window Study," 86PR1314, General Dynamics Corp., Fort Worth, TX, 12 Sep 1991.

5-4 McDonnell Aircraft Company Technical Memorandum TM 256.91.0063.01, "Early Risk Reduction -- Phase I, RF Properties of Three Wide Band Window Materials," 6 August 1991.

5-5 INTENTIONALLY LEFT BLANK

5-6 Gallium Arsenide Coating Design Report completed under Contract No. E03088, Litton/Itek Optical Systems, Lexington, MA, 02173, 1 Feb 1991.

5-7 McDonnell Aircraft Company Technical Memorandum TM 256.91.0056.01, "Early Risk Reduction -- Phase I, Effect of Humidity and Blowing Sand on Three Wide Band Window Materials," 1 August 1991.

5-8 MIL-F-48616 Filter (Coatings), Infrared Interference: General Specification For

5-9 ASTM B117-90 Standard Test Method of Salt Spray (Fog) Testing

5-10 McDonnell Aircraft Company Technical Memorandum TM 256.91.0057.01, "Early Risk Reduction -- Phase I, Effects of Salt Fog and Blowing Sand on Three Wide Band Window Materials," 15 August 1991.

5-11 MIL-STD-810D Environmental Test Methods and Engineering Guidelines, 19 July 1983

5-12 McDonnell Aircraft Company Technical Memorandum TM 256.91.0055.01, "ATA Wide Band Window -- Environmental Test -- Sand and Dust Exposure," 9 August 1991.

5-13 Dayton T. Brown, Engineering and Test Division Test Report No. DTB04R91-0543, "Sand Test Program Performed on Eighteen Sensor Window Coupons," 20 June 1991.

5-14 McDonnell Aircraft Company Technical Memorandum TM 256.91.0058.01, "Early Risk Reduction -- Phase I, Effect of Temperature/Altitude Exposure on Three Wide Band Windows," 23 August 1991.

5-15 McDonnell Aircraft Company Technical Memorandum TM 256.91.0059.01, "Early Risk Reduction -- Phase I, Effect of Fluid Exposure on Three Wide Band Window Materials," 12 August 1991.

5-16 Charles J. Hurley letter with attached Table, University of Dayton Research Institute Rain Erosion Results, June 7, 1991.

5-17 ASTM C158-84 Standard Methods of Flexural Testing of Glass (Determination of Modulus of Rupture)

5-18 McDonnell Aircraft Company Technical Memorandum TM 253.91.0140.01, "Wide Band Window -- Strength Tests," 5 July 1991.

A-1 Born, M. and Wolf, E., "Principles of Optics," Pergaman Press, NY, 1965, p. 405.

B-1 "Electro Optics Handbook," RCA Corp., 1974, pp. 89-90.

1.0 SUMMARY

Passive sensors are important for multi-mission aircraft to minimize detectability. The ability to target, navigate, and fly low level at night using visual flying techniques is a distinct advantage. Add to this the capability to autonomously lase and not be dependent upon an airborne or ground Forward Air Control provides an independent, effective Strike/Fighter aircraft.

A cost effective answer to these requirements is a passive system combining the benefits of a Forward Looking Infrared (FLIR) targeting system for weapon delivery, a FLIR navigation system, and a laser designator for air-to-ground missions, with an Infrared Search and Track (IRST) sensor for air-to-air missions. A single, compact, lightweight, highly integrated, passive multi-sensor system offers a cost effective approach to meeting these needs.

A multi-sensor system such as this requires the development of a broad-band window that transmits the wavebands of both FLIR and laser devices, attenuates radar frequency (RF) radiation, and possesses outstanding durability. The ATA Early Risk Reduction program IR Window Study assessed the state of the art in the manufacture and performance of broad-band infrared windows, acquiring design information and demonstrating the critical window system capabilities suitable for use in high performance subsonic and supersonic aircraft.

Existing and new window material technologies were surveyed, and those candidates which showed potential to meet optical environmental, structural and signature goals were identified.

Optical performance goals were chosen based on prior ATA systems studies for laser transmission at either 1.06 or 1.54 microns and infrared reception in the 7 to 12 micron wavelengths. Durability against rain erosion, blowing sand, temperature/altitude, humidity, salt fog, and aircraft fluids were measured. Exposure to radiation power of an onboard laser was also evaluated.

Zinc Sulfide/Zinc Selenide, from Hughes Danbury, and Gallium Arsenide, and Zinc Selenide from Litton/Itek were the window substrates selected. Samples of each with treatments and coatings were procured and tested. Destructive and non-destructive testing, spectral properties, Radio Frequency transmissions, thermal characteristics, and susceptibility to erosion by rain and sand were determined.

All three window systems tested had some degree of success in meeting the optical transmission and RF attenuation goals, but

all were damaged by sand and rain erosion. Zinc-Sulfide/Zinc-Selenide lost the conductive grid, and the other two materials suffered substrate damage and transmission loss.

Testing revealed a large performance variability in Gallium Arsenide. Manufacturing expertise with this material as a window substrate is not as mature as it is for Zinc Sulfide and Zinc Selenide.

Current production costs of the substrate material varies between $190 per cubic inch for Zinc Selenide to $500 per cubic inch for Gallium Arsenide. Large multi-paned windows may cost upwards of $500K. This, in addition to the low durability experienced, projects into high life cycle costs for broad-band windows unless further research and development identify solutions that mitigate these concerns.

The industrial base for substrate manufacture is critical. Currently, Morton International (formerly CVD) is the only mass producer with manufacturing experience of large window substrates in Zinc Selenide and Zinc Sulfide/Zinc Selenide. Gallium Arsenide substrate is currently unavailable in the required size, A although Litton Airtron, Texas Instruments, and Amorphous Materials continue to develop the technology in smaller sizes. Moving this technology into production will require substantial capital investment.

2.0 WINDOW PERFORMANCE REQUIREMENTS AND ACHIEVEMENTS

2.1 Introduction

The Early Risk Reduction Phase I (ERR I) Broad Band IR Window Material Test Program evaluated materials and coatings for use as an aperture for a laser target designator (LTD) and a targeting FLIR. The need for a broad band infrared window evolved from requirements documents generated by the U.S. Air Force for the Advanced Tactical Aircraft (ATA).

The addition of an LTD for the delivery of laser guided weapons on the U.S. Air Force version of the A-12 initiated several studies. These trade studies indicated the advantage to aircraft observability and performance of a coaxial configuration where an 8 to 12 micron targeting FLIR and a 1.06 micron laser target designator would use the same window. A window system (material and coatings) to support the broad band characteristics as well as to withstand the harsh environment of a high-performance, all-weather attack aircraft was challenging. To meet this challenge, the MCAIR/GDFW team was funded by the USAF (N00019-88-G-0051, Order No. 1201) to assess state-of-the-art technology and outline risk reduction activities (Figure 2.1-1)

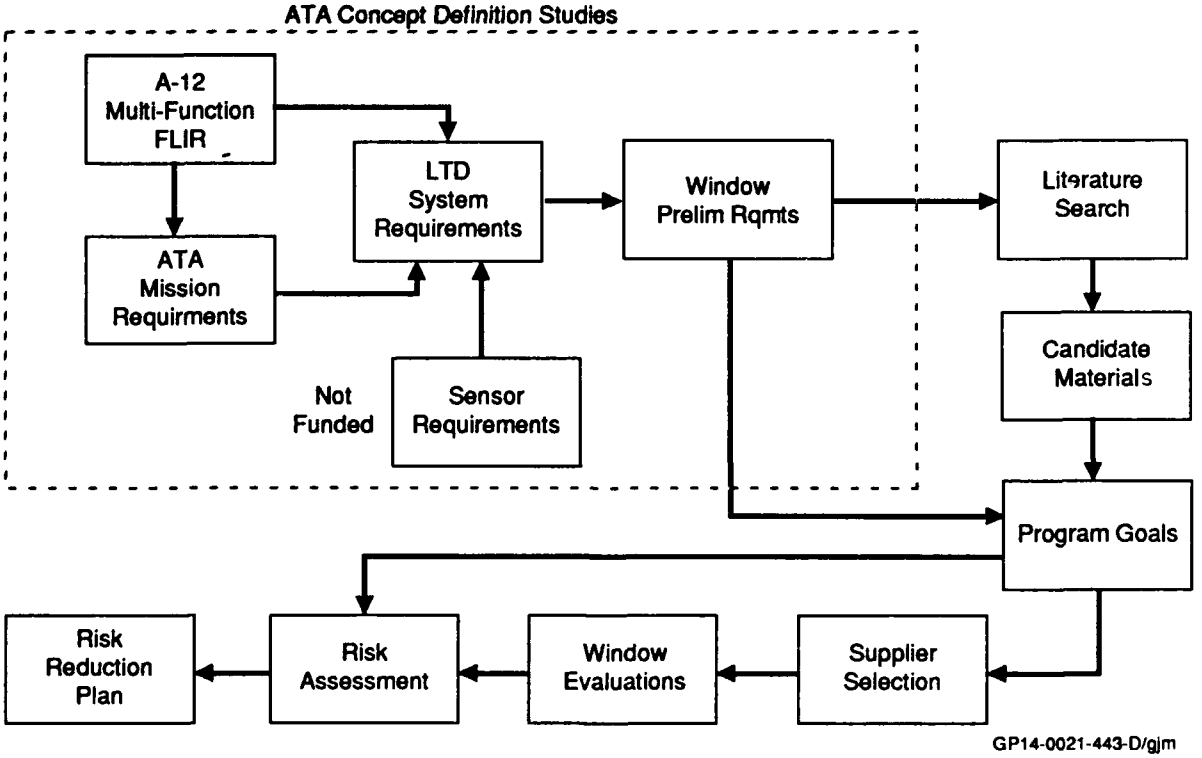

Figure 2.1-1. Program Plan

A literature search identified three materials -- Zinc Selenide (ZnSe), Gallium Arsenide (GaAs), and a combination of Zinc Sulfide and Zinc Selenide (ZnS/ZnSe) -- as having the most potential to meet broad band optical, low observability, and durability requirements. Goals were defined and an RFP was issued to established infrared window suppliers. The vendor proposals substantiated that the three materials selected earlier had the most promise of effecting a solution. Suppliers were selected to provide coupons of each of the candidate window systems and assess technical and manufacturing issues needing resolution prior to production. Contracts were awarded to Hughes Danbury Optical Systems for the ZnS/ZnSe and to Litton Itek Optical Systems for the other two materials. A

A materials evaluation test program (Figure 2.1-2) was implemented to acquire optical, environmental, RF, and laser compatibility measurements.

In concert with the suppliers, assessments and risk reduction plans were made.

2.2 Test Result Summary

The three window systems had some success in meeting optical transmission and RF attenuation goals, but performed poorly in erosive environments such as sand and dust and rain.

2.2.1 Optical Transmission - Figure 2.2-1 shows the spectral transmittance design goals and compares performance of the best optical transmission coupon from each of the three designs. The ZnS/ZnSe and ZnSe coupons consistently produced transmittances within 5% and 10%, respectively, of the values shown. GaAs performance, however, was highly variable with long wave transmittances sometimes falling below 10%. The variability is apparently due to immaturity of the GaAs substrate manufacturing process.

Although the figure shows that all designs exceeded the 1.06 and 1.54 micrometer transmission goals, laser performance of the ZnS/ZnSe design proved to be unacceptable. Its measured diffuse transmittance of 25% showed that the window scatters half the transmitted energy away from the target. This problem was observed only for the ZnS/ZnSe design and only for the laser wavelengths.

Sample Type, No. per Vendor	Lot Number	Transmission vs Wavelength (Optical)	Transmission vs Temperature (Optical)	Transmission vs AOI (Optical)	1.06 Wavefront Homogeneity (Optical)	10.6 Wavefront Homogeneity (Optical)	1.06 Coherent Imaging (Optical)	Diffuse Transmittance (Optical)	MTF (Optical)	10.6 Stray Light (Optical)	Visual/Micro/Sem Inspection (Optical)	Laser Compatibility (Laser and RF Tests)	RF Coax (Laser and RF Tests)	RF Tunnel/Arch (Laser and RF Tests)	Interferometric Thermal Lensing (Laser and RF Tests)	Temperature/Altitude (Environmental Tests)	Humidity (Environmental Tests)	Salt Spray (Environmental Tests)	Sand and Dust (Environmental Tests)	7X Fluids (Environmental Tests)	Rain Erosion (Environmental Tests)	Structural (4 Pt Bend) (Environmental Tests)	Transmission vs Wavelength (Post Environment Test)	Diffuse Transmission (Post Environment Test)	Visual/Micro/Sem Inspection (Post Environment Test)	
Coaxial Doughnuts	1	2									2		4													
(2) - 7 mm Dia x 0.25 in. Thick**	2	2									2		7													
(2) - 1.5 mm Dia x 0.25 in. Thick	3	2									2		4													
RF	1	1		1	1	1	1	1	1	1	1			1												
(1) - 12 in. x 12 in. x 0.50 in	3	1		1	1	1	1	1		1	1			1												
Environmental	1	12						12			12				1	2	2	2	6	2			22	22	22	
(12) - 3 in. Dia x 0.45 in. Thick	2	12		1	1	1	1	12	1	1	12				1	2	2	2	6	2			22	22	22	
	3	12						12	1		12				1	4	2	2	6	2			22	22	22	
Optical	1	3	3					3*			3	3											3	3*		
(3) - 1 in. Dia x 0.45 in. Thick	2	3	3					3*			3	3											3	3*		
	3	3	3					3*			3	3											3	3*		
Rain Erosion	1	12						12			12										10		10	10	10	
(12) - 1 in. x 0.625 in. x 0.25 Thick	2	12						12			12										10		10	10	10	
	3	12						12			12										10		10	10	10	
Strength	1	5									5											5				
(5) - 1.5 in. x 10 in. x 0.25 in. Thick***	2	5									5											5				
	3	5									5											5				
Total Number of Tests		104	9	3	3	3	3	83	3	3	104	9	15	2	3	8	6	6	18	6	30	15	105	96	96	733

* Implicitly included in laser hardening tests.
** Lot 1 samples are 0.05 in. thick.
*** Lot 2 samples are 1.5 in. x 8 in. x 0.25 Thick

GP23-0005-17-Dkas

Figure 2.1-2. Test Program Matrix
Number and Type of Test Performed

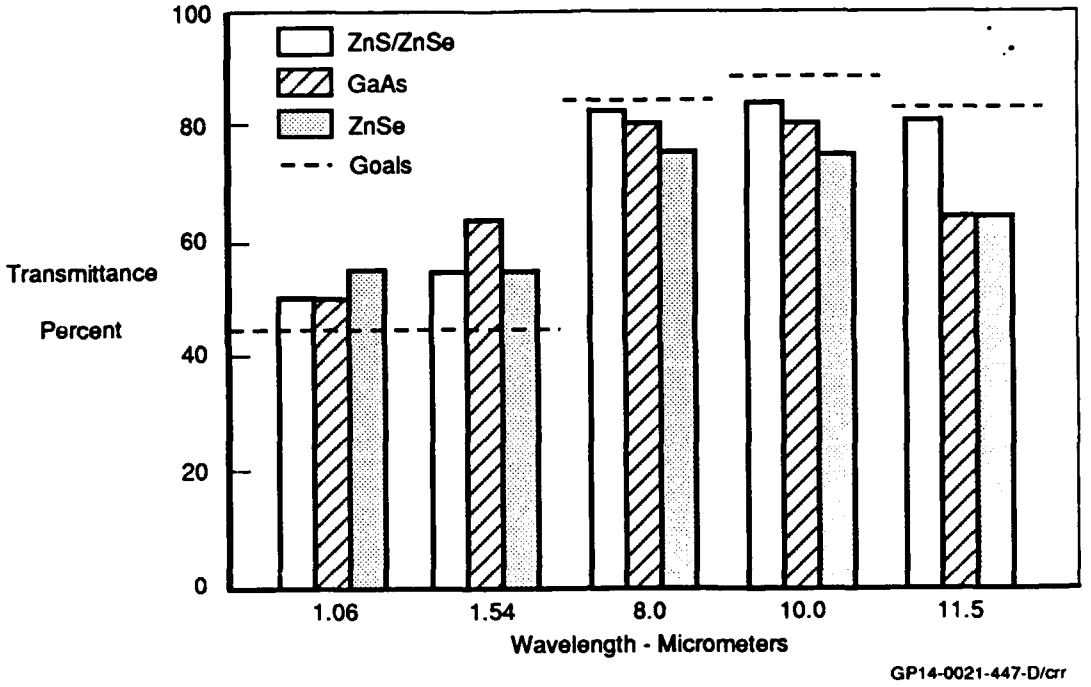

Figure 2.2-1. Measured Optical Transmittance Best Optical Transmission Coupons

The ZnS/ZnSe scattering problem may be caused by the Morton International manufacturing process for the bulk window material. A 0.040-inch ZnS layer for rain protection is deposited on the ZnSe substrate. The delivered material is milky in visual appearance, whereas material formerly produced by Raytheon is not. (Raytheon is no longer a producer.) The probable scattering source is the interface between the ZnSe and ZnS and/or the bulk scattering properties of the ZnS. Scattering produced by the RF conductive grid is limited to less than 5%.

2.2.2 RF Attenuation - Figure 2.2-2 compares attenuation of the best RF coupon from each of the three designs. The design goal is at least 20 dB power attenuation from 2 to 18 GHz. Both the ZnS/ZnSe and ZnSe designs achieve RF attenuation by using conductive grids near the outer surface of their dielectric substrates. Periodic modulation of the transmittance curve is a property of the test sample thickness, not the grid design. The GaAs design achieves RF attenuation by doping the semiconductor substrate. A

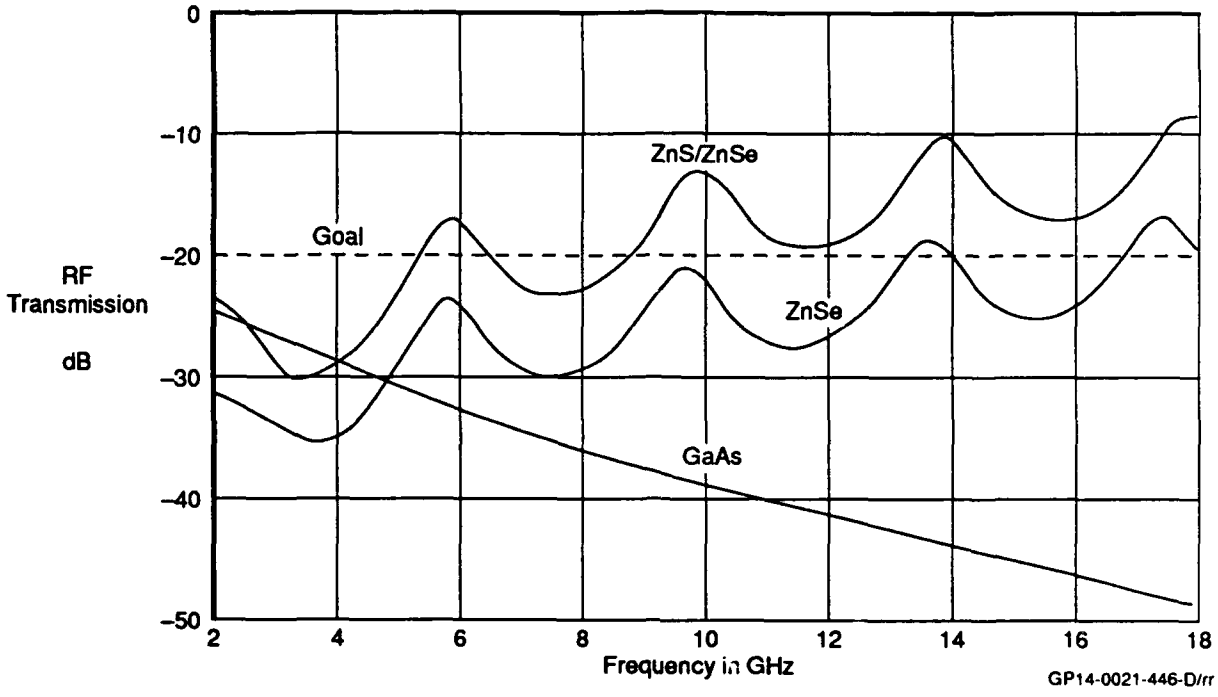

Figure 2.2-2 Measured RF Transmission Best RF Coupons

The superior performance of the ZnSe design relative to the ZnS/ZnSe is due to its tighter spacing of the conductive grid lines -- 200 micrometers compared to 400 micrometers for the ZnS/ZnSe. Unfortunately, the tighter spacing also lead to reduced long wave optical transmission, as shown above.

As with optical performance, Gallium Arsenide's RF attenuation varied considerably. The excellent RF performance shown in Figure 2.2-2 requires a high doping density, which degrades transmission at the long wavelengths. Consistent simultaneous performance in wide band optical transmission and RF attenuation is yet to be demonstrated. A

2.2.3 Durability - All three window designs were severely damaged when subjected to simulated inflight rain conditions. The goal was to survive the rain for 30 minutes with a loss of less than 5% in optical transmission. Figure 2.2-3 shows the measured change in transmission produced by 30 minutes of 1-inch/hour rainfall. The protective coatings used with the ZnSe and GaAs were unable to protect the brittle substrates, and both designs suffered substantial transmission loss. The 40-mil ZnS coat in the ZnS/ZnSe design was reasonably successful in

protecting the substrate, and the window came close to meeting the transmission loss goal. Unfortunately, the conductive grid deposited on top of the ZnS was obliterated.

All three window designs were also severely damaged by blowing sand. The test speeds of 40 to 65 mph were typical of what a parked aircraft might experience in a sand storm. The ZnSe diffuse transmittance increased from 3% before exposure to 14% after 30 minutes and 30% after 90 minutes. Damage measurements for the other designs were even worse.

All window designs were subjected to Mil spec environmental tests. All of the designs successfully passed humidity and a variety of solvent tests, including ethanol, acetone, coolanol, hydraulic fluid, de-icing fluid, and jet fuel. During the temperature/altitude tests, the ZnSe design suffered isolated flaking of the interior coating during 20^{0}C per minute temperature rate change, but optical properties were not significantly affected. During salt fog tests, the ZnSe design experienced a slight reduced 1.06 micron transmission and damage to the aluminum grid. The damage appears to be associated with pre-existing pinholes in the exterior coatings. ZnS/ZnSe and GaAs designs were not damaged. A

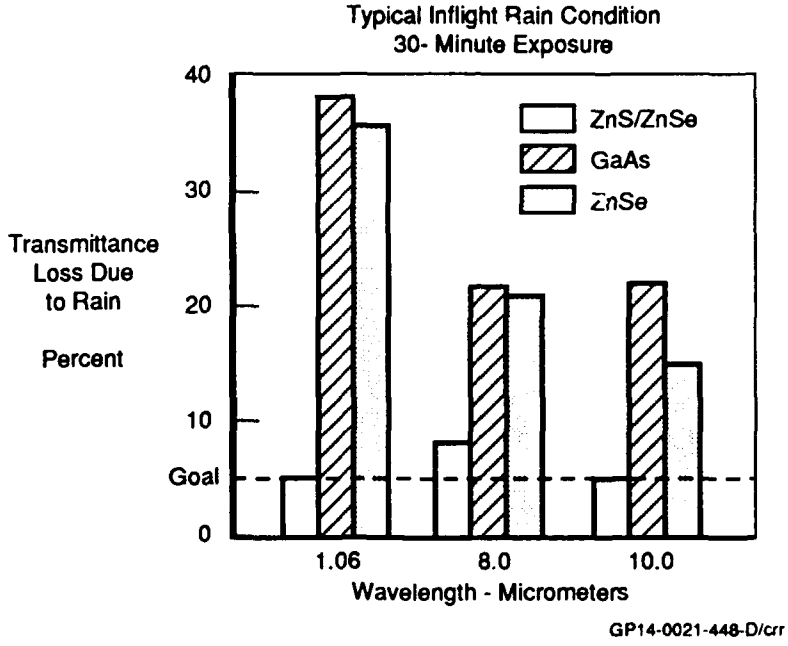

Figure 2.2-3. Effect of Rain Exposure on Optical Transmittance

3.0 LITERATURE SEARCH

The literature search provided the technical basis for window technology evaluation, identified candidate materials suitable for transmission of laser wavelengths of 1.06 micron up to transmission of long wave infrared in the 8 to 12 micron band, and provided comparative data not previously obtained. As the program evolved and test results became available, the compiled documentation became a resource for evaluation and interpretation of test results.

The industry survey identified current manufacturing capabilities and processes and confirmed the primary technology development thrust of window manufacturers. Requests for Proposal were sent to seven suppliers based on this survey: Pacific Optical (Torrence, CA); Texas Instruments (Dallas, TX); Litton/Itek Optical Systems (Lexington, MA); Morton International (Woburn, MA); Hughes Danbury (Danbury, CT); Westinghouse Electric (Baltimore, MD); and Martin Marietta Electronic Systems (Orlando, FL). The responses identified specific advances in both materials research and in thin film technology. Hughes Danbury and Litton Itek were selected to demonstrate three material types (ZnS/ZnSe clad, ZnSe, and GaAs) and three distinct manufacturing processes.

Candidate Materials. The Infrared Handbook (1978 edition, page 7-17), Reference 3-1, identifies materials that have measured performance from 1.06 micron through the 8 to 12 micron band. From that list, thirteen materials covered the wavelengths of interest and were identified as being commercially available by JANOS (1989-edition, page 6), Reference 3-2, at the time of the contract, Figure 3.0-1. Seven materials (Barium Fluoride, Sodium Chloride, Potassium Chloride, Potassium Bromide, Silver Chloride, Thallium Bromoiodide, and Cesium Bromide) were eliminated due to their solubility in water. Of the remaining candidate materials, no single material appeared to have superior performance as a broadband window. However, several window materials were being developed for advanced aircraft applications: ZnS, ZnS/ZnSe Clad, Ge, and GaAs. Because of Ge's limitations at high temperatures and lack of transmission at 1.06 micron, it was eliminated as a candidate.

Summary of Previous Material Studies

Most studies comparing ZnS, ZnSe, ZnS/ZnSe, and GaAs for specific applications were aimed at either long or mid-wave FLIR imaging applications. None addressed the transmission of a 1.06 micron laser and mid-to-long wavelength infrared through the same window.

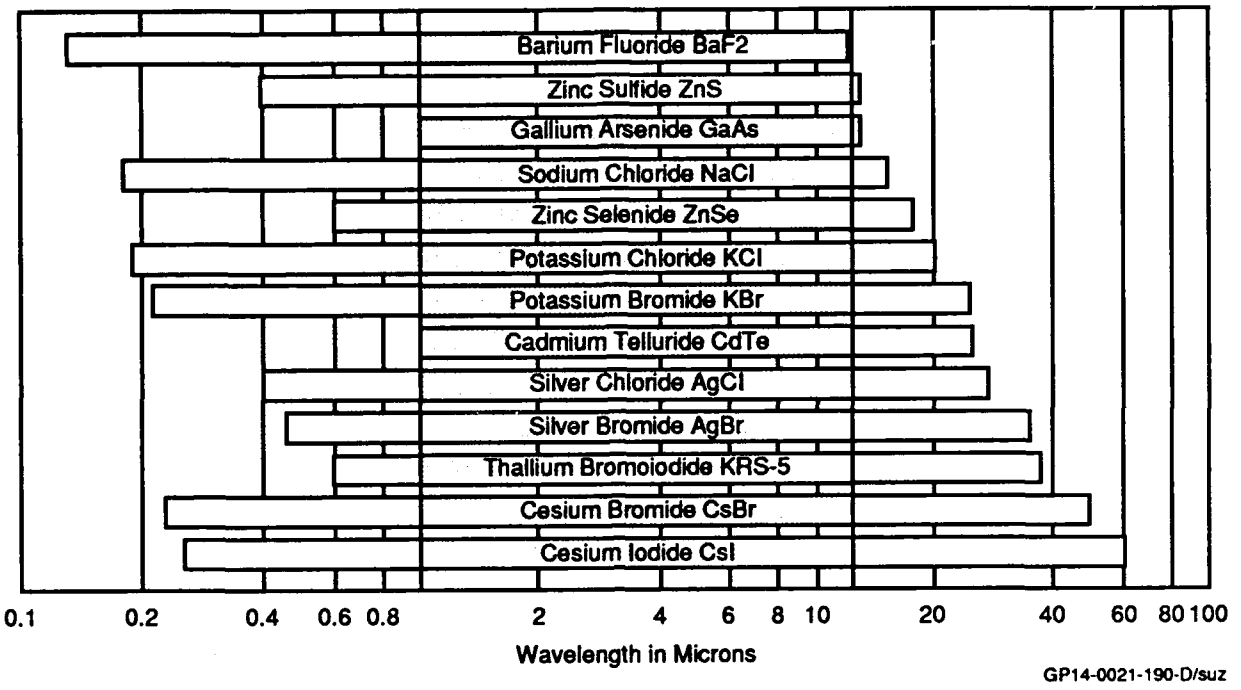

Figure 3.0-1. Transmission Range for Various Materials

AFML Contract No. F33615-75-C-5011 - This 1976 study conducted by the University of Dayton Research Institute (UDRI) was contracted by the USAF Materials Lab. The study provided a characterization of the mechanical, thermal, and physical properties of candidate optical window materials for high power laser and broad band FLIR applications (Reference 3-3).

UDRI investigated the environmentally-assisted slow crack growth behavior of ZnSe, which is a form of stress-aided corrosion commonly observed in ceramics and glass. The combined effect of tensile stress and chemical attack (usually from water vapor) produces a time-dependent growth of surface flaws which eventually reach critical dimensions. Even though the database was too limited to develop a stress-failure model, UDRI conservatively predicted that a ZnSe window would have a lifetime between 109 and 1012 hours with an applied stress of 1500 psi and a 1 mm scratch as an initial flaw.

An extensive material investigation was also performed on the Alkaline Earth Fluorides (CaF_2 and SrF_2). These materials were found to have superior thermo-optical and long wave IR performance. Consequently, these materials are considered candidates for high power Df and CO laser windows. However, they

are sensitive to thermal shock and are soluble in water making them unsuitable for external windows.

AFML Contract No. F33615-77-C-5004 - This 1979 study was conducted by the USAF Materials Lab (Reference 3-4). As part of this investigation, the mechanical properties of ZnS were studied. It was established that the critical stress intensity was significantly dependent on surface flaw orientation. In addition, experimental data on hardness and elastic properties of ZnS were compiled.

AFWAL Contract No. F33615-79-C-5044 - The purpose of this 1982 USAF Weapons Labs study was to evaluate optical substrate materials suitable for use as mirrors and windows in high energy gas laser systems (Reference 3-5). Materials investigated were polycrystalline CaF_2, hot pressed nickel niobate, and single crystal silicon. Bulk properties were extensively characterized. The ultimate strength of single crystal and small grain polycrystalline silicon were comparable. Large grain polycrystalline silicon has a 25% greater ultimate strength. The study suggested that material post processing treatment (heat treat and cold working) might enhance the ultimate strength.

In addition, the ultimate strength of a ZnS/Znse sandwich window material was characterized. The ultimate strength with ZnS in compression was 8.5 ksi; with ZnS in tension the ultimate strength increased to 10.8 ksi. Based on the published data for ZnS, ZnS/ZnSe sandwich material had an unexpectedly low ultimate strength when the ZnS was in tension.

US Army Materials and Mechanics Research Center Contract No. DAAG46-79-M-0871 - This study characterized the Bi-directional Transmissoin Distribution Function (BTDF) of ZnSe at three wavelengths and several incident angles (Reference 3-6). The study characterized three thicknesses (1/4", 3/4", and 1") of Chemical Vapor Deposition (CVD) grown ZnSe manufactured by Raytheon. Results showed that there was measurable bulk scattering at the 0.6328 micron wavelength. Since scattering varies inversely with wavelength, there could be performance implications for ZnSe at the 1.064 micron wavelength.

AFML/AFWAL/AFSC Contract No. F33615-80-C-5013 - This study developed analytical techniques to evaluate the performance of ZnS, ZnSe, and ZnS/ZnSe laminates applied to long wave FLIR systems (Reference 3-7). The study addressed the effect of window optical properties on FLIR performance.

The window can affect system performance in three ways. Low transmission reduces the signal-to-noise ratio at the detector by reducing scene energy in the optical pass-band. The window can

also generate additional noise if the material thermal spectral emittance falls within the system optical pass-band. Finally, the effects of transmitted wavefront distortion due to the window ultimately reduces the modulation transfer function of the system.

A comparison was made of the effect of temperature on absorption and refraction index for ZnS and ZnSe in the 8 to 12 micron wavelength range. The absorption coefficient of ZnS doubles when the temperature increases from 28°C to 203°C, whereas there is little temperature effect on the absorption-coefficient for ZnSe. The study attributes the temperature degradation of ZnS to multi-photon excitation mechanisms.

The study also addressed production of a ZnS/ZnSe laminate by CVD to improve rain erosion resistance of ZnSe. The premise was that laminates of 50 mil or more of ZnS provide all the rain erosion resistance of a pure ZnS window, and adequately protect the underlying ZnSe substrate.

A

4.0 MATERIALS DEVELOPMENT

Two window suppliers were contracted to integrate state-of-the-art coatings and substrates into materials systems and to fabricate test specimens for the tests described herein. One supplier, Hughes Danbury Optical Systems, utilized a zinc sulfide/zinc selenide sandwich material with a conductive grid. The other, Litton, Itek Optical Systems, integrated two materials into window systems: semiconductive gallium arsenide and zinc selenide.

4.1 Description and Manufacturing Process

4.1.1 ZnS/ZnSe (Tuftran) - ZnS/ZnSe test specimens were supplied by Hughes Danbury Optical Systems, Danbury, CT. Complete details of the development program can be found in Reference 4-1.

Figure 4.1-1 illustrates the ZnS/ZnSe sandwich design. The exterior surface is outer moldline. The ZnS/ZnSe substrate material was purchased by Hughes Danbury from Morton International, Inc. Specialty Chemicals Group. Polishing was performed by Hughes Danbury. The 0.040 +/- 0.005-inch thick layer of ZnS was grown by chemical vapor deposition (CVD) directly onto the underlying ZnSe substrate. The purpose of this layer is to increase the resistance to rain erosion. Prior testing had demonstrated that 0.04 inches provides a good trade between optical transmission and rain protection. A

Microwave attenuation is provided by a rectangular grid of gold on chromium spaced at 400 microns with a grid width of 10 microns. The grids range from 0.5 to 0.75 microns thick. The grid was applied using a lithographic process which coated the substrate with photoresist and applied an acetate mask. After the mask was exposed to UV light, the structure was developed to reveal the mesh pattern in the photoresist. Photoresist exposed to UV light was washed away. Next, the system was placed in a vacuum chamber and the metallization process was performed. An acetone wash dissolved the photoresist that remained between the substrate and the freshly deposited metal, lifting off any metal that resided on the photoresist. The metal deposited directly onto the substrate, within the voids of the photoresist left after the development process, remained intact to define the metal mesh structure.

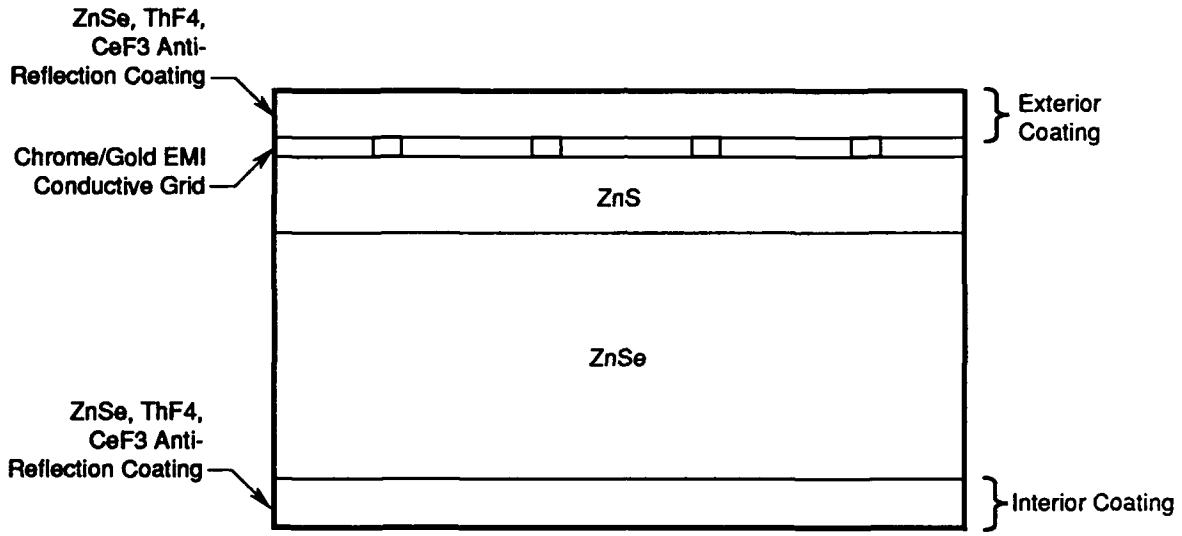

Note: Coating thickness are not to scale

Coating	Material	Thickness (microns)
Exterior	ZnSe, ThF_4, CeF_3	2.5
	Gold Grid	0.6
	Zns	1,000
Interior	Znse, ThF_4, CeF_3	2.5

GP14-0021-333-D/cm

Figure 4.1-1. Coated ZnS/ZnSe Window Material

External and internal antireflection coatings were applied by thermal co-evaporation of high and low index materials to achieve a graded refractive index increasing from near unity to nearly that of ZnS (2.38). The coating process is vendor-proprietary and consists of varying mixtures of thorium fluoride, cerium fluoride, and ZnSe. The purpose of this layer is to reduce optical reflections at the air-window interface and to protect the grids from environmental influences. Surface measurements performed by the vendor show that the surface contour is controlled by the grid, e.g., excursions from a smooth surface match the thickness and location of the grids. This surface roughness may introduce surface scattering and stress at the intersection of the coating and the ZnS layer. A

4.1.2 Gallium Arsenide (GaAs) - GaAs test specimens were supplied by Litton, Itek Optical Systems, Lexington, MA. Complete details of the development program can be found in Reference 4-2.

Figure 4.1-2 illustrates the GaAs system design. The GaAs substrates were fabricated by Airtron, Division of Litton Industries, and are Czochralski-grown single crystal GaAs doped to a conductivity of 1 to 25 Ohm cm. The conductive GaAs provides its own radio frequency (RF) and microwave attenuation and, hence, a conductive grid is unnecessary.

Itek designed the external and internal anti-reflection (AR) surface coatings shown in Figure 4.1-2. Each AR coating increases transmittance in the three bands of interest. Also, the external AR coating provides environmental protection. It was decided that the intrinsic hardness of GaAs would preclude the need for an additional coating to protect the AR coatings. Yttrium oxide and bismuth oxide were finally selected for the external surface because of their high durability compared to fluoride and sulfide materials tested. Cerium fluoride, in conjunction with bismuth oxide, was chosen as the internal AR coating because of the high refractive indices of the external coating and the durability of cerium fluoride. The external and internal AR coatings were applied by Itek using their ion-assisted deposition (IAD) process. During IAD, electron beam evaporation sources provide a continuous flux of coating material; simultaneously, argon ions bombard the growing coating to atomically compact the coating and remove weakly bound impurity atoms. | A

4.1.3 Zinc Selenide (ZnSe) - ZnSe specimens were also supplied by Litton, Itek Optical Systems, Lexington, MA. Complete details of the development program are in Reference 4-3.

Figure 4.1-3 illustrates the ZnSe system design. Chemical-vapor-deposited (CVD) ZnSe substrates from both Morton International, Inc., Specialty Chemicals Group, Advanced Materials, and II-VI, Inc. were evaluated by Itek. CVD ZnSe is polycrystalline with an average grain size of 50 to 70 microns. Since ZnSe currently cannot be doped to produce conductivity, a conductive grid of aluminum (300 nanometers thick) on chromium (0.1 nanometers thick) was incorporated into the design. The grid was produced on the substrate by means of positive photolithography described in Section 4.1.1. The grid spacing varies from sample to sample as shown below. The original plan was to deposit grids with 150 microns spacing and a 7 micron line width, but deposition problems resulted in the variation.

Sample	Grid Spacing and Line Width
Rain Erosion	150 x 11 microns
Optical	150 x 11
Environmental	200 x 16
Strength	200 x 15
12" x 12"	200 x 10

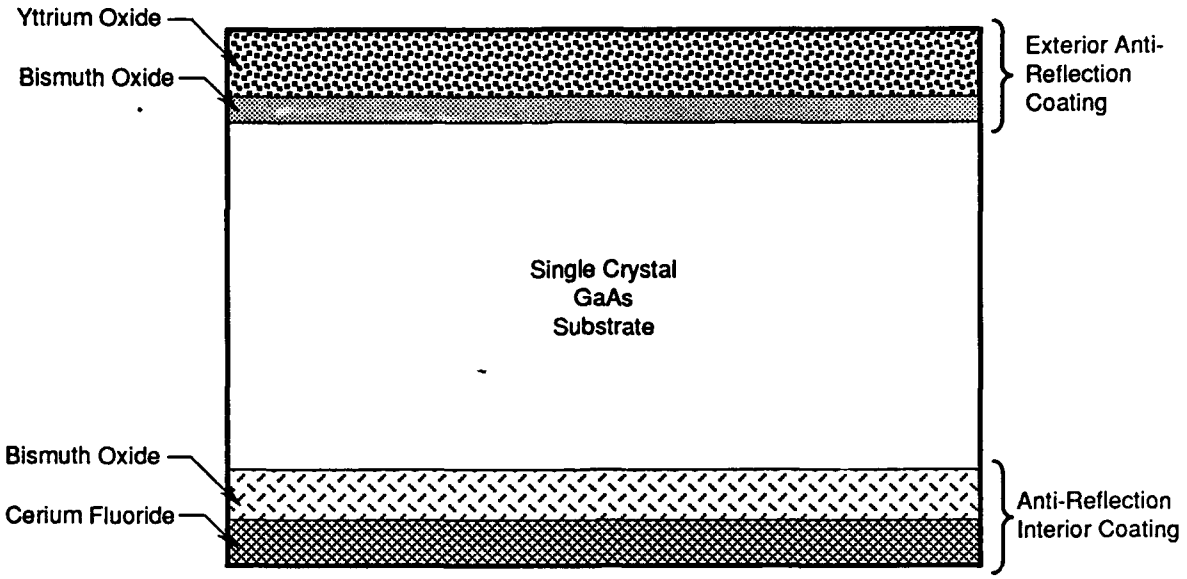

Figure 4.1-2. Coated GaAs Window Material

The grid and ZnSe substrate are environmentally protected with a thick (4 to 8 micrometers) layer of tellurium - doped Zinc Sulfide (ZnS:Te) applied by co-evaporation with ion assist. The ZnS:Te coating and the ZnS substrate have similar refractive indices, assuring little optical interference from the coating.

Itek designed the external and internal antireflection (AR) coatings shown in Figure 4.1-3. Yttrium oxide was chosen for the exterior AR coating because of its durability compared to the fluoride and sulfide materials evaluated. Cerium fluoride was selected for the interior AR coating because of its low absorption properties in the 8-11.5 micron wavelength range and its refractive index. As with the GaAs specimens, the AR coatings were applied by Itek using their ion-assisted deposition (IAD) process. A

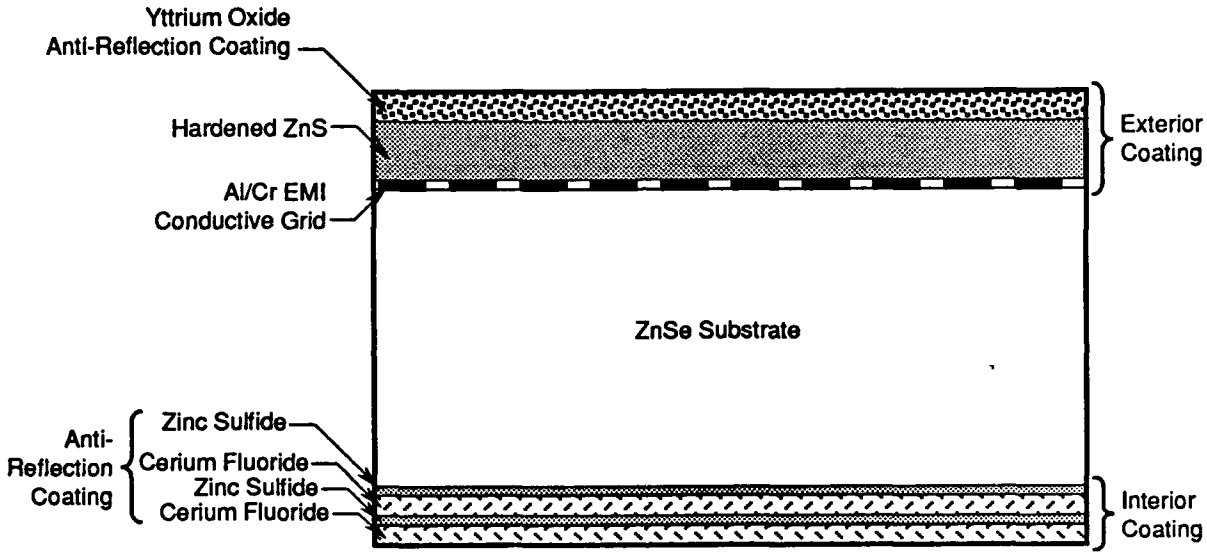

Note: Film thickness and grid dimensions are not to scale

Coating	Material	Thickness (microns)
Exterior	Yttrium Oxide	1.20
	ZnS:Te	4.2
	Grid	0.3
Interior	Cerium Fluoride	0.7
	Zinc Sulfide	0.1
	Cerium Fluoride	0.7
	Zinc Sulfide	0.1

A

Figure 4.1-3. Coated ZnSe Window Material

GP23-0005-28-D/kas

5.0 MATERIAL TESTING

The test objectives were to determine the ability of the selected window systems to satisfactorily perform to combat aircraft requirements by testing representative multi-spectral band window systems. System requirements include good optical throughput over widely spaced spectral bands (extending from 1.06 microns to 12.0 microns), survivability/durability under a diversity of stressing environments, RF shielding, and laser compatibility -- all while striving for consistency of performance and low production costs. The production window/sensor configuration could necessitate windows as large as 20" x 20" x 0.5" in size so the chosen window system must be either currently achievable in such sizes or scalable. The technical requirements of the statement of work were, therefore, oriented toward the speeds (and indirectly the corresponding temperatures) and environments associated with a subsonic aircraft. During the performance of the window study, the applicability was informally broadened to include implications of utilizing such a window system on supersonic aircraft and considering some of the factors pertinent to multi-paned flat or conformal windows.

5.1 Optical Tests

The program was structured to address the key optical performance characteristics of two infrared (IR) materials: Zinc Sulfide (ZnS) coated Zinc Selenide (ZnSe), and Gallium Arsenide (GaAs). ZnSe was coated in two ways with ZnS. The first was a relatively thick layer (1 millimeter) producing "Tuftran." The second method deposited a much thinner layer (4 microns) over the ZnSe.

Two IR material suppliers were chosen to fabricate, coat, and deliver the three types of materials. Hughes Danbury manufactured the "Tuftran", and Litton/Itek the ZnSe and GaAs. One hundred and four total samples of the three material types were delivered and tested. Figure 5.1-1 shows the configuration of those samples used in the optical tests. The number and type of optical test performed on each sample type is shown on Figure 5.1-2. The tests were selected in order to characterize the compatibility of a window to be used for a broadband lasing and imaging function and to characterize the effect of environments on window performance. Any environmental impact will be measured by transmission vs. wavelength tests and diffuse transmittance tests. All other tests shown in Figure 5.1-2 characterize optical and laser compatibility properties. Because of schedule restraints, two laboratories within MCAIR and the GDFW laboratory were used to perform the optical testing. Sample materials were initially circulated among the three laboratories to ensure that

identical results were obtained by all. The results of the laboratory testing are reported in References 5-1, 5-2, and 5-3.

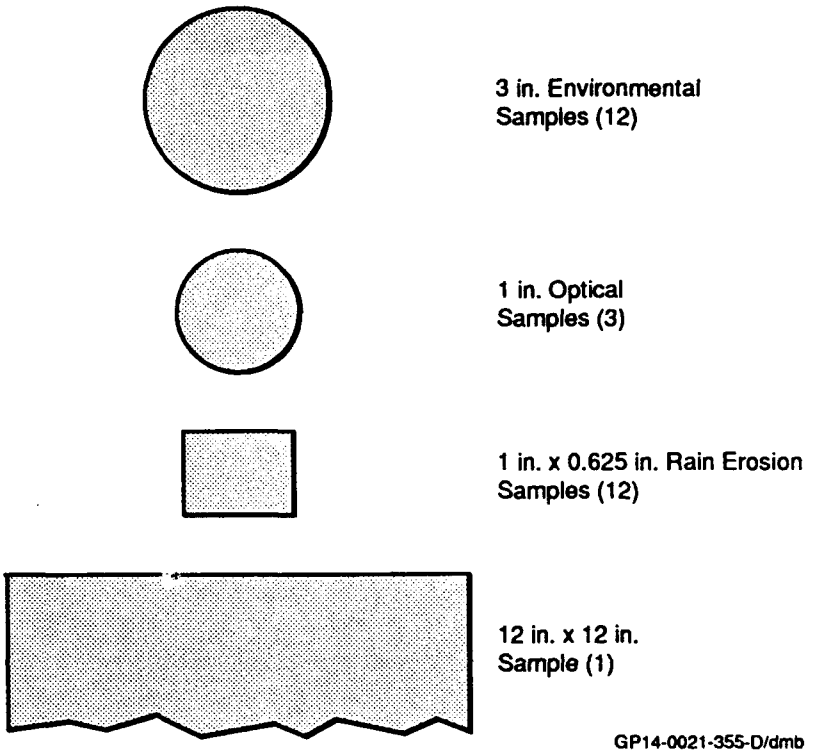

Figure 5.1-1. Window Test Program Optical Sample Configuration

5.1.1 Transmission vs. Wavelength - The results of the testing to measure specular transmission of the Environmental, Optical, Rain Erosion, and Full Size samples of the three materials in the "as received condition" is included in this paragraph. A discussion of the results is preceeded by a discussion of the test setup. Rain Erosion Test Setup is discussed in detail in Reference 5-3.

Sample Type, No. per Vendor	Lot Number	Transmission vs Wavelength	Transmission vs Temperature	Transmission vs AOI	Diffuse Transmittance	10.6 Stray Light	MTF	Laser Compatibility	1.06 Wavefront Homogeneity	10.6 Wavefront Homogeneity	1.06 Coherent Imaging	Interferometric Thermal Lensing
Coaxial Doughnuts (2) - 7 mm (2) 1.5 in. Diameter	1	2										
	2	2										
	3	2										
RF 12 in. x 12 in. (1)	1	1		1	1	1	1		1	1	1	
	3	1		1	1	1			1	1	1	
Environmental 3 in. Diameter (12)	1	12			12							1
	2	12		1	12	1	1		1	1	1	1
	3	12			12		1					1
Optical 1 in. Diameter (3)	1	3	3		3*			3				
	2	3	3		3*			3				
	3	3	3		3*			3				
Rain Erosion 1 in. x 0.625 in. (12)	1	12			12							
	2	12			12							
	3	12			12							
Strength 1.5 in. x 10 in. (5)	1	5										
	2	5										
	3	5										
Total Number of Tests		**104**	**9**	**3**	**83**	**3**	**3**	**9**	**3**	**3**	**3**	**3**

*Implicitly included in laser hardening tests.

GP14-0021-354-DU/dmb

Figure 5.1-2 Coupon Test Matrix, Number and Type of Optical Test Performed on Each Sample

Test Setup - The instrumentation used to measure transmission versus wavelength at the Physics and Optical Properties Laboratory of MCAIR and reported in Reference 5-1 was a Beckman ACTA MVII spectrophotometer for the near infrared from 0.8 to 2.5 microns; and for the 2.5 to 18 microns spectrum, an IBM FTIR IR/32 spectrometer. Data from both instruments was combined to produce a single graph from 1 to 12 microns.

In samples that do not exhibit large amounts of scattering, combining the results from two instruments provide excellent results. The match of transmission at the common 2.5 micron wavelength is perfect. However, in samples such as ZnS/ZnSe where large amounts of scattering exist, the two methods provide slightly different transmission values at the 2.5 micron point. This is a result of the differences in the detector field of view (3^{o} for the Beckman ACTA and 8^{o} for the IBM FTIR). The two spectrophotometers measure scattering as transmission. This disparity manifests itself as a slight discontinuity of transmission at 2.5 microns where the two results have been pieced together.

The Beckman spectrophotometer uses a near infrared source which measures energy from 0.8 to 2.5 microns. After transmitting through the sample, the wavelength is sorted by using a diffraction grating operating in a reflection mode. The energy contained in the discriminated wavelength is measured by a lead sulfide detector.

The IBM FTIR spectrometer uses Fourier Transform techniques in conjunction with a Michelson interferometer to measure spectral transmission.

Two different spectrophotometers were used in the Avionics Optical Systems Laboratories of MCAIR (Reference 5-2) to measure transmission for the 0.8 to 2.5 micron wavelength band and 2.5 to 12 micron band. The equipment setup is shown in Figure 5.1-3. The NIR spectrophotometer has a field-of-view (FOV) of 11^{o} whereas the LWIR system used a 20^{o} FOV. Because of this difference, again, there is a slight discontinuity in transmission at the common wavelength, i.e., 2.5 microns which becomes more apparent for very diffuse materials such as ZnS/ZnSe. No discontinuity results from the diffraction effects of the grids because of large instrument FOV in both cases. While the grids cause scattering, almost all of the scatter is intercepted by the large detector FOV. This concept is examined in more depth in paragraph 5.1.5.

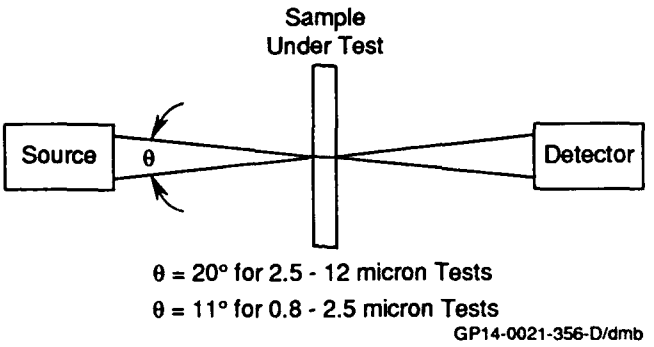

Figure 5.1-3. Transmission vs Wavelength Test Setup

A relative comparison of transmission performance of three representative sample materials along with the program goals is shown in Figure 5.1-4. The variation in transmission among the ZnS/ZnSe samples was very small whereas the variation among the GaAs samples was extensive. The variation among ZnSe samples was approximately 10%. The figure also shows that the transmission of the ZnS/ZnSe is much better than either GaAs or ZnSe. The higher transmission of ZnS/ZnSe, compared to ZnSe, is partly attributable to less geometric grid obstruction, but mainly because a more efficient graded antireflection coating was used.

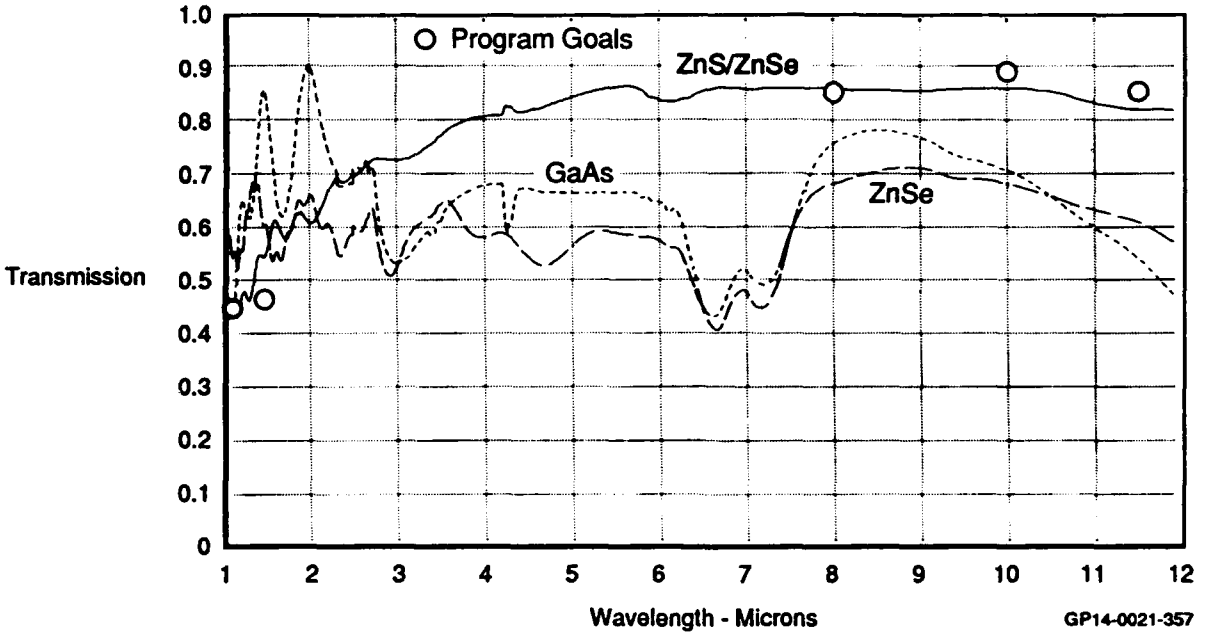

Figure 5.1-4. Performance of Candidate Materials

ZnS/ZnSe Results: Figures 5.1-5 thru 5.1-8 are the transmission curves for ZnS/ZnSe for four sample configurations. The performance is very consistent and generally meets the transmission program goals, which are also shown on the figure.

GaAs Results: Figures 5.1-9 and 5.1-11 are transmission curves for "as-received" GaAs. Figure 5.1-9 shows very large performance variation at the Long Wave Infrared (LWIR) band due to doping variation between the original boules and also the in-situ variation within a boule. The samples were made from boules whose resistivity varied from 0.03 to 42.0 ohm-cm, Figure 5.1-12. The Environmental samples, which show such large variation in transmission, originated from five different boules. Optical samples, which did not show much variation in transmission, came from a single boule.

The Optical samples exhibited less performance variation (Figure 5.1-10) because the resistivity variation, 0.2 to 0.6 ohm cm, was small, as shown in Figure 5.1-12. Rain Erosion sample results are presented in Figure 5.1-11.

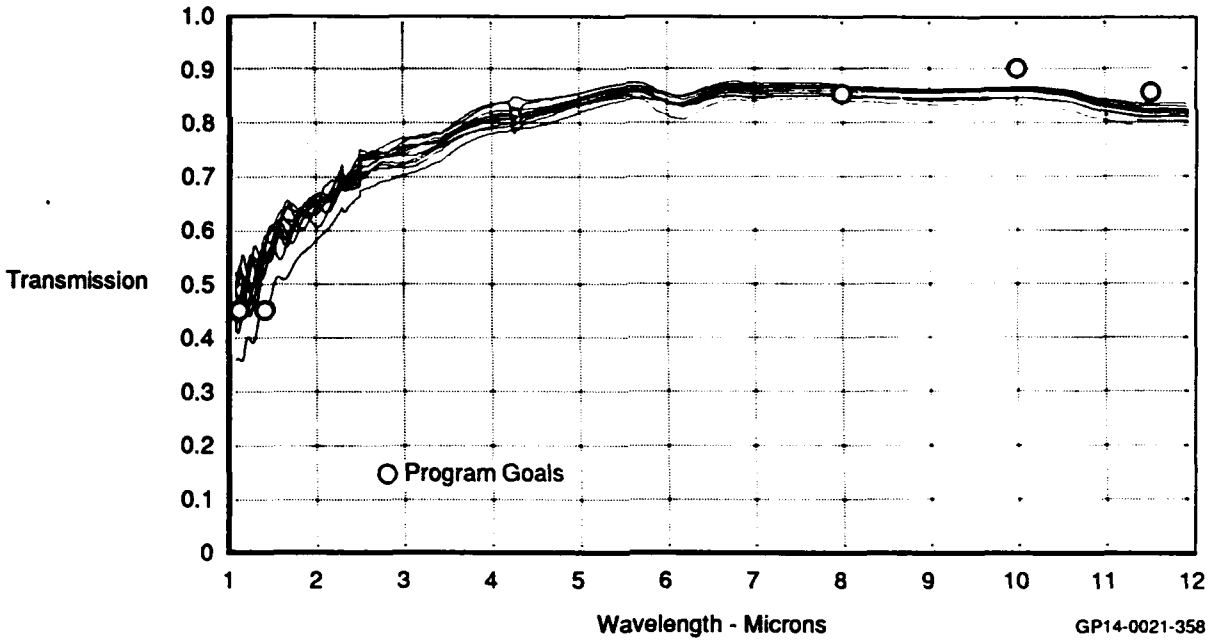

Figure 5.1-5. Performance Variation of ZnS/ZnSe Samples
Material Type - Environmental No. of Samples - 12

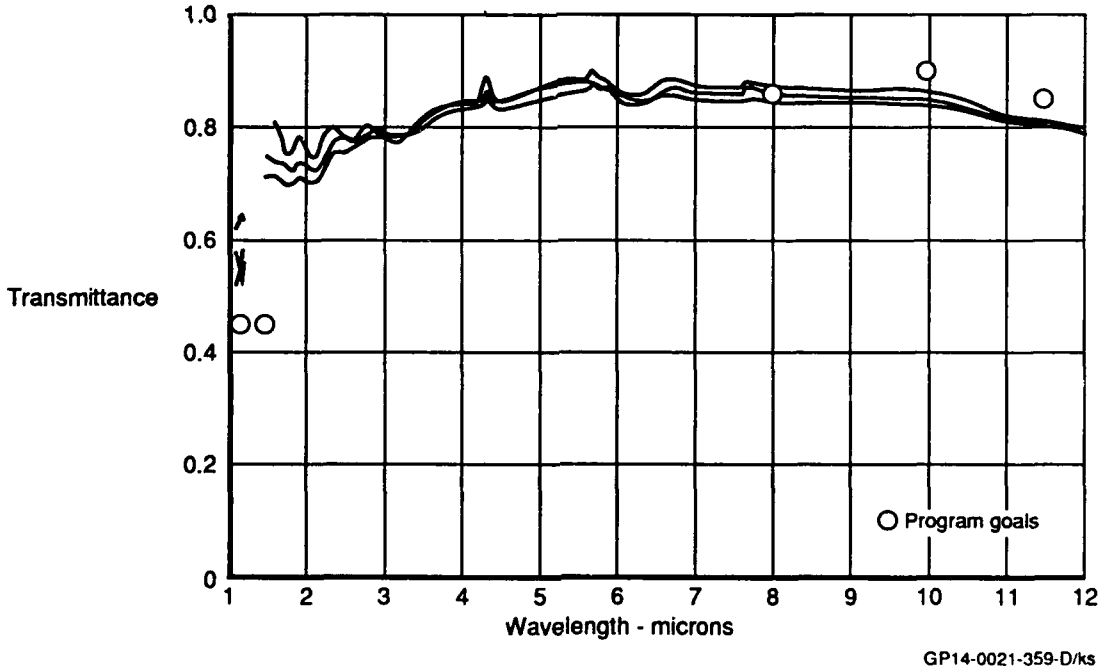

Figure 5.1-6. Perfomance Variation of ZnS/ZnSe Samples
Sample Type - Optical No. of Samples - 3

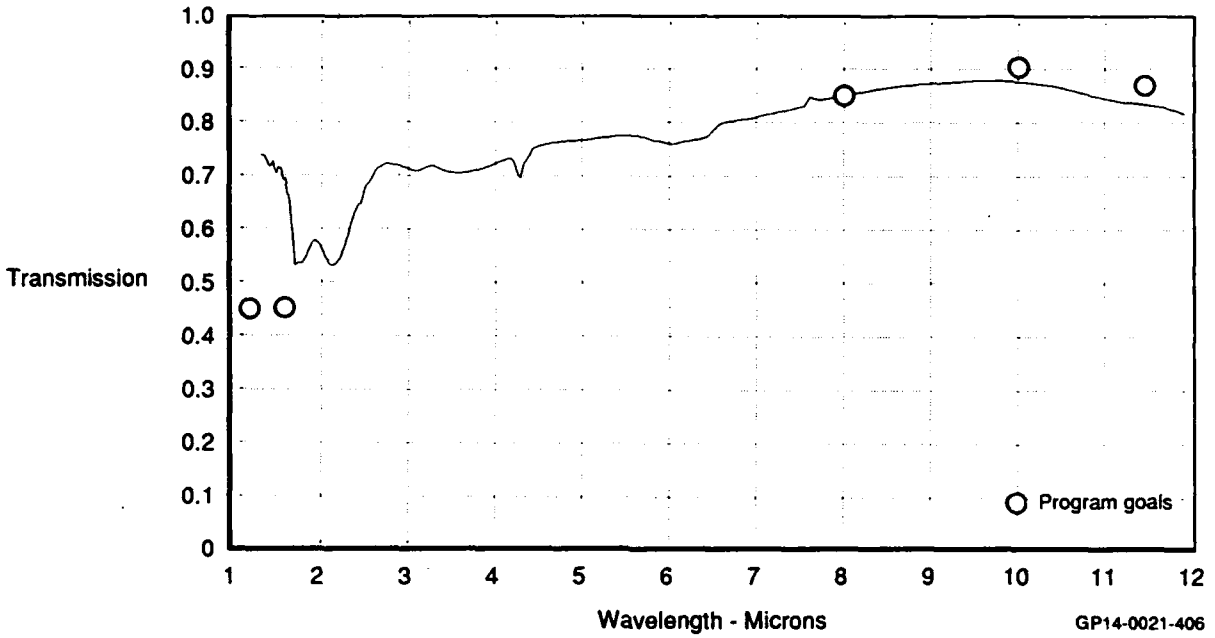

Figure 5.1-7. Optical Transmission of ZnS/ZnSe
Sample Size 12 x12 in.

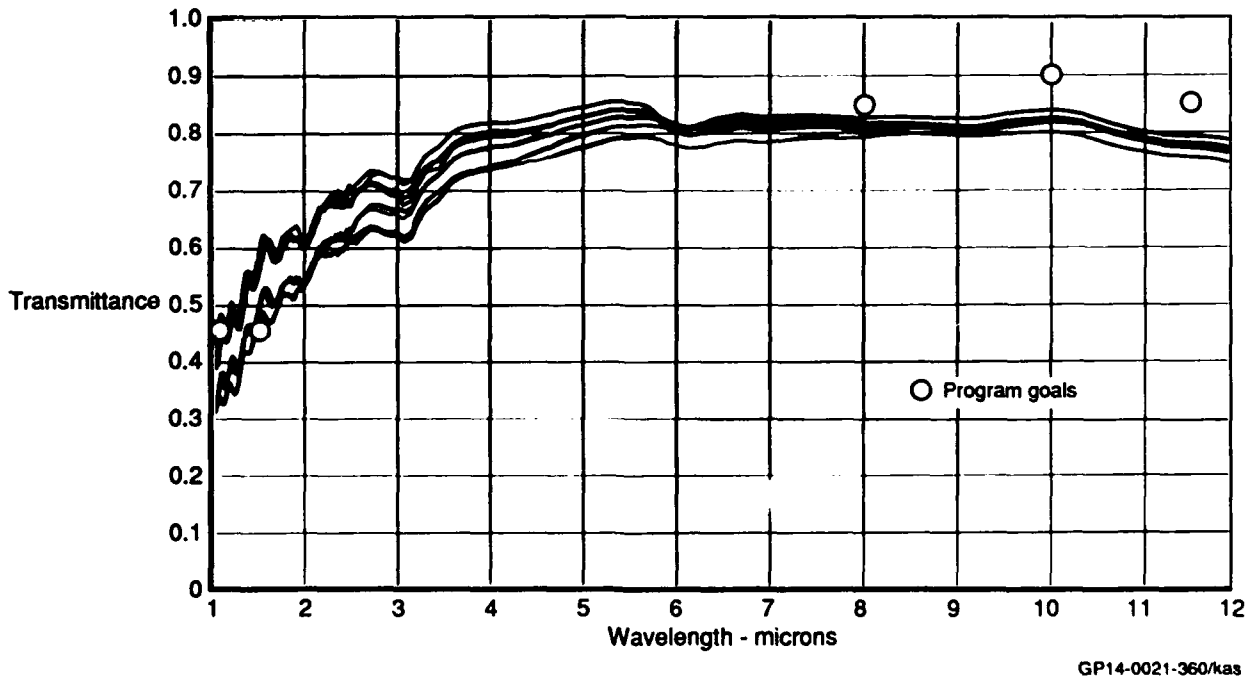

Figure 5.1-8 Performance Variation of ZnS/ZnSe Samples
Material Type - Rain Erosion No. of Samples - 9

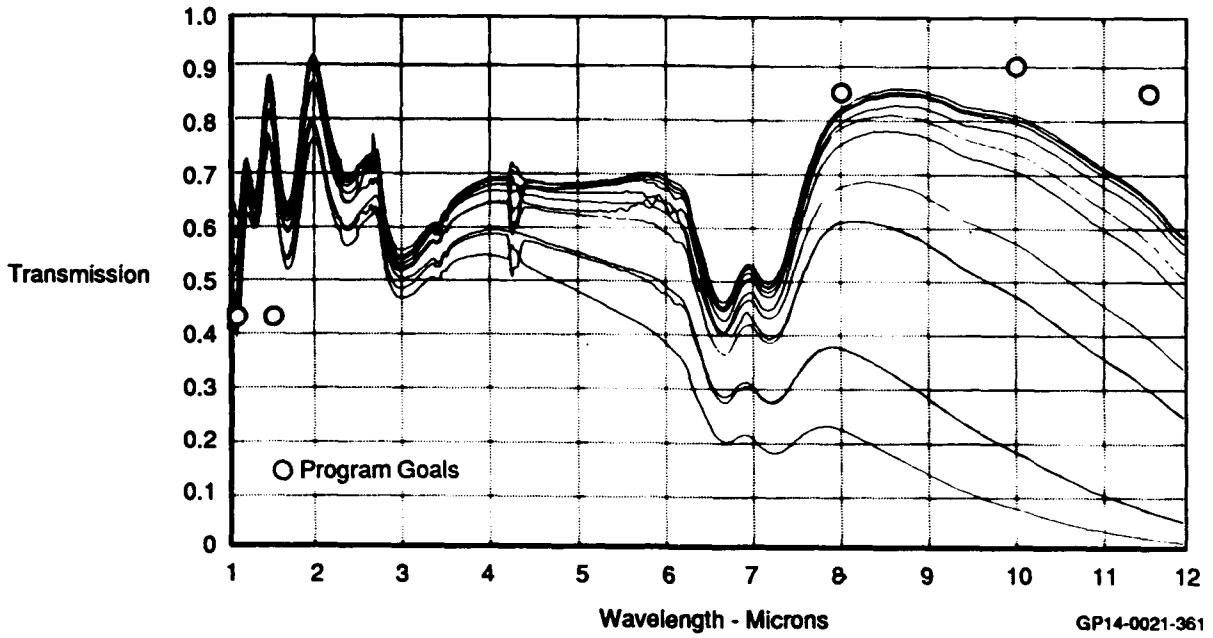

Figure 5.1-9. Performance Variation of GaAs Samples
Material Type - Environmental No. of Samples - 12

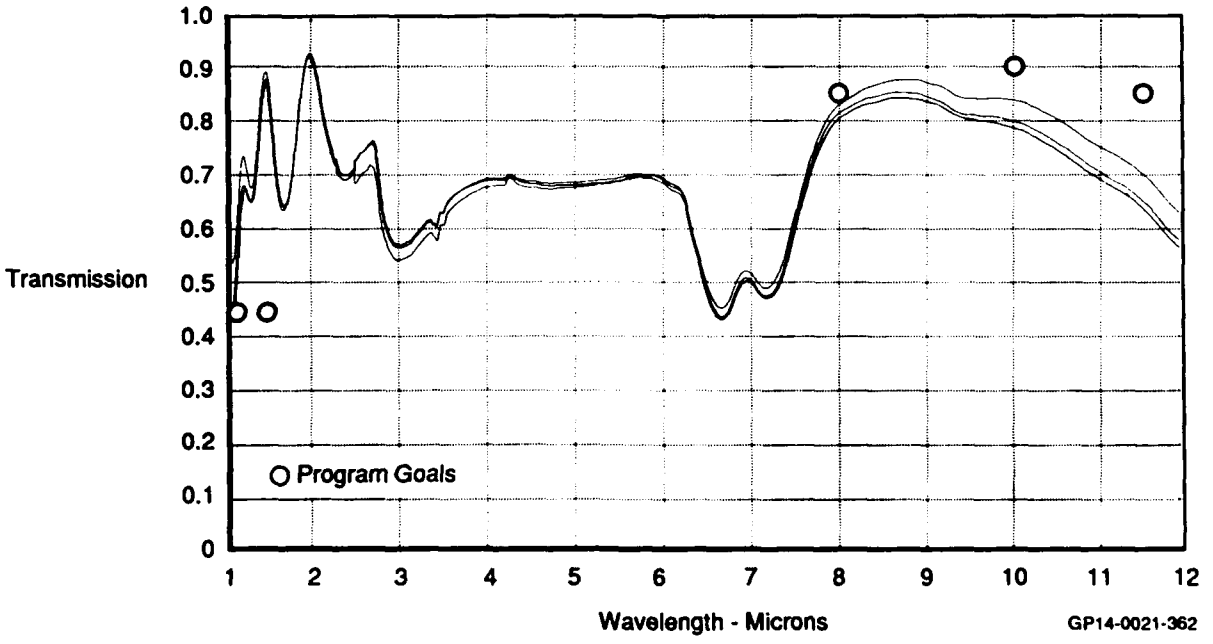

Figure 5.1-10 Performance Variation of GaAs Samples
Sample Type - Optical No. of Samples - 3

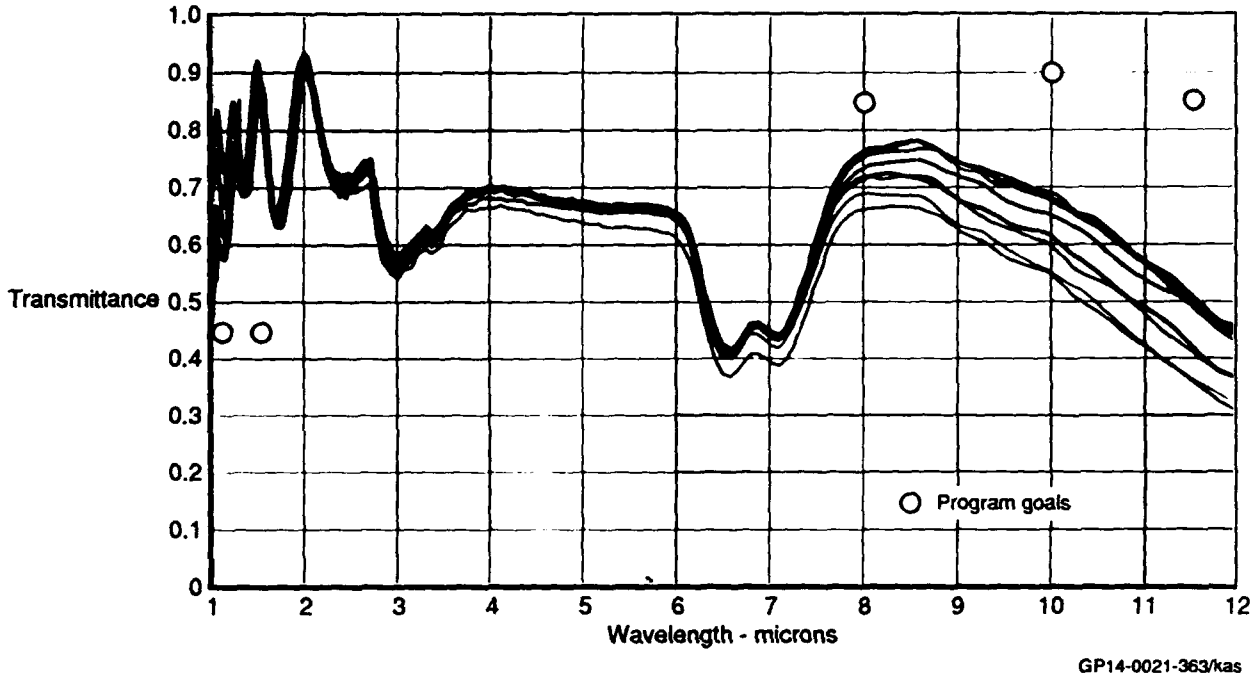

Figure 5.1-11. Performance Variation of GaAs Samples
Material Type - Rain Erosion No. of Samples - 12

Sample Description	Boule Number	Boule Seed	Boule Tail
Rain Erosion	11198	0.14 ohm cm	
Rain Erosion	5525	0.05 ◄——►	2.0 ohm cm
Environment	5521	0.40	
Environment	5522	42.0	
Environment	5523	0.03 ◄——►	0.3
Environment	5524	0.20 ◄——►	0.4
Environment	5525	0.05 ◄——►	0.2
Optical	11181	0.20 ◄——►	0.6

GP14-0021-364-D/cjg

Figure 5.1-12. Variation in GaAs Resistivity With Location Within Boule

A typical boule's conductivity varies from seed to tail; constant resistivity exists across any slice. Thus, it is likely the Optical samples were taken from the same slice or adjacent slices whereas the Environmental samples were taken from different boules and/or different slices within a boule.

GaAs exhibited large performance variability, probably due to doping variations which are the result of manufacturing processes. Transmission at 1.06 microns meets program goals while the 8 to 12 micron transmission does not. These data were developed for material from a single supplier. It is not known from this program if the GaAs performance is supplier dependent.

The chief advantage of GaAs is the inherent ability (without the aid of grids) to transmit the wide band of optical wavelengths; and, at the same time, provide rejection of electromagnetic waves in the RF spectrum. These twin abilities are dependent upon the material resistivity as a result of proper doping. Thus, the resisitivity of the Environmental samples was measured to see if any correlation existed between the optical performance and resistivity.

Six samples were chosen for this measurement which represented high, medium, and low optical transmission. Resistivity as a function of optical transmission at 10 microns was plotted and is shown in Figure 5.1-13. The monotonically increasing curve shows perfect correlation between resistivity and transmission, i.e., increasing resistivity always produces higher and, therefore, better optical transmission. Also shown in this figure is the relation between resistivity and one-way RF transmission attenuation at 2 GHz for a 0.5-inch thick sample, based on theoretical analysis of the effect of bulk resistivity. These curves may be used to tradeoff optical and RF performance. For example, if a one-way RF attenuation of 20 dB is desired, then a resistivity of less than 30 ohm-cm is required. The attendent optical transmission is no greater than 0.86. The RF performance of the materials is examined in greater depth in paragraph 5.2.

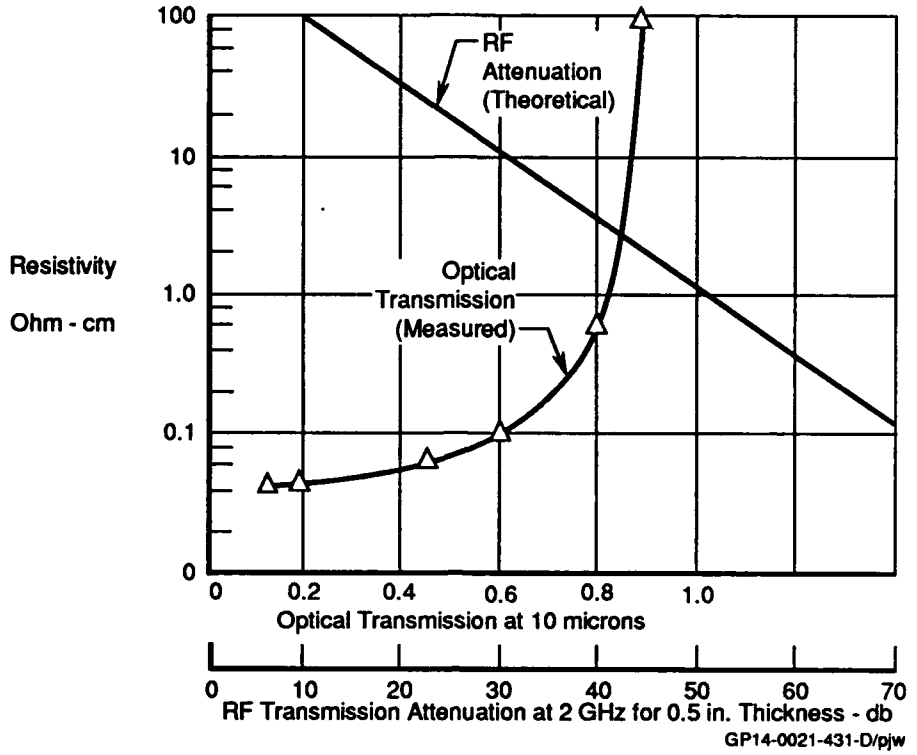

Figure 5.1-13. Effect of Resistivity of GaAs on Optical and RF Performance

ZnSe Results: The ZnSe specular transmission is presented in Figures 5.1-14 through 5.1-17. Figure 5.1-14 shows about a 10% variation in transmission in LWIR band. The Optical sample shows an approximate 2% change in performance in this same wavelength band.

The transmission at 1.06 microns is much better than the program goals while performance at 8-12 microns is approximately 15% less than the program goals.

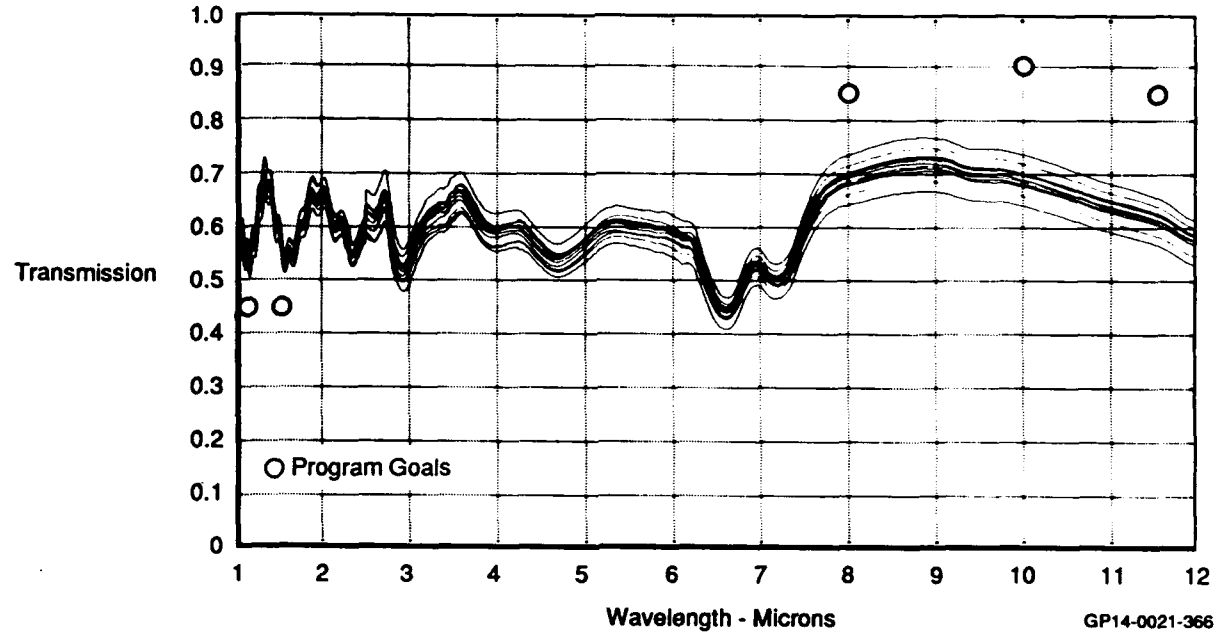

Figure 5.1-14. Performance Variation of ZnSe Samples
Sample Type - Environmental No. of Samples - 12

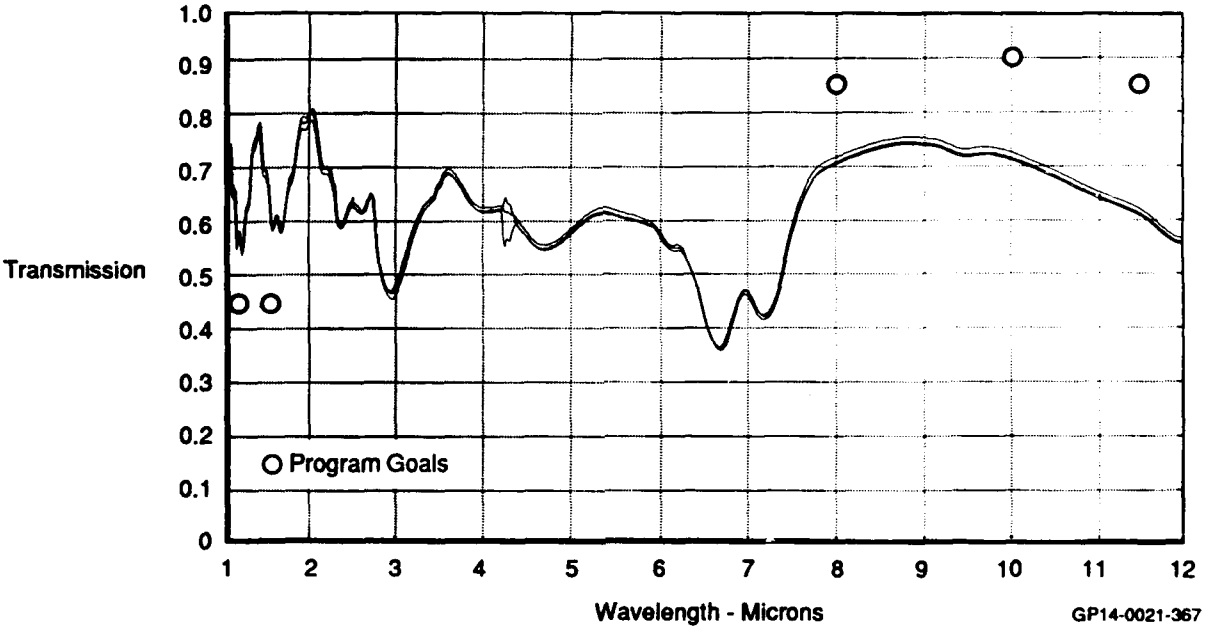

Figure 5.1-15. Performance Variation of ZnSe Samples
Sample Type - Optical No. of Samples - 3

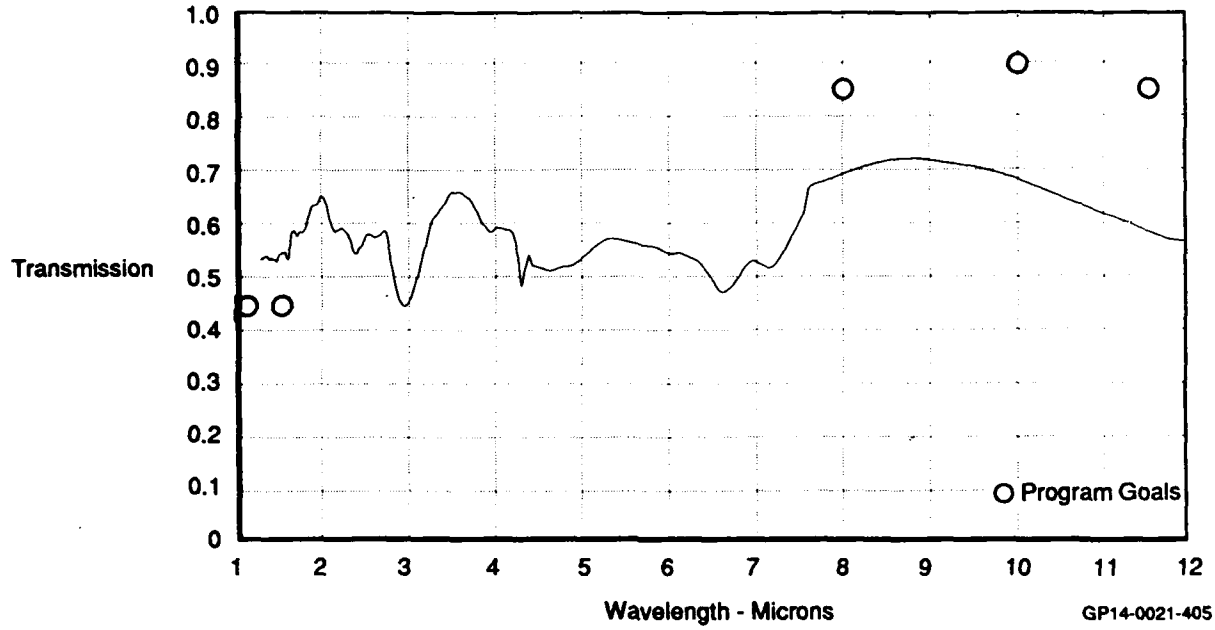

Figure 5.1-16 Optical Transmission of ZnSe
Sample Size 12 x12 in.

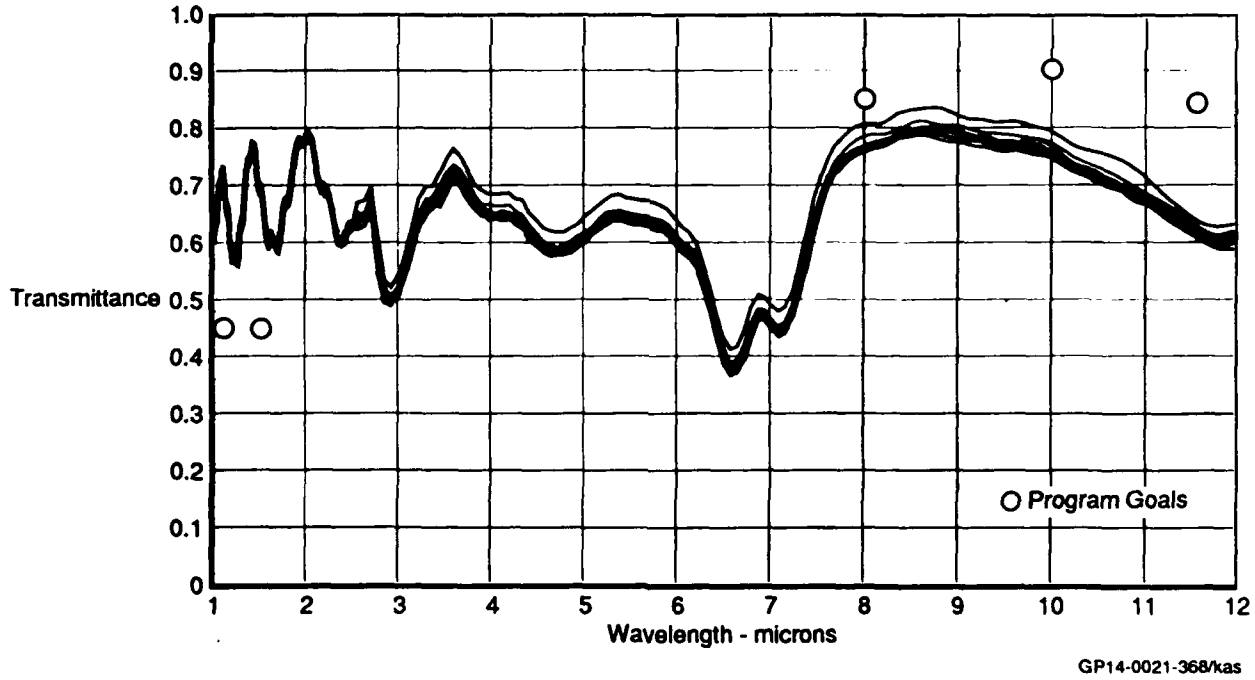

Figure 5.1-17. Performance Variation of ZnSe Samples
Material Type - Rain Erosion No. of Samples - 10

5.1.2 Transmission vs Angle of Incidence (AOI) - Window transmittance is dependent upon the angle between the direction of the transmitted light beam and the normal to the window. Usually maximum transmission occurs at zero AOI, but anti-reflection coating design may cause peak performance to occur at another angle. The shape of this curve may be different at the NIR and LWIR wavelengths.

The test setups for the AOI measurements are shown in Figure 5.1-18a) and b). The NIR test uses a 1.06 micron laser source coupled into a set of beam forming optics to obtain a narrow 0.57-inch diameter beam. This beam is incident on the sample and the transmitted energy is captured by the integrating sphere which measures both direct transmitted and diffused energy through the sample. The sample is rotated to obtain AOI changes and is translated vertically to obtain five measurements so that homogeneity of the sample may be measured.

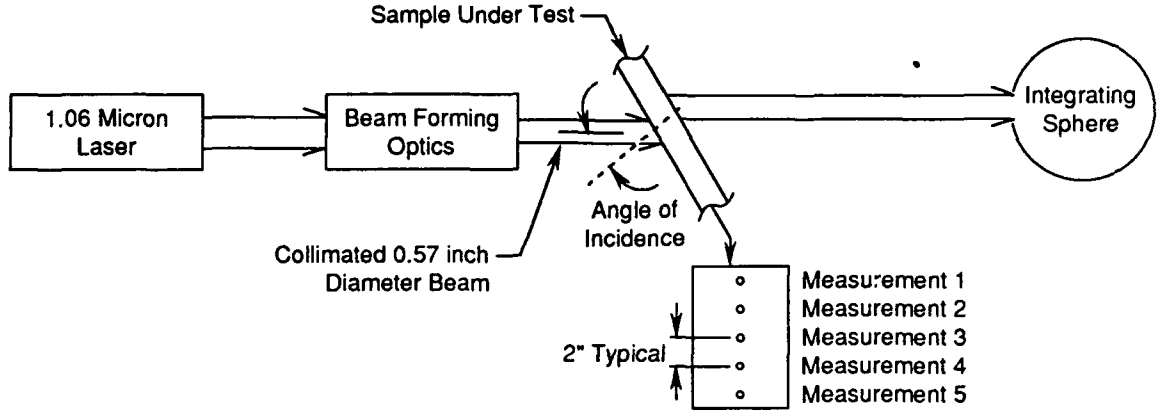

a) NIR Angle of Incidence Test Setup

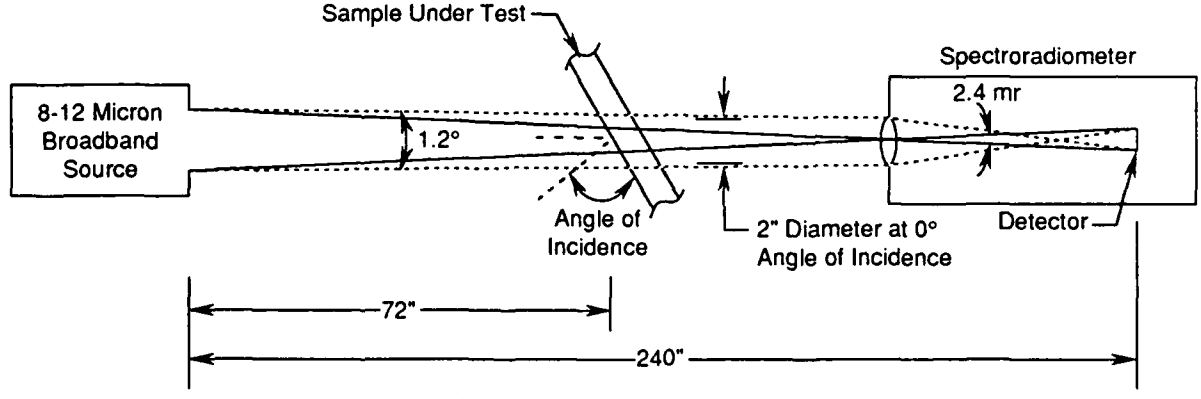

b) LWIR Angle of Incidence Test Setup

GP14-0021-369-D/scz

Figure 5.1-18. Angle of Incidence Test Setups

The LWIR AOI measurement is shown in Figure 5.1-18b). The source and detector are located so the beamwidth illuminating the sample has an angle of 1.2° resulting in a 2-inch diameter circle on the sample. The spectroradiometer has a 2.4 mr FOV. The sample is rotated on a turntable to obtain variations in AOI.

For the NIR wavelength of 1.06 microns, the results are shown in Figures 5.1-19 through 5.1-21 for ZnS/ZnSe, GaAs, and ZnSe materials, respectively. The large 12x12 samples were used because the test laser beam undergoes such an extreme offset when passing through the material. The test was repeated at five locations on the 12x12 inch samples to test for material homogeneity. Only one test location was used on the GaAs sample because of its small 3-inch diameter size; and its homogeneity was thought not to vary greatly because of this.

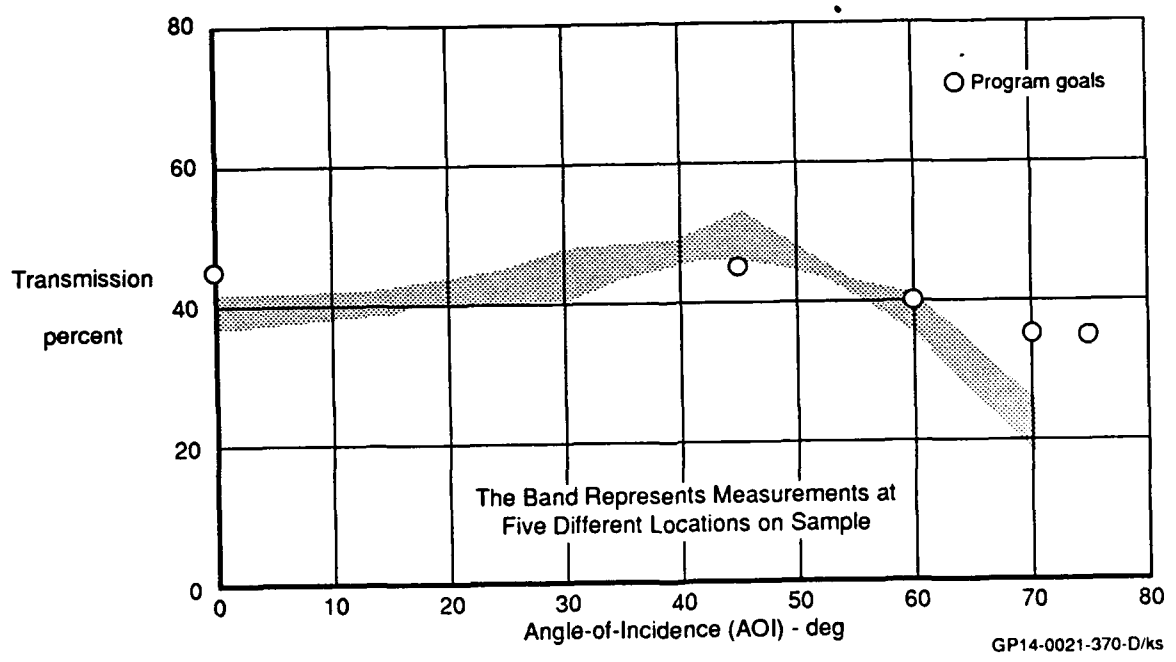

Figure 5.1-19. Effect of Angle-of-Incidence on Transmission
Material - ZnS/ZnSe 12 In. x 12 In. Wavelength - 1.06 Microns

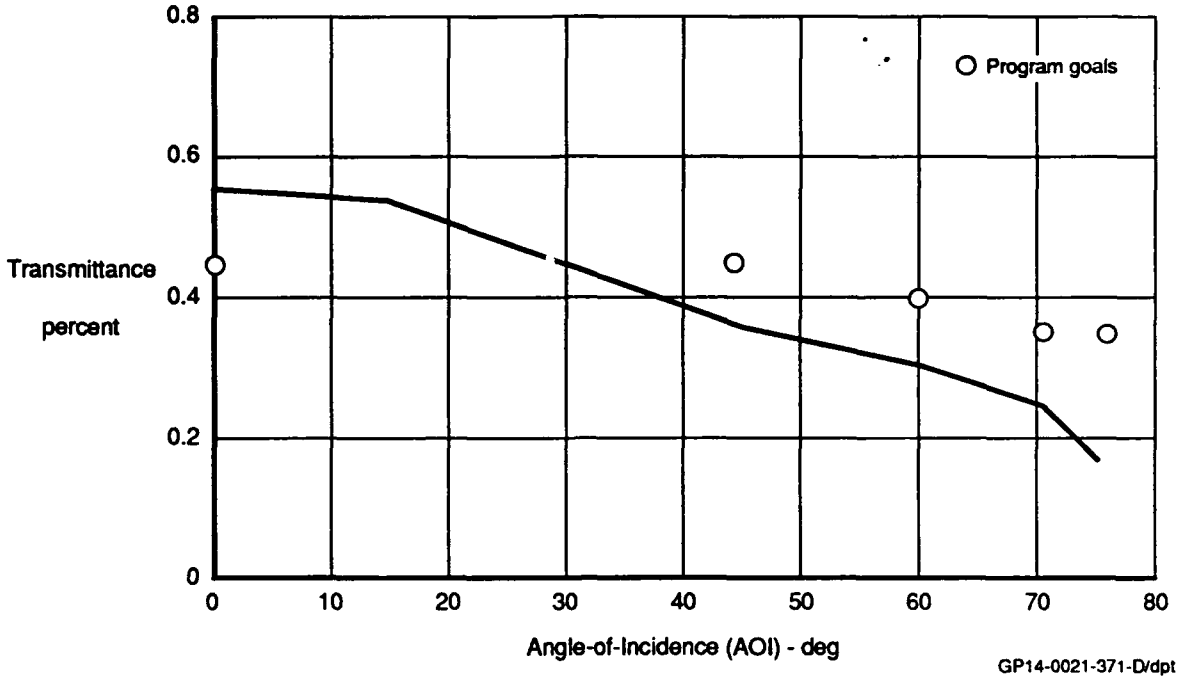

Figure 5.1-20. Effect of Angle-of-Incidence on Transmission
Material - GaAs 3 in. dia. Wavelength - 1.06 microns

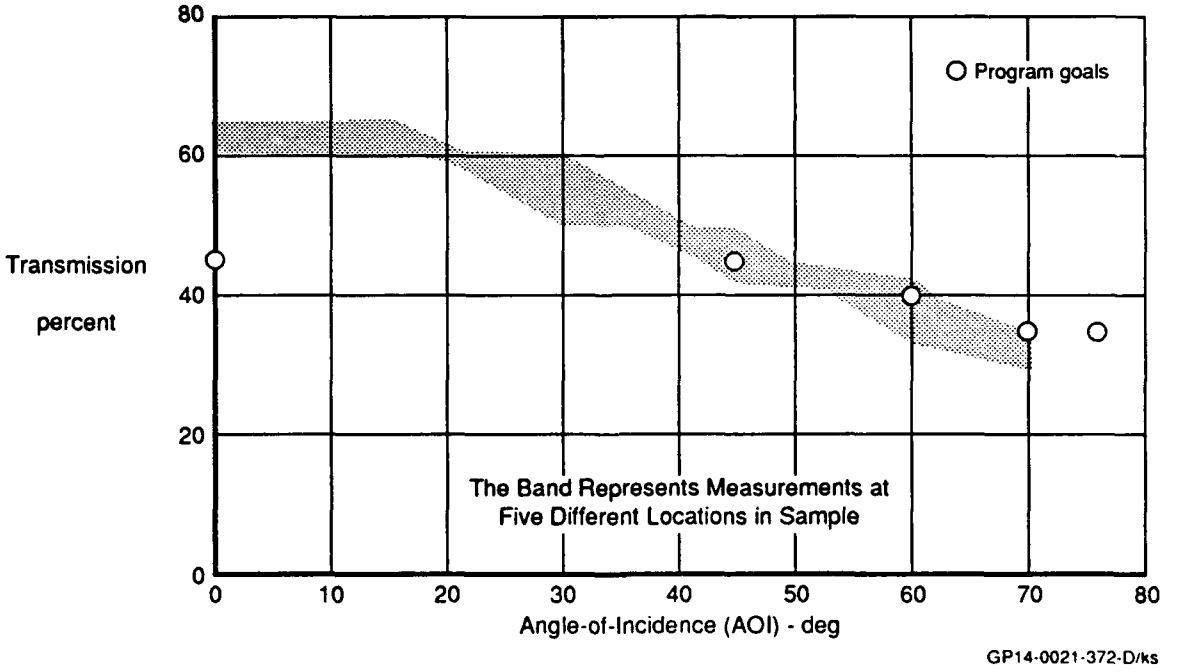

Figure 5.1-21. Effect of Angle-of-Incidence on Transmission
Material - ZnSe 12 In. x 12 In. Wavelength - 1.06 Microns

The effect of AOI on transmission for ZnS/ZnSe at 1.06 microns is shown on Figure 5.1-19. The antireflection coatings were designed to provide peak performance at 45° AOI. From 0° to 45° constant transmission was achieved. Transmission decreases dramatically at AOI greater than 45°. In contrast, GaAs, Figure 5.1-20, and ZnSe, Figure 5.1-21, exhibit maximum performance at 0° AOI with a continuous decrease at larger AOI. Clearly, windows can be designed for peak performance at AOI other than 0°. The angle for peak performance is a design consideration based on the window installation in the aircraft.

The effect of AOI on transmission at 7.5 to 12 microns is shown in Figure 5.1-22 for all three materials. The curves represent an average of multiple measurements taken through ZnSe and ZnS/ZnSe 12x12-inch samples and one measurement on the 3-inch GaAs sample. As shown earlier on Figure 5.1-9, large transmission variations exist with the GaAs and another GaAs sample may have had better or worse transmission. The important fact to be gained is the shape of the curve and the gradual drop off in transmission as AOI increases.

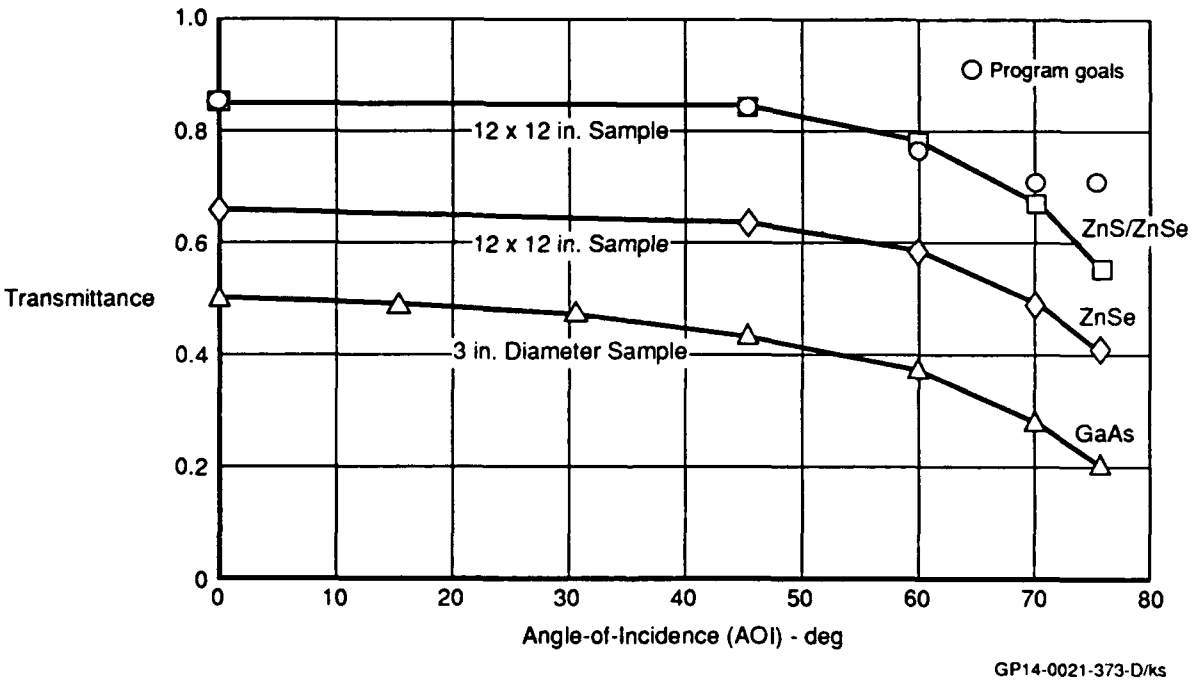

Figure 5.1-22. Effect of Angle-of-Incidence on Transmission
Wavelength - 7.5 - 12 Microns Broadband

5.1.3 Transmission vs Temperature - Because of aerodynamic heating, the effect of temperature on IR window optical performance is a key concern in any Forward Looking Infrared (FLIR) or Infrared Search and Track (IRST) sensor design. Some window materials become opaque to IR energy transmission at elevated temperatures and reduce the performance of a FLIR or IRST. All three materials were tested to establish the effect of temperature on transmission at the NIR and LWIR wavelengths. The temperature was varied from -20^{o} to 105^{o}C in approximately 20^{o}C increments to approximate the operating temperature range for subsonic aircraft. Current supersonic aircraft, such as the F-4, F-14, and F-15, typically experience stagnation temperatures up to approximately 200^{o}C.

The test setup is shown in Figure 5.1-23a), b), and c). The samples were mounted into a heat sink which was either heated above ambient or cooled below ambient temperature by an external source. In addition, the below ambient tests required insertion of the sample into a vacuum chamber to prevent surface condensation on the sample.

During testing of ZnS/ZnSe at 1.06 microns, it was discovered that transmission measurements were affected by sample location with respect to the source, Figure 5.1-24. The high diffuseness of ZnS/ZnSe caused a variation in transmission performance. The diffuseness is much less at the longer IR wavelengths. As a result, the test setup was changed to the configuration shown in Figure 5.1-23b) where the sample was moved closer to the spectroradiometer and the diffuse source was moved further from the spectroradiometer. As a result, the beam of energy being measured was more collimated and the diffuse rays were not collected by the spectroradiometer.

The test setup for the 1.54 and 8 to 12 micron wavelengths are shown in Figure 5.1-23c) and was changed from the previous setup because a longer wavelength source and spectroradiometer were used.

As shown in Figures 5.1-25 through 5.1-27, there was little effect of temperature on transmission for all three materials. No material opaqueness was evident for the -20^{o}C to 105^{o}C temperature range.

The ZnSe optical sample's anti-reflection coating was crazed prior to temperature testing. While increasing the temperature from ambient to higher levels, portions of the anti-reflection

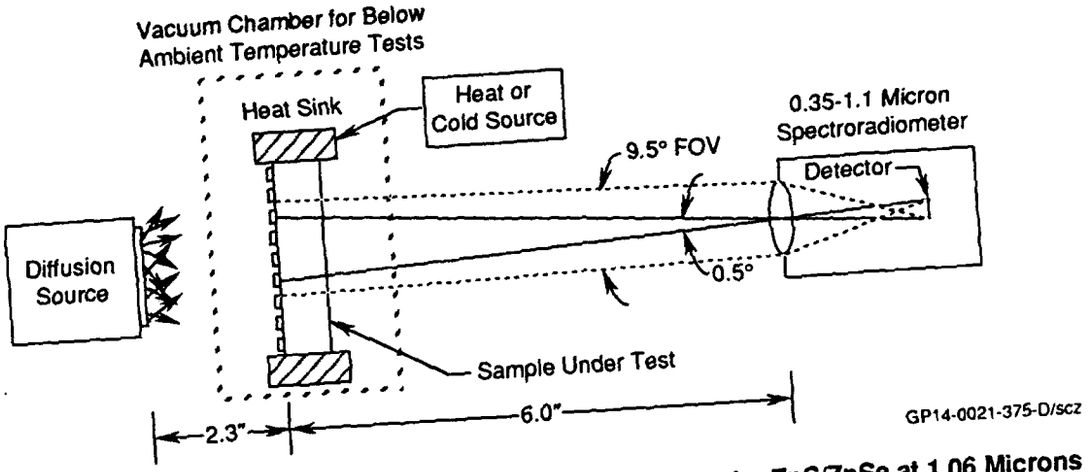

Figure 5.1-23. (a)Transmission vs Temperature Test Setup for ZnS/ZnSe at 1.06 Microns

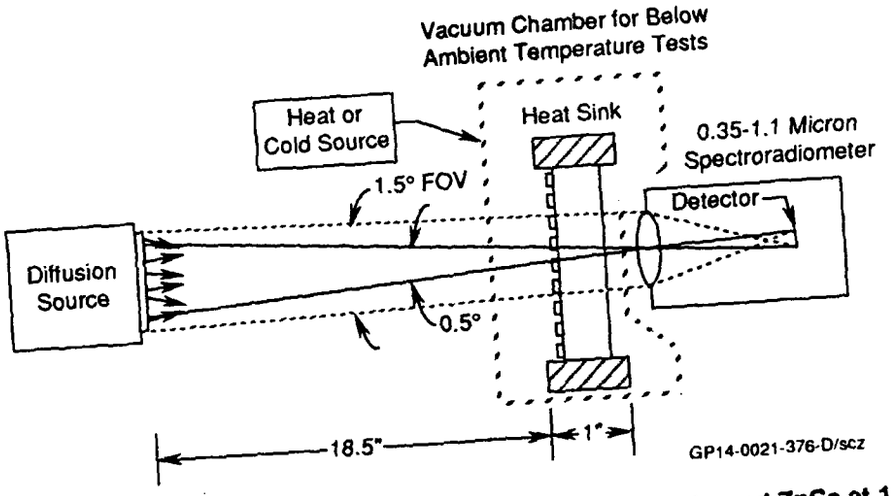

Figure 5.1-23. (b)Transmission vs Temperature Test Setup for GaAs and ZnSe at 1.06 Microns

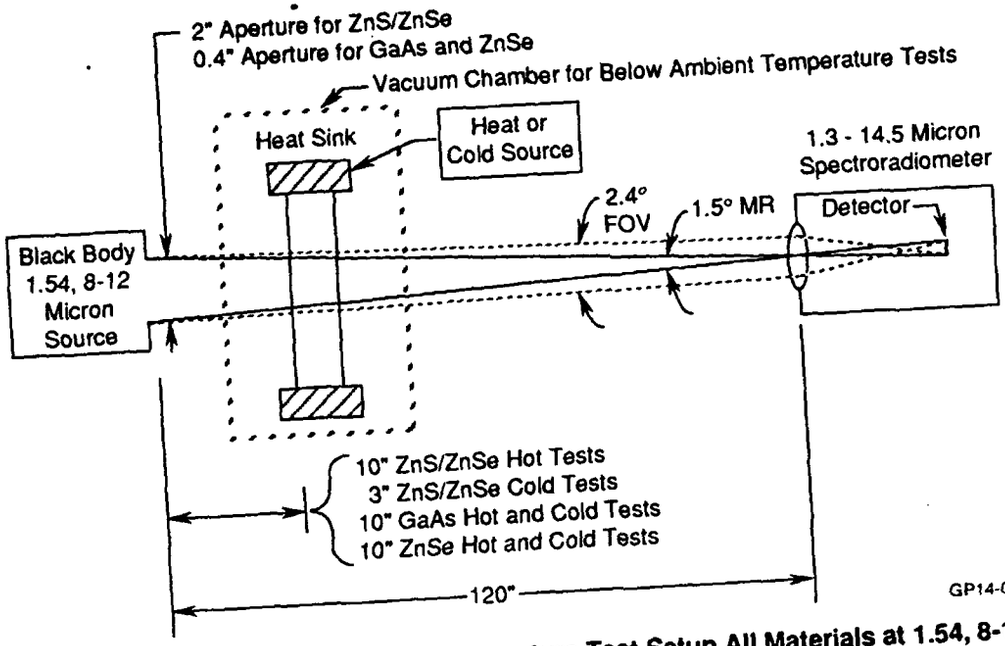

Figure 5.1-23. (c)Transmission vs Temperature Test Setup All Materials at 1.54, 8-12 Microns

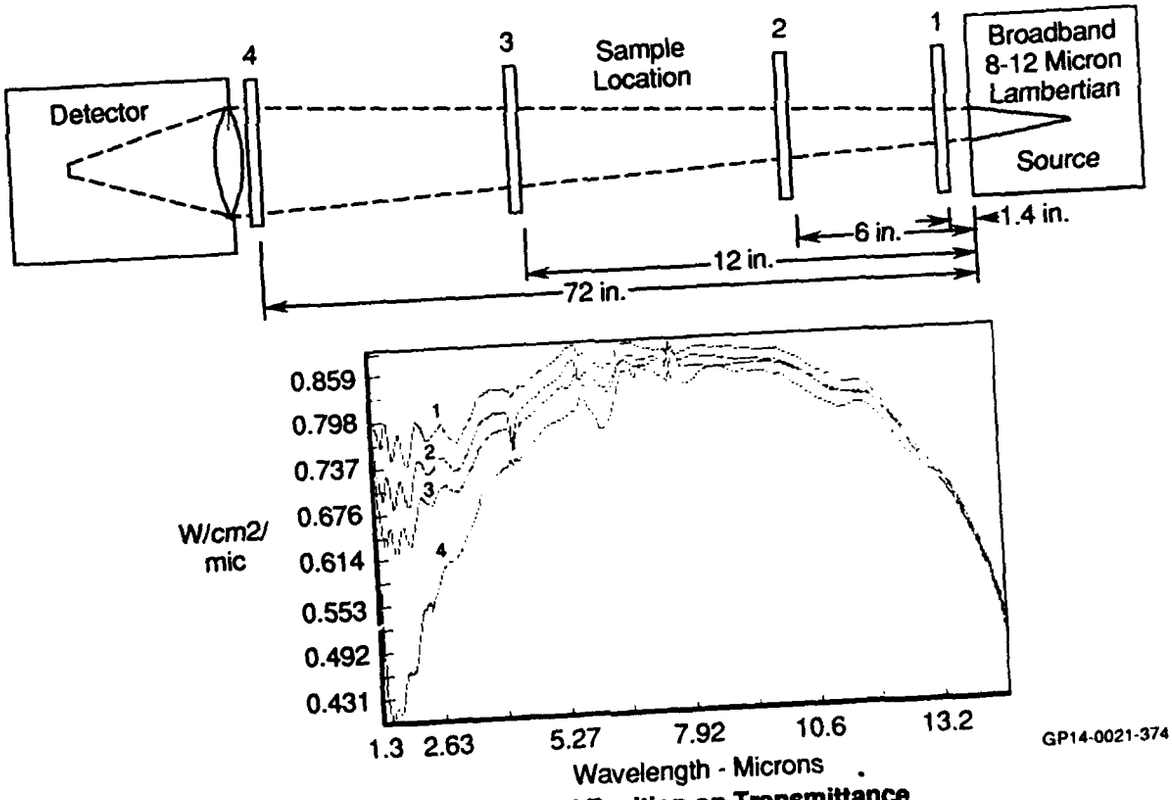

Figure 5.1-24. Effect of Position on Transmittance of Material With Large Scatter

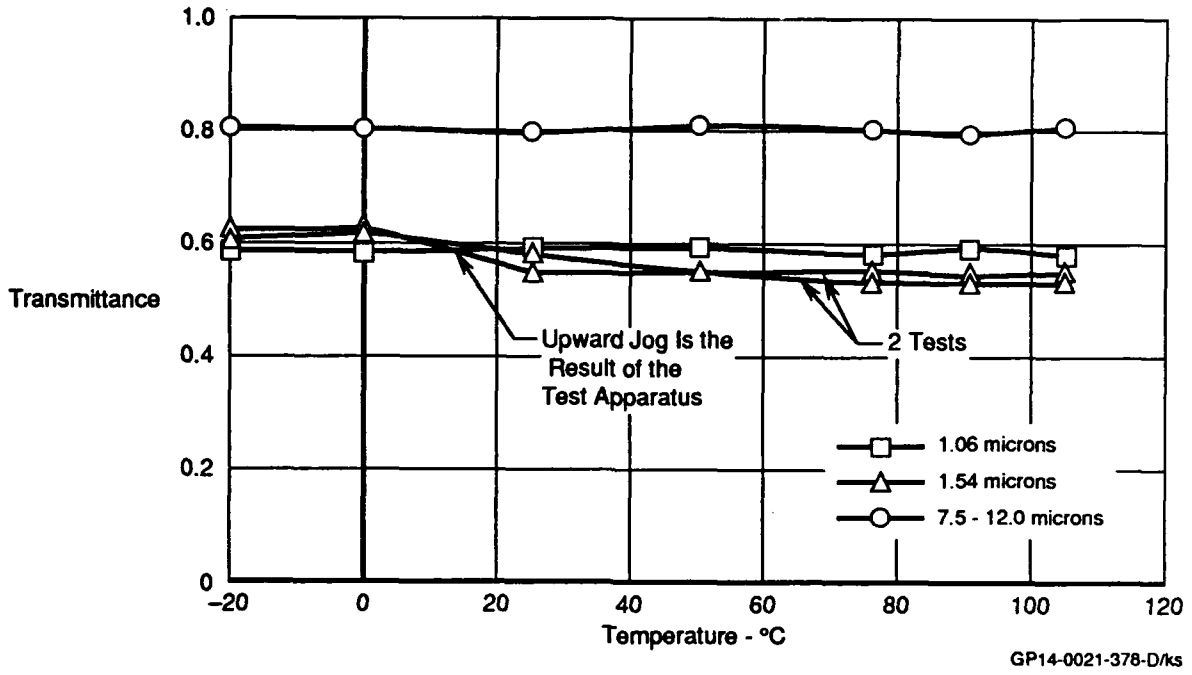

Figure 5.1-25. Temperature Effects on Transmission
Material - ZnS/ZnSe

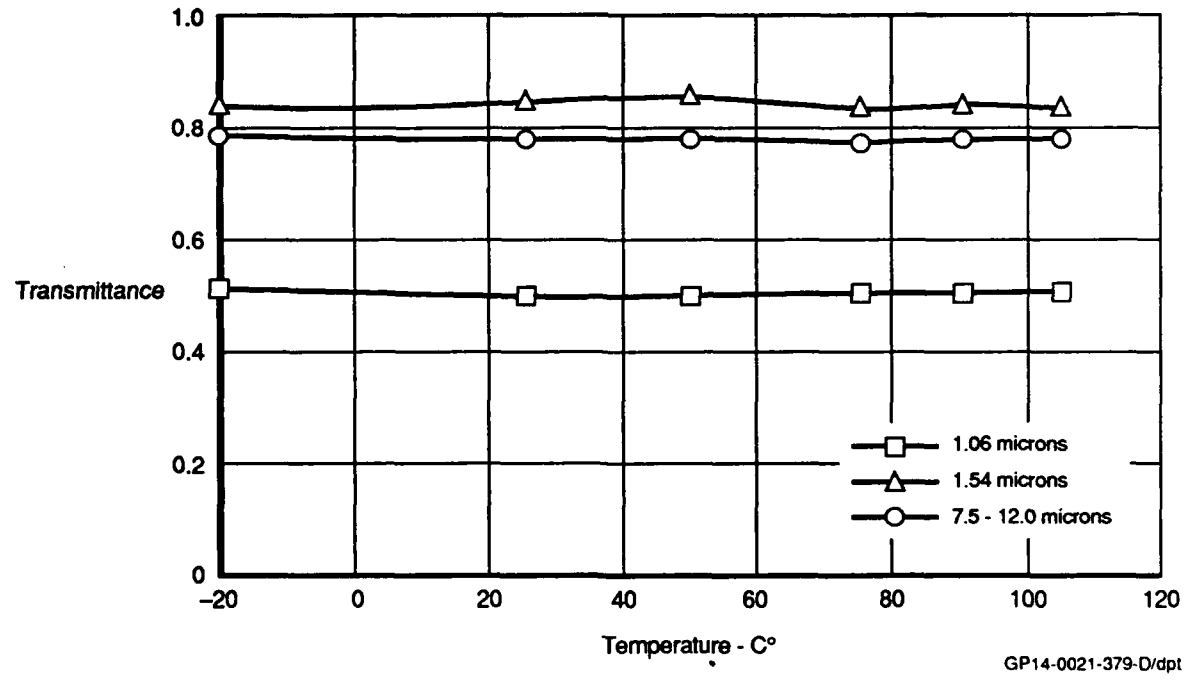

Figure 5.1-26. Temperature Effects on Transmission
Material - GaAs

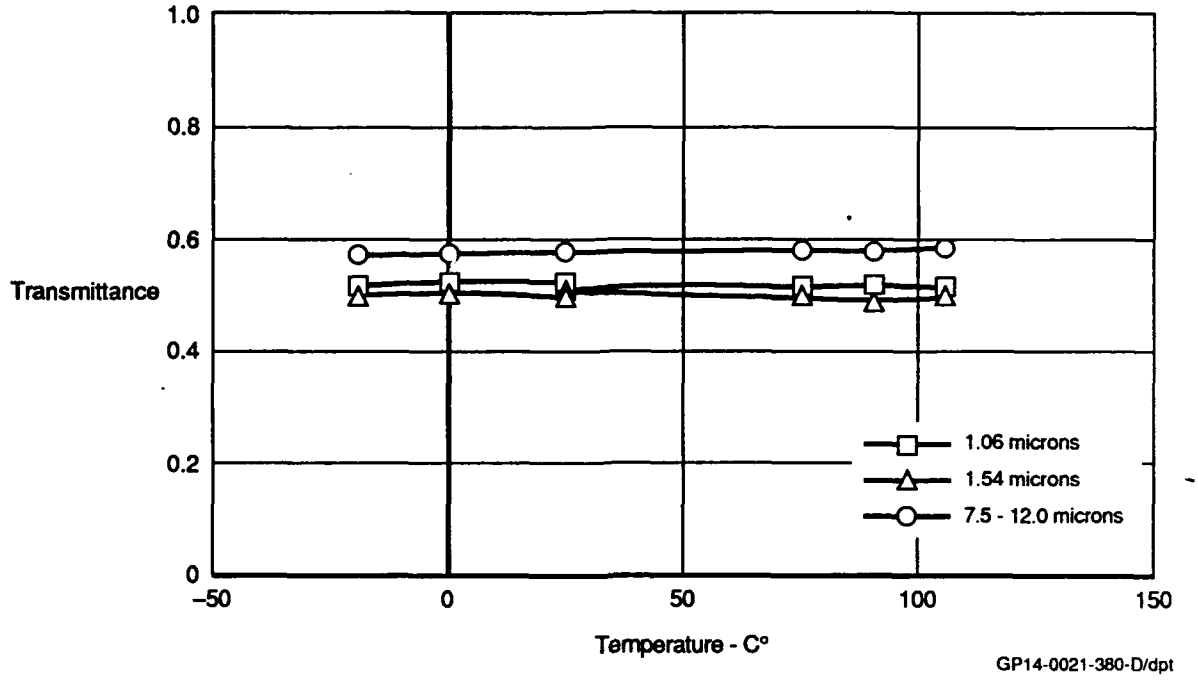

Figure 5.1-27. Temperature Effects on Transmission
Materal - ZnSe

coating flaked off causing loss of 1.06 micron transmission, as shown in Figure 5.1-28. When the sample was returned to 25°C ambient, transmission had decreased from an initial 62% to 54%, and examination under 100X magnification revealed crazing and coating flake-off. Samples not initially crazed suffered no transmission degradation during the test. The ZnSe supplier confirmed that the sample had crazing in the anti-reflection coating due to their processing. During the Ion Assisted Deposition of the Anti-Reflection (AR) coating on the samples, ITEK's chamber monitoring noted that their process had reached a point in its maintenance cycle where the chamber needed to be shut down for cleaning. After coating the optical coupons, the chamber was cleaned. The samples were inspected and crazing of the AR coating was noted. However, there was no contractural prohibition precluding crazing of coatings. Therefore, the samples were shipped. This experience suggests that window materials must be examined under magnification to screen out material which has crazed coatings. Current MIL-specs do not address this condition and should be revised to include crazing inspection.

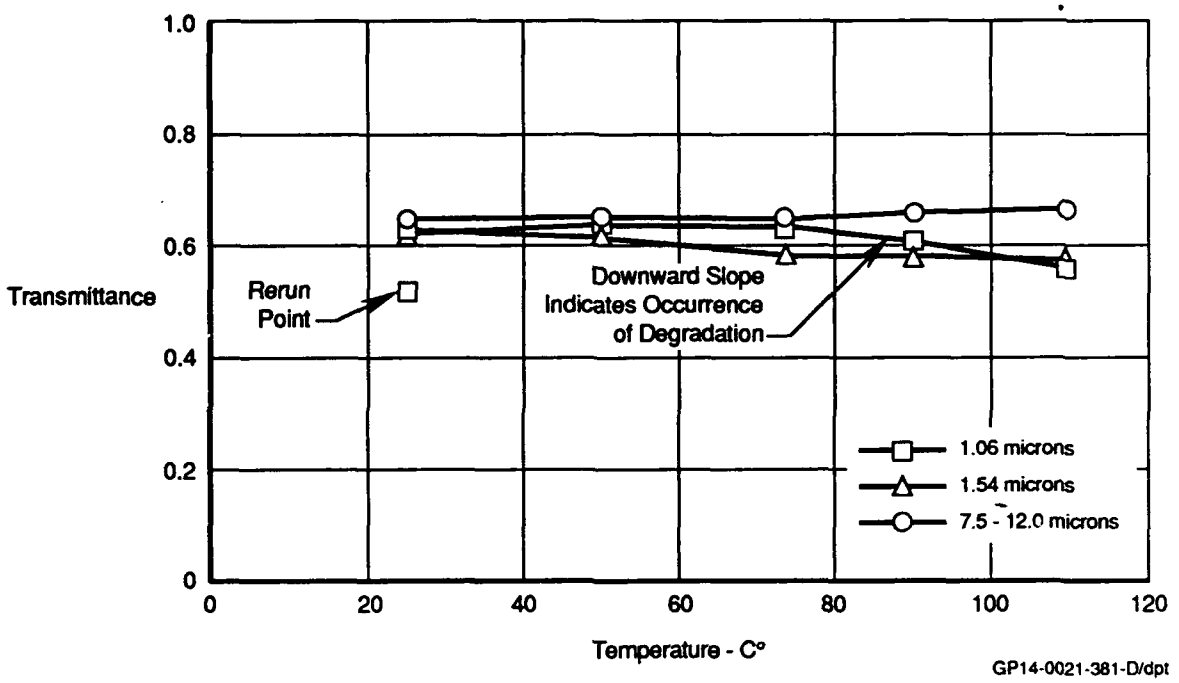

Figure 5.1-28. Effects on Transmission IF Anti-Reflection Coating Is Crazed

5.1.4 Diffuse Transmittance - An inhomogeneous refraction index will cause radiation passing through a material to scatter and diverge. Collimated laser energy will diverge causing decreased power on the target and illumination of a larger area. Material diffusion tests were performed upon the three materials. A 1.06 micron collimated laser beam was transmitted through the sample as shown in Figure 5.1-29. Beam forming optics were used to obtain a 0.57-inch diameter beam. On the exit side of the sample, all energy outside of 5° diverging beam was captured by an integrating sphere. The ratio of this energy to the energy entering the sample is defined as diffuse transmittance.

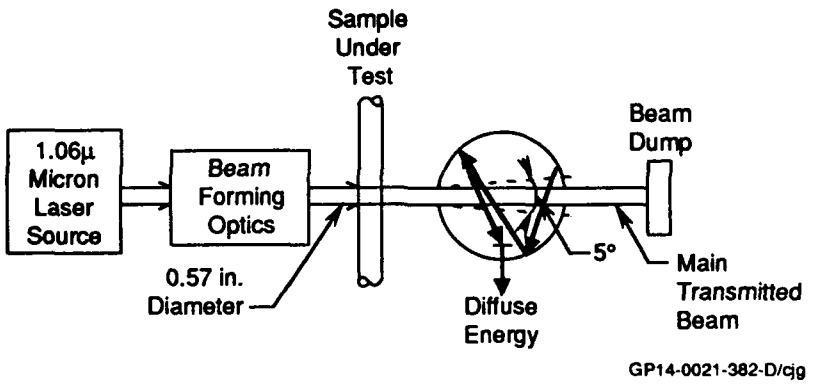

Figure 5.1-29. Diffuse Transmission Test Setup

The results are shown in Figure 5.1-30. By far the worst performance was the ZnS/ZnSe where the typical diffuse transmittance was greater than 25%; too large to be compatible with laser transmission. The large diffuse transmittance was probably caused by two factors: a thick layer (1mm) of ZnS which has an inherently large scatter characteristic, and scattering at the ZnS and ZnSe interface. The interface between the two layers was etched during manufacturing to create a rough surface for coating adhesion.

Sample Type	Statistics on 12 Samples Per Lot		
	ZnS/ZnSe (percent)	GaAs (percent)	ZnSe (percent)
Environmental Average	28.4	0.362	2.87
Standard Deviation	2.3	0.050	0.21
Rain Erosion Average	24.7	1.600	2.70
Standard Deviation	1.0	0.160	0.28

GP14-0021-383-D/cjg

Figure 5.1-30. Diffuse Transmittance at 1.06 Microns

GaAs and ZnSe had acceptable diffuse transmittance. The small diffusion exhibited by ZnSe was due only to the inherent scattering of the grid structure. The interface between the substrate and anti-reflection coating was polished and, therefore, did not cause scattering and the anti-reflection coating is too thin to produce an effect of this magnitude. A

5.1.5 Stray Light - The purpose of the stray light test was to determine the amount of 10.6 micron wavelength energy that was scattered by the window into a sensor field-of-view (FOV) as a result of the scattering properties of the window material and the diffraction effects of a grid incorporated into the window. The test simulated stray light from a source such as the sun located outside of the FOV which could cause scatter. Grid diffraction effects will cause a strong source such as the sun to appear as a starburst pattern with bright spots located along two perpendicular lines. The spot spacing and orientation is dependent on grid spacing and orientation.

The test setup is shown in Figure 5.1-31. A 10.6 micron CO_2 laser was the source and an integrating sphere captured all energy exiting the sample. Beam forming optics were used to generate a beam diameter so that it underfilled the 3-inch diameter sample at the 70^o maximum angle of incidence (AOI). The field stop and sphere-to-sample distance were adjusted to obtain three FOVs simulating a navigation FLIR, targeting FLIR, and IRST. The AOI of the CO_2 laser source was varied from 0^o to 70^o to simulate the location of the sun at various angles outside the sensor FOV. The change of AOI was in a plane parallel to a grid wire, defined as 0^o azimuth. The test was repeated with this plane rotated to 45^o and 90^o in azimuth. With a square symmetric grid, the results at 90^o should duplicate those at 0^o. The results at 45^o were expected to be different because the grid diffraction effects were several orders of magnitude less than at 0^o or 90^o. Thus, the effects at 45^o were a result of the material scatter properties only.

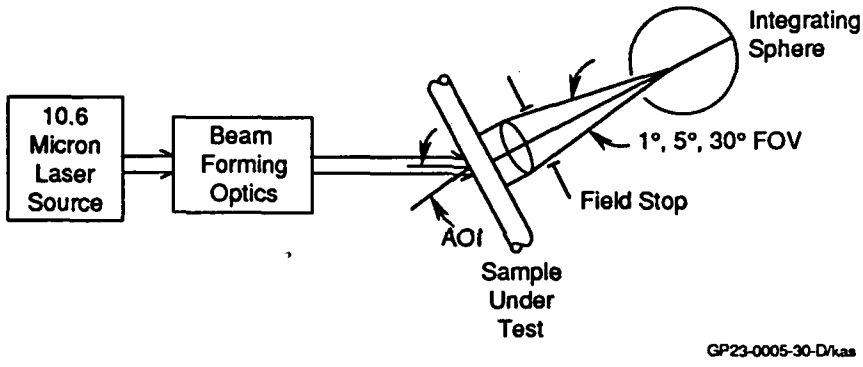

Figure 5.1-31. Stray Light Test Setup

As stated above, the magnitude of the stray light was composed of material scatter effects and diffraction effects. The scatter effects were a result of random path direction changes of the light source within the material. An explanation of diffraction effects is in Appendix A.

Figure 5.1-32 shows the stray light effect for ZnS/ZnSe for the 30^o, 5^o and 1^o sensor FOV. The meaningful portion of each curve is that section where the incidence angle is greater than the sensor semi-FOV. The 1^o FOV curve has peaks at 3^o and 6^o attributable to the diffraction higher side orders. As Figure A-1 of the Appendix showed, sidelobes occurred every 1.5^o for ZnS/ZnSe. However, only the sidelobes occurring at integer values of angle appeared because of the method of testing. Measurements of stray light were taken at AOI of 1, 2, 3 . . .

10, 20 . . . 60, 70 degrees. Thus, because of the narrowness of the lobe, the first diffracted order at 1.5° did not show up; whereas, the one at 3° did. The 5° FOV curve shows some effects of the diffraction as evidenced by the ripple between 3° and 10°. The effects are not as pronounced as the 1° field-of-view case because the wider 5° field-of-view aperture averages the effects. The stray light effects are contained in the long tails of decreasing magnitude.

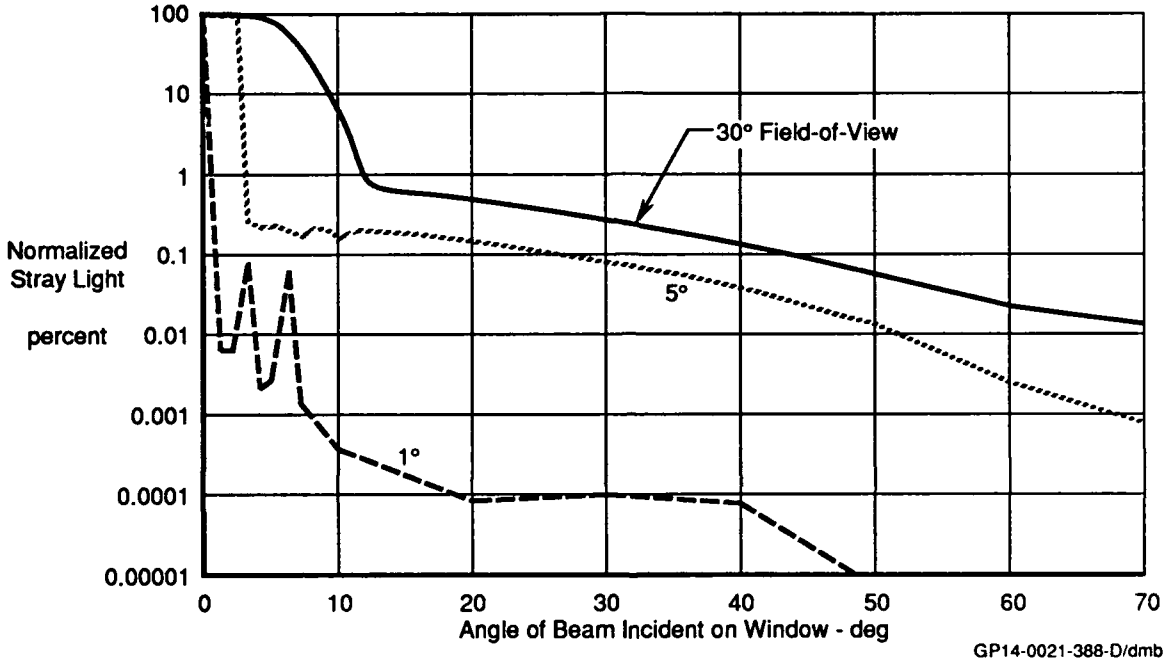

Figure 5.1-32. 10.6 μ Stray Light Test
Material - ZnS/ZnSe Azimuth Angle With Respect to Grid - 0°

Figure 5.1-33 is for ZnS/ZnSe material at 45° azimuth. It shows no effects of the higher order diffractive effects because the effects are so small, almost negligible. The tails represent only stray light effects.

Figure 5.1-34, because it is at 90° azimuth and the grid is square, should duplicate the effects of Figure 5.1-32. The results were very similar, with the difference accounted for by the method of testing.

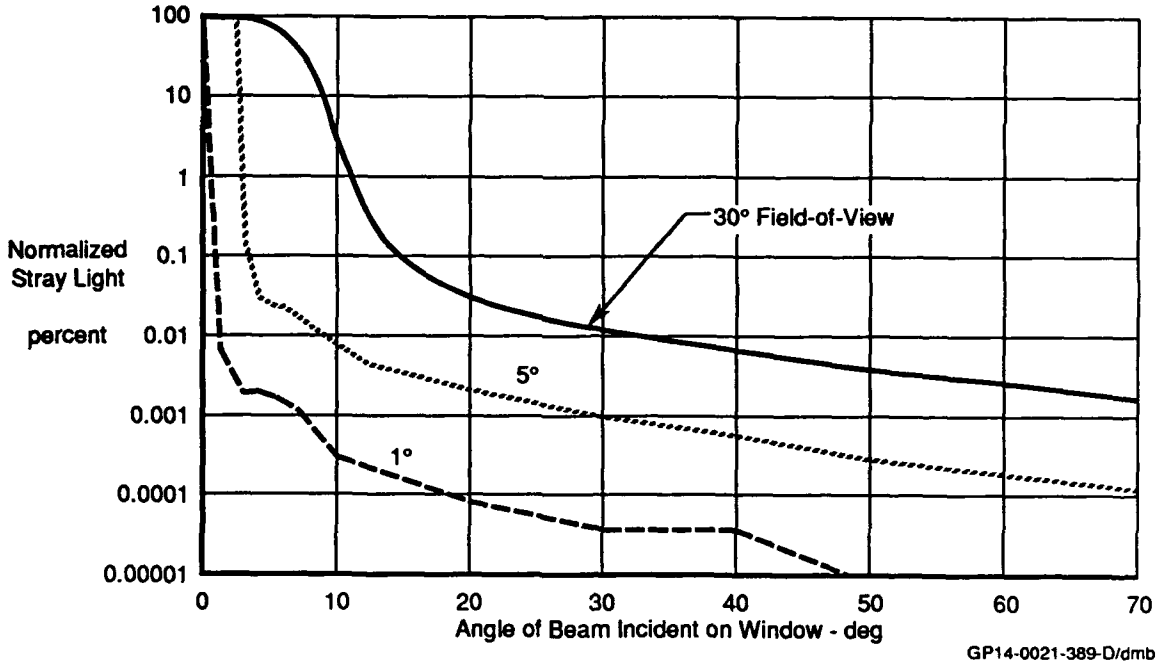

Figure 5.1-33 10.6 μ Stray Light Test
Material - ZnS/ZnSe Azimuth Angle With Respect to Grid - 45°

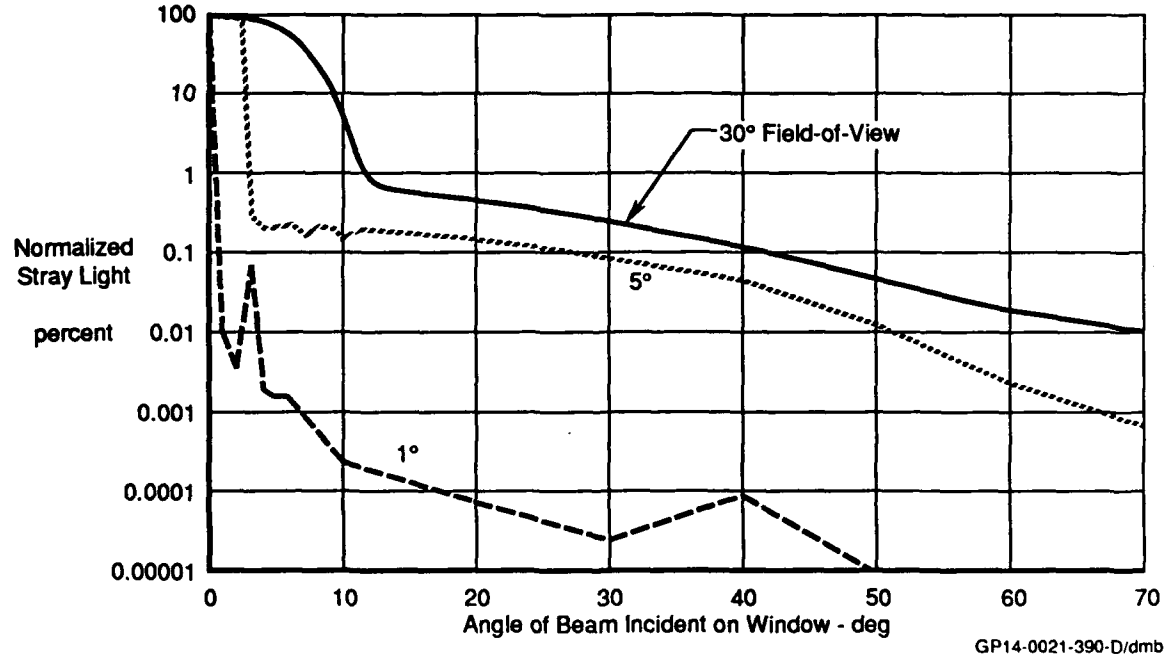

Figure 5.1-34. 10.6 μ Stray Light Test
Material - ZnS/ZnSe Azimuth Angle With Respect to Grid - 90°

Figure 5.1-35, valid for GaAs, contains the effects of scattered stray light. Since no grids are used, no diffractive effects occurred. The magnitude of the stray light was about 1/15 of the ZnS/ZnSe and ZnSe (compare Figure 5.1-35 to Figure 5.1-33).

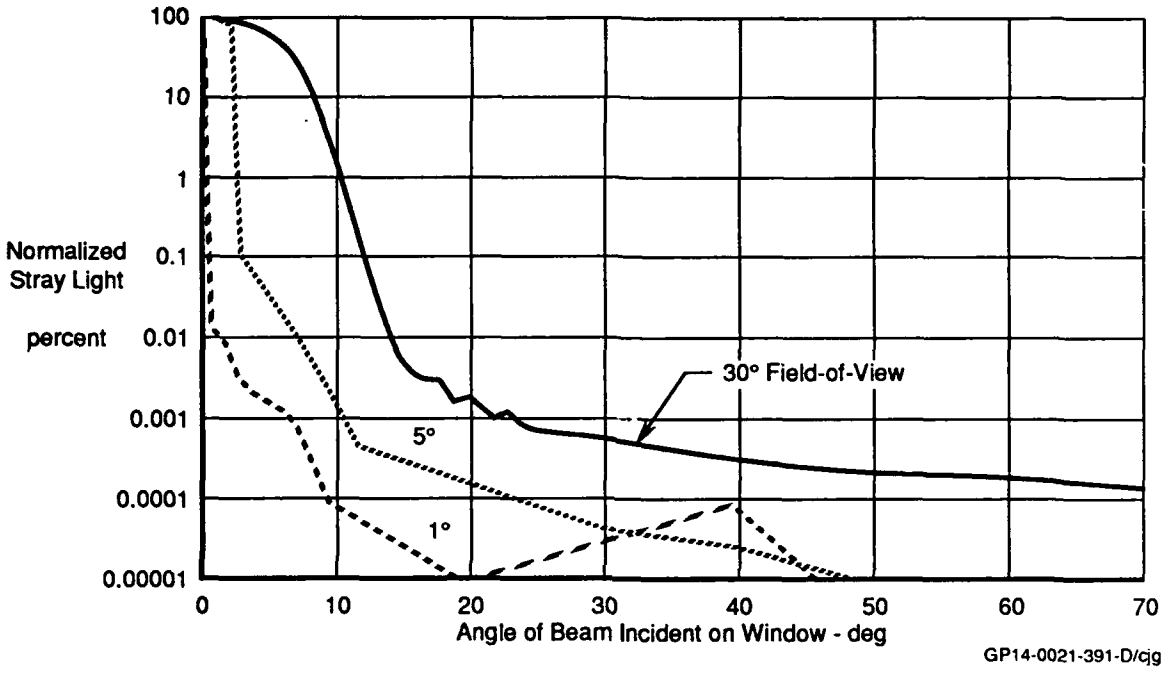

Figure 5.1-35. 10.6 μ Stray Light Test
Material - GaAs

Figures 5.1-36 through 5.1-38 are for the ZnSe material at the same three azimuth angles. The higher diffractive orders occurred at 3° intervals, so the effects show up very dramatically. The material scatter effects are very comparable to ZnS/ZnSe as noted by comparing Figures 5.1-37 to Figure 5.1-32. A wide disparity exists between the 0° azimuth 5° FOV case on Figure 5.1-36 and the 90° azimuth 5° FOV case on Figure 5.1-38 due to the method of testing.

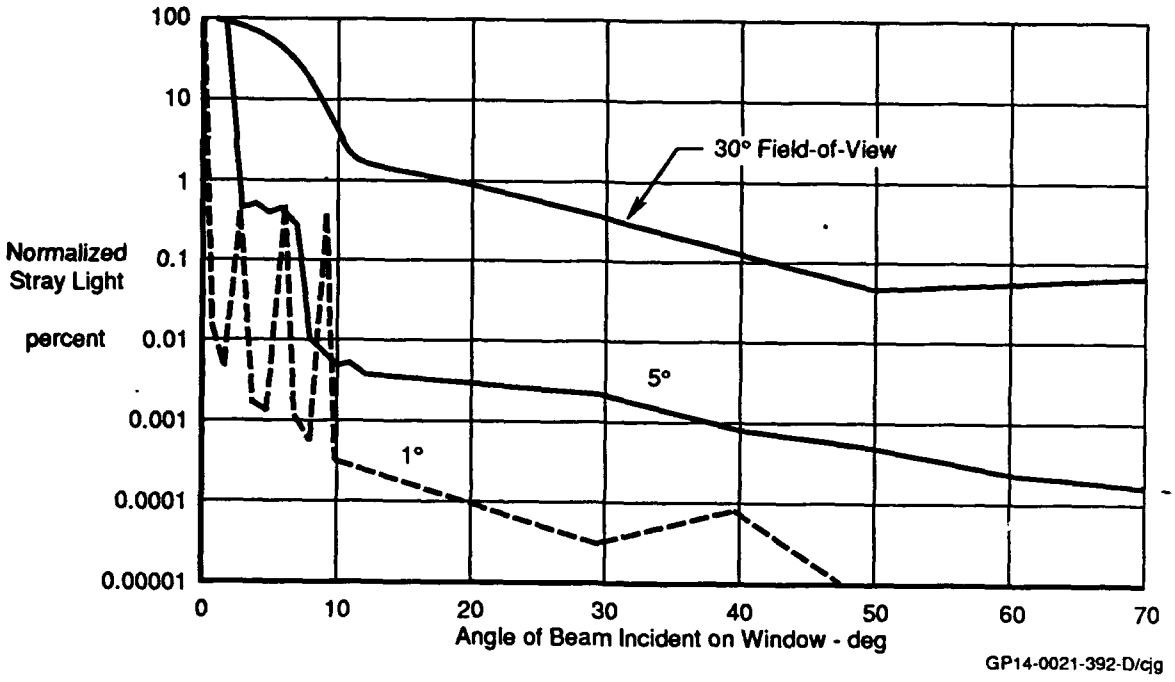

Figure 5.1-36. 10.6 μ Stray Light Test
Material - ZnSe Azimuth Angle With Respect to Grid - 0°

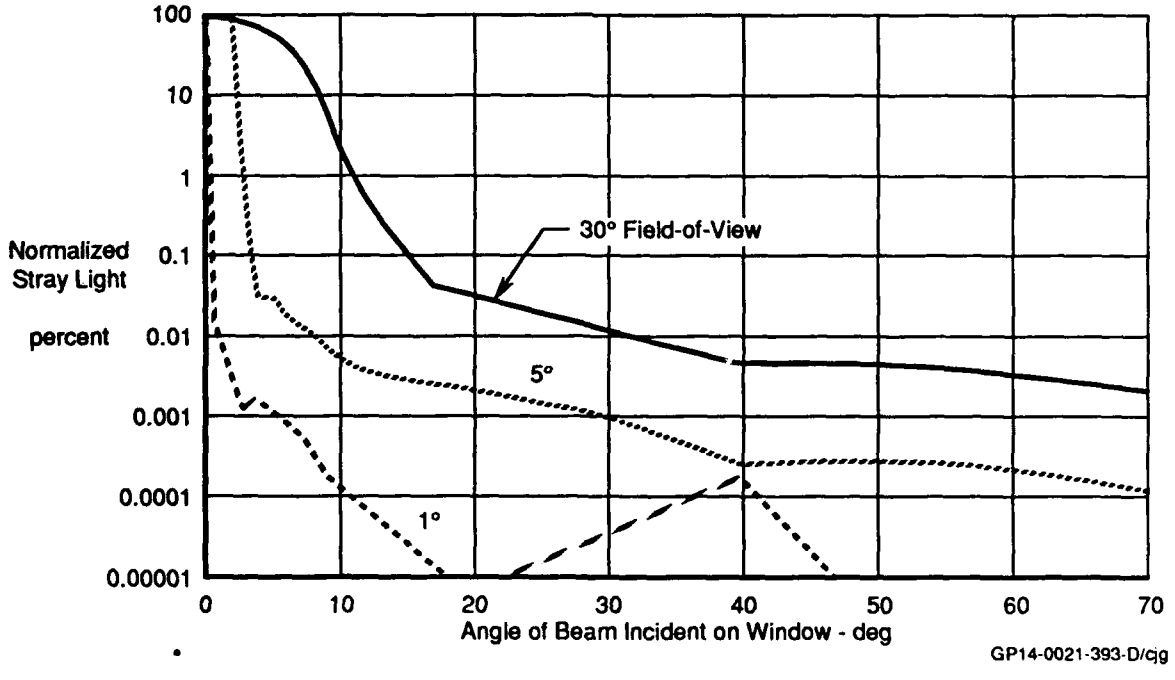

Figure 5.1-37 10.6 μ Stray Light Test
Material - ZnSe Azimuth Angle With Respect to Grid - 45°

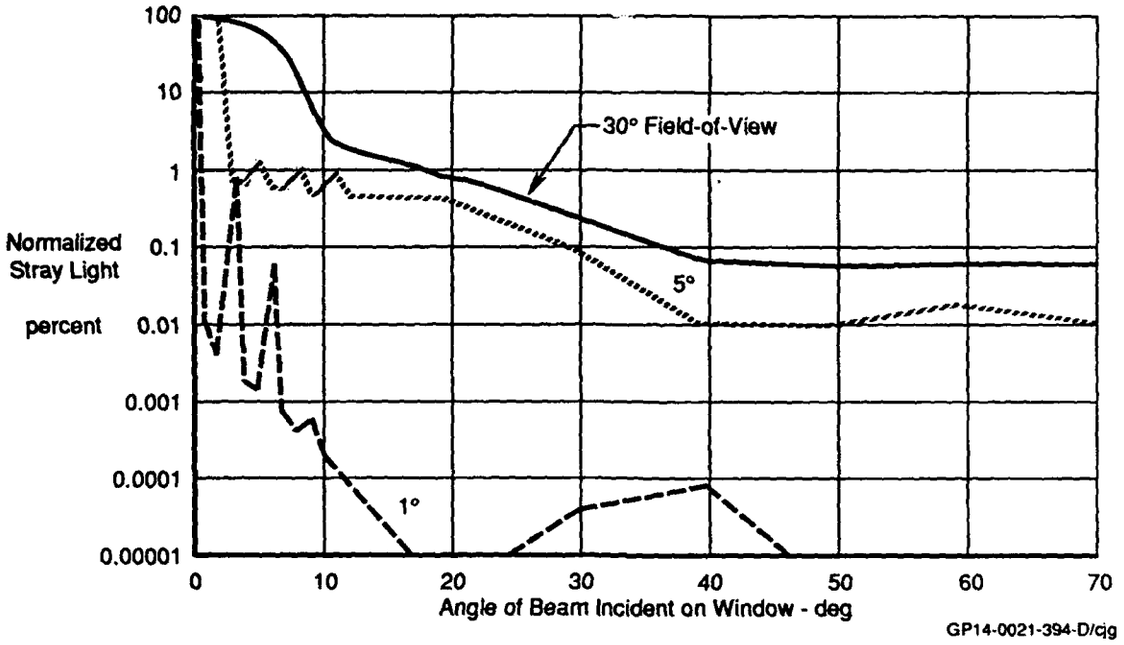

Figure 5.1-38. 10.6 μ Stray Light Test
Material - ZnSe Azimuth Angle With Respect to Grid - 90°

A comparison of the total scatter effects of all materials at a 30° angle of incidence is shown in Figure 5.1-39. The results show that GaAs had about 1/15 the scatter of the other two materials. (Compare GaAs to the 45° azimuth results of the other two). At 45° azimuth, the inherent scatter of ZnS/ZnSe and ZnSe at 10.6 microns were approximately the same.

The tests show that strong energy sources such as the sun may appear within the sensor FOV due to diffraction even if the source is not within the sensor FOV. The results of the stray light testing at 10.6 microns show that all three materials do not have as much scatter or diffuse transmission at the imaging wavelengths as they evidenced at the lasing wavelengths.

5.1.6 Modulation Transfer Function (MTF) - The MTF is a measure of how well an optical system can image the detail contrast or modulation of a source object. Poor MTF quality causes degradation of sensor resolution. Generally, low spatial frequencies are imaged better than high spatial frequencies.

Material	Azimuth Angle	Figure Number	Scatter at 30° AOI		
			30° FOV	5° FOV	1° FOV
ZnS/ZnSe	0°	5.1-32	0.26	0.08	Below Test Equipment Noise Level
ZnS/ZnSe	45°	5.1-33	0.012	0.0009	
ZnS/ZnSe	90°	5.1-34	0.24	0.08	
GaAs	N/A	5.1-35	0.0008	0.00006	
ZnSe	0°	5.1-36	0.41	0.003	
ZnSe	45°	5.1-37	0.014	0.001	
ZnSe	90°	5.1-38	0.29	0.117	

GP14-0021-387-D/dpt

Figure 5.1-39. Stray Light Tests and Applicable Figure Number

MTF is determined by measuring the spatial intensity of a re-imaged point source through the window-under-test and a diffraction limited lens in series and then mathematically calculating the spatial frequency content of the imaged point source or "Point-Spread-Function (PSF)." Any degradation to image quality is manifested by a wider PSF and lower MTF and will be the result of diffraction caused by the finite lens diameter and any aberrations in the window. To determine the degradation caused by window aberrations, the diffraction-caused lens degradation is divided out of the window-lens MTF measurement.

The test setup is shown in Figure 5.1-40. A pinhole IR source was expanded into a collimated beam for transmission through the sample under test. The test sample causes deformation of planar optical wavefronts if optical path length differences exist. The deformed wavefront was imaged as a point by the diffraction limited lens. The intensity distribution of the point, the PSF, is shown on the figure. The Fourier transform of the PSF is the Modulation Transfer Function of the window and lens combination.

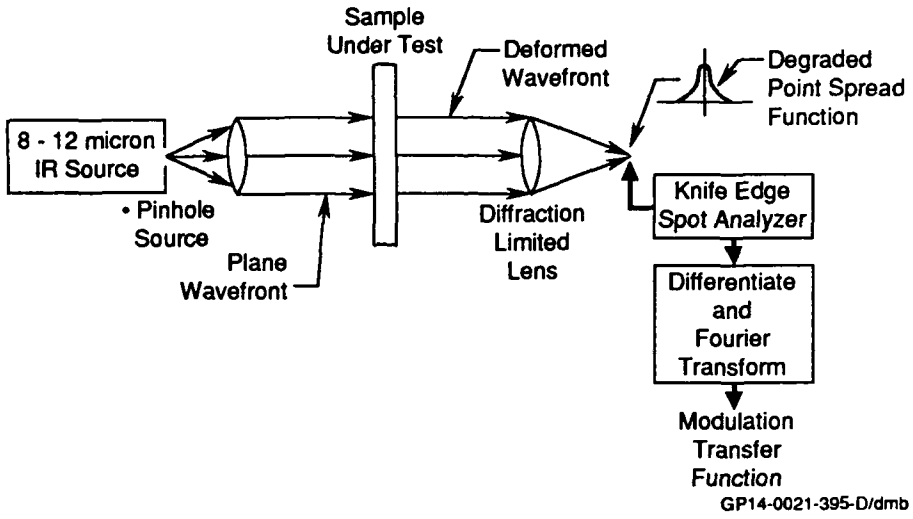

Figure 5.1-40. Modulation Transfer Function Test Setup

The MTF of each material was characterized in LWIR. The results are shown in Figures 5.1-41 through 5.1-43 and were normalized by dividing the test results by the results of a perfect aperture (the diffraction limited case). Thus, a perfect window would have a response of 1.0 for all spatial frequencies. Both ZnS/ZnSe and ZnSe were very close to diffraction limited performance. The performance of GaAs was somewhat less; the reduced performance was approximately equal to a $\lambda/8$ wavefront quality and is due to the index of refraction and thickness variation in the sample.

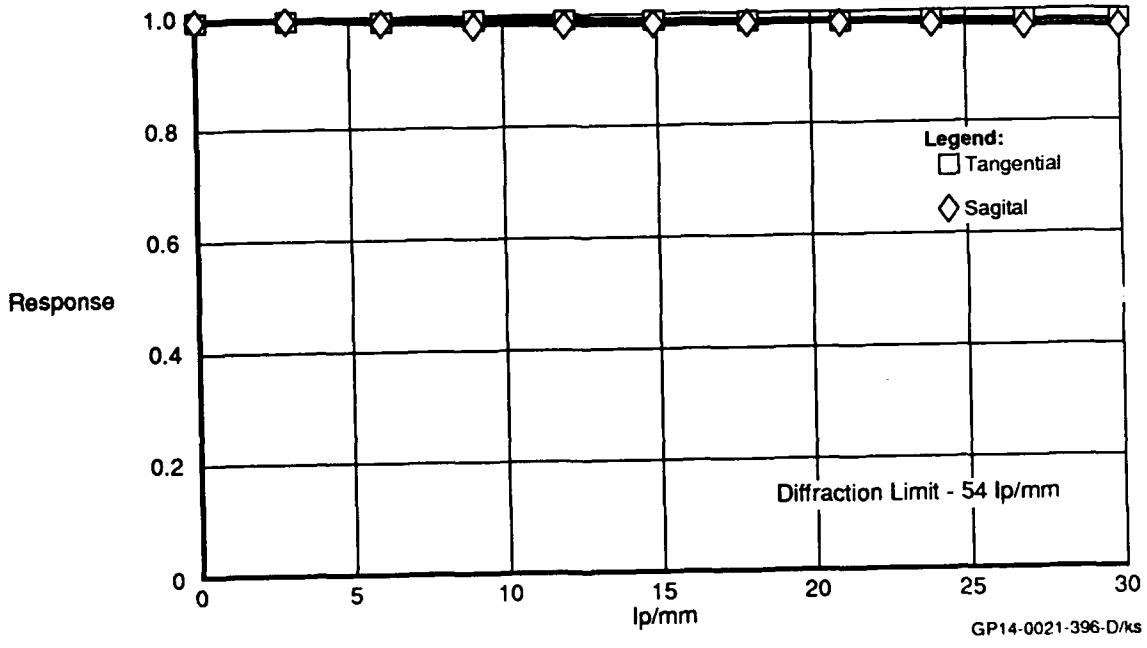

Figure 5.1-41. Modulation Transfer Function
Material - ZnS/ZnSe Wavelength - 7.5 - 12 Microns Sample Size - 12 x 12 In.

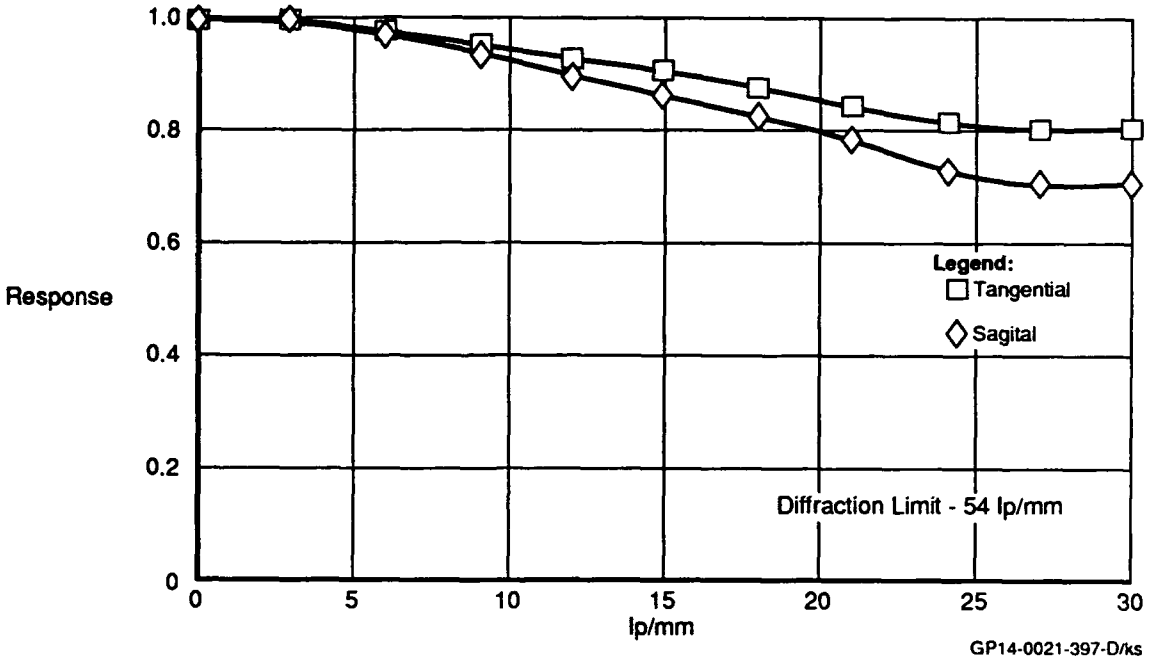

Figure 5.1-42. Modulation Transfer Function
Material - GaAs Wavelength - 7.5 - 12 Microns Sample Size - 3 In. Diameter

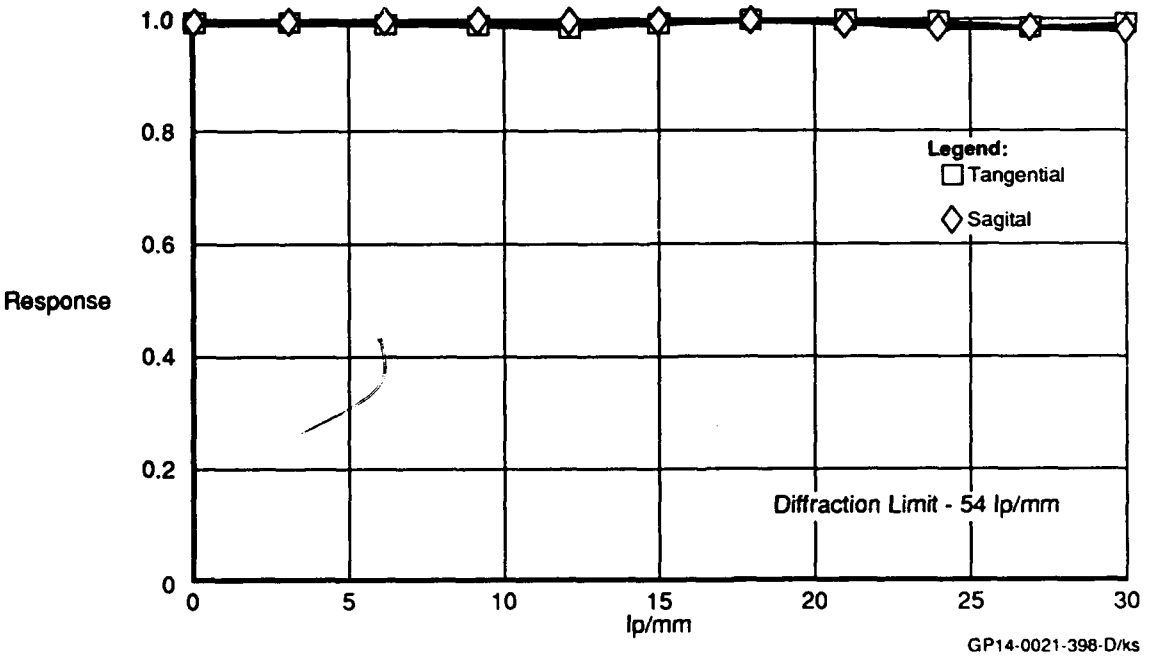

Figure 5.1-43 Modulation Transfer Function
Material - ZnSe Wavelength - 7.5 - 12 Microns Sample Size - 3 In. Diameter

The MTF qualify of all three materials was adequate for use in current or near-term FLIR and IRST applications.

5.1.7 Laser Compatibility - All three materials were tested to determine if the substrate, coatings, or grids could be damaged by laser transmission. As shown in Figure 5.1-44, a Quantel Laser was used to produce 10 nanosecond pulses of 1.064 micron energy. The fluence levels of .1, 1, 10, 33, 100, and 170 mj/cm^2 were set by using the attenuator as shown. The remainder of the optical system was used to produce a 0.25-inch diameter collimated beam directed at the test sample. Failure was established arbitrarily and defined as a 25% loss of transmission or 25% increase in reflected energy. All reflected energy was captured with an integrating sphere and transmitted energy was measured by appropriate instrumentation. The ratio of these quantities to the input energy, suitably calibrated, defined the reflection and transmission ratios.

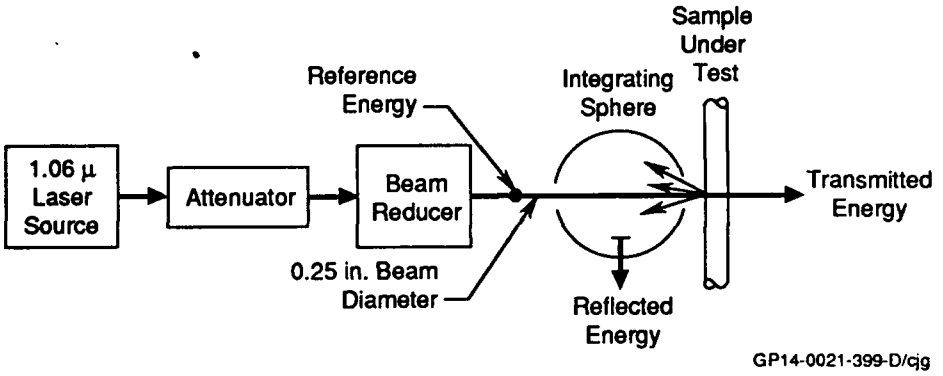

Figure 5.1-44. Laser Compatibility Test

Each material was exposed to a single pulse at the specified fluence level. The reference, transmitted, and reflected energies were recorded and the material was inspected for damage using 10X magnification. If no damage was incurred, a 20 Hz, 400 shot sequence was started. A computer monitored every third pulse and if measurable damage occurred, the laser shutter was closed and the test ended. If no measurable damage occurred, the material was again visually examined for damage using 10X magnification, and if there was no visible damage, the process was repeated using a full 100,000 shots at 20 Hz. At the end of these shots (assuming no measurable damage) the material was re-examined with the 10X magnification. A

No damage occurred to any grid, substrate, or coating at 10 millijoule/cm^2 which is a typical airborne laser operating value. However, at 33 millijoules/cm^2, grid melting occurred in ZnSe but not ZnS/ZnSe. The ZnSe grid was made from aluminum with a chrome binder which melts at 675°C compared to the grid made from gold with a chrome binder in ZnS/ZnSe which melts at 1060°C. In addition, the ZnS/ZnSe grid thickness was 0.6 micron compared to 0.3 microns for the ZnSe. Consequently, the ZnSe grid melted locally, whereas the ZnS/ZnSe grid did not. In fact, the ZnS/ZnSe grid withstood 170 millijoules/cm^2 without damage. All three substrates and their coatings withstood 170 millijoules/cm^2 without being damaged.

5.1.8 Second Harmonic (Green Light) Generation - During laser compatibility testing with a 1.06 micron laser, ZnS/ZnSe and ZnSe converted some of the transmitting laser energy into green light. A photograph of this phenomenon is included as Figure 5.1-45. In addition, pure samples of ZnSe, ZnS, and Cleartran were also subjected to the 1.06 micron energy and all exhibited this green light characteristic. The material "clearness" affected the degree of diffusion of the green light. Clear materials, such as ZnSe and Cleartran, retained beam collimation and produced a narrower beam of green light. The more diffuse material such as ZnS/ZnSe produced a Lambertian green light pattern on the ZnS surface of the material that was visible throughout the forward viewing hemisphere. The green light which was generated was found to be a second harmonic of the incident 1.06 micron laser energy and results from the non-linear relationship between the electric field in the material caused by the laser and the resulting material polarization. Details of the theory which provides an explanation of the generation of the green light is contained in Appendix B.

Because the green light is visible, the covertness of the aircraft may be compromised. A first order analysis was made to determine the visibility range of the green light when viewed by an observer at night, since the human eye is most sensitive under darkness conditions. The significant effects on visibility such as atmospheric attenuation and the effect of range were included in the analysis and the green light was considered to be a point source because of the large distance. The conversion efficiency of the laser into green light was measured. Approximately 1 part in 10^6 to 10^7 is converted for ZnS/ZnSe.

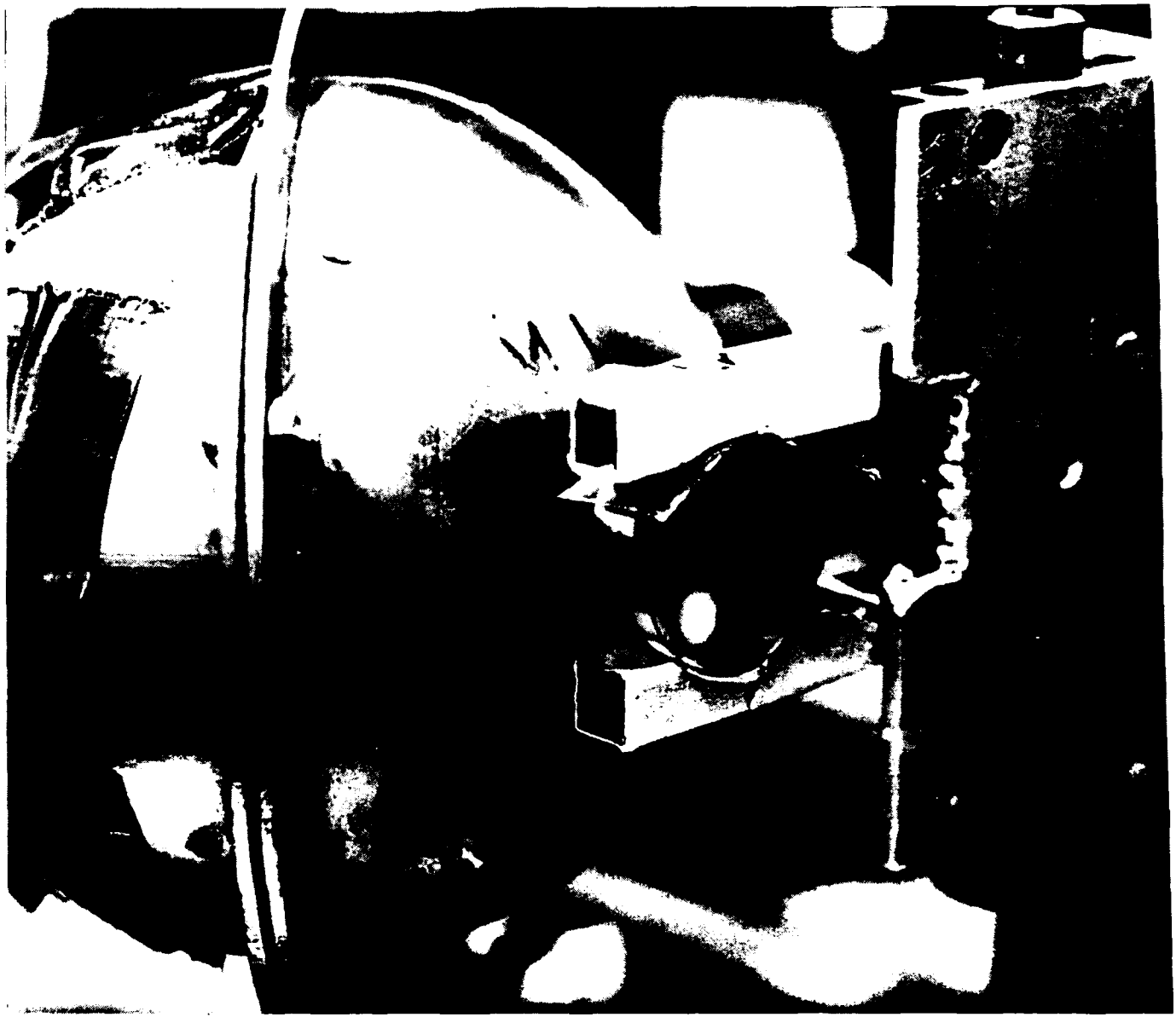

GP14-0021-449/pls

Figure 5.1-45. Sample Converting 1.06 Micron Energy Into Green Light

Figure 5.1-46 shows the results of our initial analysis based upon the following parameters:.

Laser energy	= 300 millijoules
Laser pulse rate	= 20 Hz
Conversion efficiency	= 10^{-6} and 10^{-7}

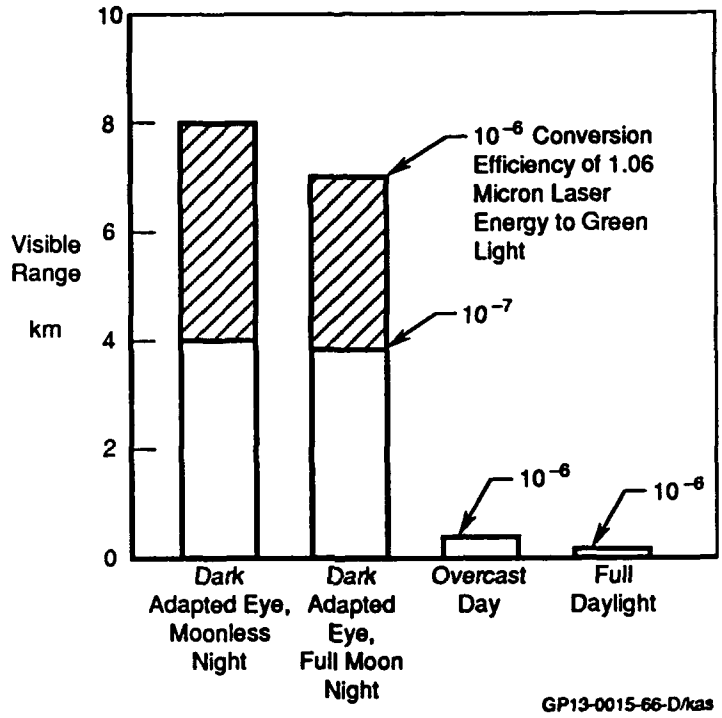

Figure 5.1-46. Maximum Visibility Range of Green Light

Human eye thresholds for four background lighting conditions are shown on this figure: dark adapted moonless night, dark adapted full moon night, overcast day, and full daylight. The dark adapted cases include the eye's response for scotopic viewing at 0.532 microns. The daylight cases are photopic viewing at the same wavelength. Figure 5.1-47 indicates that the light source can be detected at ranges greater than 4 kilometers on a moonless night and 4 to 7 kilometers on a full moon night. Because the eye is not as sensitive for daylight viewing, the range is much less, in the range of 100-200 meters on an overcast day or full daylight day.

5.1.9 Grid Transmission Loss - As shown in Appendix A, light passing through a grid produces a diffraction pattern consisting of a central peak on axis and lower magnitude multiple peaks off axis. The RF attenuation requirements of dielectric materials

require grid spacings in the order of 100-400 microns. The attendant diffraction effects which result from this dense spacing cause scattering of the light being transmitted through the window. The scattering angle depends upon grid spacing and light wavelength. If the light energy test equipment detector does not have a large enough FOV, some of the diffracted or scattered light is not intercepted and is manifested by an apparent transmission loss.

The calculated transmission loss for the ZnS/ZnSe grids due to obstruction was 5%, but tests showed a 7-8% loss. Similarly, calculated transmission losses for the ZnSe grids were 13%, but had a 17% loss. The difference was attributable to the off axis peaks which contained some of the energy, but were not detected because of being outside the sensor FOV.

5.1.10 Wavefront Homogeneity - Wavefront optical path differences (OPD) resulting from material surface irregularity or index of refraction inhomogeneities were evaluated at both 1.06 and 10.6 micrometers wavelengths. All measurments were made at normal incidence on 3-inch diameter and 12 x 12-inch samples.

A WYKO IR3 interferometer was used for the 10.6 micrometers wavefront homogeneity test. The test arrangement is shown in Reference 5-3. Repeatability of OPD data is a major concern when doing interferometry. The WYKO IR3 interferometer employs the state-of-the-art phase-shifting technique to analyze fringe patterns and is designed to perform with a root-mean-square (RMS) repeatability of 0.005 wavelength. This capability minimized measurement errors for the 10.6 micrometers wavefront homogeneity test.

An Nd:YAG laser provided the source for the 1.06 micrometers wavefront homogeneity test. The Nd:YAG laser (operating in TEM_{00} single mode) was spatially filtered and collimated with a 50.8 mm diameter, 250 mm focal length achromatic doublet. Collimation was verified using a lateral shearing interferometer plate. The collimated light was directed into the first cubic beam splitter of a Mach-Zehnder interferometer. Each sample was inserted in the cavity of the Mach-Zehnder normal to the collimated light. The test arrangement is shown in Reference 5-3.

An image of the interference pattern from one of the output ports of the Mach-Zehnder was formed on a screen to allow a Pulnix TM-34K CCD camera with an 8 mm lens to capture the fringes. The video image from the CCD camera was sent to a WYKO 6000 interferometer to be frame-grabbed and analyzed (with WYKO 6000 version 4.20 software).

Phase-shifting interferometry was not available for the 1.06 micrometers wavefront homogeneity test. The combination of the Mach-Zehnder interferometer and the WYKO 6000 version 4.20 fringe analysis software employs a computer-controlled fringe-following algorithm to interpret fringes. Repeatability of this technique is dependent on various characteristics of the fringe pattern; for example, the intensity, the contrast, and the shape of the fringes. Based on observations, the 1.06 micrometers wavefront homogeneity test arrangement was not expected to perform better than an RMS repeatability of 0.02 wavelength.

Because the aperture of the 1.06 micrometers wavefront homogeneity test equipment was limited to a 2-inch diameter, the test was repeated at nine locations on the 12 x 12-inch samples (Reference 5-3) and only once on the 3-inch diameter samples. Measurement areas on the 3-inch diameter samples for the 1.06 micrometers and the 10.6 micrometers wavefront homogeneity test are shown in Reference 5-3.

5.1.10.1 Results - The Wavefront Homogeneity test results are provided in Reference 5-3.

5.1.11 Coherent Imaging Test - The purpose of the Coherent Imaging Test was to determine the effect of material inhomogeneity and grid structure on the far field diffraction patterns as a result of a 1.06 micrometer Nd:YAG laser radiation transmitted through each material. This test simulates ground target illumination by an airborne laser designation system, neglecting the effects of atmospheric turbulence and platform vibration.

Five samples were tested -- a 3-inch diameter of each of the three materials, and a 12 x 12-inch sample of ZnS/ZnSe and ZnSe. The 3-inch ZnS/ZnSe had the worst coherent imaging performance of the five samples tested. The 12-inch ZnS/ZnSe had better properties than the 3-inch. GaAs had significant aberration in the central term. The 12-inch and 3-inch ZnSe samples produced the best coherent imaging, having virtually no effect on the central term.

The conductive grids on the ZnS/ZnSe and ZnSe produce a complex far-field diffraction pattern consisting of a bright central term and an array of evenly spaced sidelobes approximately 20 dB down in intensity from the central term. The angular spacing between sidelobe grating orders, 1060/D milliradians, where D is the grid wire spacing in micrometers. The wire spacing for the ZnS/ZnSe grids is 400 micrometers, and 200 micrometers for the ZnSe. Grating order spacings were, therefore, 2.65 mr and 5.30 mr, respectively.

A schematic drawing of the coherent imaging test equipment arrangement is shown in Reference 5-3. The Nd:YAG laser (operating at 1.06 micrometers in TEM_{00} single mode) was spatially filtered and collimated with a 19-inch focal length achromatic doublet. Collimation was verified using a lateral shearing interferometer plate. Each sample was inserted in the collimated space between the doublet and one of two imaging telescopes. Images from either telescope were captured by a COHU 4800 series CCD camera and analyzed using a Big Sky Laser Analyzer system.

A Nikkor 200 mm focal length telephoto lens was selected to image the diffraction sidelobes produced by the gridded samples. The 200 mm focal length provided sufficient image scale on the CCD camera to image several diffraction sidelobes.

A second telescope of roughly 200X longer focal length was arranged to provide an image scale sufficient to resolve detail in the central term for the gridded samples and the Point Spread Function (PSF) of the GaAs sample. An Ealing 36-inch focal length collimator formed an intermediate aerial image at its focus, and a 43X microscope objective relayed this image to its conjugate image, focused on the CCD camera focal plane. This combination produced an effective focal length of nearly 40 meters.

The YAG laser output beam was reflected from a 5% beam splitter to greatly reduce the power for the coherent imaging test. Laser power was further adjusted using neutral density filters, inserted between the 5% beam splitter and the spatial filter. This maintained image intensity to within the CCD camera dynamic range (about 11 dB) and provided proper video output levels for the Big Sky analyzer.

5.1.11.1 Results - The Coherent Imaging test results are provided in Reference 5-3.

5.1.12 Interferometric Thermal Lensing (ITL) Optical Testing - A relatively high power laser beam often has to share a window and/or other imaging optical elements coaxially with another optical system. An example is a laser target designator operating coaxially within a FLIR system, transmitting and receiving through a broadband IR window and a portion of the internal optical elements. The optical properties of some infrared-transmitting materials are particularly dependent on localized heating, induced by aerodynamic heating and/or transmission of high-power laser beams. An interferometric thermal lensing test was designed for this study to quantify optical impacts of medium-energy Nd:YAG laser irradiation and propagation on the three types of window materials investigated.

Samples of all three materials were placed in an interferometer cavity, and briefly exposed to a 1.06 micrometers YAG laser beam of variable intensity. Video imagery of the transmitted laser beam far field pattern and interferograms at both 1.06 micrometers and 10.6 micrometers were simultaneously recorded. Changes in the material index or surface profile caused by laser heating results in changes in the transmitted wavefront OPD, shown by the interferometers. By adjusting the laser power and examining interference patterns, the laser power range was identified before thermal lensing effects take place for a particular operating wavelength.

The raw multi-mode beam coming out of the Nd:YAG laser was used to heat the material. Its intensity profile was not uniform; thus, power density was a function of location. Although the power density level used in the test was cautiously measured to determine the cutoff power level of each sample, a uniform beam might yield a slightly different result.

Two equipment arrangements were used to characterize the three 3-inch samples. A 1.06/1.06 micrometers setup using a 1.06 micrometers Mach-Zehnder interferometer and a CCD video camera for fringe pattern analysis and a 1.06 micrometers laser beam as the heating element. A 10.6/1.06 micrometers arrangement using a WYKO 10.6 micrometers interferometer for fringe pattern analysis and a 1.06 micrometers YAG laser beam as the heating element.

5.1.12.1 Results - The ITL Tests are provided in Reference 5-3.

5.2 RF Tests

The RF attenuation and reflection characteristics of ZnS/ZnSe, GaAs, and ZnSe were tested using a transmission tunnel, co-axial airline, and bistatic receiver/transmitter reflection testing. A significant manufacturing facility scale-up would have to have been made to obtain GaAs samples in the 12" x 12" size required for the transmission tunnel and reflection testing. Therefore, only co-axial samples were procured for GaAs RF testing. The results of the RF attenuation testing are included in Reference 5-4 and the results of the reflection testing are in Reference 5-3.

The transmission tunnel is the preferred method of obtaining RF attenuation characteristics but may require sample sizes too large and too expensive to explore the required frequency range. For this reason, smaller sample sizes (12 in x 12 in) were tunnel tested which provided data over a portion of the required range only. In order to extend this data to a broader range, co-axial airline (7mm and 1.5 in diameter) tests were performed. A 20 db one way power attenuation from 2 to 18 GHz was the program A requirement.

The transmission tunnel test system is a free-space measurement technique which can provide transmission attenuation data from 2-18 GHz. The tunnel consists of a symmetric, anechoic chamber divided by a metal plate with a round aperture at the center, as shown in Figure 5.2-1. Two horn antennae (one the source and one the detector) are mounted at opposite ends of the chamber. To perform a measurement, the sample is placed over the aperture with its surface perpendicular to the axis of the antennae. When measuring highly conductive samples in the tunnel, metal-tape with a conductive adhesive is used to electrically seal the sample to the aperture.

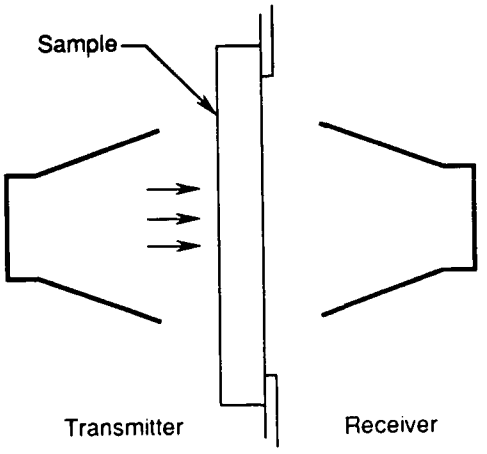

GP14-0021-437-D/bcb

Figure 5.2-1 Transmission Tunnel Test Setup

Coaxial transmission airlines are used as sample holders, as shown in Figure 5.2-2, for broadband low frequency measurements. The 1.5-inch coaxial airline test system provides measurements of the transmission attenuation and reflectance at frequencies below 4 GHz. The 7mm coaxial airline test provides the same data in the 2-18 GHz frequency band. When using the coaxial airline tests to quantify highly conductive specimens, it is necessary to provide a good electrical path between the sample holder and the inner and outer edges of the test specimen. This is best achieved with a tight-fitting specimen that does not allow any air gaps between the sample and sample holder. If this is not possible, a conductive paint can be applied to the inner and outer edges of the test specimen to seal the air gaps and minimize microwave leakage.

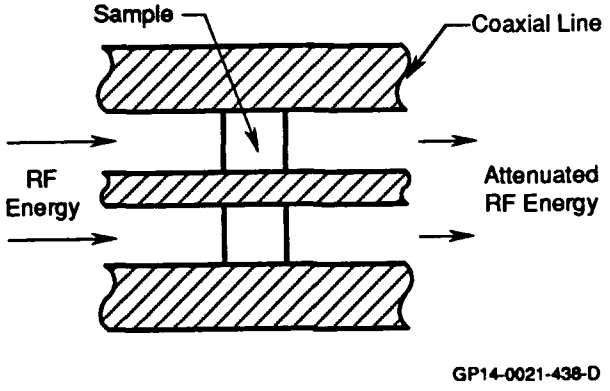

Figure 5.2-2. Coaxial Line Test Setup

In addition to these transmission tests, tests to determine the microwave reflectivity of the 12 x 12 in samples were performed using a test devised by the Naval Research Laboratory (NRL). The NRL arch test system provides a free-space measurement of the microwave energy reflected from a sample. Measurements are referenced to the total energy reflected from a metal plate of the same size. The test system consists of two horn antennae mounted to a vertical arch and positioned above the sample to provide equal angles of incidence and reflection, as shown in Figure 5.2-3. The sample is placed on a styrofoam table located at the center-of-curvature of the arch. Measurements were made at bistatic angles ranging from 20^{o} - 120^{o} over the 2-18 GHz frequency band.

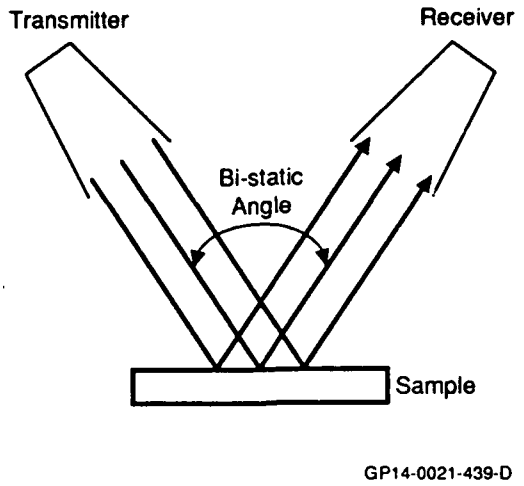

Figure 5.2-3. NRL Arch Reflection Test Setup

5.2.1 Results of ZnS/ZnSe RF Tests - Five ZnS/ZnSe specimens were tested -- two 7mm and two 1.5-inch diameter samples, and one 12" x 12" sample. The co-axial samples were supplied with a conductive treatment of the center hole and outer circumferential surface. The samples were manufactured with no bevel on the gridded face so that grid would be continuous to the edge and make contact with the conductive treatment. The 7mm diameter samples were 0.05 inch thick and the 1.5-inch diameter was 0.25 inch thick. The 12 x 12-inch had conductive bus bars on the edge which contacted the grid wires and were 0.5 inch thick.

The coaxial measurement results reveal that none of the coaxial samples tested met the program specifications. The attenuation values for the samples were less than 20 dB across the 2-18 GHz frequency band (Figures 5.2-4 through 5.2-5). The average attenuation levels were close but the shapes of the curves are different because each sample tested had a different thickness which affected the attenuation values. Thicker samples display a higher attenuation value than thinner samples.

The coaxial samples were retested with a film of silver conductive paint between the inner and outer surfaces and the coaxial line. Some improvement of attenuation was experienced for frequencies below 2 GHz. Photographs taken of the coaxial

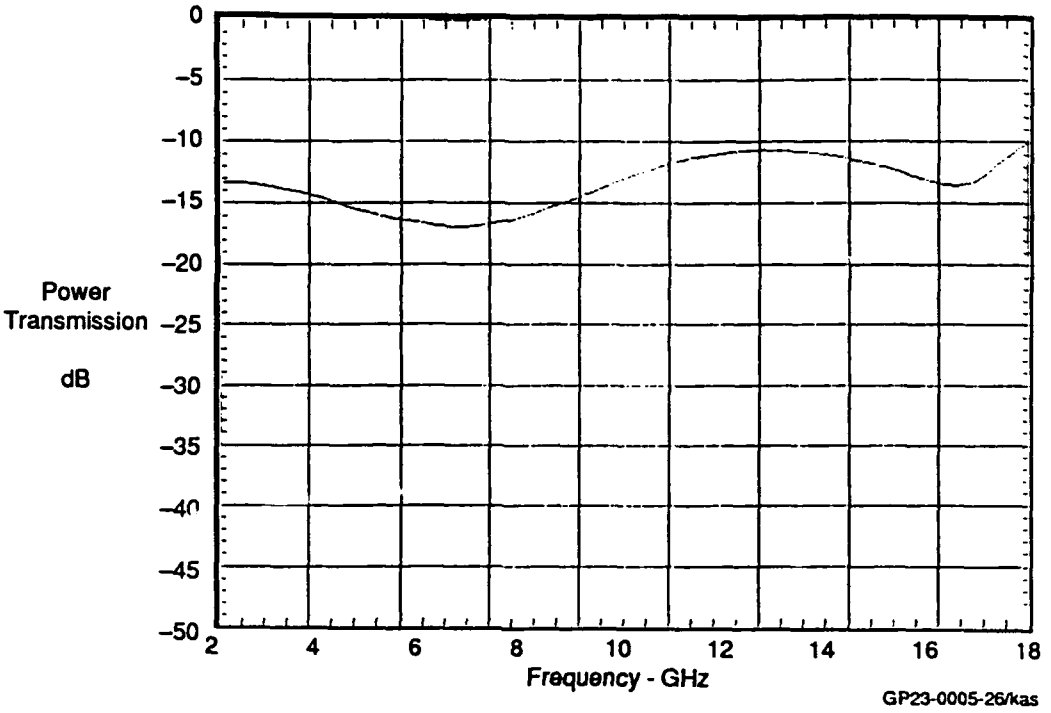

Figure 5.2-4. RF Transmission
Sample Type: ZnS/ZnSe
Sample Size: 7 mm Coaxial
Test Type: Airline Coaxial

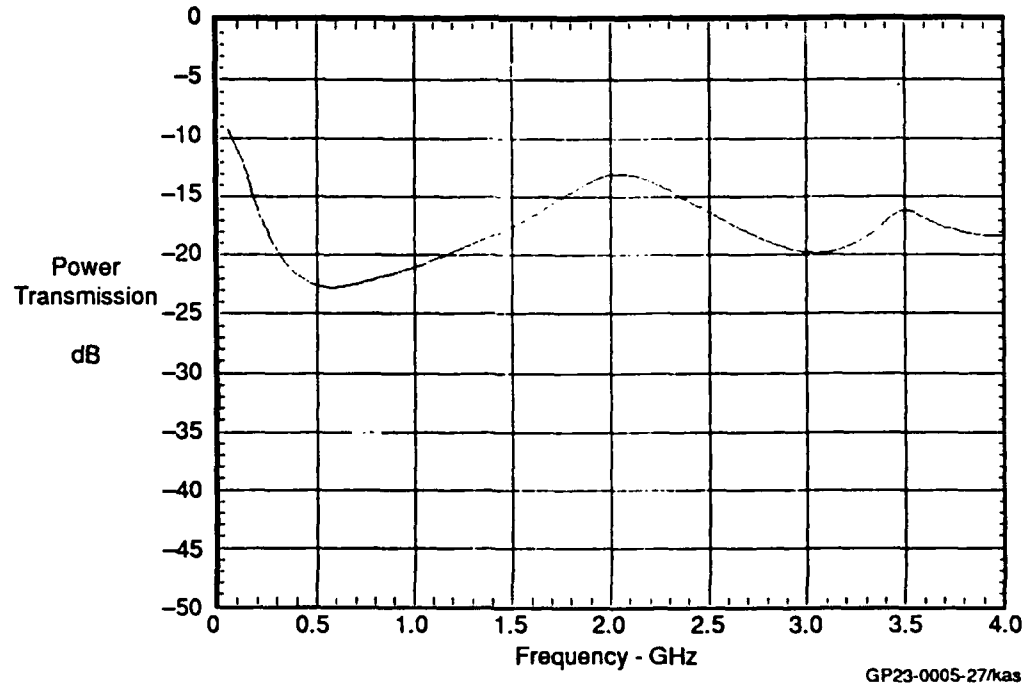

Figure 5.2-5. RF Transmission
Sample Type: ZnS/ZnSe
Sample Size: 1.5 Inch Coaxial
Test Type: Airline Coaxial

specimens showed discontinuities in the grid pattern and surface fractures at the edge of the specimens (Figure 5.2-6). These edge fractures were a result of fabricating coaxial samples without edge bevels in order to have electrical grid contact with the outer and inner conductive surfaces. The discontinuities could have prevented the grid from making good electrical contact with the sample holder, thereby causing inconsistency in the coaxial airline data.

Transmission tunnel testing results show that from 2-5 GHz, the 12 x 12-inch sample meets the program specifications with attenuation values greater 20 dB (Figure 5.2-7). However, from 5-18 GHz the attenuation values are less than 20 dB.

The NRL arch testing results revealed that the ZnS/ZnSe gridded system is highly reflective for near-normal to within 60^{o} incidence angles. Details are found in Reference 5-3. The reflection loss was nearly zero over most of the 2.0 to 18.0 GHz band. This is true at all of the incidence angles at which the tests were done. Only in the 10.0 GHz to 18.0 GHz region and at 60^{o} angle of incidence does the reflection loss become noticeable (approaching 1 dB). Otherwise, for other angles less than 60^{o}, the transition to greater loss is confined to 16.0 GHz or higher frequencies. The increasing loss, as a function of incidence angle, occurs in the parallel polarized (TM) mode of propagation. The other polarization -- perpendicular (TE) -- exhibits better reflectivity at higher incidence angles, as expected.

5.2.2 Results of GaAs RF Tests - Four Gallium Arsenide (GaAs) specimens were to be tested, but one sample was broken during test. Therefore, only three samples were tested -- two 7mm and one 1.5-inch. A silver conductive paint was applied to the inner and outer edges of the sample to ensure good electrical contact with the sample holder and achieve accurate results. But, because test results indicated that the co-axial samples did not meet program specifications, Litton/Itek suggested that an oxide layer on the inner and outer edges of the samples could have prevented the samples from making good electrical contact with the airline. The samples were returned to the manufacturer where the oxide layer was removed and a gold conductive coating was applied to the edges of each specimen. After the samples were returned, they were silver-painted to ensure good electrical contact with the sample holder before the attenuation was measured again.

a. 7mm Coaxial Specimen – Tuftran 2 – 10.5x

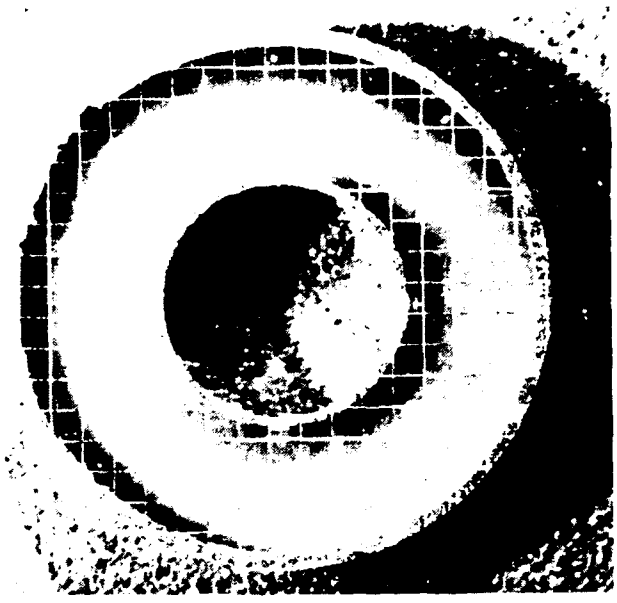

b. 1.5 in. Coaxial Specimen – Tuftran 4 – 1.5x

GP14-0021-419/pls

Figure 5.2-6. ZnS/ZnSe Showing Edge Defects

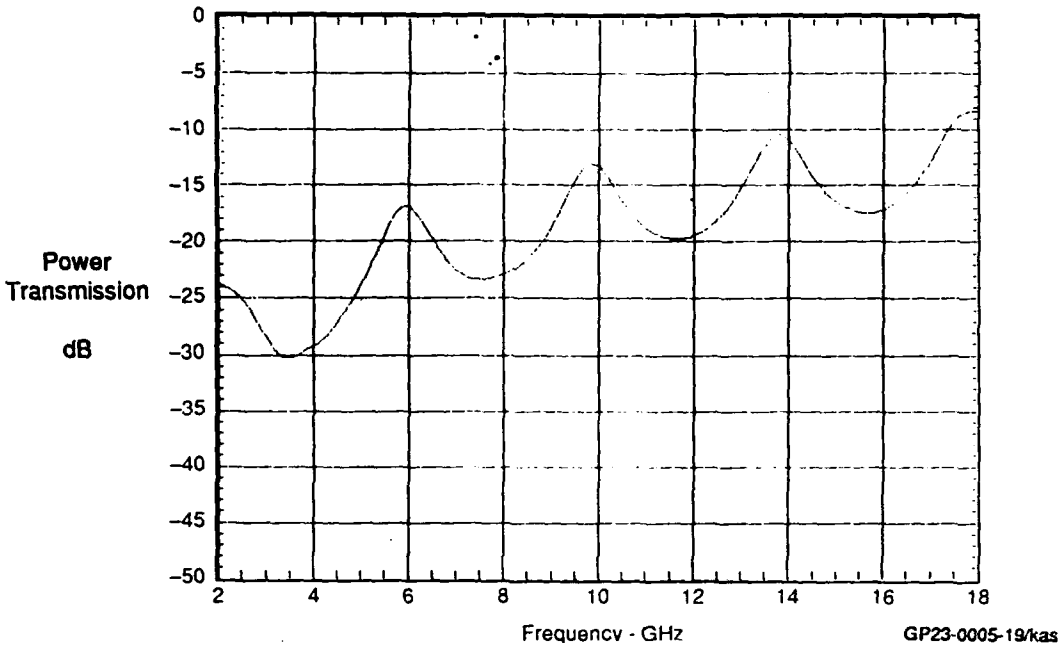

Figure 5.2-7. RF Transmission
Sample Type: ZnS/ZnSe
Sample Size: 12 x 12 Inch
Test Type: Tunnel

On retest, the 7mm and a 1.5-inch diameter samples met the program attenuation specifications. As shown in Figures 5.2-8, Curve A and 5.2-9, the attenuation values were greater than 20 dB across the specified 2-18 GHz frequency band. Another 7mm sample, shown in Figure 5.2-8, Curve B, showed that even after rework, the sample did not meet the program specifications. The attenuation value measured was less than 10 dB from 2-18 GHz.

Reference 5-6, provided by Litton/Itek, specified a surface resistivity for these co-axial specimens of less than 20 ohms per square which correlated to an attenuation greater than 20 dB. The 7mm and 1.5-inch diameter samples were consistent with the manufacturer's specified resistivity. But the 7mm sample, Figure 5.2-8, Curve B had a resistivity greater than 100 ohms per square.

RF transmission results for the GaAs co-axial specimens before and after manufacturer rework are shown in Reference 5-4. The good correlation shown by the 7mm and 1.5-inch diameter samples indicate they came from the same boule and slice, while the other 7mm sample came from a boule or slice with vastly different composition. A

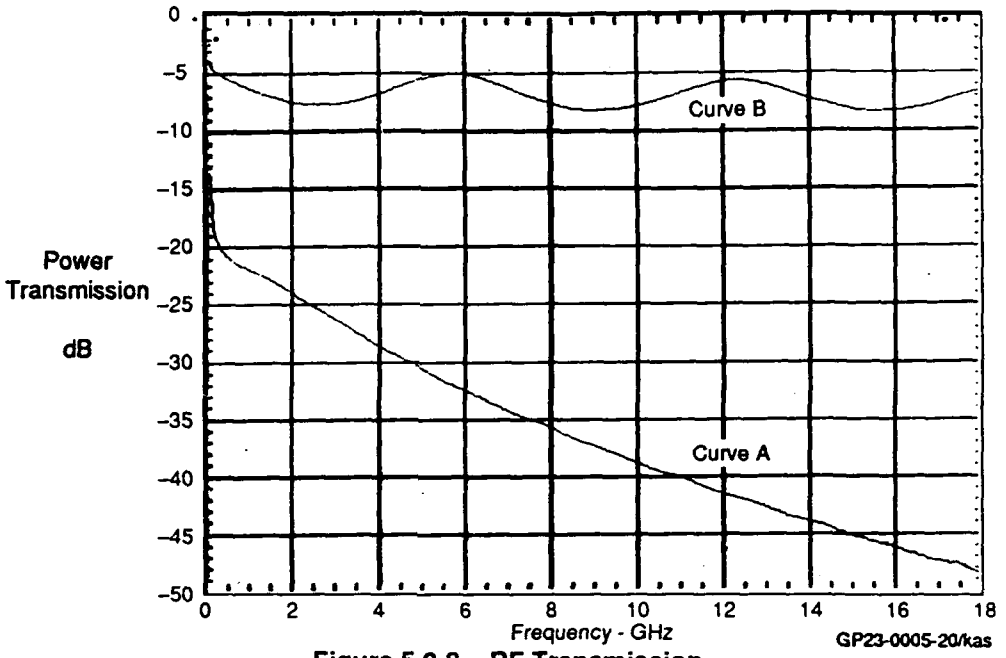

Figure 5.2-8. RF Transmission
Sample Type: GaAs (Gold Coated/Silver Edge Painted)
Sample Size: 7mm Coaxial
Test Type: Airline Coaxial

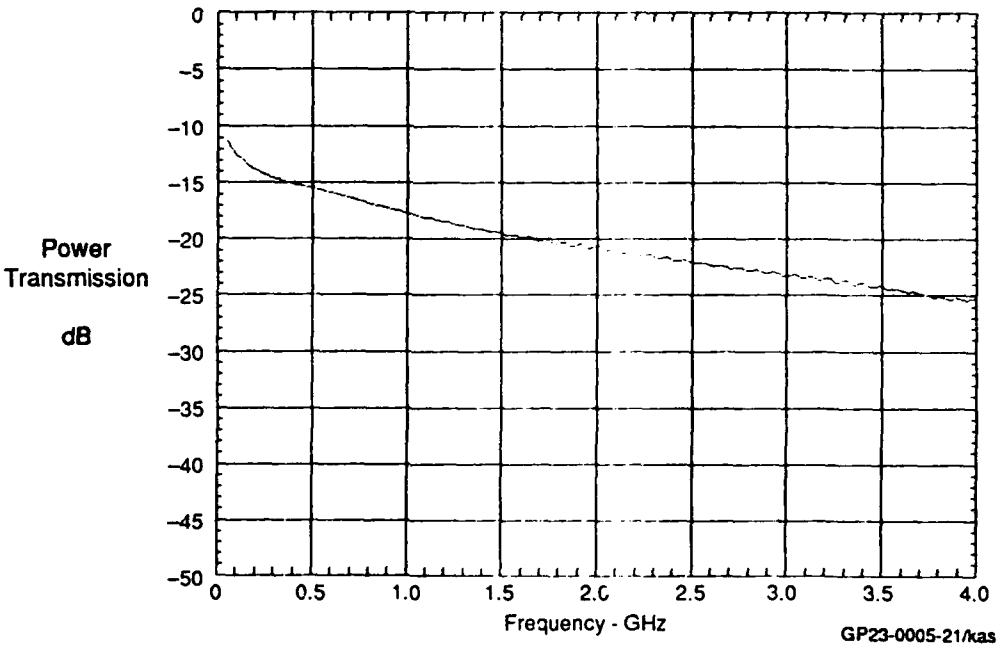

Figure 5.2-9. RF Transmission
Sample Type: GaAs (Gold Coated/Silver Edge Painted)
Sample Size: 1.5 in. Coaxial
Test Type: Airline Coaxial

5.2.3 Results of ZnSe Tests - Five Zinc Selenide (ZnSe) specimens were tested -- two 7mm and two 1.5-inch diameter samples, both 0.25-inch thick and one 12 x 12, 0.50-inch thick. None of the coaxial samples had conductive edge treatments. The coaxial samples were visually inspected before testing and some discontinuities were noted in the grid pattern, but no significant damage was observed. The initial coaxial tests revealed that none of the samples met the program specifications, so additional testing with silver conductive paint on the edges was performed.

As seen in Figure 5.2-10, the 12 x 12-inch sample met the program specifications over a portion of the frequency band. Although the average attenuation values from 2-18 GHz are greater than 20 dB, there were areas where the transmission curve was less than 20 dB. The oscillations of the curve were due to the interaction of the energy reflected from the front and back faces of the window sample. | A

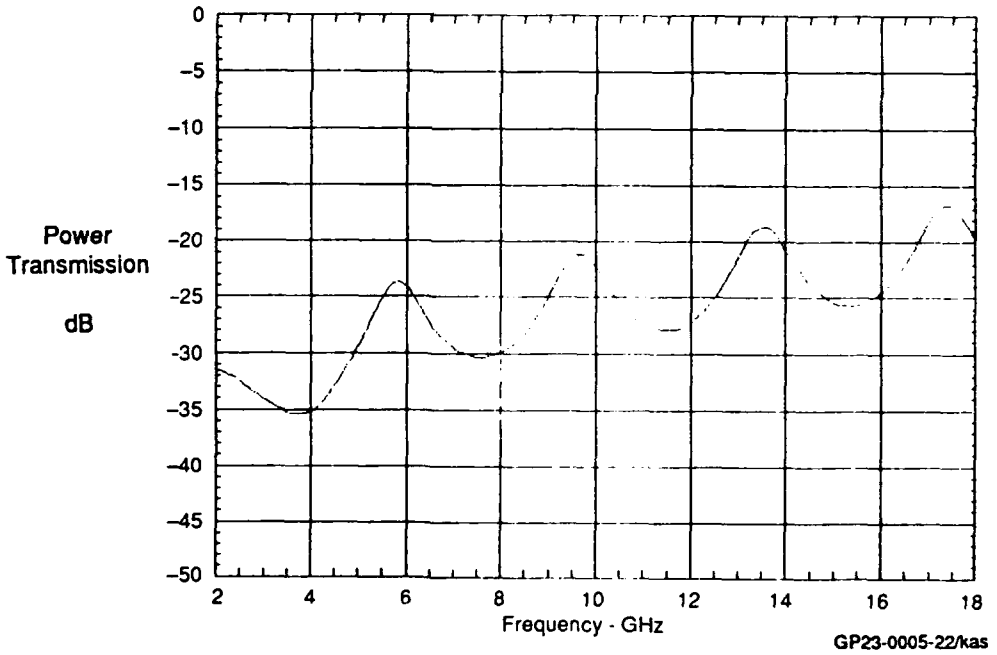

Figure 5.2-10. RF Transmission
Sample Type: ZnSe
Sample Size: 12 x 12 in.
Test Type: Tunnel

As shown in Figures 5.2-11 and 5.2-12, all of the ZnSe, silver-painted coaxial airline specimens have attenuation values less than 20 dB across the 2-18 GHz frequency band and fail to meet the program specifications. A comparison, shown on Figure 5.2-13 between the two small coaxial specimens in Figure 5.2-11 and the two large samples on Figure 5.2-12 reveals they were in agreement with each other.

The small and large ZnSe coaxial data can be compared to each other because the specimens that were tested had the same thickness. An overlay of the small and large coaxial airline data in the 0-4 GHz frequency range illustrates that the general shape of the curves is similar but the average attenuation levels differ by approximately 3 dB (Figure 5.2-13). The 12 x 12-inch panel was thicker than the coaxial airline specimens, so it was difficult to compare the tunnel data with the coaxial airline data. Although the tunnel specimen has a much greater attenuation than the coaxial airline samples, this entire difference cannot be accounted for by the thickness alone.

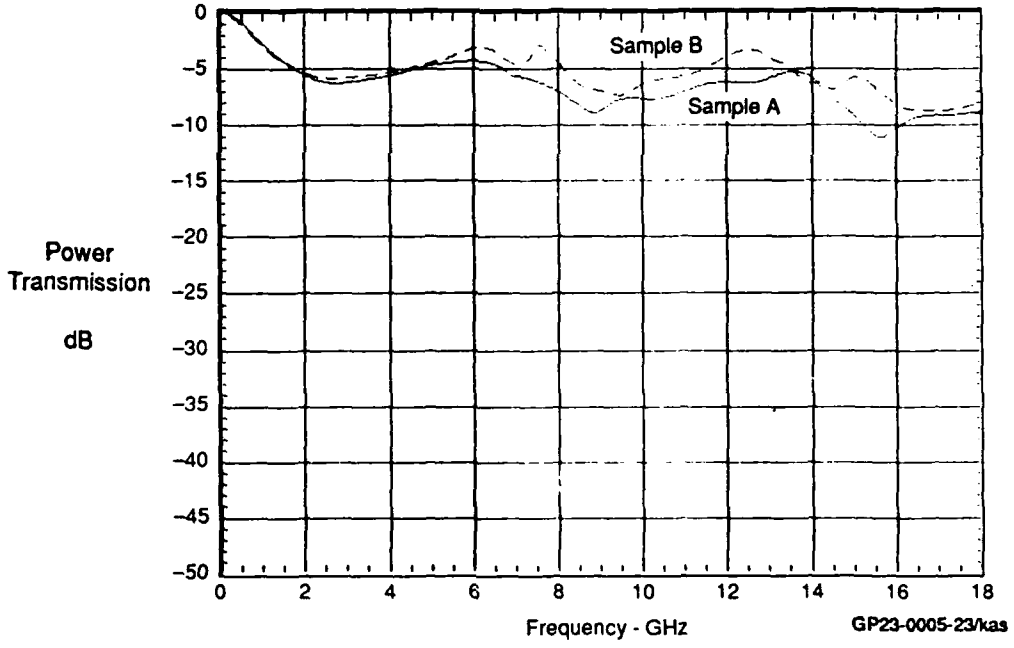

Figure 5.2-11. RF Transmission
Sample Type: ZnSe (Silver Edge Painted)
Sample Size: 7MM Coaxial
Test Type: Airline Coaxial

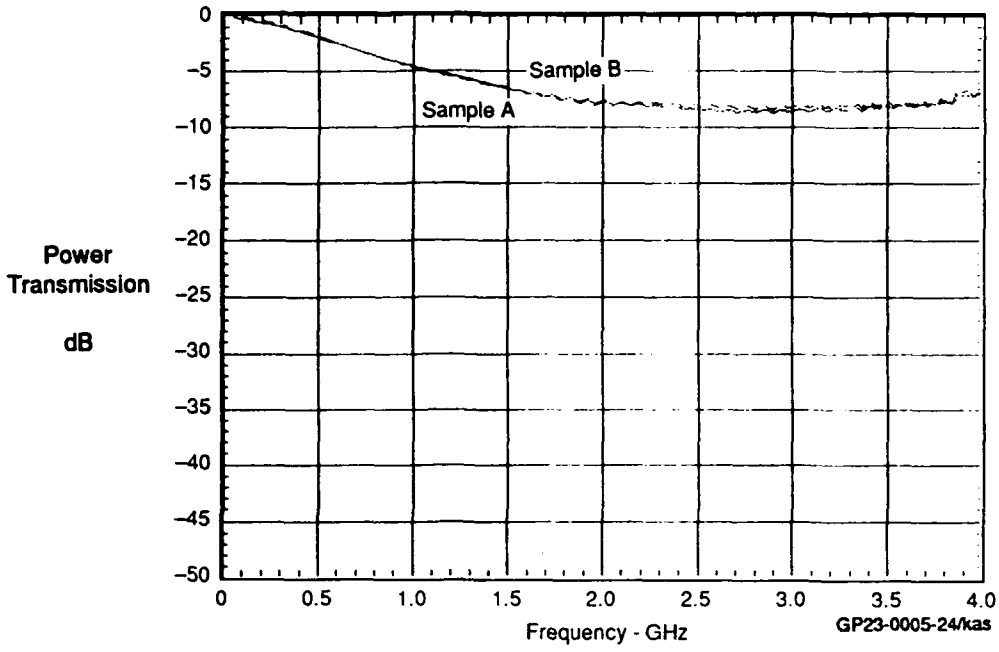

Figure 5.2-12. RF Transmission of Large and Small Coaxial Samples
Sample Type: ZnSe (Silver Edge Painted)
Sample Size: 1.5 Inch Coaxial
Test Type: Airline Coaxial

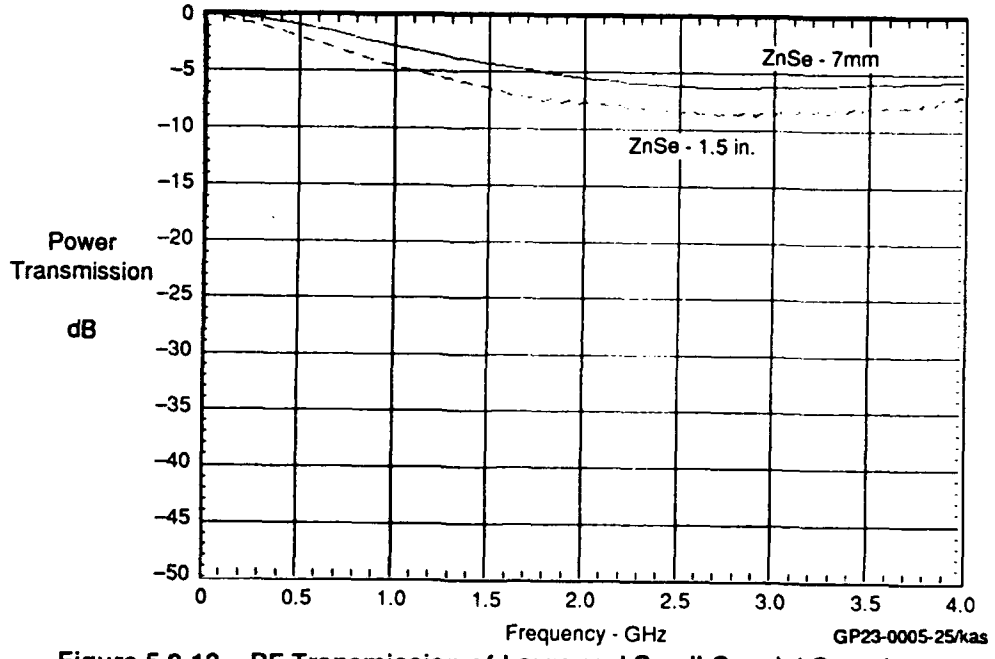

Figure 5.2-13. RF Transmission of Large and Small Coaxial Samples
Sample Type: ZnSe (Silver Edge Painted)
Test Type: Airline Coaxial

The photographs of the ZnSe coaxial specimens, taken after testing, reveal that the small coaxial specimens were damaged during the test procedure (Figure 5.2-14). Although the nature of the damage is uncertain, it appears that the specimens contain internal fractures which may have affected the testing results. In addition, there are discontinuities in the grid pattern and surface fractures at the edges of the specimens. The discontinuities may have prevented the grid from making good electrical contact with the sample holder during testing. All of these factors could account for the difference between the tunnel test results and the coaxial airline test results.

Litton/Itek provided a prediction of the transmission attenuation for four different grid designs on ZnSe. The average attenuation value for each grid design was greater than 20 dB across the 2-18 GHz frequency band. When comparing the tunnel data from the 12 x 12-inch with the predictions provided by Litton/Itek, the measured transmission curve indicates that the ZnSe had a higher dielectric constant than expected. However, the general shape and attenuation levels of the curves were in agreement. The coaxial samples did not achieve the attenuation values as specified by the manufacturer.

The reflection characteristics of the ZnSe panel, as measured on the NRL arch, are similar to those of the ZnS/ZnSe sample. These results are presented in Reference 5-3. Reflectivity was high -- zero loss -- throughout the frequency range. There are differences between the two sets of test results that are indicative of the differences between the grid systems used on the panels. For the higher frequency range, greater than 10 GHz, for all angles of incidence, the reflection loss was no greater than 0.5 dB. This is to be compared with losses greater than 1.0 dB for the ZnS/ZnSe grid system. Since the grid spacing for the ZnSe system was set at 200 micrometers, the high pass transition will begin at a higher frequency than for the ZnS/ZnSe system with a grid spacing of 400 micrometers. Consequently, the reflection will remain high over a broader frequency range and at higher incidence angles.

5.2.4 Conclusions - Three prospective IR window materials (ZnS/ZnSe, GaAs, and ZnSe) were tested and their microwave properties were compared to program specifications. Two of three GaAs specimens met the program specifications after reprocessing by the manufacturer. However, the third GaAs specimen did not pass the criteria. Closer investigation of that sample revealed the probability of inadequate bulk conductivity levels. The ZnSe tunnel specimen met the program specifications but the ZnS/ZnSe specimens did not. Grid geometry was the major factor controlling the reflection/transmission performance differences between ZnS/ZnSe and the ZnSe samples.

a. 7mm Coaxial Specimen – ZnSe 1 – 10x

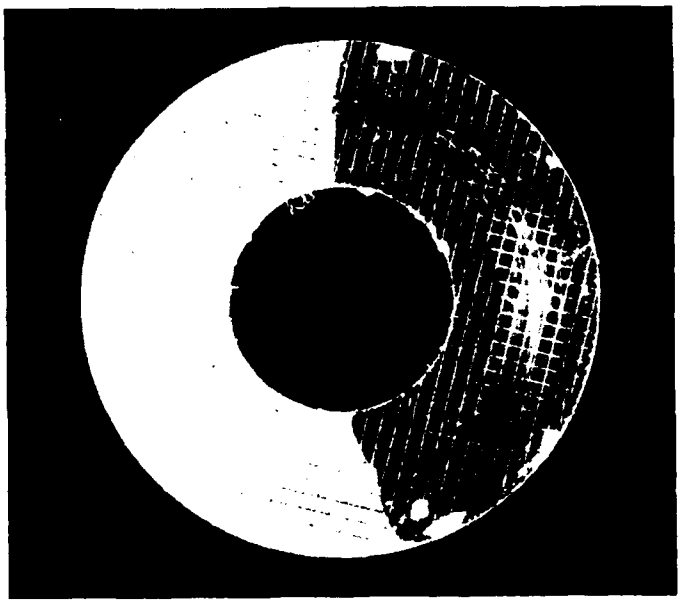

b. 7mm Coaxial Specimen – ZnSe 2 – 10x

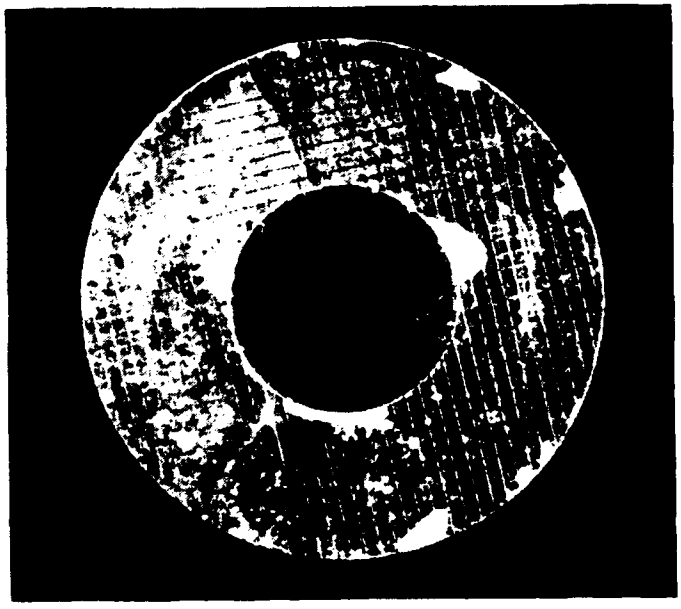

GP14-0021-426/pls

Figure 5.2-14. ZnSe Coaxial Samples Showing Damage Accumulated During Testing

c. 1.5 in. Coaxial Specimen – ZnSe 3 – 2.5x

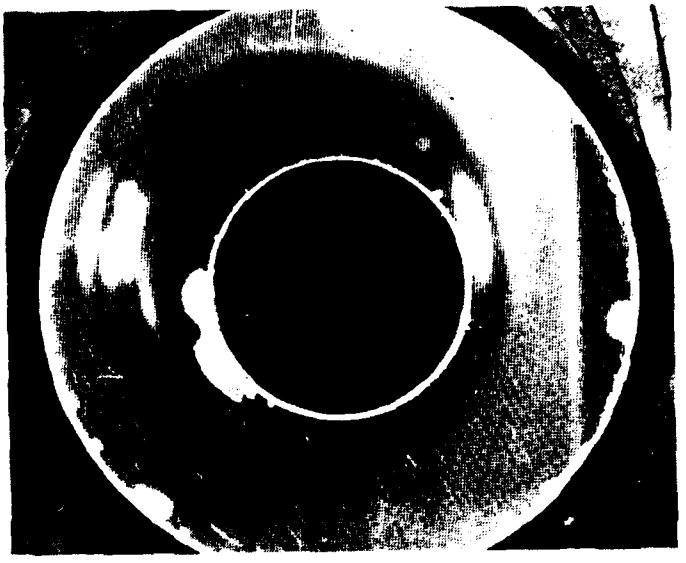

d. 1.5 in. Coaxial Specimen – ZnSe 4 – 2.5x

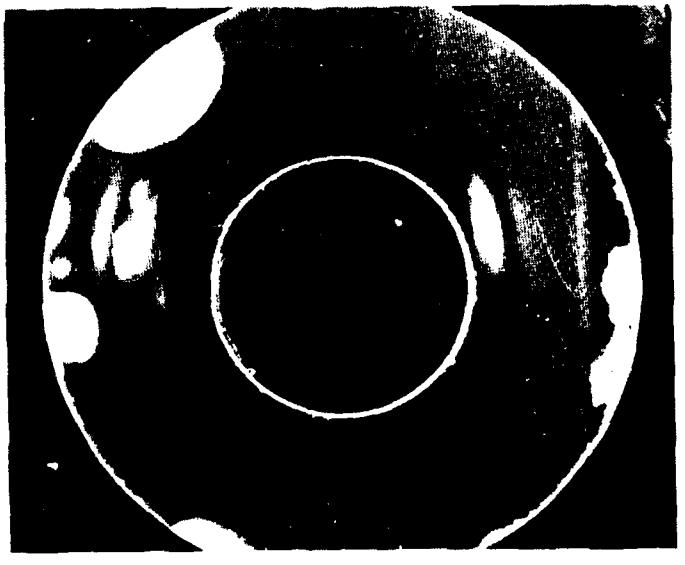

GP14-0021-427/pls

Figure 5.2-14. (Cont) ZnSe Coaxial Samples Showing Damage Accumulated During Testing

The electrical performance of the GaAs material relies on its bulk properties. Therefore, surface fractures will not significantly change its characteristics. The ZnS/ZnSe and ZnSe materials are coated with a conductive grid which determines their electrical performance. Surface fractures which cause damage to this grid will affect the characteristics of these two materials. Photographs of the ZnS/ZnSe and ZnSe materials show that surface fractures did exist in the coaxial specimens. Some of these fractures were present upon sample receipt and some were incurred during sample testing. The photographs also reveal that the specimens were manufactured with discontinuities in their grid patterns. The inconsistent coaxial airline test results for the ZnS/ZnSe and ZnSe materials may be attributed to these fractures and discontinuities in their gridded coatings.

These problems were not encountered when the ZnS/ZnSe and ZnSe materials were tested in the transmission tunnel. Metal-tape with a conductive adhesive was used to electrically seal the specimens to the aperture. This method of sample mounting helped to minimize damage to the gridded surface and, therefore, produce more reliable test results.

Coaxial airline testing provided accurate results for the GaAs material because the electrical performance was determined by the bulk properties and not a gridded coating. When testing materials with a gridded coating, such as ZnS/ZnSe and ZnSe, the transmission tunnel provides a more accurate measurement of the attenuation.

Figure 5.2-15 is a microwave performance prediction of two grids of different dimensions. Both grids are surrounded by free space and consequently have no phase interference peaks or valley occurring as a function of frequency. It is, however, evident that the transmission characteristics can be controlled by varying the spacing and/or line width of the grid. The addition of a substrate (dielectric constant >1) will impact the theoretical performance to the extent that closer spacing of the grid elements will be required to achieve the same amount of transmission loss, at the highest frequency, as the free space configuration.

For the ZnSe sample, the grid dimensions were better tailored to achieve the specified insertion loss than those of the ZnS/ZnSe sample. Since the type of substrate is only a secondary parameter of performance control, with the proper grid dimensions, the ZnS/ZnSe sample can be configured to perform within the specifications over the complete frequency range. Low frequency performance is not only a function of grid spacing, but also of grid element thickness and bulk conductivity of the metal

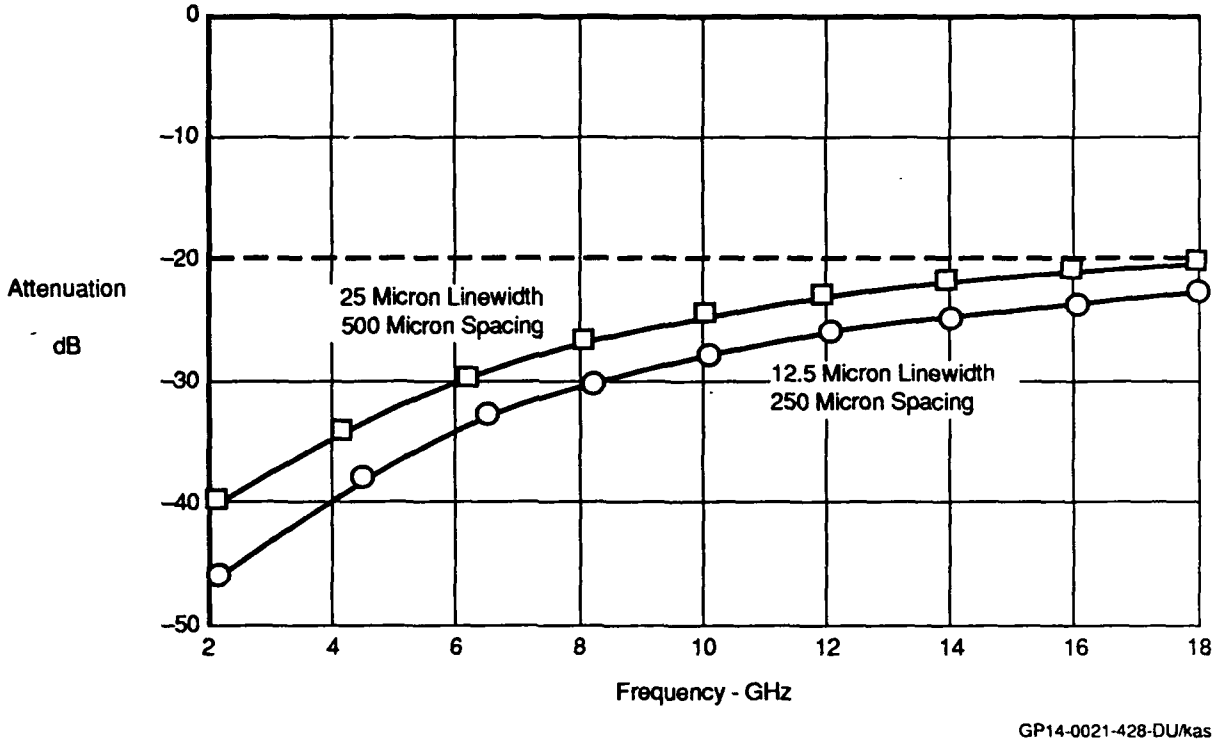

Figure 5.2-15. Microwave Attenuation in dB Through Inductive Grids

elements. As the frequency decreases, a point will be reached where the skin depth -- a function of bulk conductivity -- will be greater than the thickness of the metal. Shielding currents will consequently diminish allowing an increased transmission of energy. If frequencies lower than S-band are going to be specified for signature reduction, then this will require selection of metal type and grid thickness dimensions based on the requirement at the lowest specified frequency.

GaAs, when properly doped to achieve an adequate resistivity to maximize microwave reflectivity and IR transmission, will satisfy all of the requirements established for this program (Figures 5.2-16 and 5.2-17). However, this program has shown that more R and D is required with this material to achieve the blend of doping needed to meet both microwave reflectivity and IR transmission requirements. The effect on IR transmission has been presented previously in paragraph 5.1.1 and shown in Figure 5.1-14. Thickness of the windows will play a role in determining the lower frequency transmission/reflection characteristics, but this should not be a concern unless the thickness is less than 0.50 inch, or the low end frequency specifications extend into the 1-2 GHz L band or 0.2-1.0 UHF bands. The RF attenuation capability of GaAs decreases rapidly as frequency decreases as

shown in trends in the curves shown on Figure 5.2-17. The major control parameter in the fabrication of semiconductor windows is the doping level. Adequate quality control and assurance techniques are required in order to achieve the performance specified.

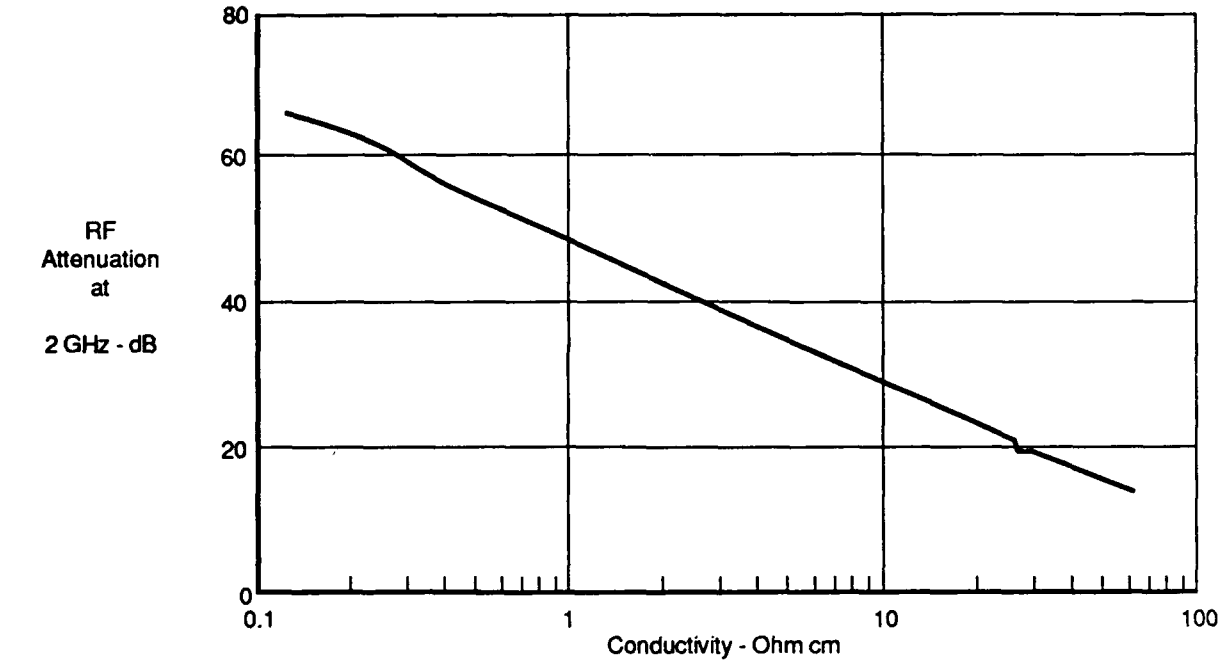

Figure 5.2-16. Theoretical GaAs RF Attenuation Characteristics
Thickness - 0.5 Inch

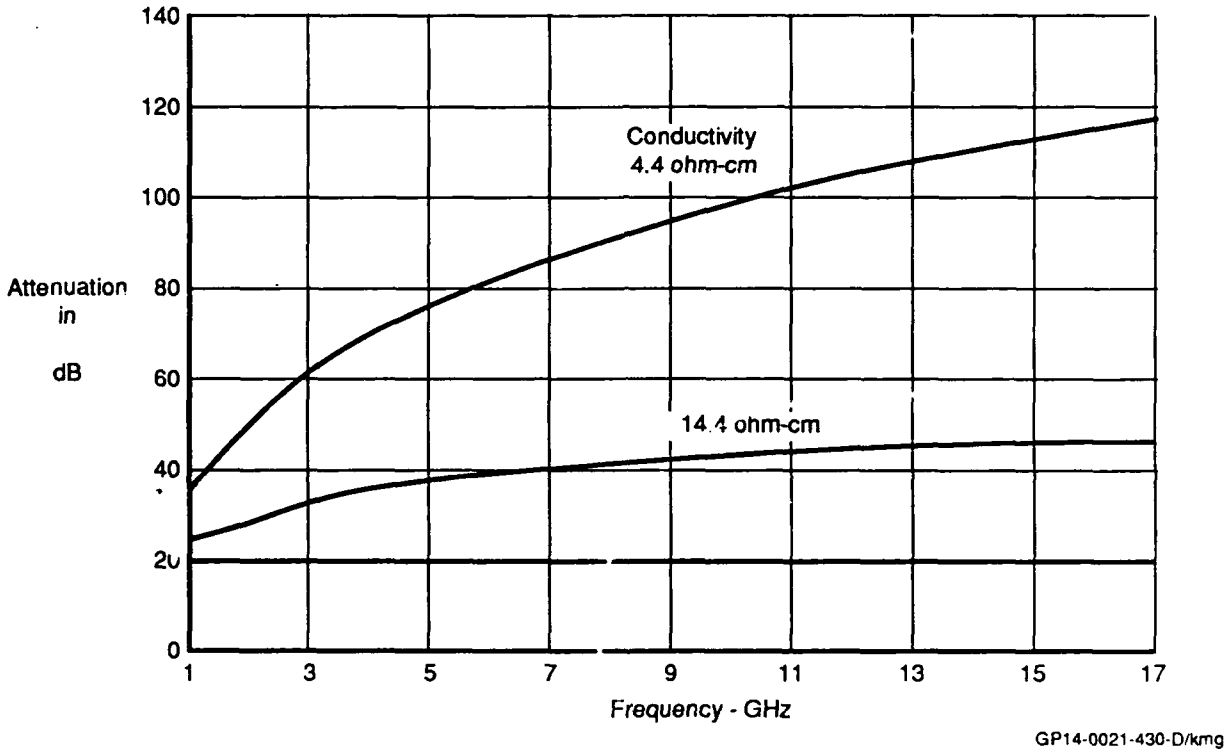

Figure 5.2-17. RF Attenuation of 0.5 Inch Thick GaAs at a Temperature of 297° K

5.3 Environmental Tests

The 3-inch diameter x 0.45-inch thick material specimens acquired from Itek and Hughes were subjected to a variety of environments to assess the effect of environment on material durability and optical performance. Environments were chosen to represent conditions expected to be experienced in the field and included salt spray, humidity, fluids, blowing sand, and temperature/altitude cycling. Rain erosion was also selected and is reported in Section 5.4. Figure 5.3-1 illustrates the sequencing of the environmental exposure and subsequent evaluation while the coupon test matrix is shown in Figure 5.3-2.

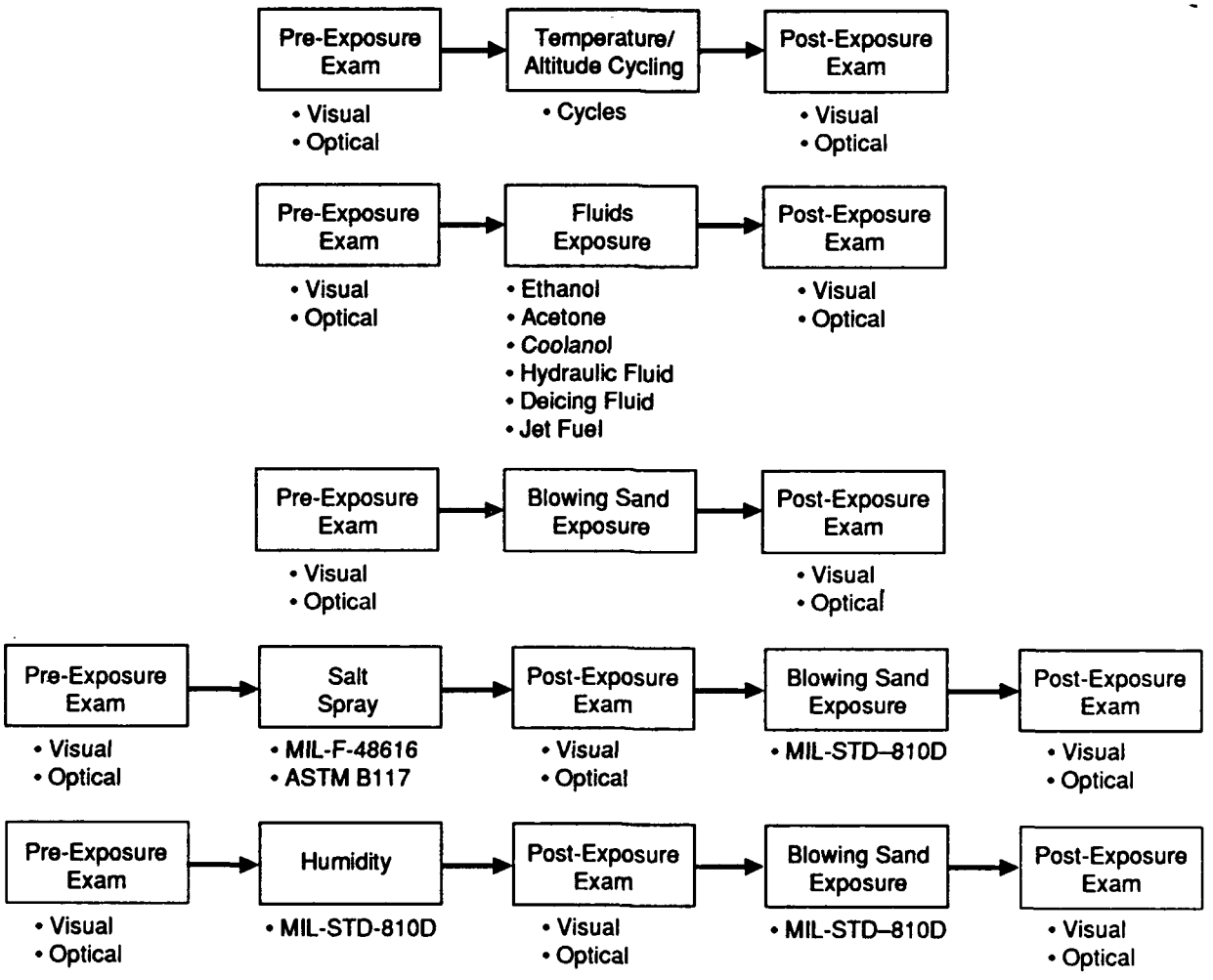

Note: Optical testing consisted of transmission versus wavelength and diffuse transmission

GP14-0021-135-DU/cm

Figure 5.3-1. Summary of Environmental Exposures for Each Material

Sample Type, No. per Vendor	Lot Number	Visual/Micro/Sem Inspection	Humidity	Salt Spray	Sand and Dust	Temperature/Altitude	7X Fluids	Rain Erosion	Visual/Micro/Sem/Inspection	Transmission vs Wavelength	Diffuse Transmission
Coaxial Doughnuts (2) - 7 mm (2) 1.5 in. Diameter	1	2									
	2	2									
	3	2									
RF 12 in. x 12 in. (1)	1	1									
	3	1									
Environmental 3 in. Diameter (12)	1	12	2	2	6	2	2		22	22	22
	2	12	2	2	6	2	2		22	22	22
	3	12	2	2	6	4	2		22	22	22
Optical 1 in. Diameter (3)	1	3								3	3
	2	3								3	3
	3	3								3	3
Rain Erosion 1 in. x 0.625 in. (12)	1	12						10	10	10	10
	2	12						10	10	10	10
	3	12						10	10	10	10
Strength 1.5 in. x 10 in. (5)	1	5									
	2	5									
	3	5									
Total Number of Tests		**104**	**6**	**6**	**18**	**8**	**6**	**30**	**96**	**105**	**96**

GP14-0021-436-DU/rwr

Figure 5.3-2. Coupon Test Matrix, Number and Type of Environmental Test Performed on Each Sample

In addition to visual examination, two optical tests were selected to evaluate the exposure effects, these being diffuse transmittance and transmission as a function of wavelength. These optical tests were performed on each specimen before and after environmental exposure. Diffuse transmittance measures scatter due to internal structure or external surface condition. By measuring diffuse transmittance before and after environmental exposure, the change due to surface condition can be isolated. Transmission versus wavelength measures degradation of transmission quality due to environmental damage of the exterior surface.

5.3.1 Humidity Exposure. Two specimens of each material, i.e., ZnS/ZnSe, GaAs, ZnSe, were exposed to temperature/humidity cycles per MIL-STD-810D, Method 507.2, Procedure 3 (Reference 1) to simulate aircraft deployment in a warm, humid environment. Method 507.2, Procedure 3 is designed to expose the specimens to temperature and humidity levels more extreme than found in normal operation, but for shorter durations. The temperature/humidity cycle used for this test is shown in Figure 5.3-3. Each specimen was exposed for 10 cycles (240 total hours) after which they were visually and optically examined to determine the effect of exposure.

There was no change in the physical appearance of any of the materials due to humidity exposure. Also, the optical performance was not significantly affected. The complete data on humidity testing and results can be found in Reference 5-7.

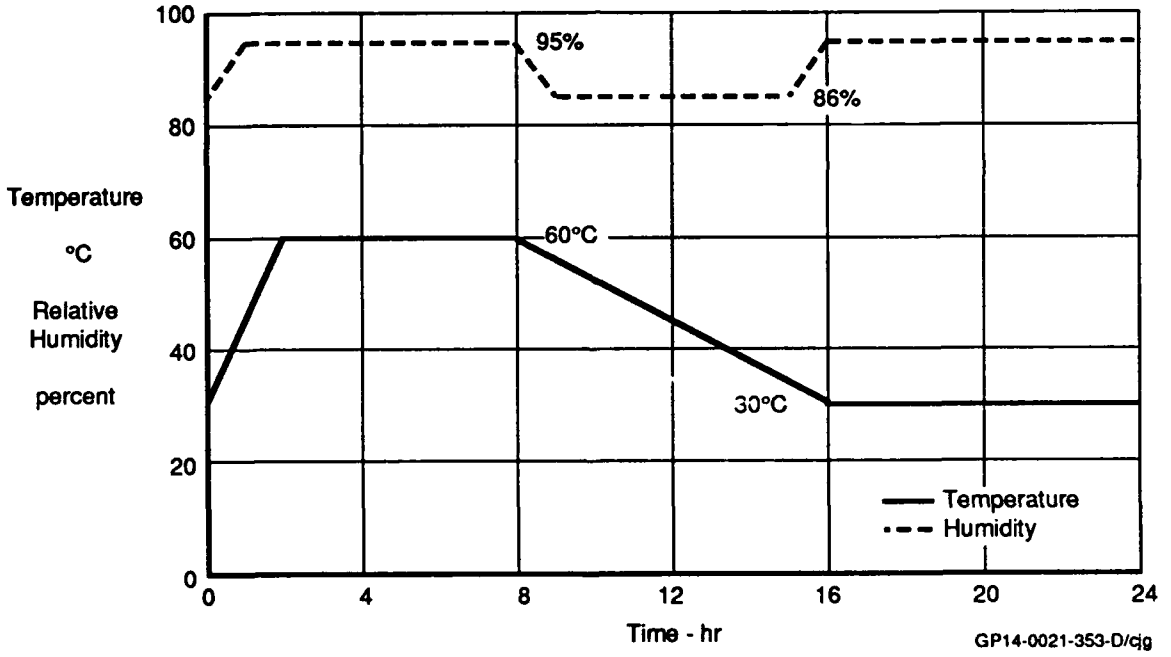

Figure 5.3-3 Temperature /Humidity Cycle

5.3.2 Salt Fog Exposure. Two specimens of each material, were subjected to salt fog testing according to MIL-F-48616, paragraph 3.4.2.3.4 and ASTM B117 (References 5-8 and 5-9). The salt fog test is intended to compare the relative salt fog resistance of various materials. Actual natural exposure tests are required to establish the absolute resistance of materials. The specimens were exposed for 168 hours to a 5% salt fog at 95°F.

After exposure, the three materials were visually examined for changes due to exposure. There was no physical change in the surface condition of ZnS/ZnSe and GaAs; however, ZnSe exhibited some damage, Figure 5.3-4. Subsequent examination at 200X to 500X revealed as-received ZnSe contained pin holes in the coating and ZnSe exposed to salt fog appears to have damage associated with the pre-existing pin holes. Damage to the ZnSe grid, Figure 5.3-5, is due to the choice of aluminum used with a chrome binder for grid material which could be eliminated by use of less corrosion-susceptible material.

The optical properties of ZnS/ZnSe and GaAs were not significantly degraded by salt fog exposure. ZnSe experienced a slight decrease in transmission at 1.06 microns.

Complete details on the salt fog tests and results can be found in Reference 5-10.

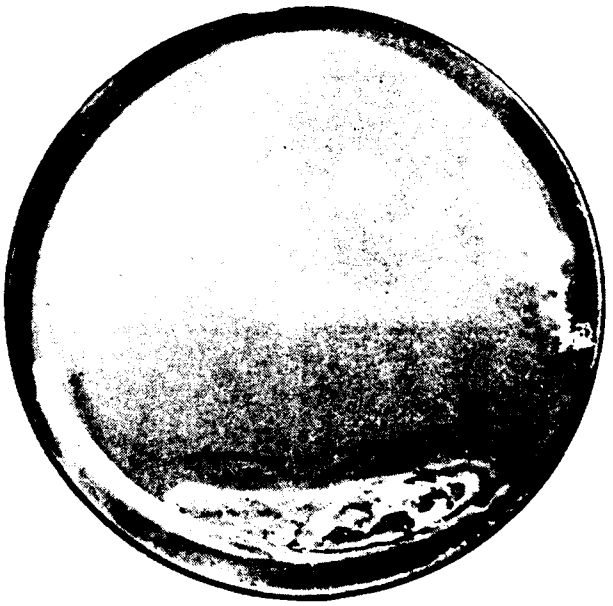

GP14-0021-434/pls

Figure 5.3-4 Photograph of Damage to ZnSe After Salt Fog Exposure

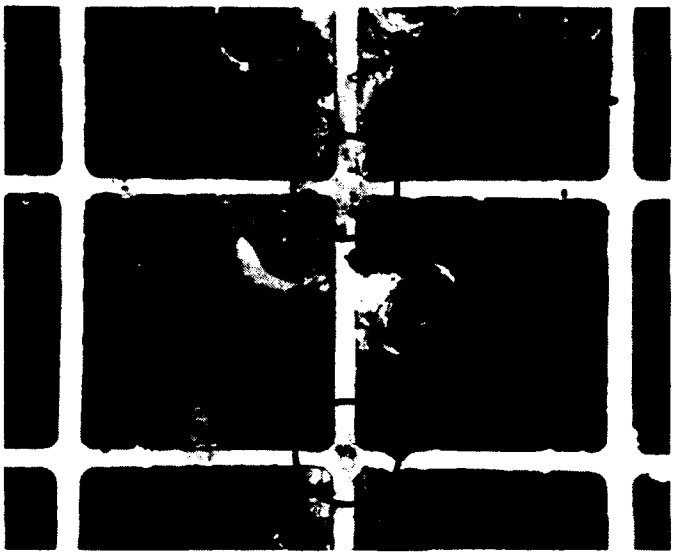

GP14-0021-435/pls

Figure 5.3-5. Photograph of Damage to Grid in ZnSe After Salt Fog Exposure

5.3.3 Blowing Sand Exposure. Blowing sand exposure was conducted by Dayton T. Brown, Inc., Long Island, NY under contract. Prior to exposure, Dayton T. Brown weighed each material specimen and visually examined them for coating anomalies such as flaking, cracking, and blistering, and for general surface condition.

The exterior surface of each specimen was subjected to blowing sand according to MIL-STD-810D, Method 510.2 (Reference 5-11). The test parameters were:

Air velocity - 4,000 ft/min (44 mph)
Chamber temperature - 84° to 99°F
Chamber relative humidity - 26% to 47%
Sand concentration - 0.0623 $\pm$0.015 gm/ft^3
Angle of incidence - 45 degrees.

The sand composition was as specified in MIL-STD-810D, Method 510.2, paragraph I-3.2d(2). Six specimens each of ZnS/ZnSe, GaAs, and ZnSe were exposed. As shown in Figure 5.3-1, some of the specimens had previously been exposed to salt-fog or humidity to determine cumulative exposure effects. The sand exposure times for each material is shown in Figure 5.3-6.

Following sand exposure, Dayton T. Brown weighed each specimen and visually examined them to assess damage. The results are summarized in Figure 5.3-7.

Material	Pre-Exposure	Sand Exposure Time (min)
ZnS/ZnSe	None	30, 60
	Humidity	30, 60
	Salt Fog	90
GaAs	None	60
	Humidity	30, 90
	Salt Fog	30, 90
ZnSe	None	30, 60
	Humidity	30, 90
	Salt Fog	60, 90

GP14-0021-130-DU/cm

Figure 5.3-6. Exposure Time For Blowing Sand

Material	Exposure Time (Min)	Exterior Surface Condition
ZnS/ZnSe	30	Exterior Surface Opaque; Surface Was Abraded Evenly; No Damage to Substrate
	60	No Further Damage
	90	Increased Opaqueness ⚠
GaAs	30	Exterior Surface Opaque; Surface Was Abraded Evenly; No Damage to Substrate
	60	Increased Opaqueness ⚠
	90	Increased Opaqueness ⚠
ZnSe	30	Exterior Surface Opaque; Surface Was Abraded Evenly; No Damage to Substrate
	60	Increased Opaqueness ⚠
	90	Increased Opaqueness and Roughness

⚠ Increased opaqueness compared with previous exposure

GP14-0021-200-D/suz

Figure 5.3-7. Condition After Blowing Sand Exposure

All three materials were similarly affected by the blowing sand exposure. The exterior surfaces were generally abraded evenly causing the surface to become opaque. Microscopic examination indicated that the underlying substrate was not damaged by the blowing sand; however, the grids were damaged (Figure 5.3-8).

The optical performance was significantly degraded by the exposure, as shown in References 5-7, 5-10, and 5-12.

The transmission of all three materials at 1.06, 1.54, and 8 to 12 microns were reduced by 5% or more after only 30 minutes exposure. The average transmission loss was greater at 1.06 microns than 8 to 12 microns, Figure 5.3-9. Diffuse transmission was also significantly affected by blowing sand, Figure 5.3-10. The diffuse transmission of all three materials was significantly increased after only 30 minutes exposure.

Further details on the blowing sand exposure conducted by Dayton T. Brown can be found in Reference 5-13.

5.3.4 Temperature/Altitude Cycling. Two samples of each material were subjected to temperature and altitude cycling. Environmental cycling was conducted in a Thermotron Combined Environmental Test chamber. The selected thermal/altitude cycle is described below.

a. Chamber temperature was reduced from ambient to -66°C.
b. Chamber pressure was reduced to that at 50,000 feet.
c. Chamber temperature was increased to +60°C.
d. Chamber pressure was returned to ambient while the temperature was increased to +100°C.
e. Chamber temperature was reduced to -66°C.

The temperature rate of change was 5°C/min. while the pressure rate of change was 900 feet/min. All materials were exposed to 18 cycles. Each sample was visually examined and the optical performance of each material was measured to determine the effect of the exposure. The effect of a more aggressive temperature rate of change was investigated. Two cycles were performed using a 20°C per minute rate of change. Both ZnS/ZnSe and GaAs were physically and optically unaffected, but ZnSe exhibited isolated areas where flaking of the interior AR coating occurred. However, this flaking did not significantly degrade the optical properties.

Further details on the testing can be found in Reference 5-14.

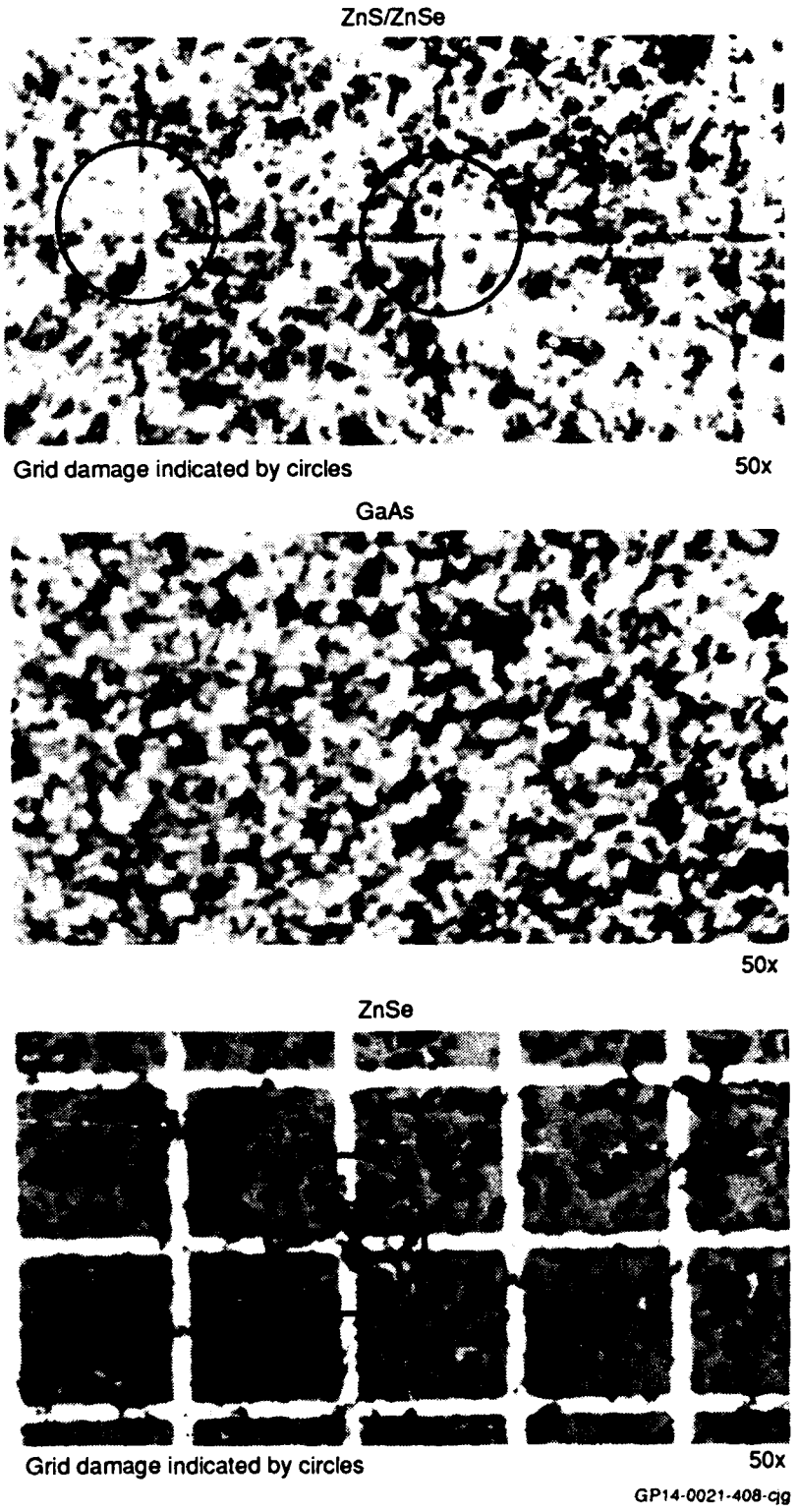

Figure 5.3-8. Typical Surface Damage After Exposure to Blowing Sand
44 Miles per Hour Air Velocity

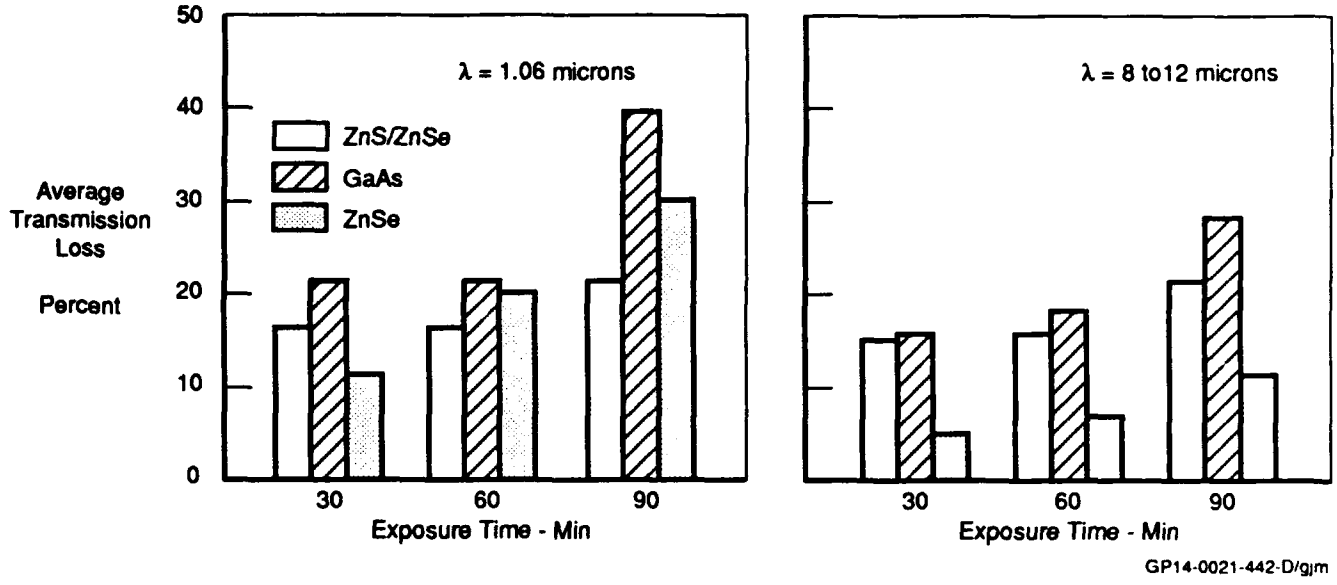

Figure 5.3-9. Average Transmission Loss Due to Blowing Sand

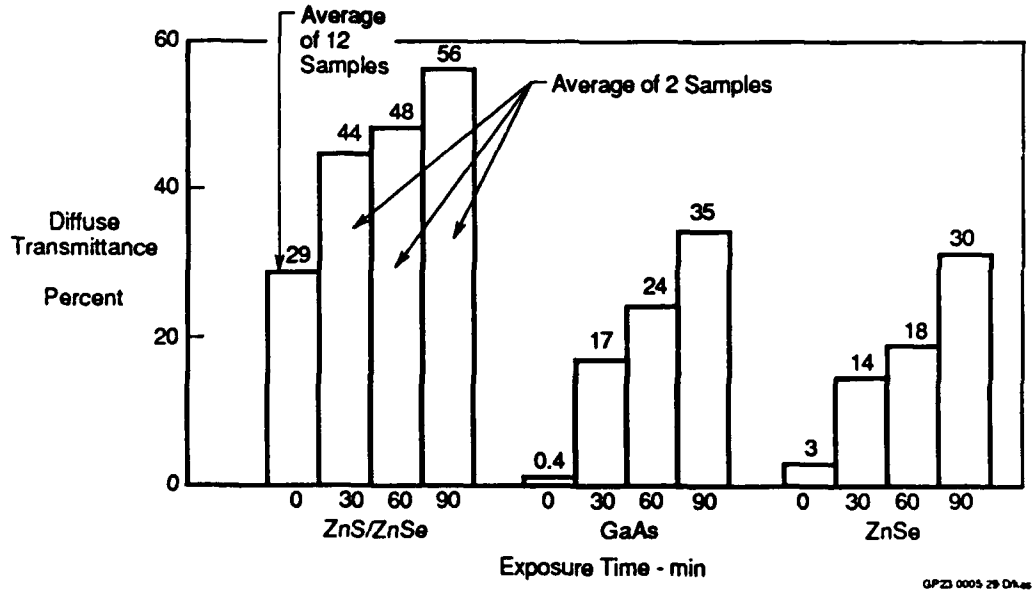

Figure 5.3-10. Degradation of Diffuse Transmittance at 1.06 Microns as a Result of Sand and Dust Exposure for 3 Exposure Times

A

5.3.5 Fluid Exposure. Two specimens of each material were exposed to a variety of fluids expected to be encountered during normal aircraft basing and usage. The chosen fluids were ethanol, acetone, coolanol (Monsanto Coolant No. 25R), MIL-H-83282 hydraulic fluid, MIL-A-8243 deicing fluid, and JP-4 jet fuel. Each specimen was exposed sequentially for 30 minutes. Following each exposure, the specimens were examined visually and optically to determine the effect of fluid exposure.

None of the fluids caused either a change in the physical appearance nor optical performance for the three materials. Complete data on the fluid exposure testing and results can be found in Reference 5-15.

5.4 Rain Erosion Tests

Erosion of window exterior surfaces exposed to rain is a general concern. Consequently, each material was subjected to rain erosion testing to learn, on a subjective basis, the relative durability of the three materials.

Rain erosion tests were conducted at the Materials Directorate System Support Division's Rain Erosion Test Facility at Wright-Patterson AFB. This facility has conducted rain erosion tests on a variety of materials since 1947 and is operated by the Aerospace Vehicle Coatings Group, Materials Engineering Division, University of Dayton Research Institute (UDRI).

Test specimens were attached to the tip of a knife-edge propeller-like blade which was rotated at a selected velocity through a simulated rainfall as shown in Figure 5.4-1.

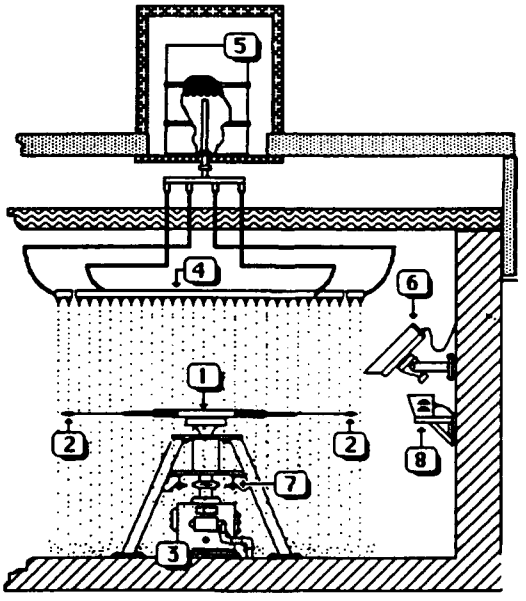

1. DOUBLE ARM BLADE
2. MATED TEST SPECIMENS
3. VERTICAL DRIVE GEAR BOX AND SHAFT
4. CURVED MANIFOLD QUADRANT
5. WATER STORAGE TANK FOR RAIN SIMULATION
6. REMOTE CONTROLLED CAMERA
7. MAGNETIC PICK-UPS FOR FIRING THE STROBE
8. HIGH INTENSITY STROBE LIGHT FOR STOP MOTION VIEWING

GP14-0021-133-/suz

Figure 5.4-1. Rain Erosion Test Apparatus

The test specimens used for this test were 0.625" x 1.00" x 0.25" thick as prescribed by UDRI. The test matrix shown in Figure 5.4-2 documents the exposure times and examination intervals for each material. The specimens were subjected to a rainfall rate of 1 inch/hour at a velocity of 470 mph at an angle of 45 degrees.

5.4.1 Physical Degradation - Following each exposure interval, the coupons were examined at 10X by a technician and his subjective observations were recorded. Rain erosion damage is described by URDI as the extent of coating loss, pitting, cratering, ring fractures, and surface microcracks (see Figure 5.4-3). Pitting is confined to the coating layer. When pits extend through the coating into the substrate, the resulting damage is called cratering. Surface microcracks are considered to be in the substrate near the surface and ring fractures are interior to the substrate. Erosion failure is that point where penetration extends to the substrate. Details of the rain erosion tests can be found in Reference 5-16. A summary of the material condition after exposure is shown in Figure 5.4-4. Photographs of each sample, along with their optical performance curves, are in Appendix C.

Figure 5.4-4 shows erosion failure occurring to ZnS/ZnSe within 6 minutes exposure and within 2 minutes for GaAs and ZnSe. Also, each material experienced a variety of damage after short exposure. For example, all three materials experienced some coating removal after 2 minutes exposure and some pitting after 4 minutes exposure. Also, all three materials experienced at least some severe damage after 30 minutes exposure. GaAs suffered severe coating removal after 8 minutes exposure and well before the other two materials. Seventy to ninety percent of the GaAs coating was removed. Litton, Itek Optical Systems, who fabricated the GaAs specimens, examined one GaAs specimen and concluded that the yttria oxide layer, the hard outer coating, had been removed, exposing the softer bismuth oxide layer. Since GaAs is opaque, it was not possible to determine if that material experienced ring fractures. Based upon the overall visual examination, UDRI subjectively rated ZnS/ZnSe better than ZnSe which was ranked significantly better than GaAs.

Material	Specimen Number	Examination Interval - min										
		2	4	6	8	10	12	14	16	20	22	30
ZnS/ZnSe	1					√				√		√
	2					√				√		√
	3					√				√		√
	4					√				√		√
	5					√				√		√
	7					√				√		√
	8	√	√	√								
	9	√	√	√								
	10				√							
	11				√							
	14						√		√		√	
	15						√		√		√	
GaAs	1			√	√							
	2			√	√							
	3					√				√		
	6					√				√		
	8					√				√		
	9					√				√		
	11					√				√		√
	12					√				√		√
	13	√										
	14	√										
	15		√									
	16		√									
ZnSe	1					√				√		
	2					√				√		√
	3					√				√		√
	4					√				√		
	5					√				√		
	6					√				√		
	7	√										
	8	√										
	9			√	√							
	10			√	√							
	12						√					
	15						√					

GP14-0021-139-DU/cm

Figure 5.4-2. Examination Intervals for Rain Erosion Tests

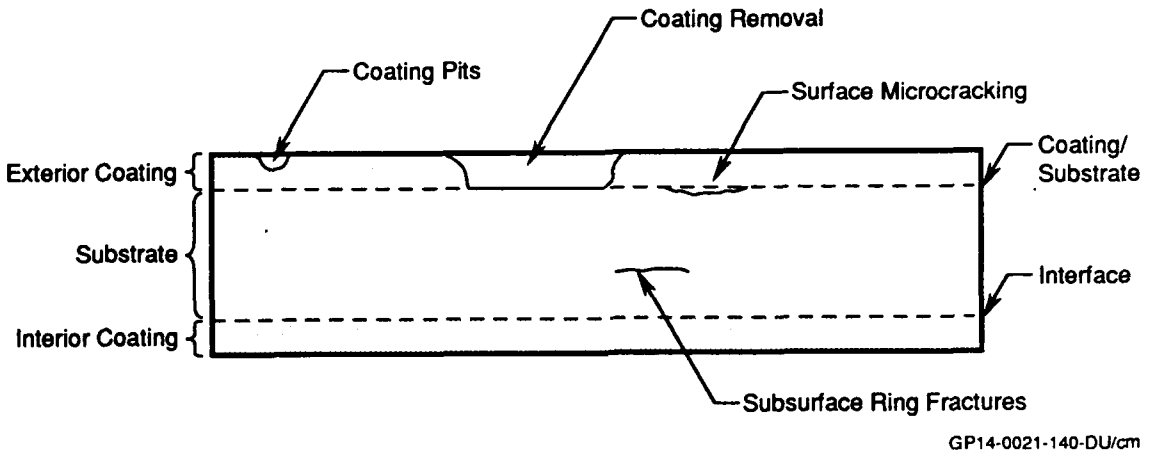

Figure 5.4-3. Categories of Rain Erosion Damage

5.4.2 Optical Performance Degradation - Following rain exposure, the material optical properties were measured and compared with pre-exposure properties to document degradation. The optical properties selected for comparison were 8 to 12 micron transmission and diffuse transmittance at an optical wavelength of 1.06 microns. This wavelength was the most sensitive (in our examination of broadband or 1 m-12 m bandpass windows) to the microscopic damage caused by rain erosion. A five percent decrease in specular transmission or increase in diffuse transmittance was considered significant degradation.

The primary mechanisms for optical degradation are delamination or removal of the AR coatings and substrate microcracks associated with impact craters. AR coating delamination/removal results in increased first-surface Fresnel reflection which reduces the specular transmission. Subsurface microcracks can have a similar effect on specular transmission but also introduce significant optical scattering which increases the diffuse transmission. These phenomena are accentuated by materials with a large indices of refraction. The optimum erosion resistant window material would, therefore, have a low refractive index and high mechanical toughness. Full details concerning the optical performance after rain erosion can be found in Reference 5-3.

Material	Exposure Time (min)	Conditions				
		Coating Removal	Pitting	Surface Microcracks	Cratering	Ring Fracture
ZnS/ZnSe	2	Slight (<10%)	None	None	None	Slight
	4	Slight (<10%)	Very Slight	None	None	Increased
	6 (1)	No Increase	Increased	None	None	Increased
	8	No Increase	No Increase	None	1 or 2 Craters	No Increase
	10	No Increase	No Increase	None	No Increase	No Increase
	12	No Increase	No Increase	None	No Increase	No Increase
	14	No Increase	Increased	None	No Increase	Increased
	16	No Increase	Increased	None	No Increase	Increased
	20	No Increase	No Increase	None	No Increase	No Increase
	22	Increased	Increased	None	No Increase	Increased
	30	5 - 20%	Severe	None	No Increase	No Increase
GaAs	2 (1)	Slight (<10%)	Slight	None	1 Crater	None
	4	50%	Increased	Some	No Increase	None
	6	50%	No Increase	No Increase	No Increase	None
	8	70 - 90%	Increased	No Increase	Increased	None
	10	70 - 90%	No Increase	No Increase	No Increase	None
	20	100%	Severe	No Increase	Severe	None
	30	100%	Severe	Severe	Severe	None
ZnSe	2 (1)	<10%	Some	Some	Some	Some
	6	<10%	No Increase	No Increase	No Increase	No Increase
	8	<10%	Increased	Increased	Increased	Increased
	10	<10%	No Increase	No Increase	No Increase	No Increase
	12	<10%	No Increase	No Increase	No Increase	No Increase
	20	<10%	Increased	Increased	Increased	Increased
	30	<10%	Severe	Severe	Severe	Severe

(1) Time at which pitting penetrated through coating to substrate

GP14-0021-138-DU/cm

Figure 5.4-4. Summary of Rain Erosion Damage

5.4.2.1 ZnS/ZnSe - As shown in Figure 5.4-5, ZnS/ZnSe experienced less optical degradation than GaAs or ZnSe. There was some loss of transmission for ZnS/ZnSe primarily due to lost AR coating. For example, after 30 minutes exposure, there was a five percent decrease in transmission at 1.06 microns and a seven percent decrease at 8 microns. As shown in Figure 5.4-5, there appears to be some correlation between exposure time and transmission loss, as expected. In addition, there was a minimal increase in diffuse transmittance, as shown in Figure 5.4-6. Diffuse transmittance was found to increase rapidly with exposure time after 8 minutes exposure, probably due to increased exterior surface roughness as the grids and coating became more eroded.

5.4.2.2 GaAs - GaAs experienced significant optical degradation, as shown in Figure 5.4-5 and Reference 5-3. For example, after 20 minutes exposure, there was a 19 percent decrease in transmission at 1.06 microns and 8 microns. This is directly related to the physical damage suffered by the coating and substrate. As expected, the transmission reduction was a function of exposure time. Diffuse transmittance was also significantly increased by rain erosion due to severe pitting and coating removal damage, Figure 5.4-6. GaAs exhibited the largest increase in diffuse transmittance for shortest exposure time.

5.4.2.3 ZnSe - Transmission was significantly reduced in ZnSe due to rain erosion damage, as shown in Figure 5.4-5. For example, after 12 minutes exposure, there was a 16 percent decrease in transmission at 1.06 microns and an 8 percent decrease at 8 microns. Transmission losses increased with exposure time, probably due to increasing substrate fractures.

Diffuse transmittance was found to increase rapidly after 8 minutes exposure, as shown in Figure 5.4-6. The increase in diffuse transmittance was due to fractures within the substrate. As exposure time was increased, surface pitting occurs and the diffuse transmittance increased.

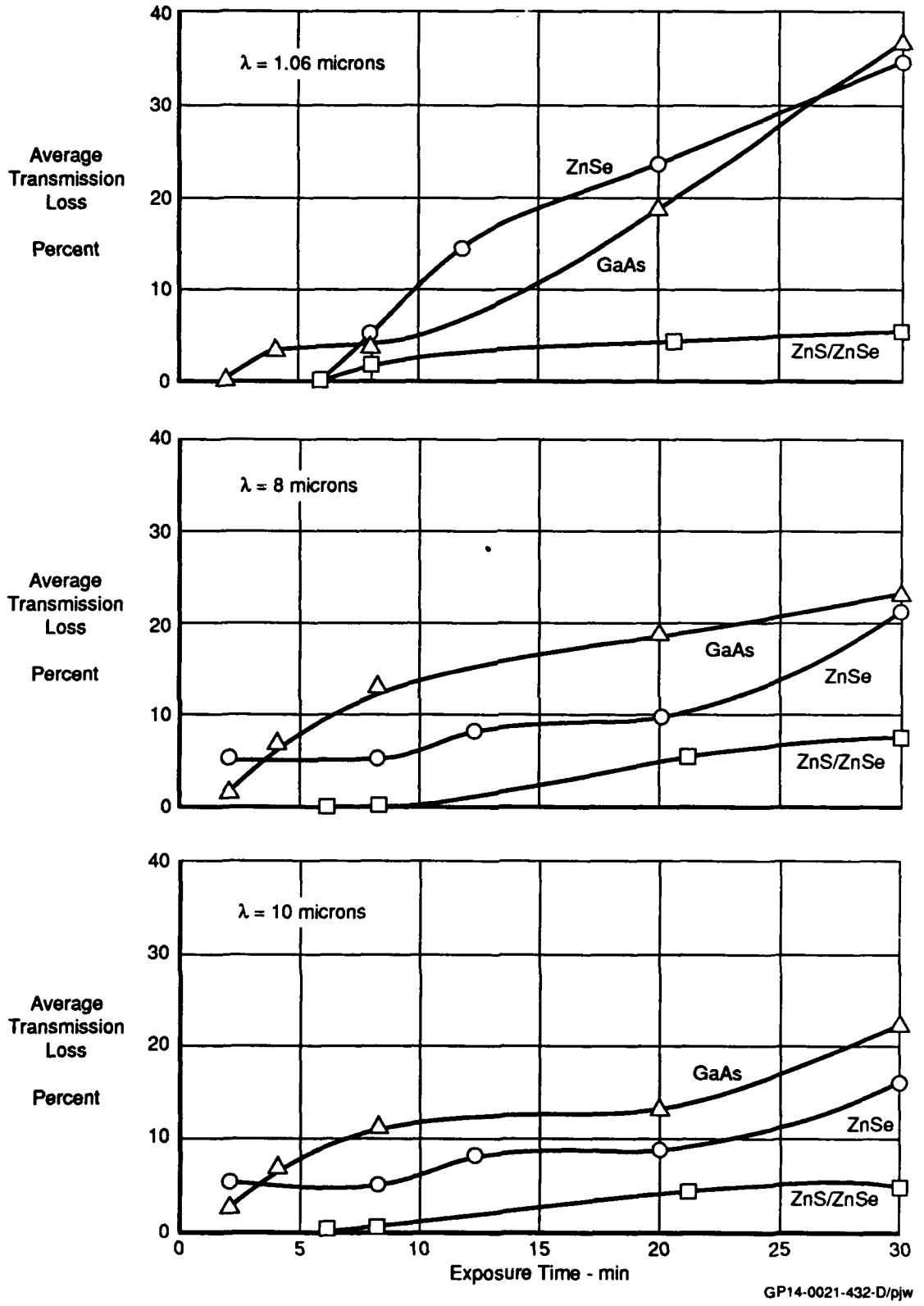

Figure 5.4-5. Average Transmission Loss Due to Rain Erosion for Three Wavelengths

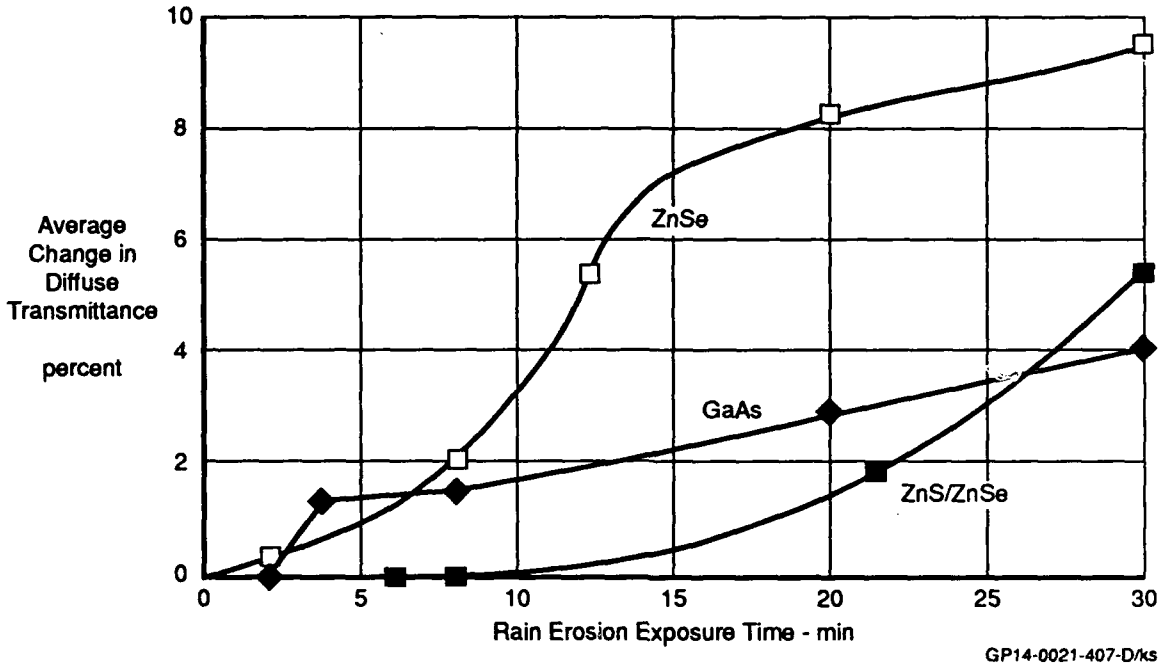

Figure 5.4-6. Effect of Rain Erosion on Diffuse Transmittance

5.5 Structural Tests

Five specimens of each material were subjected to a room temperature four-point bend test in accordance with ASTM C-158-84 (Reference 5-17) to measure the modulus of rupture.

Prior to testing, each specimen was visually examined for evidence of anomalies such as surface cracks and internal defects. These were recorded as to their location and size. During four-point bending, the load points were as shown in Figure 5.5-1. The specimens were oriented so that the exterior coating side was loaded in compression. The specimens were tested in a Universal test machine. Half-inch wide loading blocks were used to protect the specimens from the loading

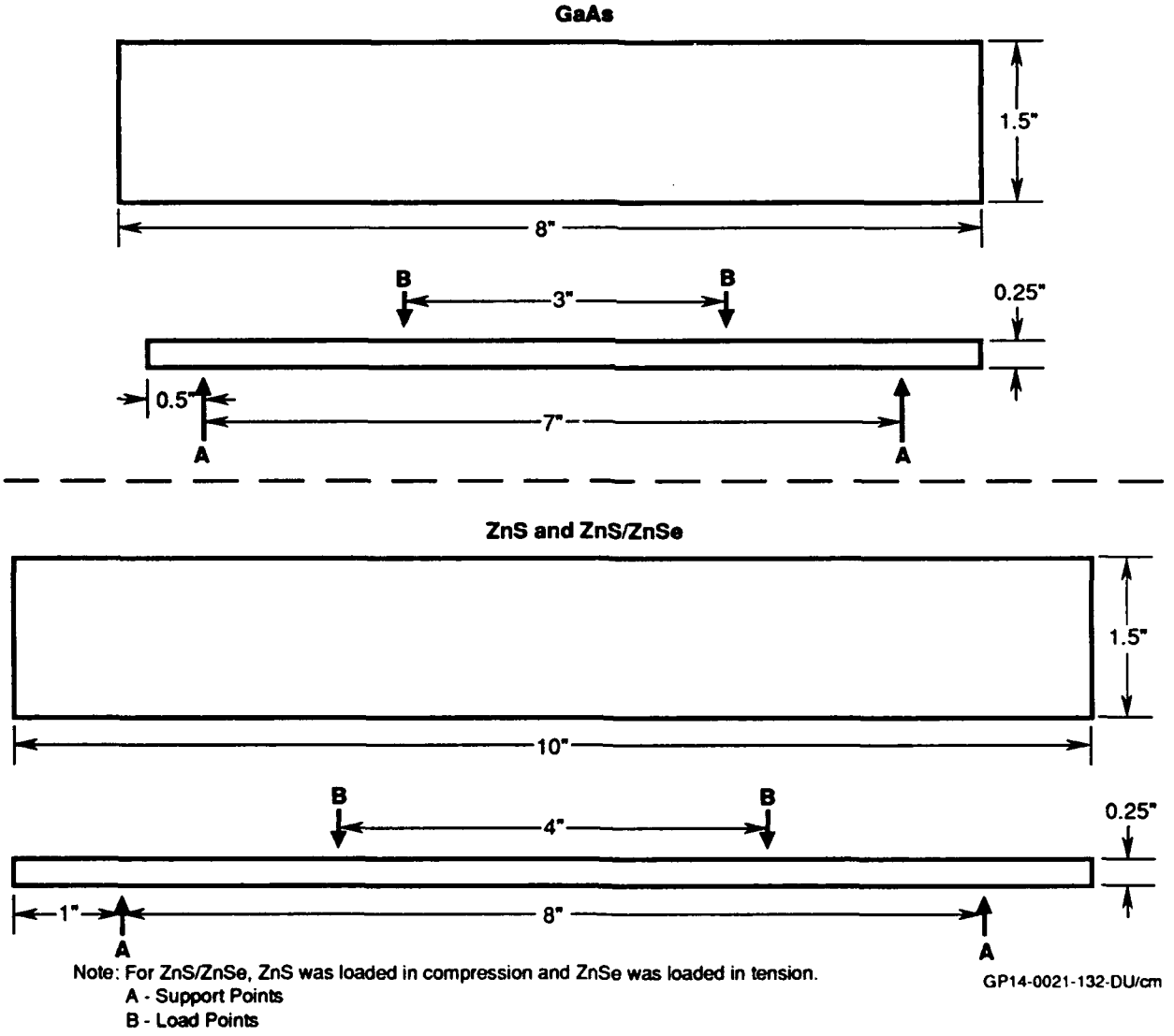

Figure 5.5-1. Load Point Locations for Four-Point Bending Test

fixture. The loading fixture swiveled so as to distribute load evenly across the specimen and between the two load points. Masking tape was used on the compression surface between load points to keep fractured pieces together. The loading rate was selected to cause failure within 50 to 70 seconds. The test arrangement is shown in Figure 5.5-2.

Following the test, the modulus of rupture was calculated from the failing load as specified in ASTM C-158-84. A comparison of the modulus of rupture for each material is shown in Figure 5.5-3. These values should only be used for qualitative comparison since the sample size was small and the data variability is significant, as shown by the coefficient of variation. However, the modulus of rupture compared favorably with published values and were similar for the three materials.

GP14-0021-170-U/vc

Figure 5.5-2. Four Point Bend Test Arrangement

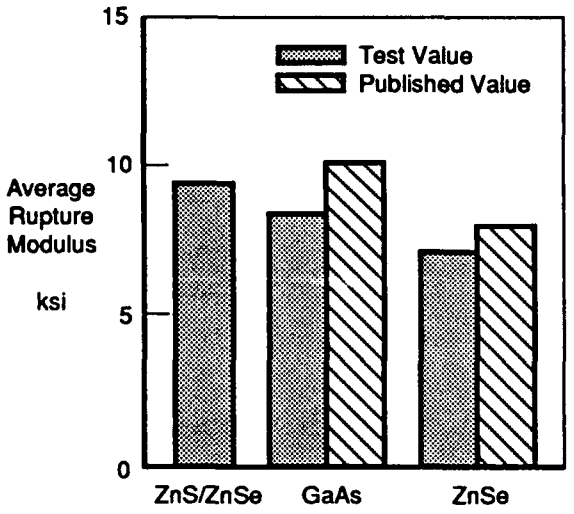

Material	Rupture Modulus (ksi)	Mean Rupture Modulus (ksi)	Coefficient of Variation (%)
ZnS/ZnSe	7.7 8.2 8.4 11.0 11.3	9.3	18.4
GaAs	5.6 7.5 7.6 9.0 12.0	8.4	28.7
ZnSe	4.6 7.0 7.4 7.9 8.2	7.0	20.0

Coefficient of Variation = $\frac{S}{\bar{X}}$

GP14-0021-131-DU/cm

Figure 5.5-3. Rupture Modulus

Typical photographs of fractured specimens are shown in Figures 5.5-4 and 5.5-5. A summary of the failure points is shown in Figure 5.5-6. As expected, the materials exhibited brittle fracture surfaces. There did not appear to be any correlation between pre-existing anomalies and the failure mode or location.

Further details on the four-point bend testing can be found in Reference 5-18.

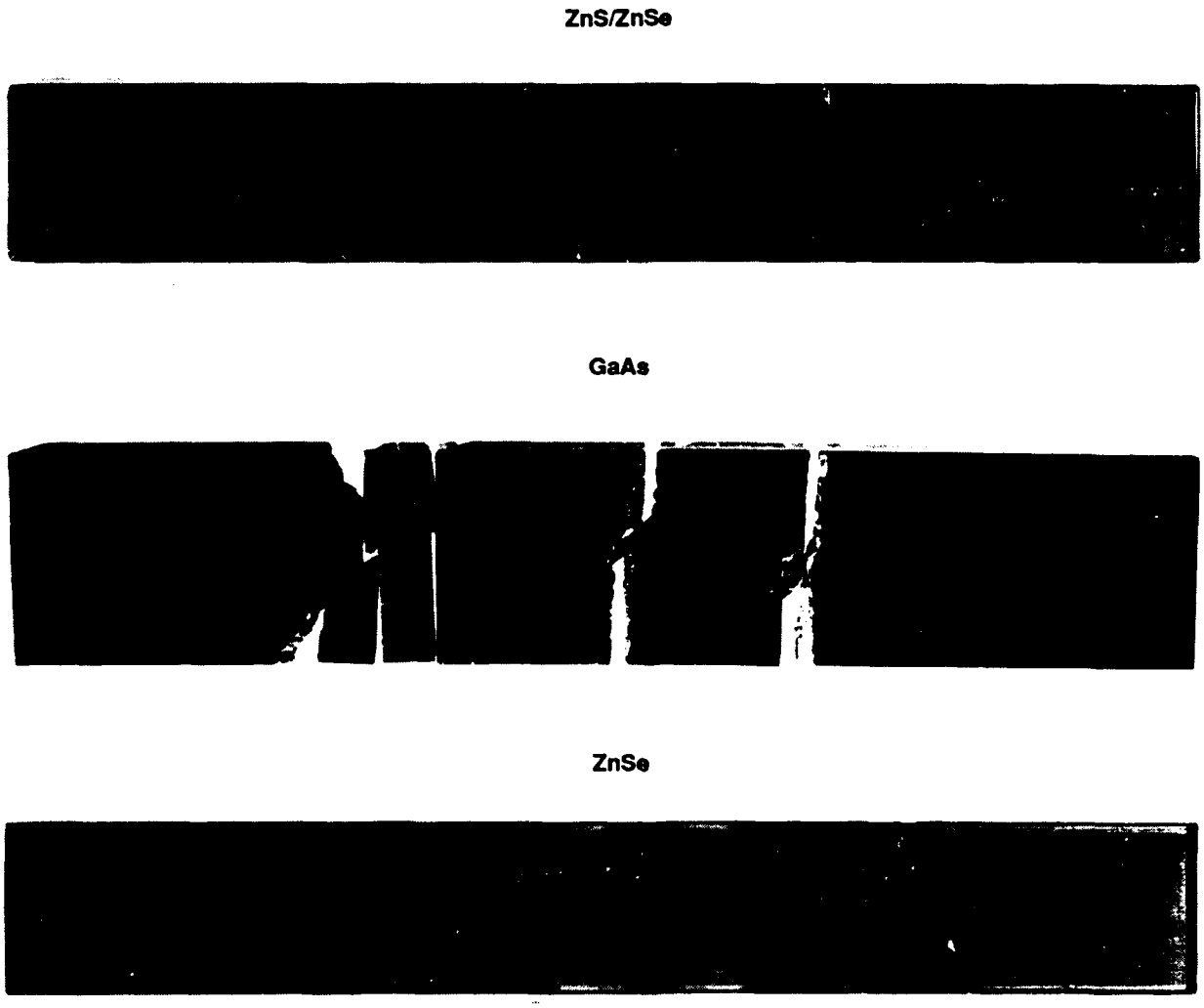

GP14-0021-137/suz

Figure 5.5-4. Photographs of Typical Failures
Surface In Tension Is Shown

ZnS/ZnSe
Compression Side

GaAs
Compression Side

ZnSe
Compression Side

GP14-0021-136/suz

Figure 5.5-5. Photographs of Typical Fracture Surfaces
Locations Shown Are Failure Points

Material	Specimen	Failure Point			Comment
		Between Reaction Point and Load Point	At Load Point	At Reaction Point	
ZnS/ZnSe	1		X		Fans From Middle to Both Sides
				X	Fans From Edge
	2			X	Fans From Edge
			X		Fans From Edge
	4		X		Fans From Edge
			X		1/2" Inside Load Point, Fans From Edge
	5			X	Fans From Edge
	6			X	Fans From Edge
ZnSe	SN 001			X	Fans From Edge
	SN 003			X	From Middle Fans to One Side/Single Crack to Other Side
	SN 004		X		Fans From Edge
			X		1/2" Inside Load Point, Fans From Edge
	SN 006		X		3/4" Inside Load Point, Fans From Edge
	SN 007		X		1/2" Inside Load Point, Fans From Edge
			X		1/2" Outside Load Point, Fans From Edge
GaAs	SN 002	X			
		X			Small Shear Lip on Compression Side
	SN 003		X		Small Shear Lip on Compression Side
	SN 004		X		1/2" Inside Load Point, Small Shear Lip on Compression Side
			X		Stepped Shear Failure (Failure at B)
	SN 005		X		Stepped Shear Failure (Failure at D)
	SN 006		X		Stepped Shear Failure (Failure at B), Fan Mark on Failure Surface
					Stepped Shear Failure, Fan Mark on Failure Surface

Note: Unless otherwise noted, ZnS/ZnSe and ZnSe specimens had numerous stress cracks at the failure site which originated on the tension side, but, in general, did not grow to compression side.

GP14-0021-169-D/vc

Figure 5.5-6. Summary of Failure Locations

6.0 RISK ASSESSMENT AND RISK REDUCTION

Litton Itek Optical Systems and Hughes Danbury Optical Systems determined and assessed risks to producing full-scale sensor windows and recommended areas of future investigation to be included in a risk reduction plan.

6.1 Material Risks - It is expected that sensor windows for future aircraft will need to be on the order of 20"L x 20"W x 0.5" to 0.75" thick. At least two vendors -- Morton International and II-VI Incorporated have large scale facilities (Reference 4-3). Morton has the facilities to produce ZnSe by chemical vapor deposition (CVD) in pieces up to 40" x 60" with thicknesses approaching 2". However, Morton has not yet produced a piece this large. Morton's current capacity is estimated at approximately 300,000 cubic inches per year. The II-VI facilities can produce CVD ZnSe in smaller sizes -- 24" x 36" in thicknesses up to .05", and 20" x 24" in thicknesses of 1.0". Itek chose Morton to produce the ZnSe substrate for this program.

Several risk factors need to be considered with ZnSe. The substrate takes weeks to grow, which may adversely affect production rates. ZnSe requires very careful handling to avoid scratches and chipping throughout the grinding, polishing, coating, and installation processes. Figure 6.1-1 shows an approach to reduce risk.

Litton Airtron supplied the GaAs substrate to Itek. GaAs crystals are grown as cylindrical boules in crucibles and must be optically shaped. Currently, the largest possible GaAs boule is 10" in diameter. Consequently, GaAs is not available in sufficient size for large sensor windows. During this program, Litton Airtron grew 10" diameter boules from which the 8"-long strength samples were produced. In order to yield 10" x 10" windows, boules 15" to 20" in diameter would be required. This requires significant cost and involves high technology risks for large scale facility scale-up. Substrate growth rates are in terms of days. The risks with GaAs are in consistency of meeting both broad band infrared transmission and electrical conductivity in the same sample. Figure 6.1-1 provides a plan to approach this risk.

Hughes also selected Morton to manufacture the ZnS/ZnSe substrate. Morton uses the CVD process to form the ZnS/ZnSe substrate sandwich which is available in sizes of 20 x 20 inches. However, this substrate, like the ZnSe, takes weeks to grow. Unlike ZnSe, this sandwich material can have poor transmission which is attributed to scattering in the ZnS material and at the interface of the ZnS and ZnSe. Figure 6.1-1 addresses a potential material risk reduction approach.

Risk Area	Description	Risk Reduction Approach					Comments	Degree of Risk
		Existing Data	Analysis	In-House Test of Samples	Coupon Test	Full Scale Panel Test		
Durability	Resistance to Sand/Dust	X		X	X		• Understand Speed Dependence • Investigate Hardened Coatings Such as Hard Carbon or Polycrystalline Diamond • Investigate Additional Material Hardening Processes • Understand Damage Mechanism • Higher Speed and Diff Duration • Establish Standard Conditions	Moderate
	Resistance to Rain	X	X	X	X		• Investigate Additional Material Hardening Processes • GaAs Polycrystalline Growth and Testing to Determine Strength vs Percent of Transmission and Conductivity • GaAs Crystal Growth Orientation to Determine Strength Trade-Offs	Moderate to High
	Slow Crack Growth and Scratch/Pitting	X	X		X		• 10 - 20 Samples to Provide Additional Strength Data and Quantify Effects of Scratches/Pits on Substrate Strength • Strength vs Configurtion, Strength Degradation vs Time and Environment	Moderate
RCS Development	Mesh Metals	X	X			X	• Large Mesh Deposition Needs Further Development • Trade Transmission With RF Conductivity • Demonstrate Other Materials • Need Less Geometric Obstruction So Trade-Offs Required of Grid Wire Size/ Mesh Spacing vs Spectral Transmission	Significant Cost and Technology Driver, High Risk
	Conductive Coatings IR Transmission vs RCS Compatibility	X	X	X	X	X	• Trade Transmission With RF Conductivity • R&D on Types of Conductive Busbar Material Adhesion Strength • R&D on Conductive Bonds Between Panes and Conductive Frames • Confirm Mating Methods Work • Confirm Need for OHMIC Contact. Need Maximum dB Attenuation	Significant Cost and Technology Driver, High Risk High
	Range Test		X			X	• Determine Effect of Multi-Panes on Optical Performance and RCS Characteristics	Low to Moderate

GP14-0021-413-D/kch

Figure 6.1-1. Risk Management Summary

Risk Area	Description	Risk Reduction Approach					Comments	Degree of Risk
		Existing Data	Analysis	In-House Test of Samples	Coupon Test	Full Scale Panel Test		
Coating Development	Graduated AR Coatings	X	X	X	X	X	• Need Higher Transmission Efficiency for Broadband ARs	Significant Cost and Tech Driver, High Risk
	Adhesion		X		X		• Quantitative Adhesion Measurements for All Layers to Allow Optimization Beyond That Possible With Tape	Moderate
	Improved Coating Design	X	X	X	X		• Optimization of Production Scale IAD Process Needed • Rain Erosion Resistant Coatings	Life Cycle Cost Driver, High Cost Risk
	Visual Signature Reduction in ZnS/ZnSe, and ZnSe	X	X		X	X	• Design Coatings to Eliminate Green Light Transmission • Coating Durability Testing • Trade-Off Studies for IR/Laser Transmission vs Green Light Attenuation	High
	Improve 1.06 Transmission in ZnS/ZnSe		X		X	X	• Establish Reason for Low Transmission • Determine Source and Amount of Scatter and Correlate vs Processing Conditions • Vary/Modify Processing to Reduce Scatter	High
Material Development	ZnS/ZnSe	X	X		X	X	• Substrate Takes Weeks to Grow • Need to Correlate Source and Amount of Scatter Against Processing Conditions Then Modified Processing to Reduce Scatter	High Raw Material Cost Can Be Reduced by Process Devlpmt and Facilities
	GaAs	X	X		X	X	• Substrate Takes Days to Grow • Substrate Material Not Currently Available in Sufficient Sizes for Large Windows • Only One Source - Litton Airtron • Further R & D to Meet Trans and Elect Conductivity Simultaneously and Continuously	Very High Material Cost-Boule Growth and Consistenancy of Parameters Is Major Problem. High Significant Cost/Technology Risk for Large Scale Facility Scale Up
	ZnSe	X	X		X	X	• Substrate Takes Weeks to Grow • Large Scale Facilities Exist at Least at 2 Vendors • Production Capability Presently Sufficient Without Adding New Fabrication Chambers • Requires Very Careful Handling to Avoid Scratches and Chipping	Moderate Cost/Low Technical Risk
	Large Pane Producibility					X	• Growth Scale-Up • Yield Improvements	High for GaAs Moderate to High for Others

GP14-0021-414-D/jsl

Figure 6.1-1. Risk Management Summary Continued

During this program, Itek and Hughes used a production-scale, ion-assisted deposition (IAD) method to apply coatings to the substrates. Itek is equipped to coat pieces up to 72" in diameter while Hughes can coat pieces up to 32" in diameter. Both suppliers consider themselves production-ready for coating full scale substrates.

It became evident during this program that there is potential for manufacturing quality problems when the window material fabrication process is scaled up to a production quantity process. For example, crazing and pinholes were encountered in the coatings. As-manufactured surface defects such as scratches or pits are clearly significant when dealing with inherently brittle materials such as these. Production process control and quality inspection in a production scale environment need to be addressed before these materials are fully ready for production.

Safety risks in producing the three materials were assessed by Itek and Hughes. In their judgement, there are no risks associated with the production of ZnSe or ZnS/ZnSe windows. However, during optical manufacturing steps, such as grinding, precautions must be taken to avoid breathing GaAs dust. Also, the GaAs slurry must be recovered and disposed of properly.

6.2 Risk Reduction - Production technology for producing broadband infrared sensor windows from ZnS/ZnSe, GaAs, or ZnSe is somewhat immature and merits a risk reduction program prior to production of full-scale windows. There are several factors which need to be considered when establishing a risk reduction program. The window assembly is more than just an outer moldline cover to protect the sensor -- it is an optical element of the sensor. As such, it must meet several criteria.

6.2.1 Mechanical Requirements - Mechanical requirements such as aeroloads, temperatures, vibration, durability, and weight will affect the window assembly structure. Window panel size and shape, installation and panel removal, and field maintenance are factors in life cycle cost and require engineering attention. Installation and maintainability drive certain aircraft compromises in configuration, location, drag, and signature. All these factors, plus optical performance, material cost, and producibility drive window design decisions.

6.2.2 Broadband Infrared Material - This program investigated three types of broadband infrared material, their coatings, and their effect on broadband transmission requirements and window durability. Optical performance characteristics of a window assembly affect a sensor's sensitivity, detection range, resolution, and tracking accuracy. Coatings are a major

contributor to window optical performance. The risk associated with coating development can be approached as shown in Figure 6.1-1.

6.2.3 RCS characteristics - RCS characteristics of the three materials were investigated in this program. Aircraft RCS requirements will determine the window assembly configuration, orientation, and conductivity requirements. Figure 6.1-1 shows a risk reduction approach which may be considered for future window RCS development work.

6.2.4 Environmental testing - The infrared window materials were subjected to environmental testing in this program to determine their resistance to environments such as sand, rain, humidity, and salt fog. Since durability requirements affect the design concept, they must be accommodated at the beginning of the design cycle. Figure 6.1-1 provides a plan to approach this risk.

6.2.5 Development risk - In the long run, the material used will depend on the primary aircraft mission (super or subsonic cruise velocities, aircraft RCS requirements, etc.). Figure 6.1-1 provides an assessment of the degree of cost, weight, and material development risk for some of these factors.

6.2.6 Element overview - Figure 6.2-1 provides an overview of elements of a typical window assembly demonstration/validation program leading to an FSD ready optimum design concept.

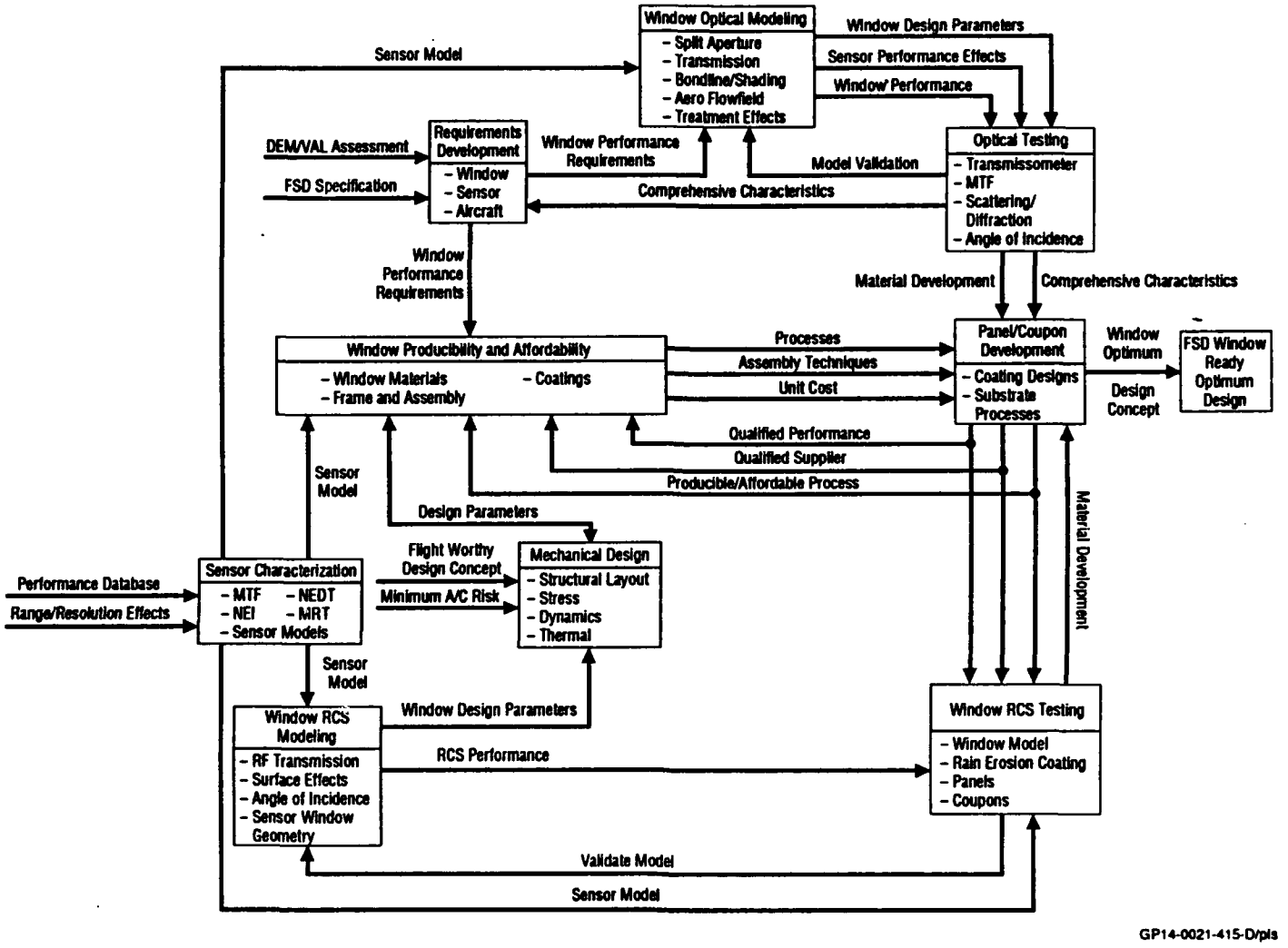

Figure 6.2-1. Typical Window Assembly Demonstration/Validation Program

7.0 SIGNIFICANT FINDINGS AND RECOMMENDATIONS

7.1 Significant Findings

The Early Risk Reduction Phase 1 Broad Band Infrared Window Material Test Program was intended to evaluate three materials, ZnS/ZnSe, GaAs, and ZnSe, and assess their suitability for simultaneous use as an aperture for a Laser Target Designator and Targeting FLIR. As the program evolved, certain findings were significant.

7.1.1 Laser Compatibility - ZnS, ZnSe, ZnS/ZnSe, and Cleartran have a non-linear polarization characteristic at 1.06 microns which results in frequency doubling and the production of green light at the 0.53 micron frequency. This phenomenon was initially observed during testing at approximately 3 millijoules/cm^2 in a darkened laboratory, and at 10 millijoules/cm^2 with the lights on. If necessary to minimize or eliminate this occurrence, special coatings will have to be developed and applied to the inside window surface which will reflect the green light back into the cavity of an electro-optical system. Most probably, a new coating will either be a multi-layer or rugate coating. Testing and trade-off studies will have to be performed to address the issues related to rain-erosion, durability, and transmission of this new coating design.

7.1.2 Grid Structure - Grid materials and grid designs are available to meet laser energy and RCS requirements. Grid spacing should be chosen to avoid being similar to transmitted wavelength.

7.1.3 Substrate Manufacturers - During the testing of ZnS/ZnSe, Hughes noted that the transmission of the polished substrates was not meeting their specification at 1.06 microns. Morton International, who supplied the material to Hughes, attributed the poor performance (28-47%) to scattering in the ZnS layer and also to the interface between ZnS/ZnSe. Hughes' previous experience with ZnS/ZnSe from Raytheon showed transmission greater than 60% at 1.06 microns. Raytheon no longer makes the material, leaving Morton the only supplier of large window substrate in both ZnSe and ZnS/ZnSe material.

7.1.4 GaAs Consistency - Inconsistency of GaAs characteristics was noted throughout the program. Transmission varied greatly as a result of substrate conductivity. The tests concluded that the optimum point to meet both the electrical conductivity and infrared transmission requirements was not satisfied. The material characteristics varied from sample to sample - probably due to the growth and consistency of the boules from which the samples came.

7.1.5 Material Durability - All three materials were subjected to humidity, temperature/altitude, salt fog, and various fluids without significant physical or optical degradation. Blowing sand at 44 mph significantly damaged all three materials, both physically and optically. Rain erosion significantly degraded the optical performance of ZnSe and GaAs, whereas the optical performance of ZnS/ZnSe was marginally degraded.

7.1.6 As-Manufactured Quality - All three materials exhibited as-manufactured quality defects such as edge chips and surface defects. ZnSe exhibited both crazing and pinholes in the AR coating.

7.2 Recommendations

7.2.1 ZnS/ZnSe

Material Studies

1. Further study of the ZnS/ZnSe diffuse transmittance at 1.06 microns is recommended to determine if the prime contributor was the thick ZnS layer or the interference between the ZnS and ZnSe.

2. Trade-off studies between optical transmission and electrical conductivity need to be done.

3. Bend bar testing of several groups (10-20 samples each) of mechanical samples needs to be done to quantify the effects of scratches and pits on the substrate strength.

4. Durability to blowing sand needs to be improved.

5. Grid manufacturing capability requires improvement, in adherence quality, denser mesh to improve RF attenuation, and reduced grid wire height to improve rain erosion resistance.

Coating Development

1. Coating development is necessary to eliminate the green light produced when the material is subjected to a 1.06 micron laser. Trade studies to address durability and transmission need to be performed.

7.2.2 GaAs

Material Studies

1. Further research and development should be conducted on meeting spectral transmission and electrical conductivity simultaneously and consistently between boules and within the same boule.

2. Investigation should continue on additional material hardening processes (such as post-processing of the GaAs boules) and the subsequent effect on bulk strength, stress, blowing sand, and rain erosion resistance, transmission, and conductivity.

Coating Development

1. The IAD process for Y_2O_3 needs to be optimized to improve its consistency of deposition, adhesion, sand/dust and rain durability, and 8-11.5 micron transmittance.

2. Investigation should continue for new GaAs exterior AR designs that provide better transmittance from 9.5 to 11.5 microns. (i.e., Itek has a new design that promises an additional 3% transmittance at 11.5 microns.)

7.2.3 ZnSe

Material Studies

1. Additional blowing sand erosion testing should be conducted to include higher wind velocity and a larger sampling of exposure times.

2. Investigation should continue on finer grid widths for reduced obscuration losses.

3. Replacment of the metallic mesh with a conductive coating which would not decrease the transmission below the goal should be explored.

APPENDIX A
SCATTER EFFECT OF GRID DIFFRACTION

A grid placed in the optical path of a light beam will act as a diffraction grating and cause a diffraction pattern to be produced. The Fraunhofer diffraction pattern is shown in Figure A-1. The pattern is composed of a central peak located on-axis and numerous side lobes or orders located at N λ/d radians off-axis where N is any integer, λ is wavelength, and d is grid spacing. The energy in each order is shown as a function of angle off normal. Note that two x-axes are shown in Figure A-1, one valid for 1 micron energy and one axis valid for 10 micron energy. The first side lobe for 1 micron energy occurs at approximately 0.28^{o} and for the 10 micron energy at 2.8^{o}. This means that the 10 micron energy is "scattered" or diffracted over a wider angle. When the wavelength of energy is the same order as the size of the grid wire width, the Fraunhofer diffraction theory is not completely valid. The theoretical predictions of side order positions is correct, but the magnitude of these orders is qualitative. Thus, with a 10 micron grid, the theory gives valid answers for magnitude and side order angle location for 1.06 micron wavelengths, but only gives valid side order location for the 10.6 micron wavelengths (Reference A-1).

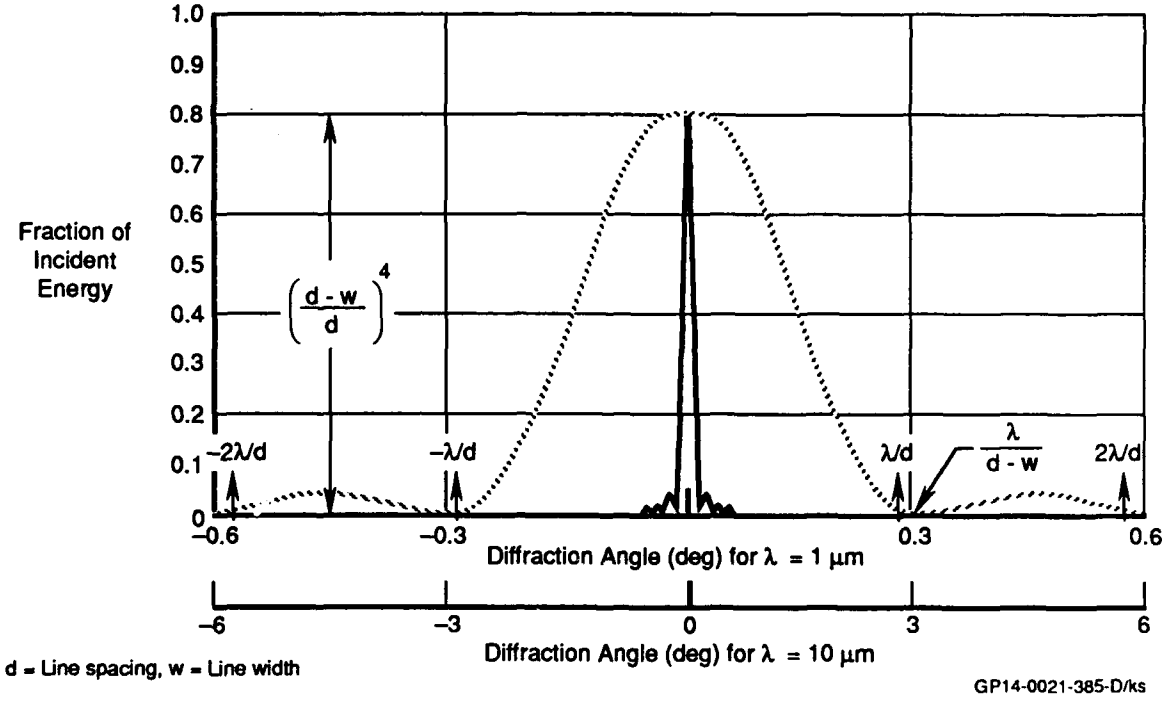

Figure A-1. Energy Spread Caused by Diffraction of a Grid Pattern
Line Width = 10 μm Line Spacing = 200 μm

Thus, a sensor with a 1.0 degree FOV would intercept the main beam and any side lobes within the $\pm 0.5^{o}$ diffraction angle. The normalized magnitude of each order can be computed by the equation:

$$\text{Energy (N)} = \left(\frac{d-w}{d}\right)^{4} \quad \text{sinc}^{2} \quad \left[\frac{N(d-w)}{d}\cdot\right]$$

where: d = line spacing
w = line width
N = Integer order number

The spacing between orders is λ/d. Figure A-2 shows the fraction of incident energy contained in each diffraction order and order spacing for both gridded materials for the main beam and four side lobes. Further computation shows that a significant percentage of the energy exists out to the 10th order.

	Material	
	ZnS/ZnSe	ZnSe
Line Spacing	400 microns	200 microns
Line Width	10 microns	10 microns
Spacing Between Orders	1.52°	3.04°
Order Number		
0	0.904	0.815
1	0.00059	0.0022
2	0.00058	0.0022
3	0.00058	0.0021
4	0.00057	0.00197

GP14-0021-386-D/dpt

Figure A-2. Fraction of Incident Energy in Each Order

APPENDIX B
THEORY OF SECOND HARMONIC (GREEN LIGHT) GENERATION AND ITS VISIBILITY RANGE

When subjected to high energy 1.06 micron laser transmission, some window materials exhibit non-linearities and convert some of this energy into 0.53 micron green light. The green light is a result of the non-linear relationship between the electric field (E) in the material caused by the laser and the resulting material polarization (P). The relationship between these two quantities is shown in Figure B-1.

For low energy systems, P and E, are linearly related. When stronger fields are incident on the window material, non-linear operation results, as shown in Figure B-1. Linearity exists for electric fields of strength less than some E_{max}. Stronger electric fields cause a non-linearity between the electric field and the resulting polarization.

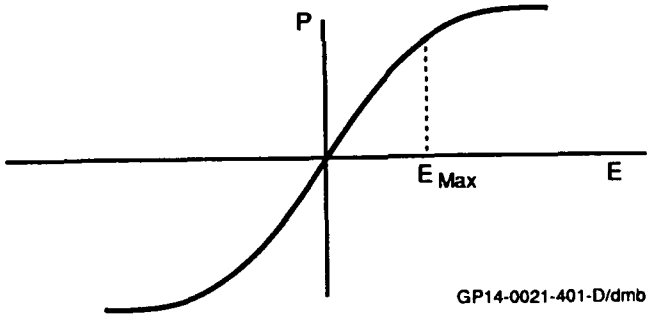

Figure B-1. Polarization and Electric Field

The generation of the second harmonic can be determined from Maxwell's Equation, which relates the electric field and polarization in a dielectric:

$$D = \epsilon E + P$$

where D = Flux density in dielectric
ϵ = Permittivity of dielectric
E = Electric field strength
P = Polarization

In general P can be related to E by a polynomial

$$P = a_1 E + a_2 E^2 + a_3 E^3 \ . \ . \ .$$

where the constants a_i are of decreasing value for the higher powers. For low power systems, the coefficients higher than a_1 are very small and can be neglected. For higher power levels, they must be included.

If E is a sinusoid:

$$E = E_o \cos wt$$

where E_o = magnitude
w = frequency

The second order term can be written as

$$a_2 E^2 = a_2 E_o^2 \cos^2 wt$$

$$= \frac{a_2 E_o^2}{2} (1 + \cos 2wt)$$

Thus:

$$P = a_1 E + \frac{a_2 E_0^2}{2} (1 + \cos 2wt) \ . \ . \ .$$

Thus we have shown that the non-linearity between E and P results in a second order harmonic as shown above.

Because the green light is visible, the covertness of the aircraft may be compromised. A first order analysis was made to determine the visibility range of the green light when viewed by an observer at night, since the human eye is most sensitive under darkness conditions. The significant effects on visibility such as atmospheric attenuation and the effect of range were included in the analysis. The conversion efficiency of the laser into

green light was measured. Approximately 1 part in 10^6 to 10^7 is converted for ZnS/ZnSe.

At large distances, the light source appears as a point source. The power density (P) of the source at a range R is

$$P = \frac{E}{\pi} \rho \tau \quad PRF/R^2$$

where E = Incident laser energy (joules)
ρ = Conversion efficiency
τ = Atmospheric transmission
PRF = Laser pulse repetition rate (Hz)
R = Range from source to observer (cm)

The effect of the atmosphere can be modeled by the equation:

$$\tau = e^{-\sigma R}$$

where σ = Atmospheric attenuation coefficient (km^{-1})
R = Range (km)

The attenuation coefficient is very dependent upon the atmospheric conditions, viewing path, and altitude between source and observer. Figures B-2 and B-3, taken from RCA, Reference B-1, may be used to determine σ. From Figure B-2, the sea level attenuation coefficient for green light on a clear day is:

$$\sigma_{SL} = 0.27$$

A typical viewing scenario might have the observer on the ground looking up at the source located at an altitude of 20,000 feet. Thus, the correction factor taken from Figure B-3 is:

$$\sigma_{corr} = 0.2$$

thus $\sigma = \sigma_{SL} \cdot \sigma_{corr}$
$= 0.054$

Figure B-4 shows the results of our initial analysis based upon the following parameters:

Laser energy	= 300 millijoules
Laser pulse rate	= 20 Hz
Conversion efficiency	= 10^{-6} and 10^{-7}

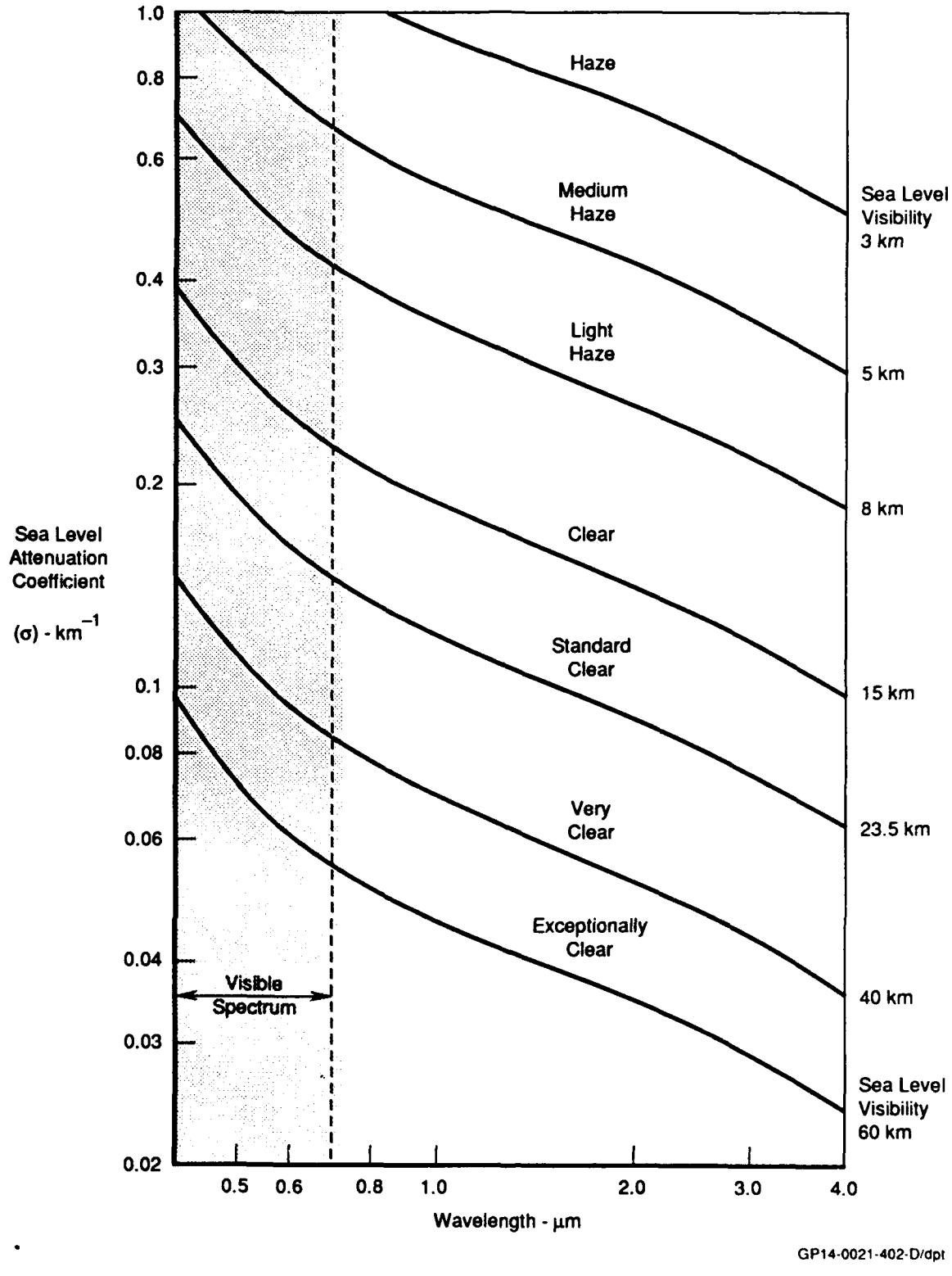

Figure B-2. Approximate Variation of Attention Coefficient With Wavelength at Sea Level for Various Atmospheric Conditions. Neglects Absorption by Water Vapor and Carbon Dioxide

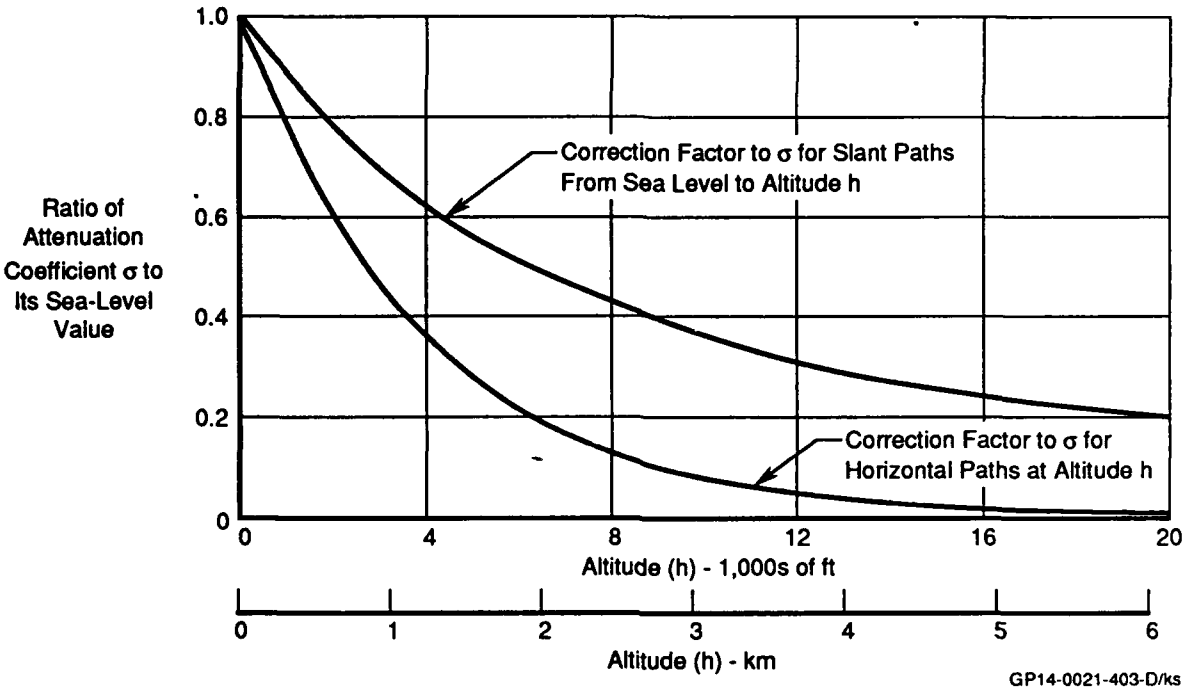

Figure B-3. Approximate Ratio of Attenuation Coefficient to Sea-Level Value for Slant Paths and Horizontal Paths. Neglects Absorption by Water Vapor and Carbon Dioxide

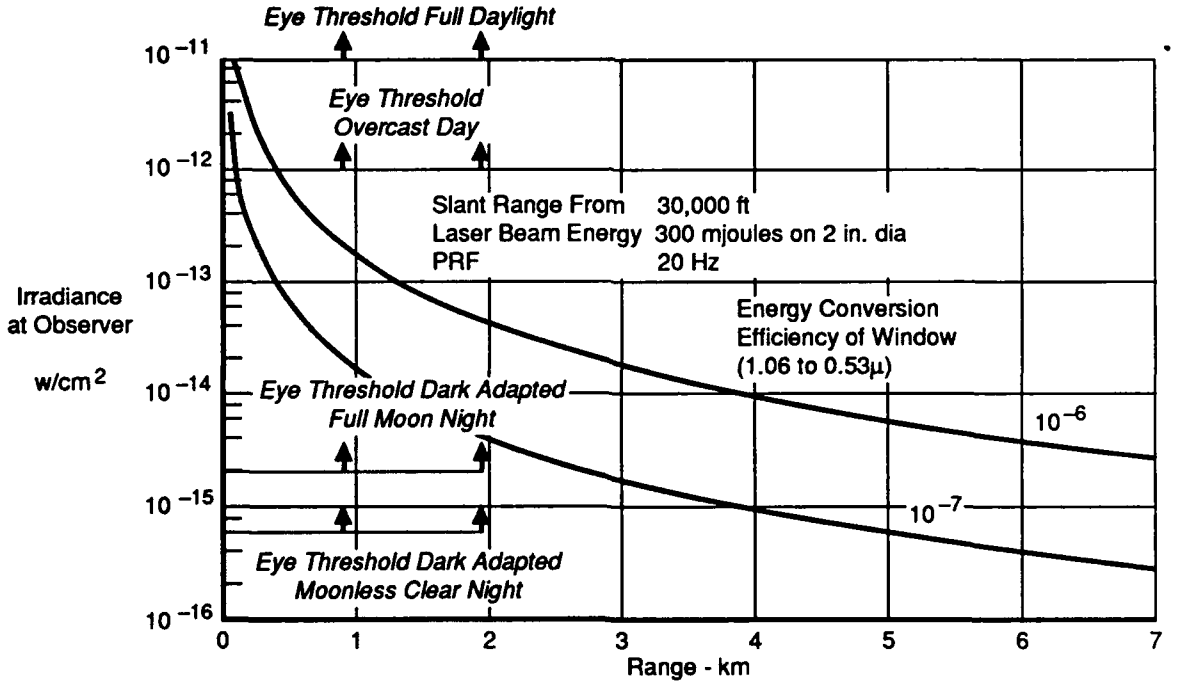

Figure B-4. Visibility of Green Light as Affected by Atmosphere

Also shown plotted on this Figure are the human eye thresholds for four background lighting conditions: dark adapted moonless night, dark adapted full moon night, overcast day, and full daylight. The dark adapted cases include the eye's response for scotopic viewing at 0.532 microns. The daylight cases are photopic viewing at the same wavelength. Figure B-4 indicates that the light source can be detected at ranges greater than 4 kilometers on a moonless night and 2 to 3 kilometers on a full moon night. Because the eye is not as sensitive for daylight viewing, the range is much less, in the range of 100-200 meters on an overcast day or full daylight day.

APPENDIX C

RAIN EROSION TEST RESULTS

This appendix contains detailed documentation of the effect of rain erosion on the physical condition and optical performance of ZnS/ZnSe, GaAs, and ZnSe window materials. The rain erosion tests were conducted under contract by the University of Dayton Research Institute at the Materials Directorate System Support Division's Rain Erosion Test Facility, Wright Patterson AFB. The optical tests before and after rain erosion were conducted by General Dynamics-Fort Worth.

6 minute Exposure
Sample #8

6 minute Exposure
Sample #9

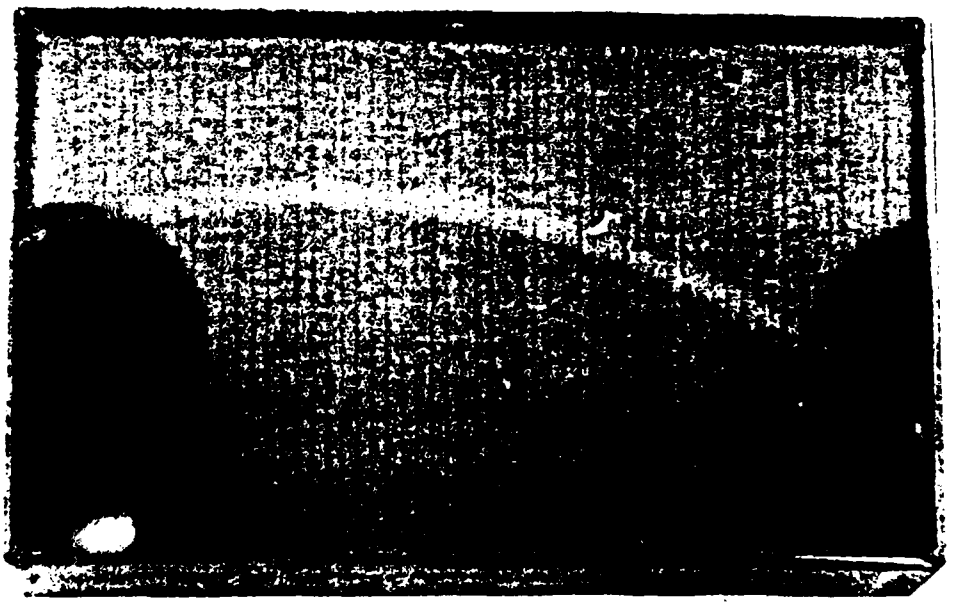

GP14-0021-335

Figure C-1. Photographs of Samples After Rain Erosion Exposure ZnS/ZnSe

8 minute Exposure
Sample #10

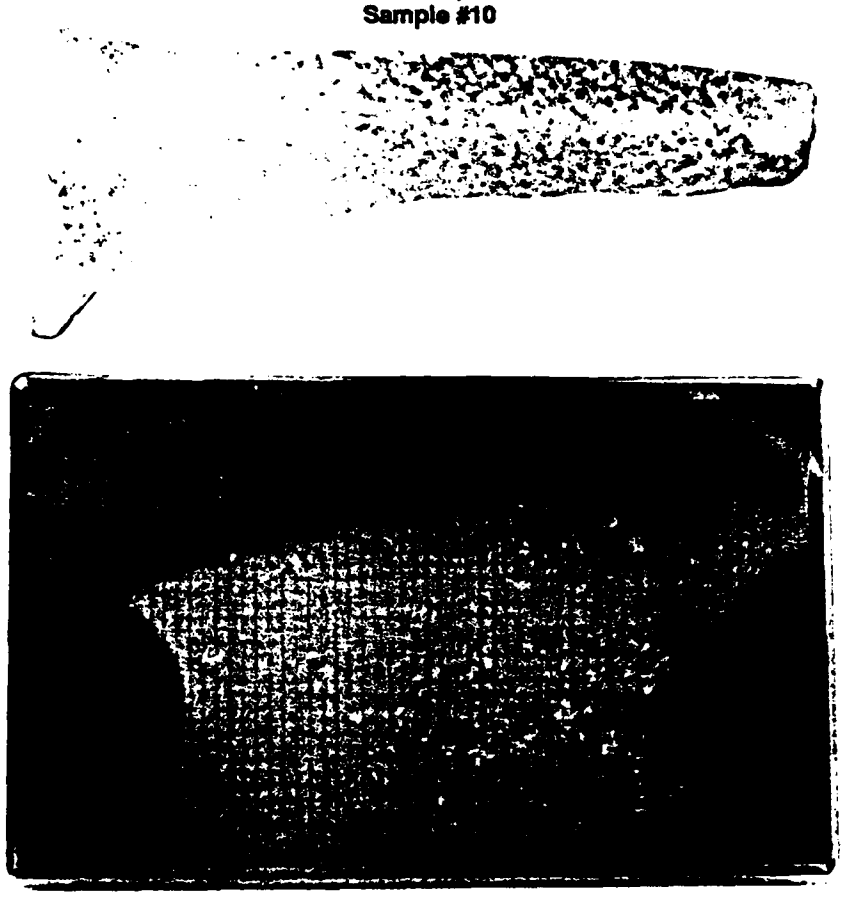

8 minute Exposure
Sample #11

GP14-0621-336

Figure C-1. (Concluded) Photographs of Samples After Rain Erosion Exposure ZnS/ZnSe

22 minute Exposure
Sample #14

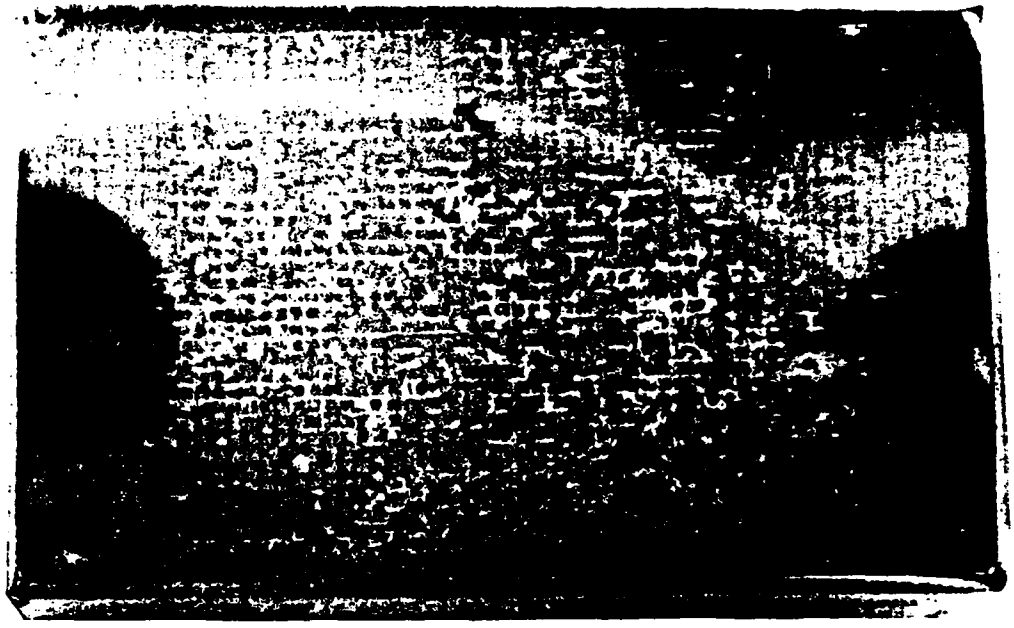

22 minute Exposure
Sample #15

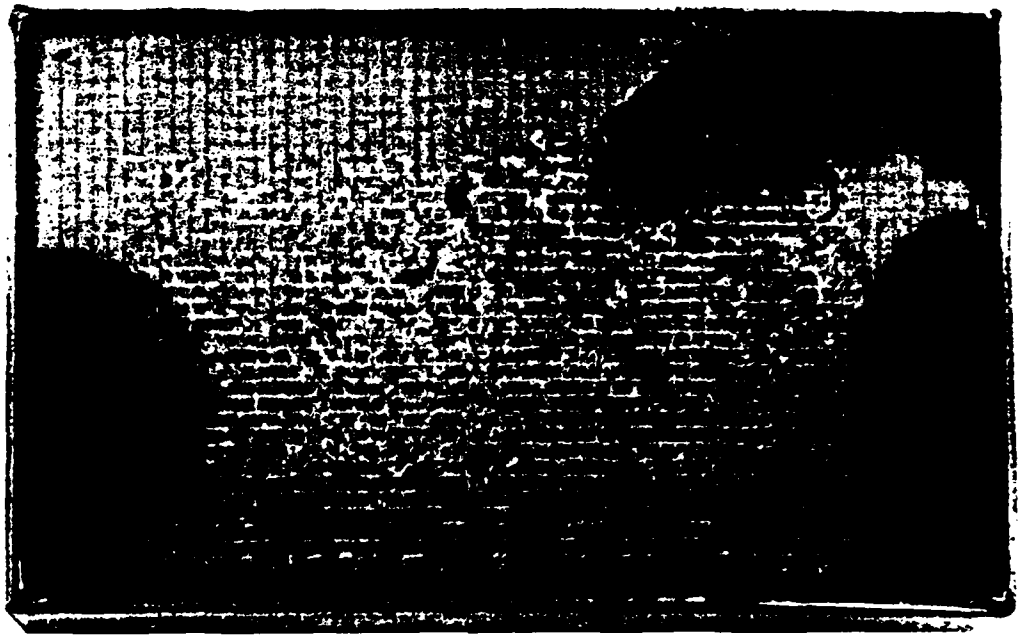

GP14-0021-337

Figure C-1. (Continued) Photographs of Samples After Rain Erosion Exposure ZnS/ZnSe

30 minute Exposure
Sample #1

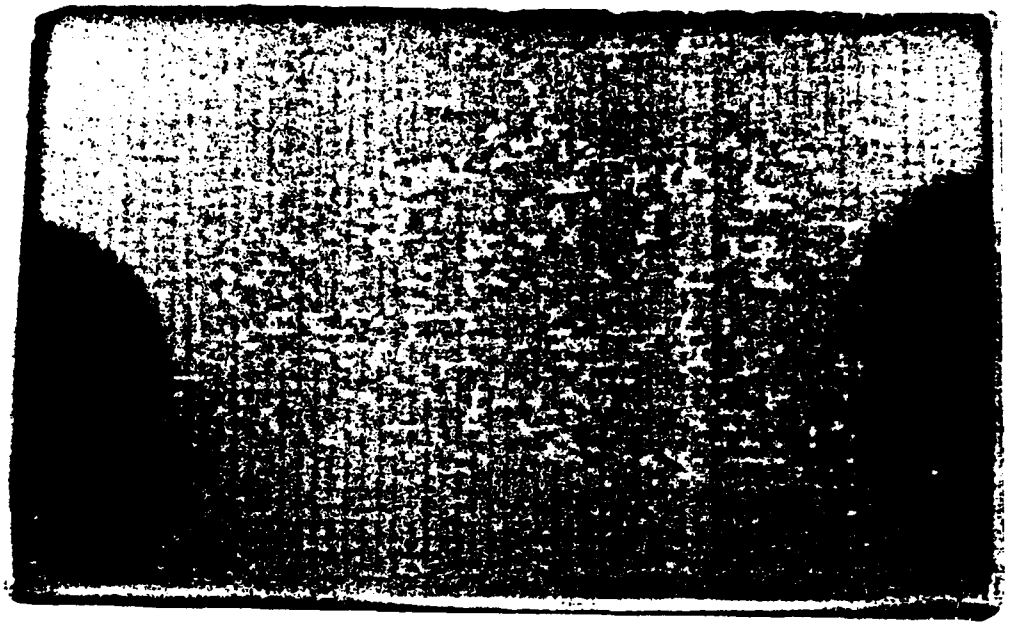

30 minute Exposure
Sample #2

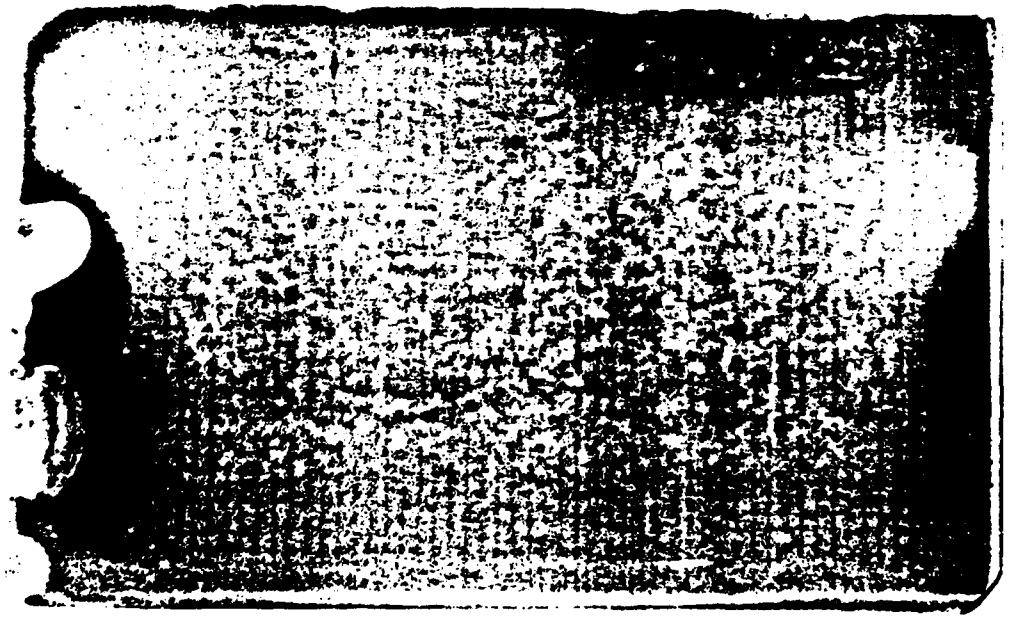

GP14-0021-338

Figure C-1. (Continued) Photographs of Samples After Rain Erosion Exposure
ZnS/ZnSe

30 minute Exposure
Sample #3

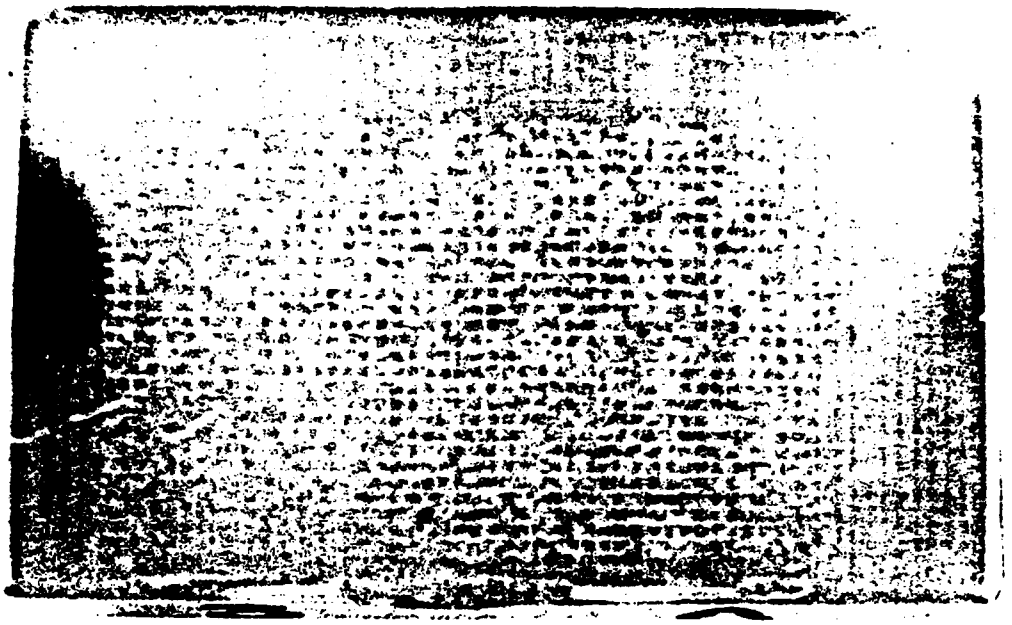

30 minute Exposure
Sample #4

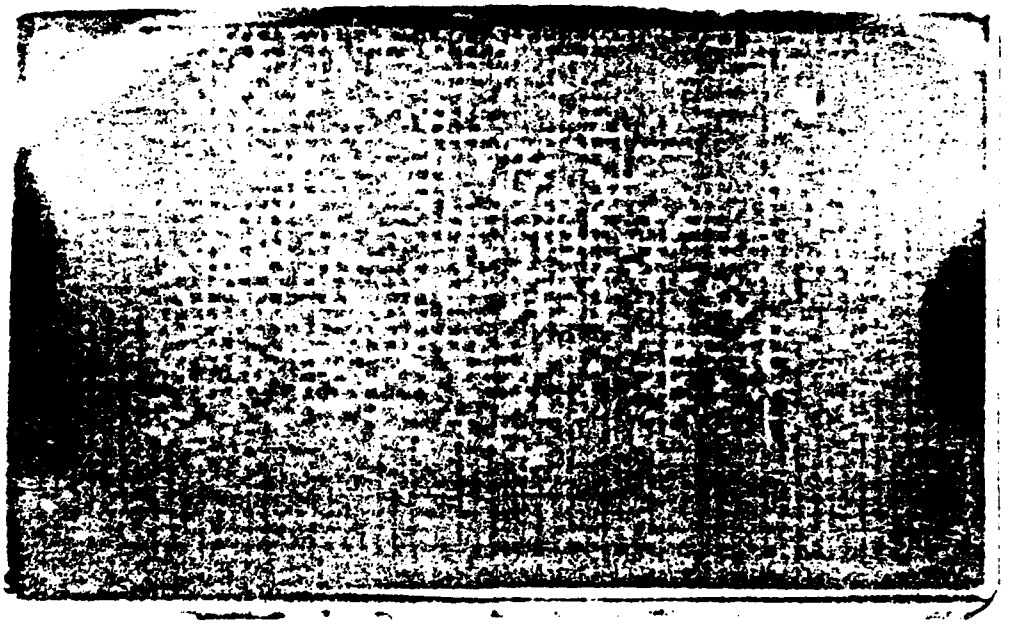

GP14-0021-339

Figure C-1. (Continued) Photographs of Samples After Rain Erosion Exposure ZnS/ZnSe

30 minute Exposure
Sample #5

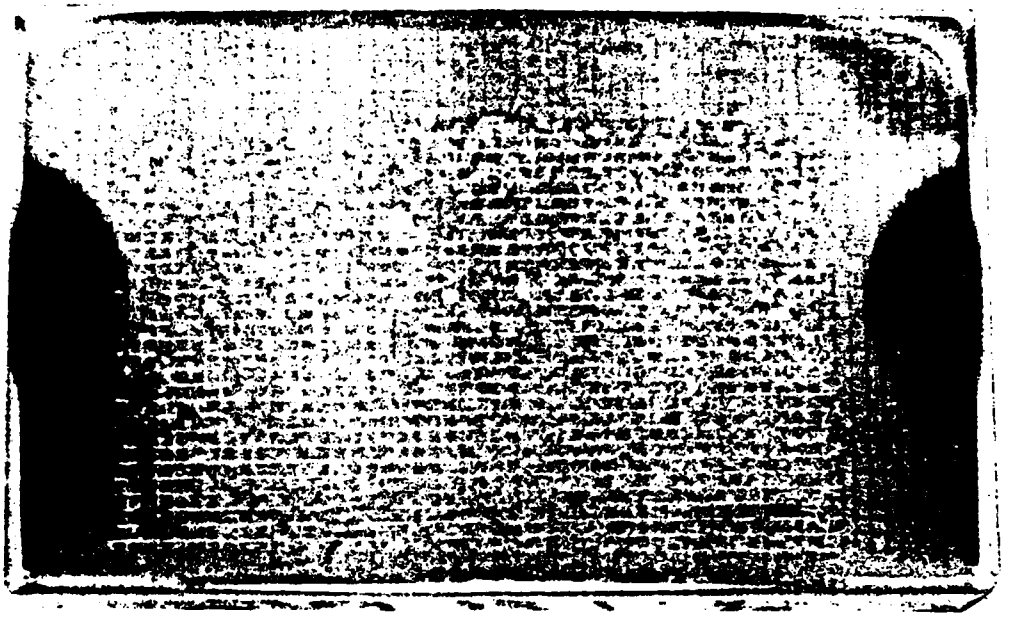

30 minute Exposure
Sample #7

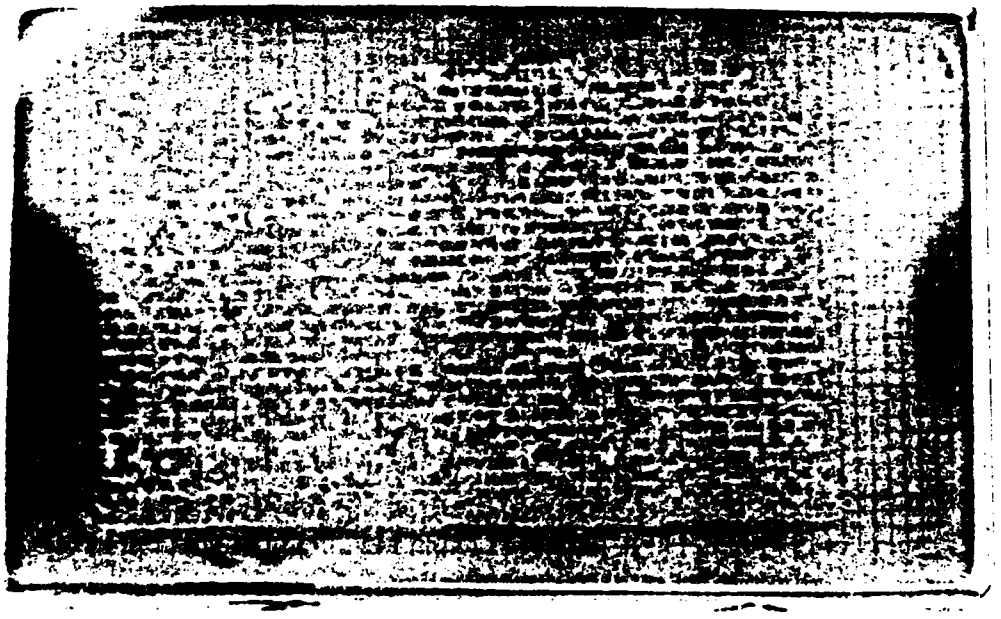

GP14-0021-340

Figure C-1. (Continued) Photographs of Samples After Rain Erosion Exposure ZnS/ZnSe

2 minute Exposure
Sample #13

2 minute Exposure
Sample #14

GP14-0021-341

Figure C-2. Photographs of Samples After Rain Erosion Exposure GaAs

4 minute Exposure
Sample #15

4 minute Exposure
Sample #16

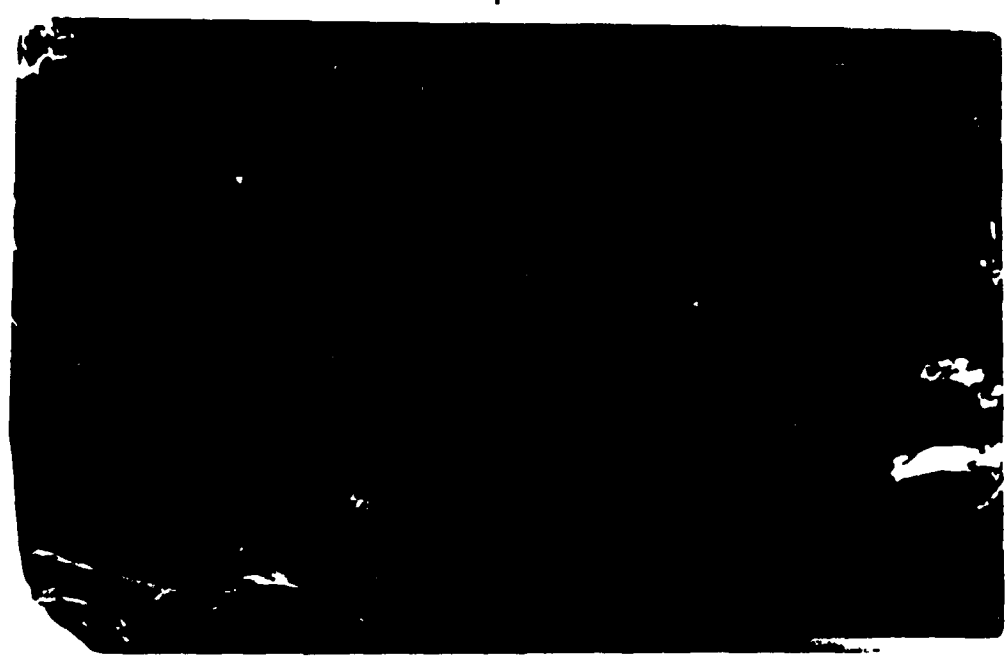

GP14-0021-342

Figure C-2. (Continued) Photographs of Samples After Rain Erosion Exposure GaAs

8 minute Exposure
Sample #1

8 minute Exposure
Sample #2

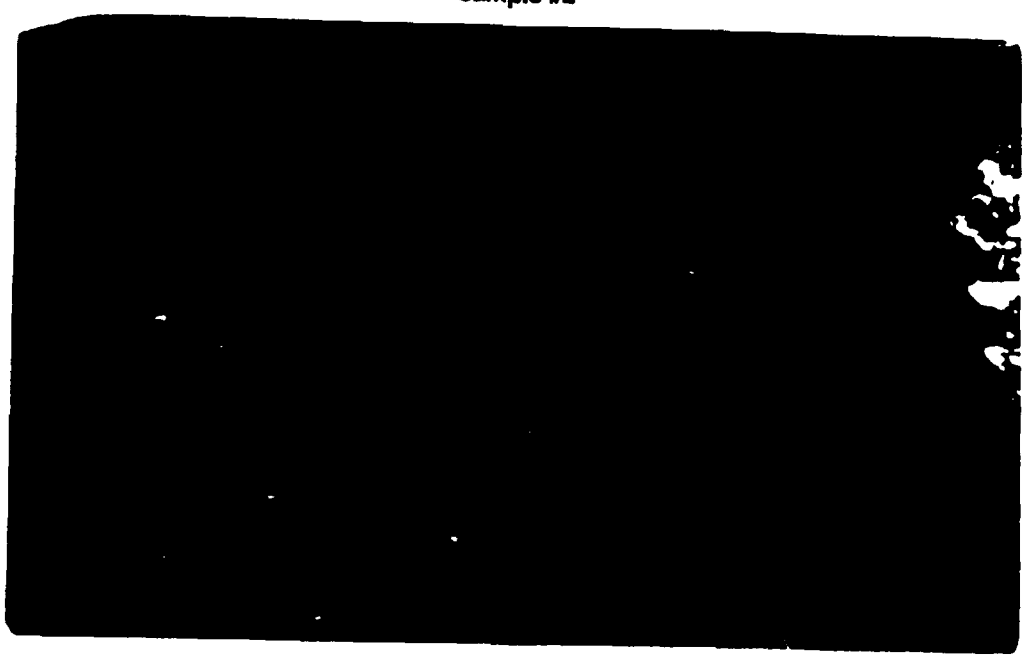

GP14-0021-343

Figure C-2. (Continued) Photographs of Samples After Rain Erosion Exposure
GaAs

20 minute Exposure
Sample #3

20 minute Exposure
Sample #6

GP14-0021-344

Figure C-2. (Continued) Photographs of Samples After Rain Erosion Exposure GaAs

20 minute Exposure
Sample #8

20 minute Exposure
Sample #9

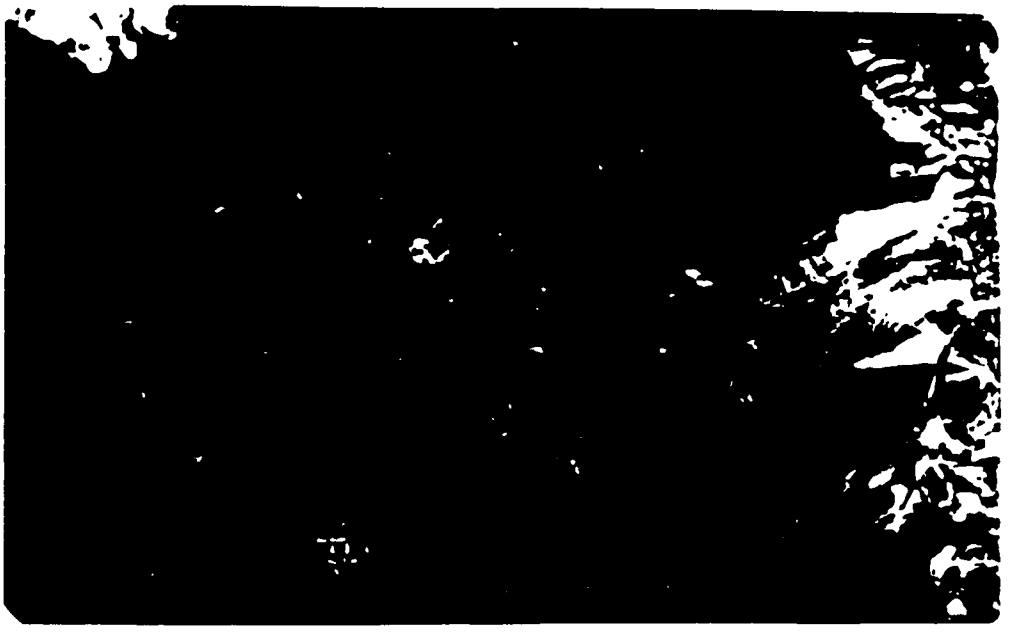

GP14-0021-345

Figure C-2. (Continued) Photographs of Samples After Rain Erosion Exposure GaAs

30 minute Exposure
Sample #11

30 minute Exposure
Sample #12

GP14-0021-346

Figure C-2. (Concluded) Photographs of Samples After Rain Erosion Exposure GaAs

2 minute Exposure
Sample #7

2 minute Exposure
Sample #8

GP14-0021-347

Figure C-3. (Continued) Photographs of Samples After Rain Erosion Exposure ZnSe

8 minute Exposure
Sample #9

8 minute Exposure
Sample #10

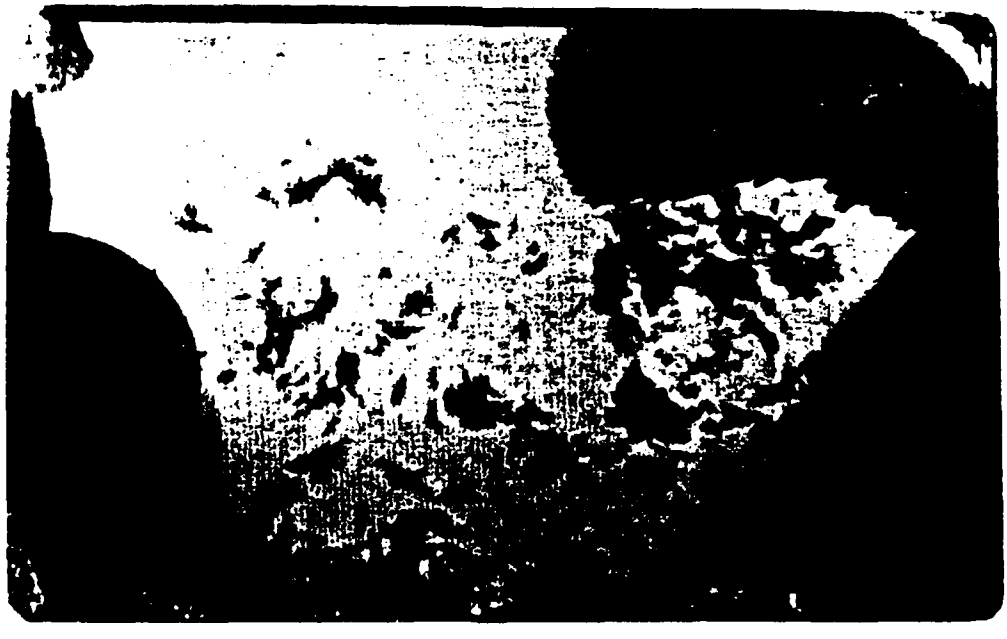

GP14-0021-348

Figure C-3. (Continued) Photographs of Samples After Rain Erosion Exposure ZnSe

12 minute Exposure
Sample #12

12 minute Exposure
Sample #15

GP14-0021-349

Figure C-3. (Continued) Photographs of Samples After Rain Erosion Exposure
ZnSe

20 minute Exposure
Sample #1

20 minute Exposure
Sample #4

GP14-0021-350

Figure C-3. (Continued) Photographs of Samples After Rain Erosion Exposure
ZnSe

20 minute Exposure
Sample #5

20 minute Exposure
Sample #6

GP14-0021-351

Figure C-3. (Concluded) Photographs of Samples After Rain Erosion Exposure
ZnSe

30 minute Exposure
Sample #2

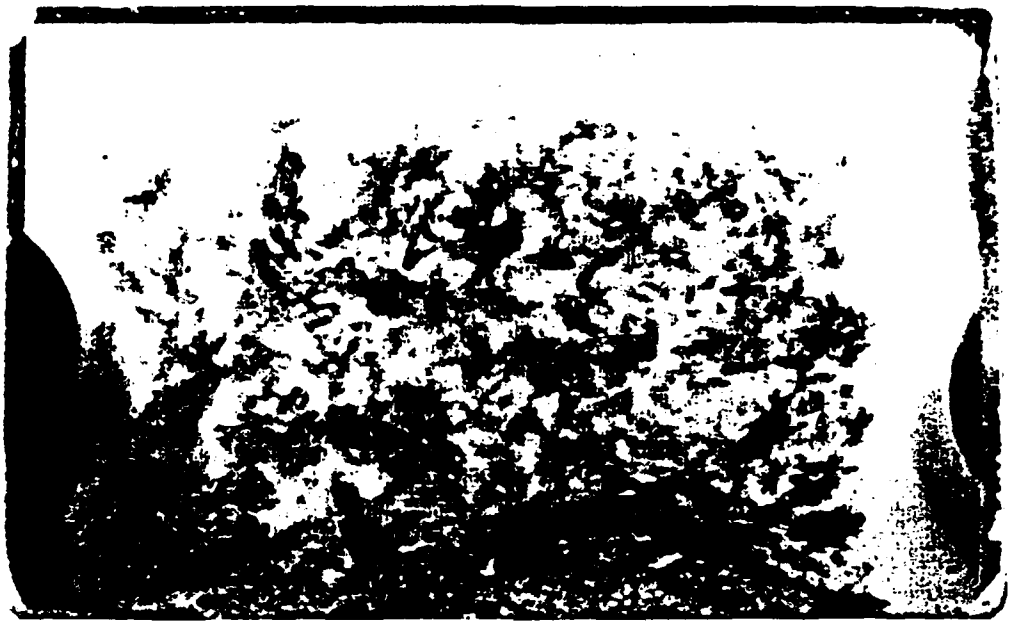

30 minute Exposure
Sample #3

GP14-0021-352

Figure C-3. Photographs of Samples After Rain Erosion Exposure
ZnSe

Sample Number	Exposure Time (min)	Diffuse Transmittance (%)		
		Before Exposure	After Exposure	Difference
ZnS/ZnSe				
8	6	24.0	23.1	–0.9
9	6	25.8	25.5	–0.3
10	8	24.7	23.4	–1.30
11	8	23.3	23.4	0.10
14	22	25.9	27.7	1.80
15	22	25.7	27.7	2.00
1	30	24.9	27.7	2.80
2	30	23.1	27.7	4.60
3	30	25.2	31.5	6.30
4	30	25.4	31.9	6.50
5	30	23.1	31.9	8.80
7	30	25.3	29.8	4.50
GaAs				
13	2	0.5	0.2	–0.3
14	2	0.4	0.2	–0.2
15	4	0.4	1.7	1.3
16	4	0.5	1.5	1.0
1	8	N/A	N/A	–
2	8	0.1	1.5	1.4
3	20	0.1	1.9	1.8
4	20	0.1	2.9	2.8
8	20	0.1	3.2	3.1
9	20	0.2	3.4	3.2
11	30	0.6	4.5	3.9
12	30	0.5	4.7	4.2
ZnSe				
7	2	2.9	3.2	0.3
8	2	2.2	2.6	0.4
9	8	2.2	4.0	1.8
10	8	2.6	4.4	1.8
12	12	2.7	9.7	2.0
15	12	3.1	7.4	4.3
1	20	2.5	13.2	10.70
4	20	2.6	10.9	8.30
5	20	2.9	12.6	9.70
6	20	2.9	9.7	6.80
2	30	2.9	13.2	10.30
3	30	2.9	12.6	9.70

GP14-0021-314-D/df

Figure C-4. Change In Diffuse Transmittance Due to Rain Erosion

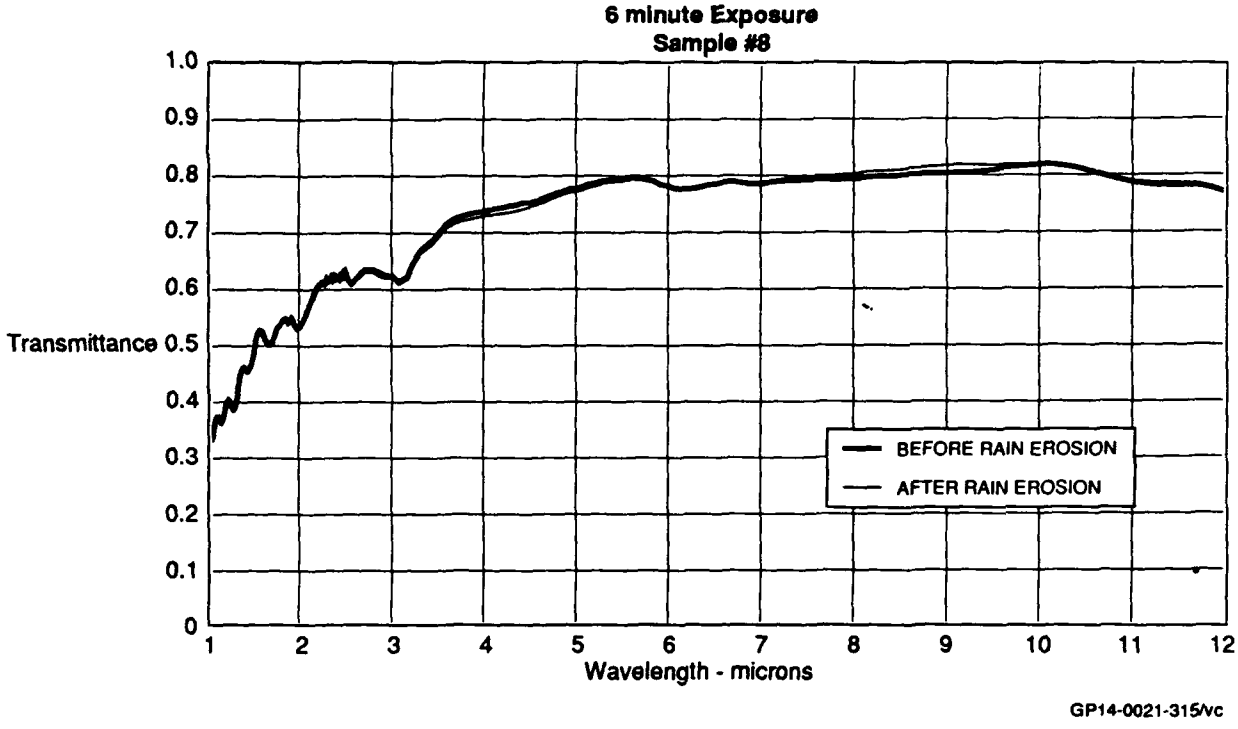

Figure C-5. Change in Transmission Following Rain Erosion Exposure
ZnS/ZnSe

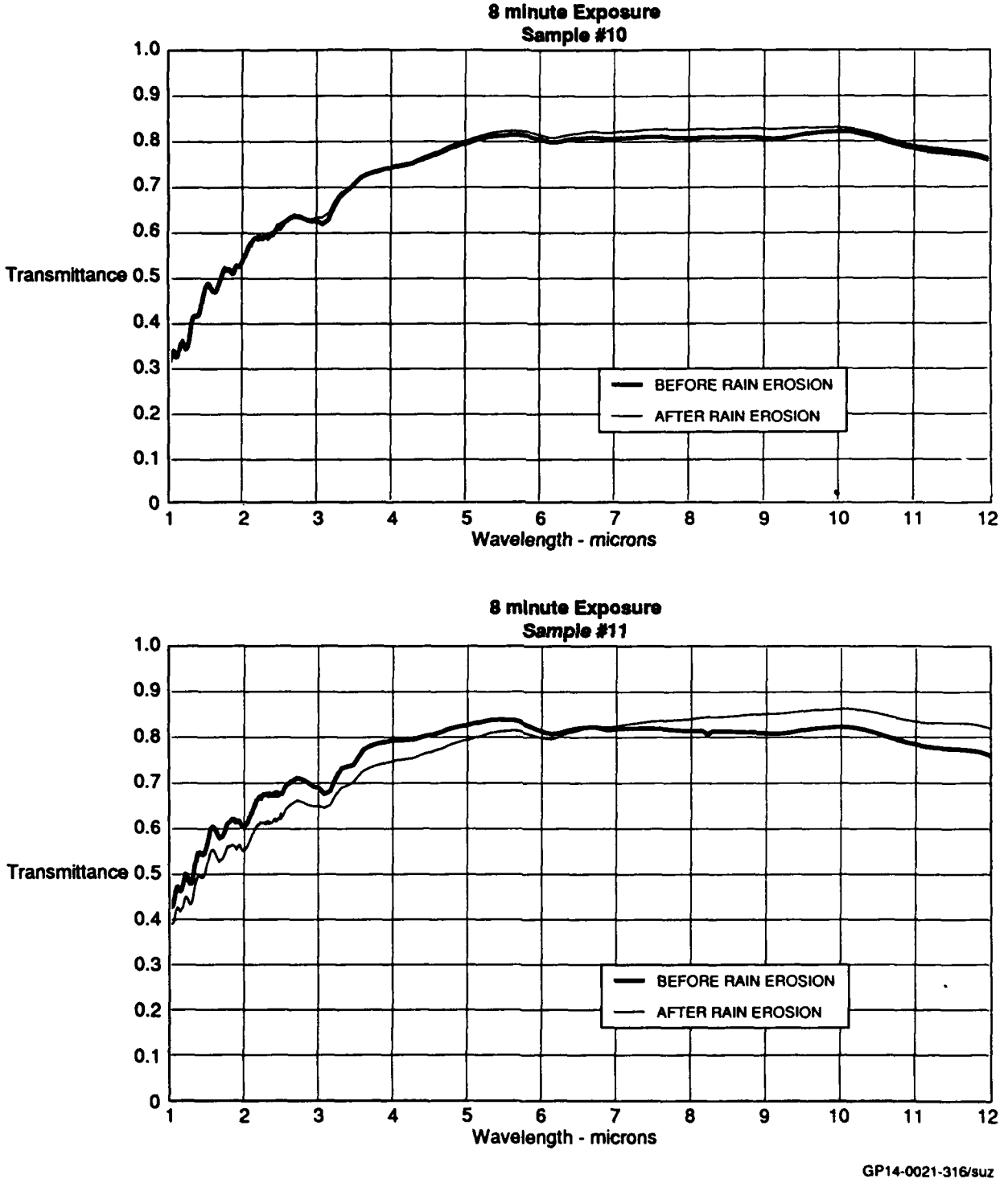

Figure C-5. (Continued) Change in Transmission Following Rain Erosion Exposure
ZnS/ZnSe

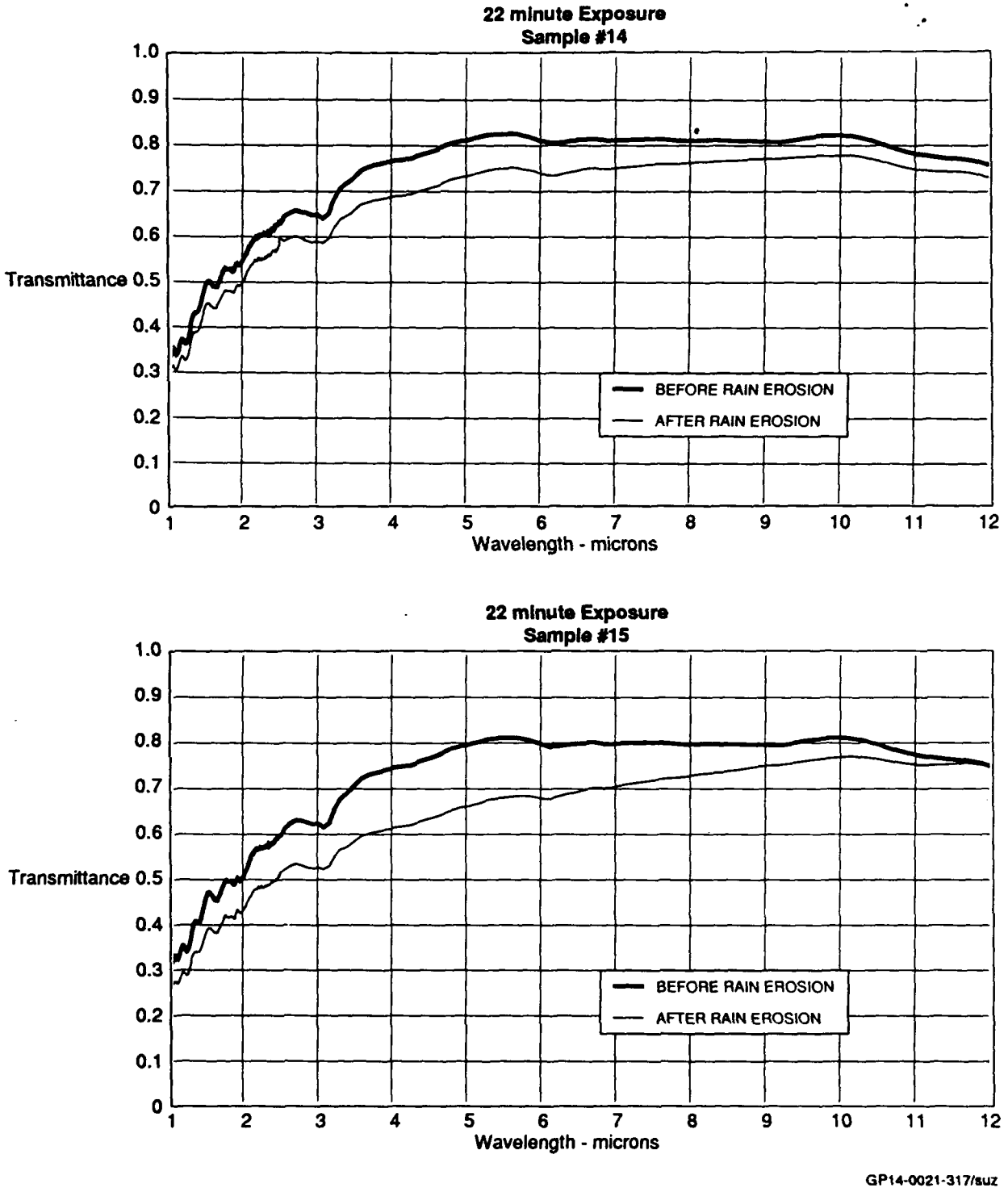

Figure C-5. (Continued) Change in Transmission Following Rain Erosion Exposure
ZnS/ZnSe

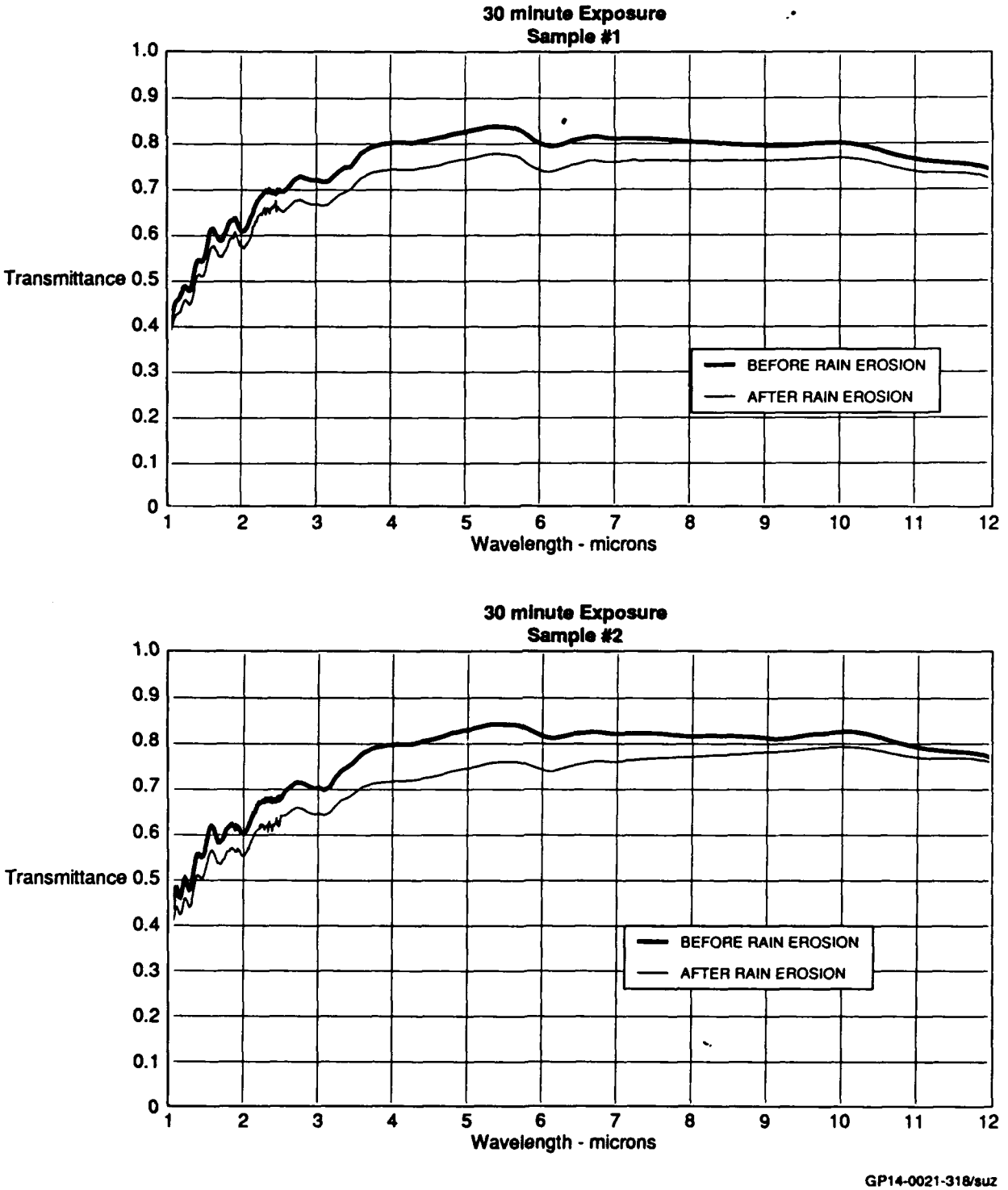

Figure C-5. (Continued) Change in Transmission Following Rain Erosion Exposure
ZnS/ZnSe

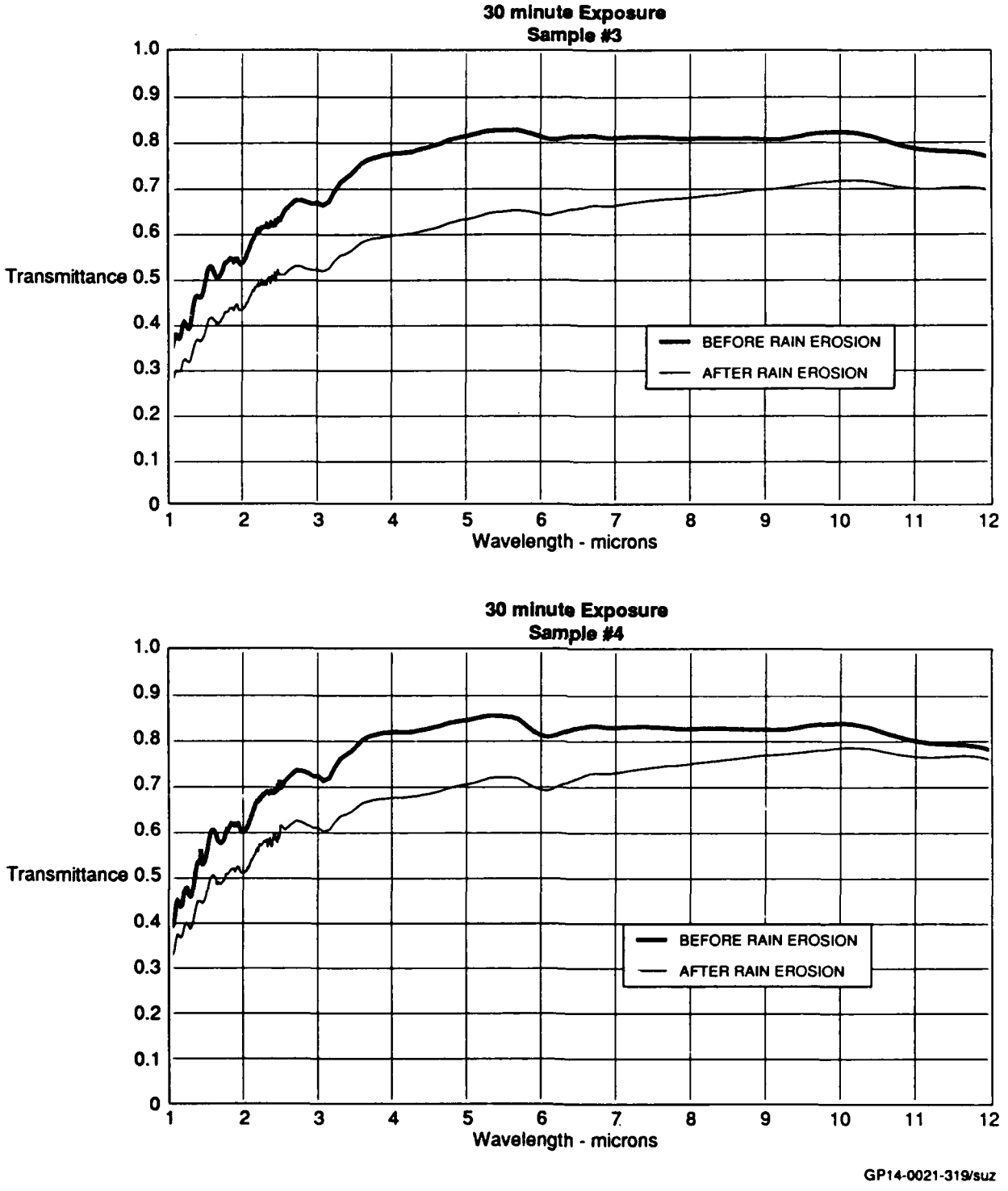

Figure C-5. (Continued) Change in Transmission Following Rain Erosion Exposure
ZnS/ZnSe

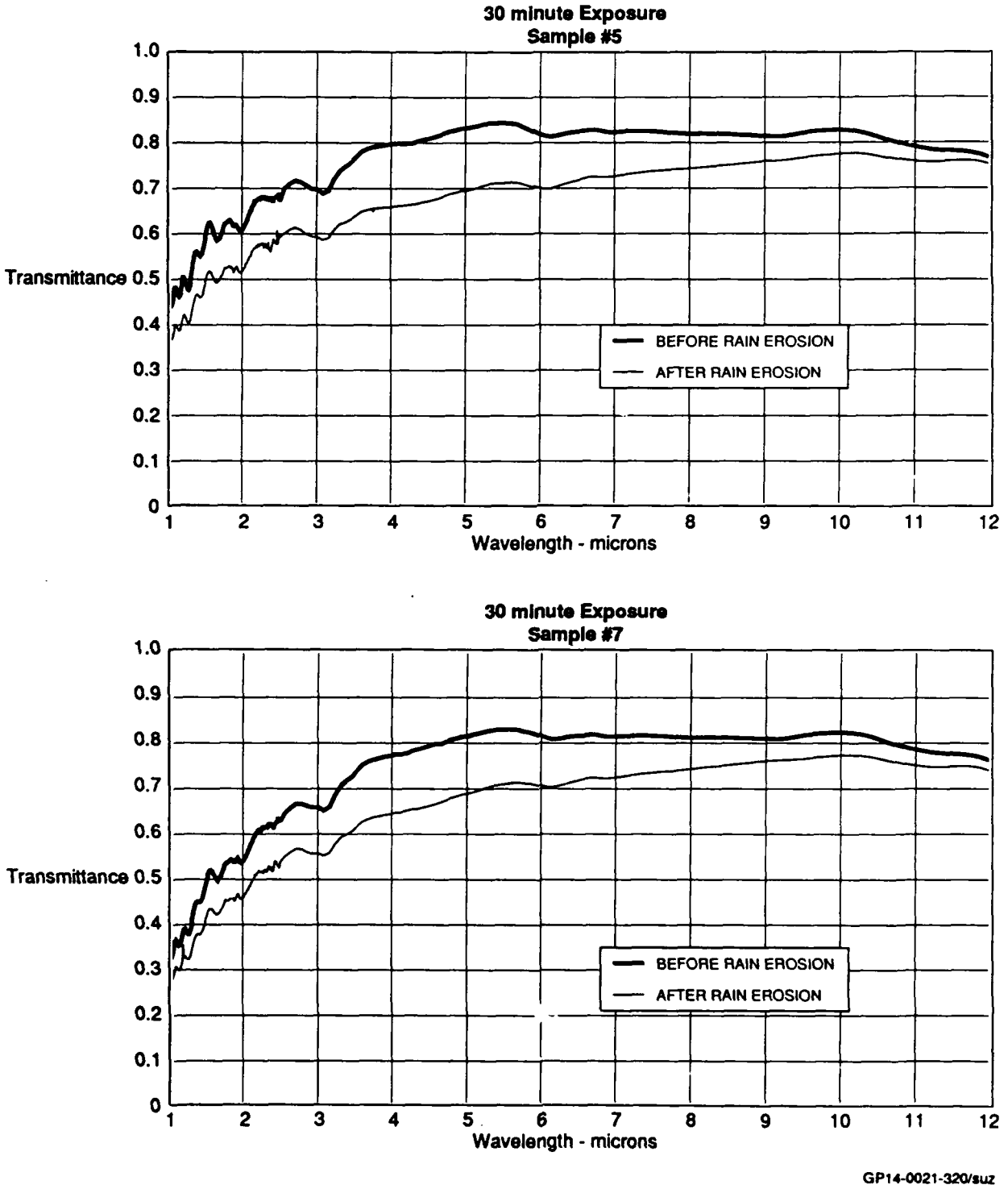

Figure C-5. (Concluded) Change in Transmission Following Rain Erosion Exposure
ZnS/ZnSe

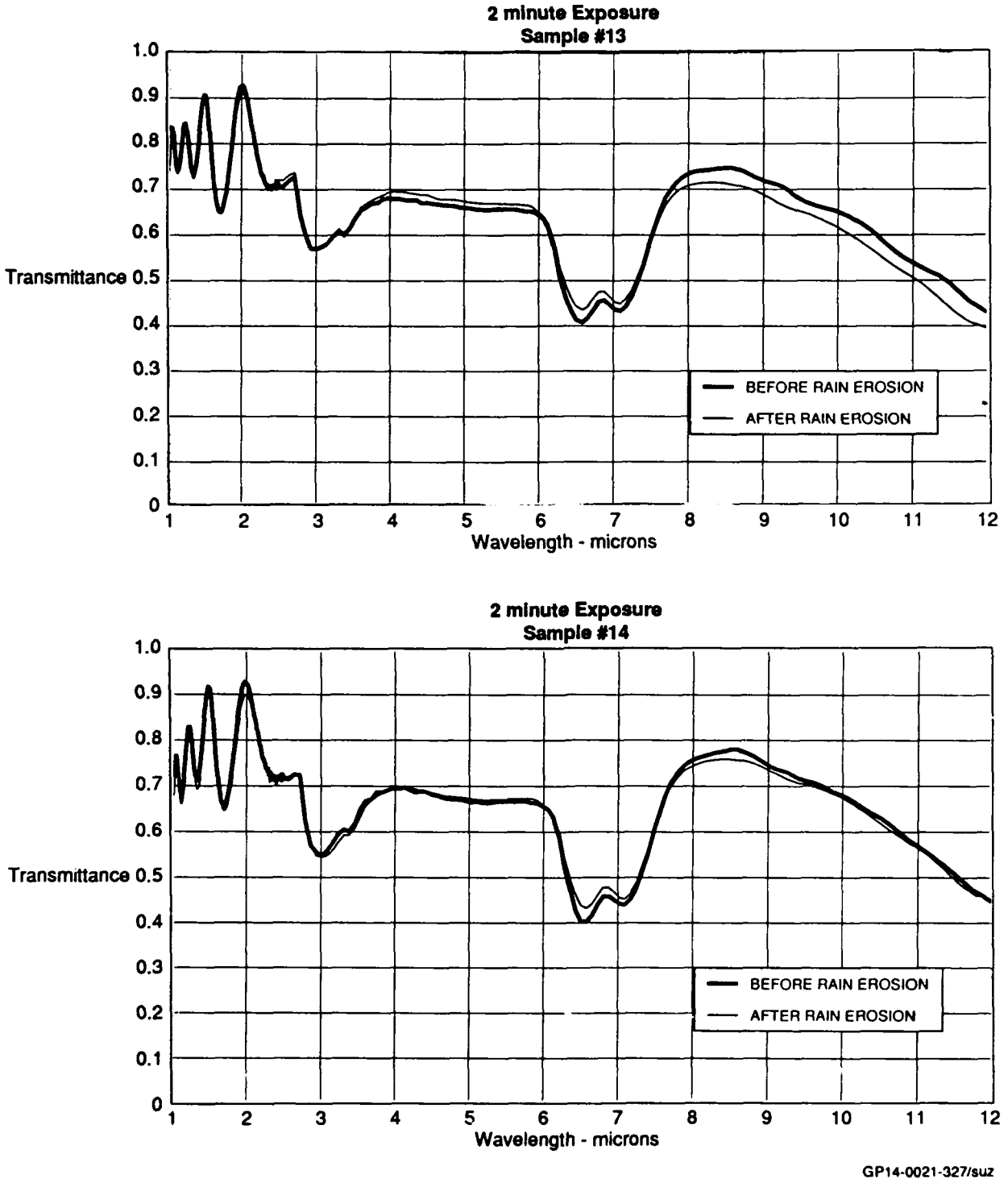

Figure C-6. Change in Transmission Following Rain Erosion Exposure GaAs

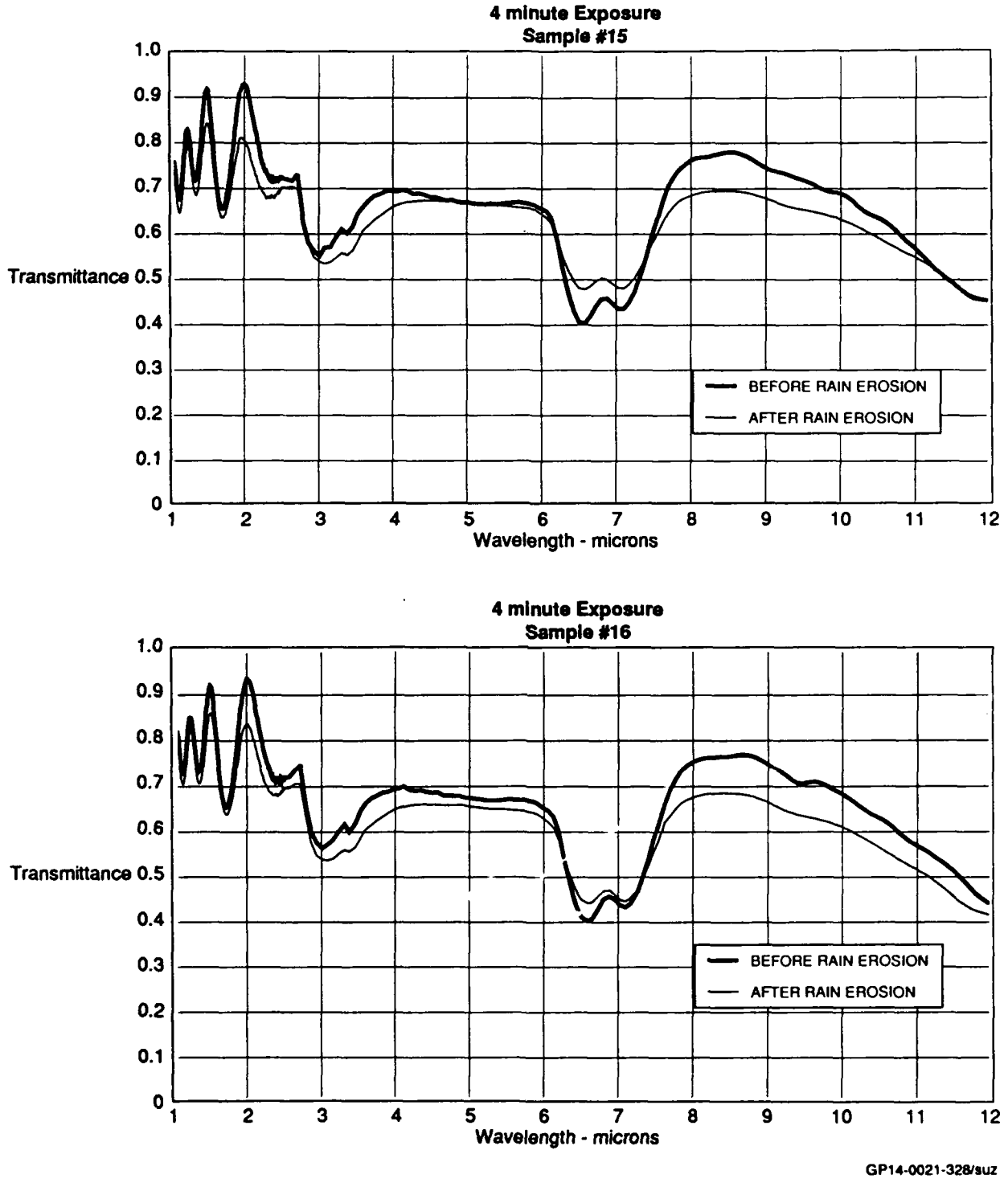

Figure C-6. (Continued) Change in Transmission Following Rain Erosion Exposure GaAs

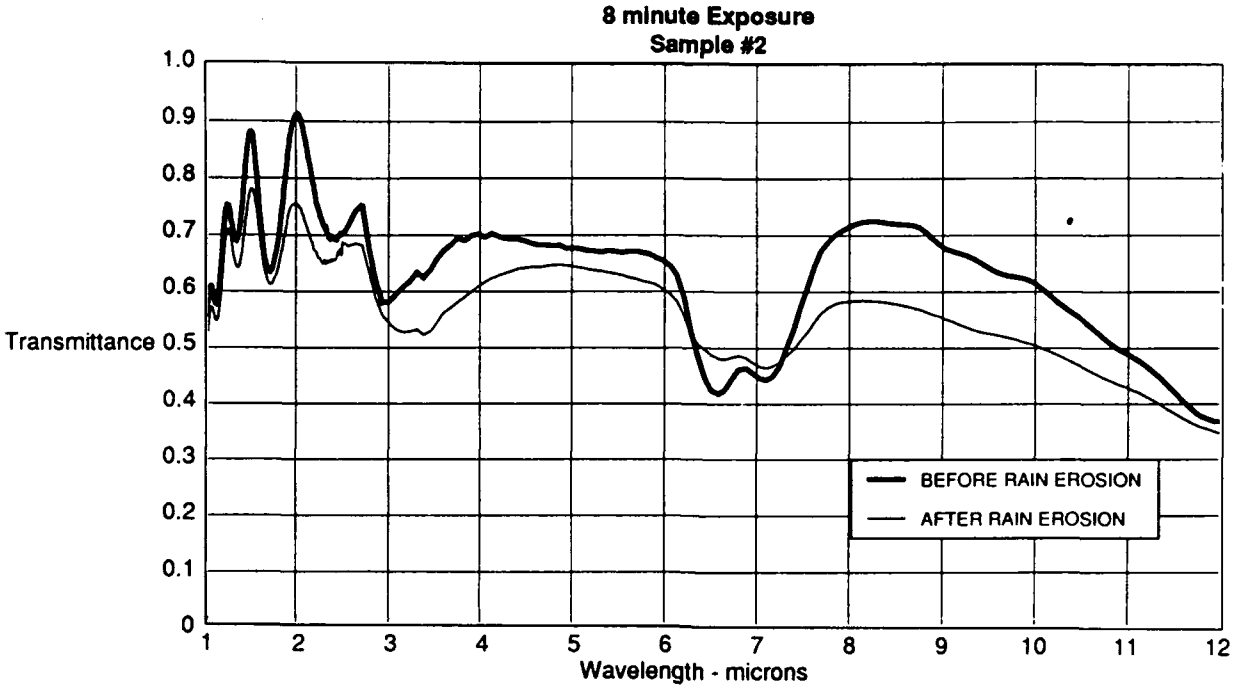

Figure C-6. (Continued) Change in Transmission Following Rain Erosion Exposure
GaAs

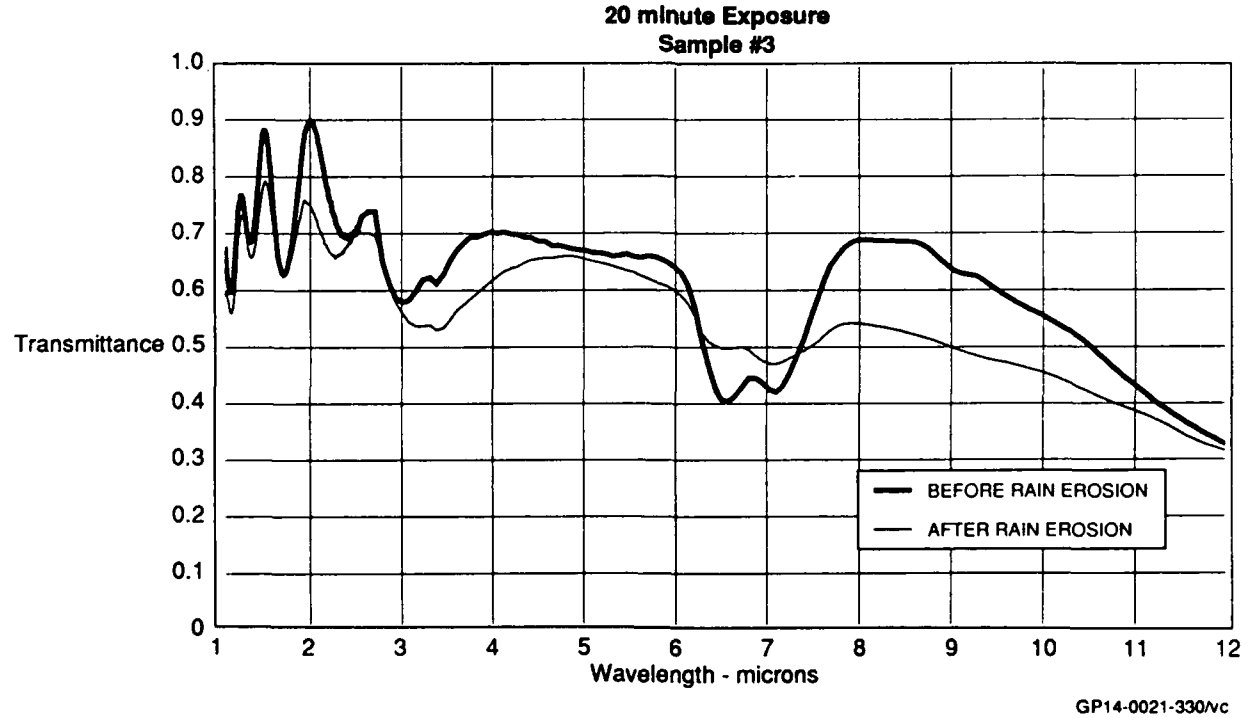

Figure C-6. (Continued) Change in Transmission Following Rain Erosion Exposure
GaAs

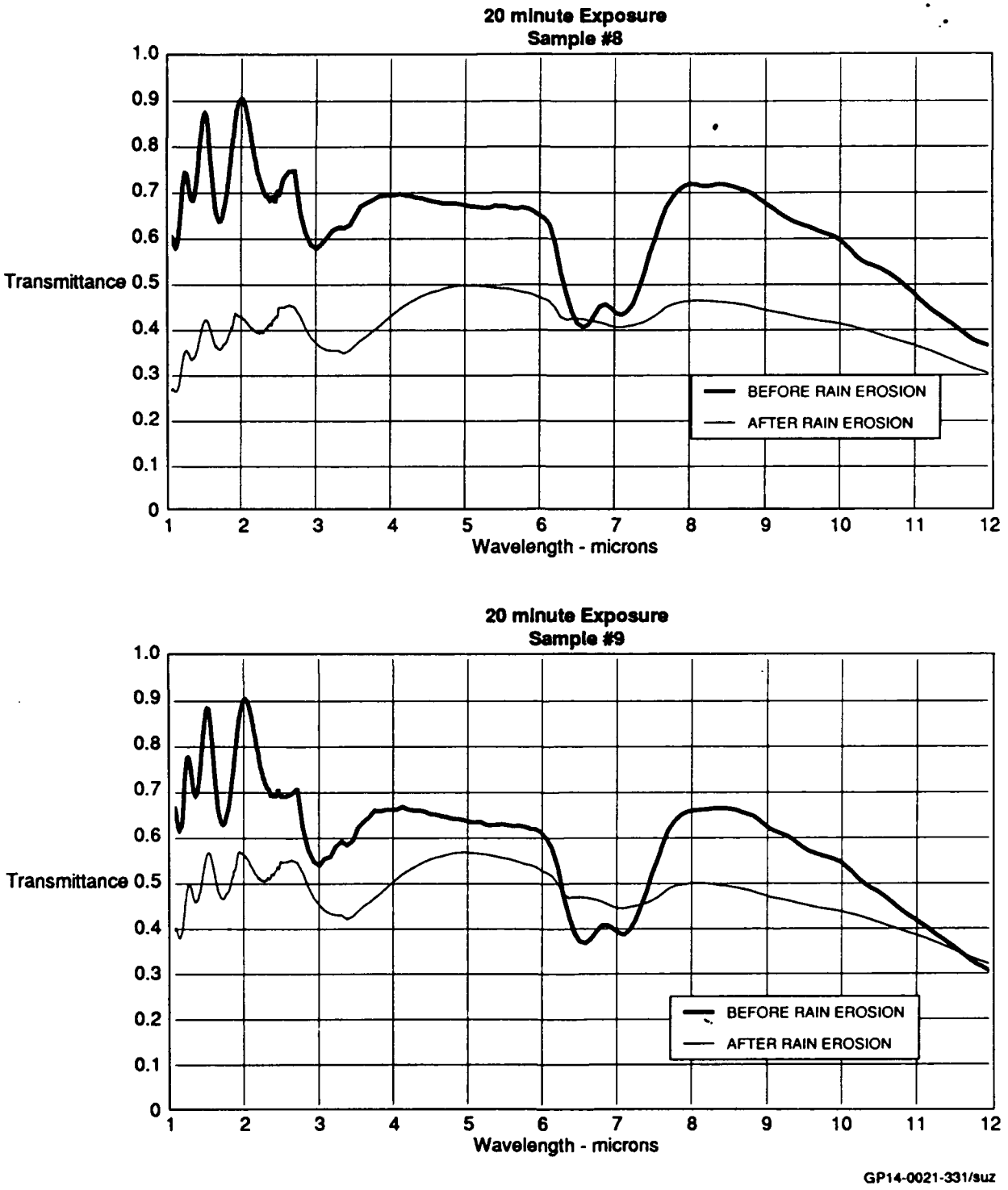

Figure C-6. (Continued) Change in Transmission Following Rain Erosion Exposure GaAs

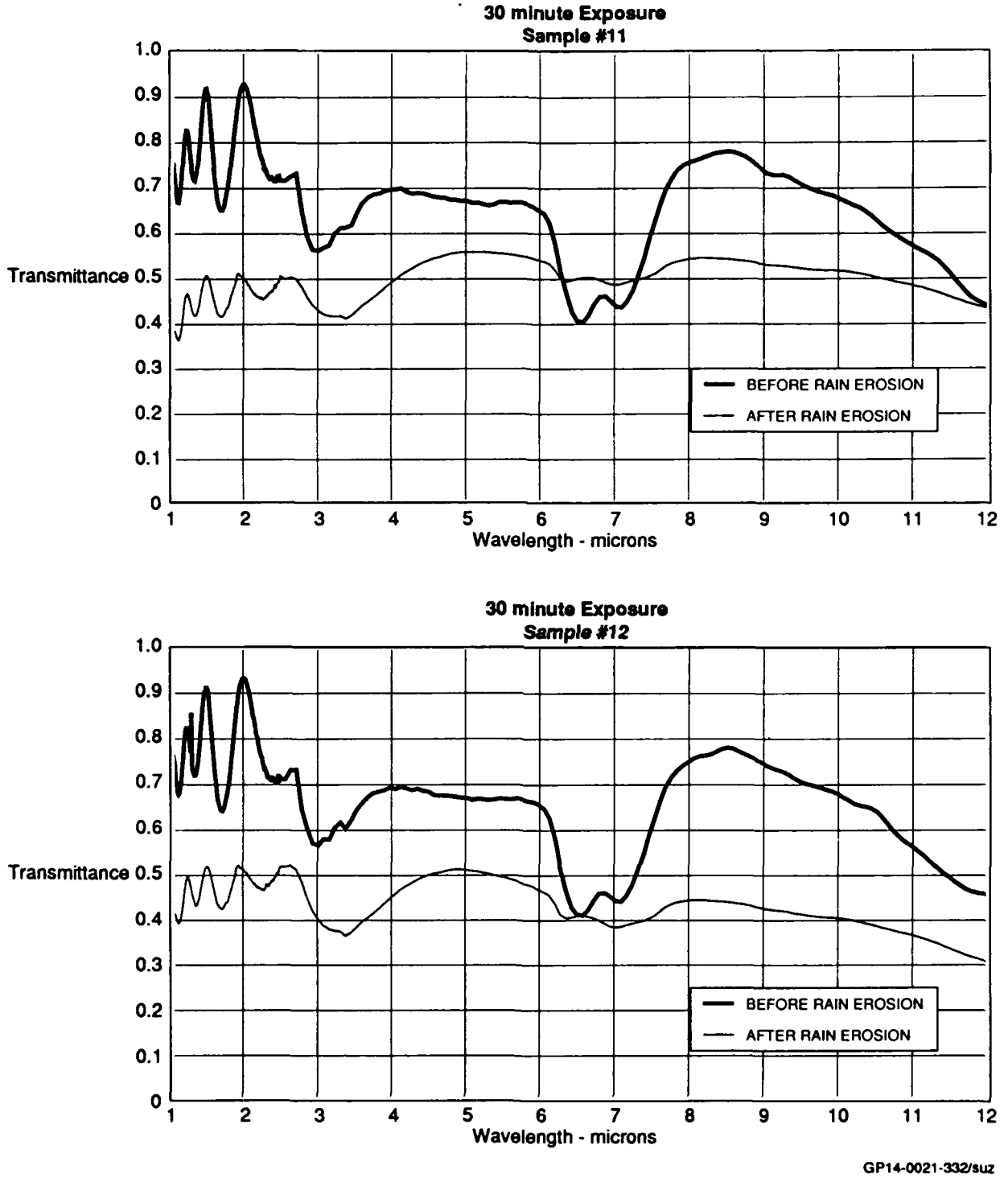

Figure C-6. (Concluded) Change in Transmission Following Rain Erosion Exposure GaAs

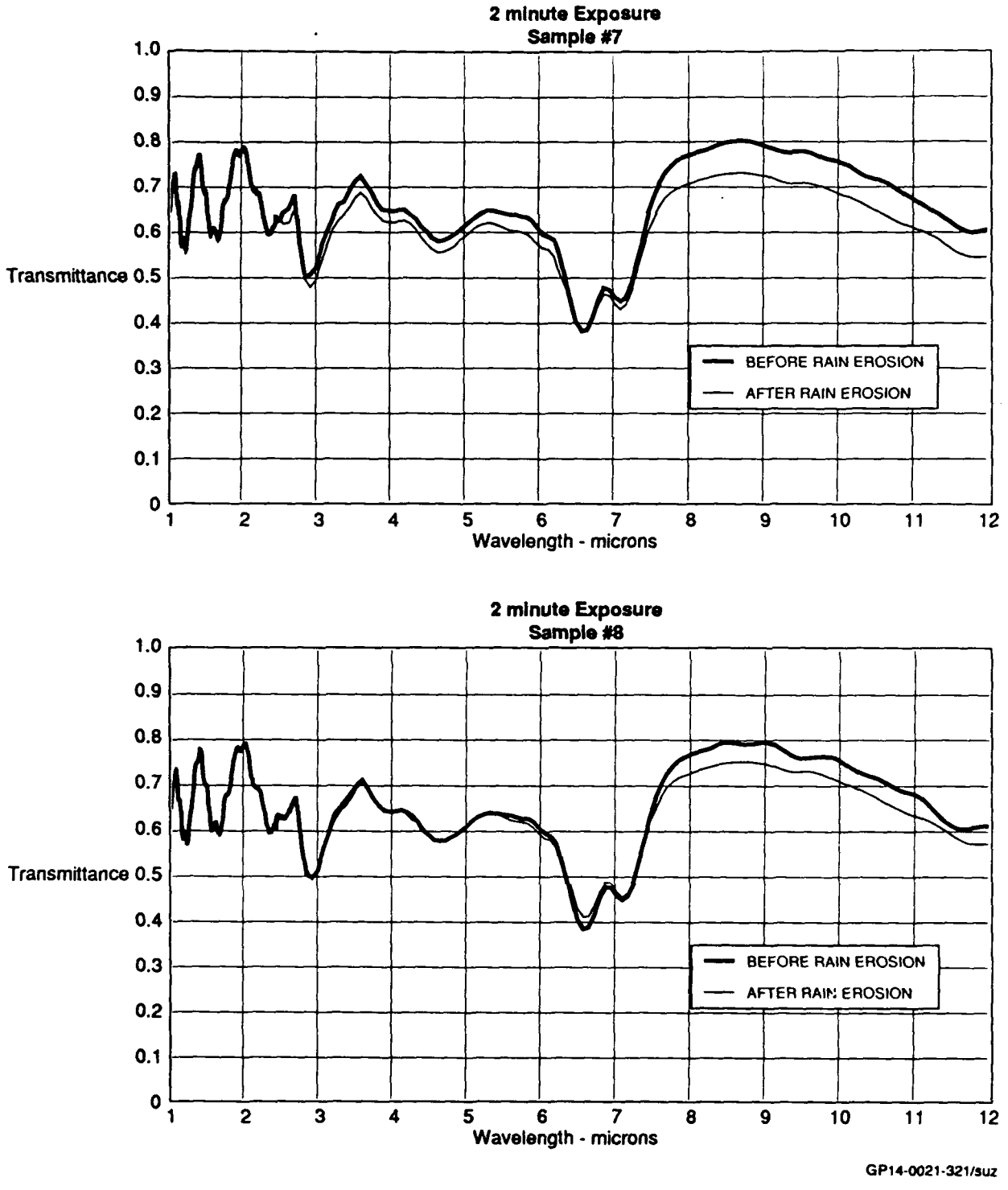

Figure C-7. Change in Transmission Following Rain Erosion Exposure
ZnSe

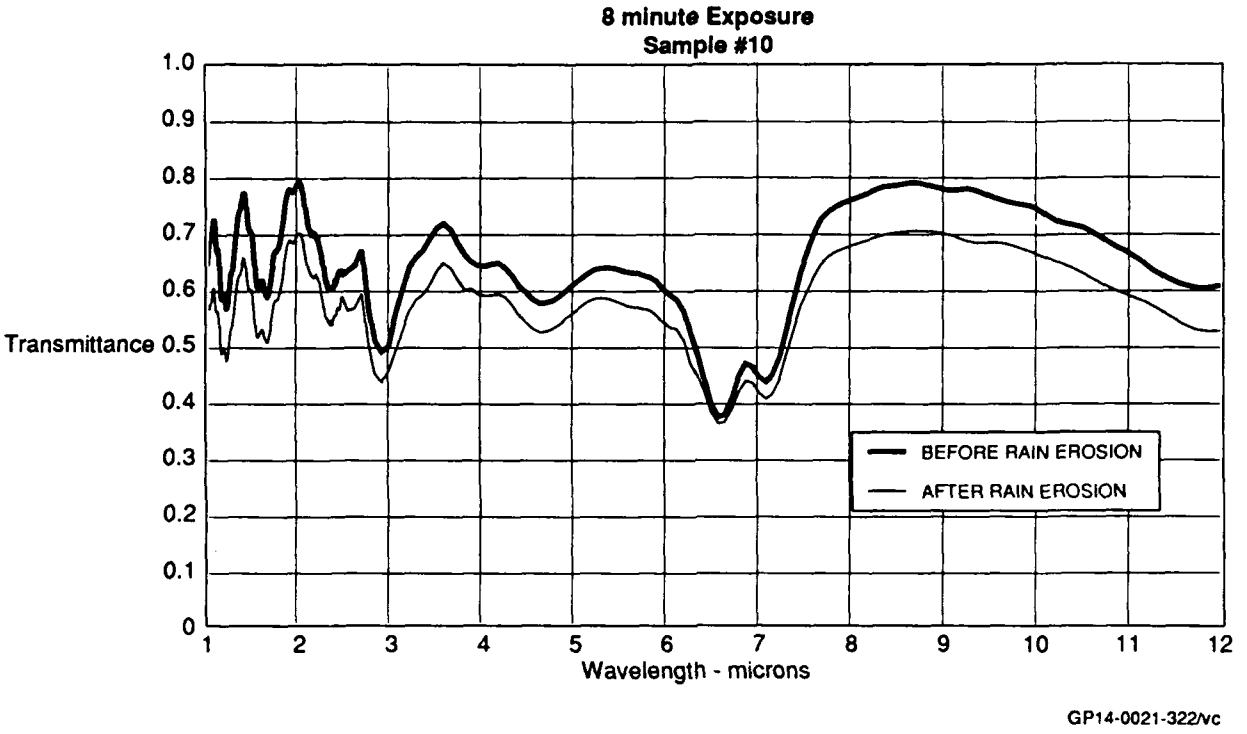

Figure C-7. (Continued) Change in Transmission Following Rain Erosion Exposure
ZnSe

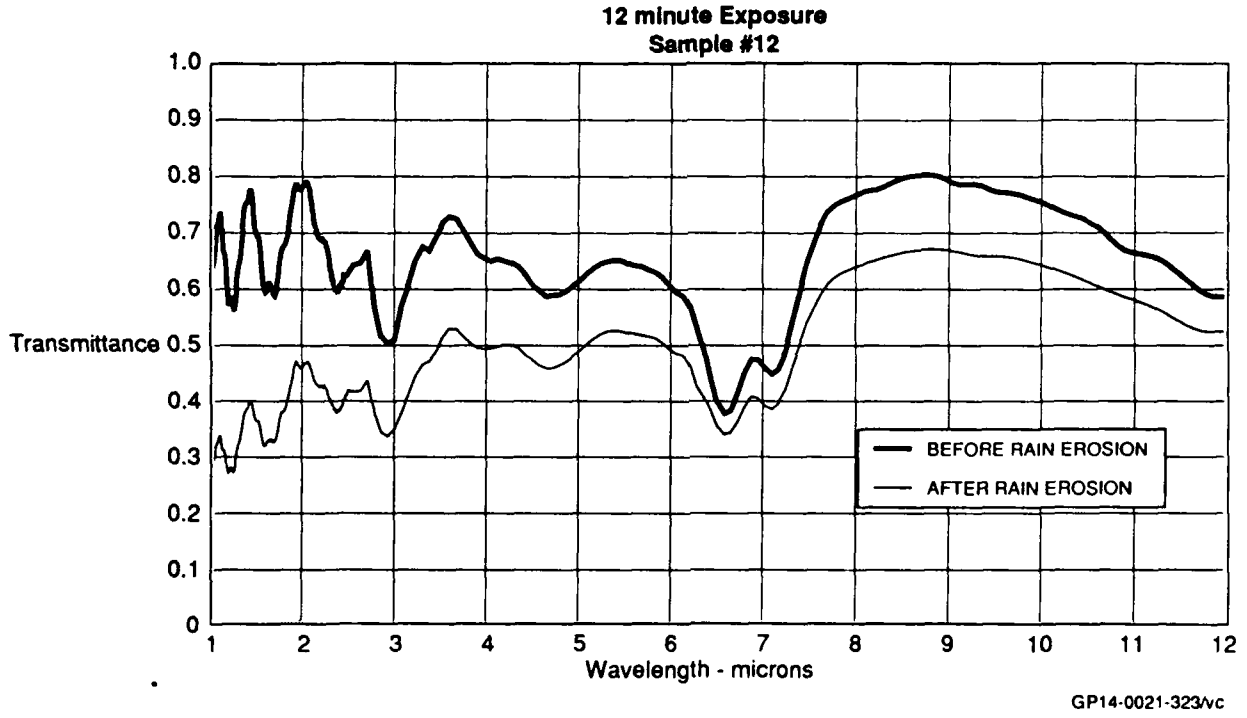

Figure C-7. (Continued) Change in Transmission Following Rain Erosion Exposure
ZnSe

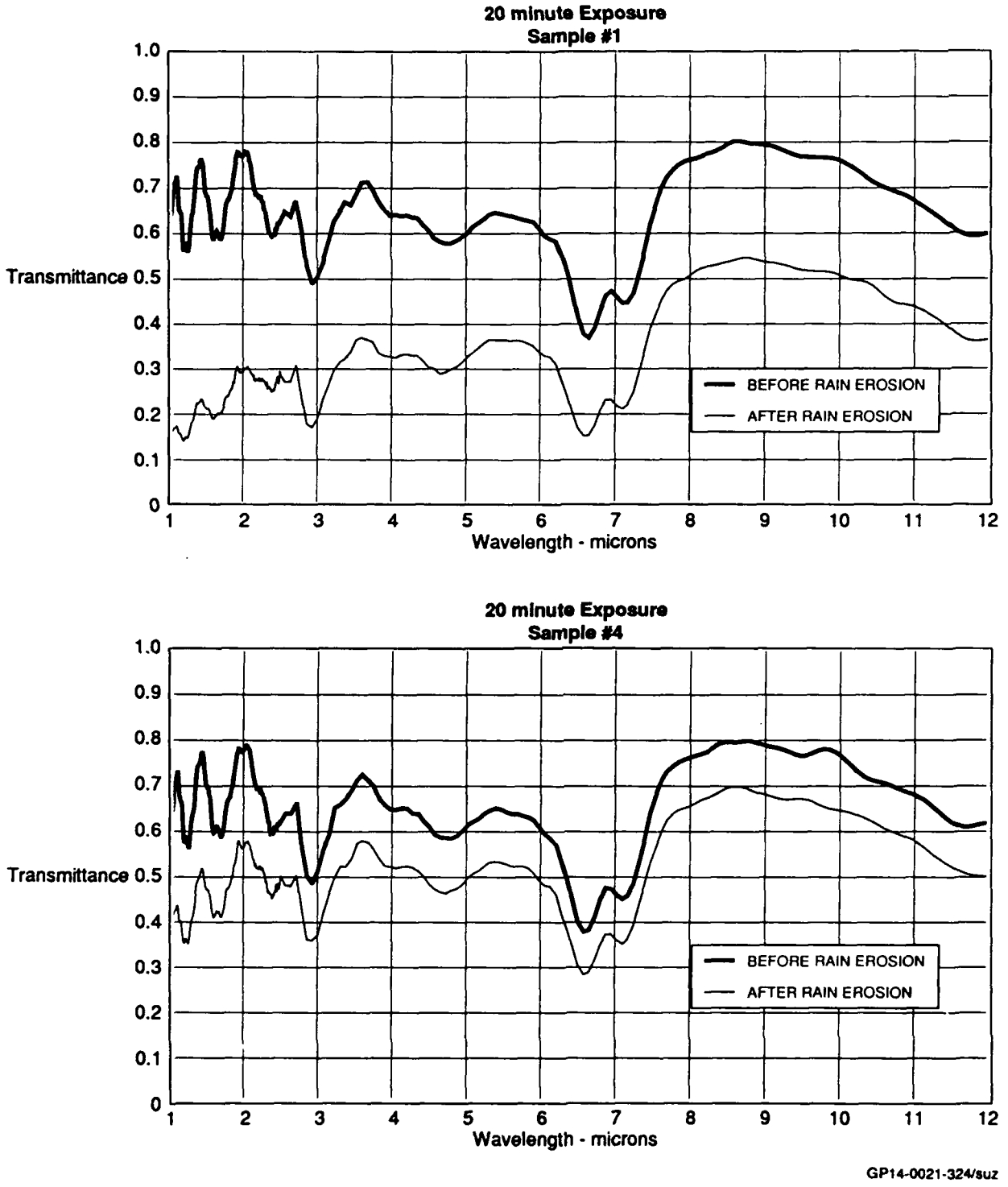

Figure C-7. (Continued) Change in Transmission Following Rain Erosion Exposure
ZnSe

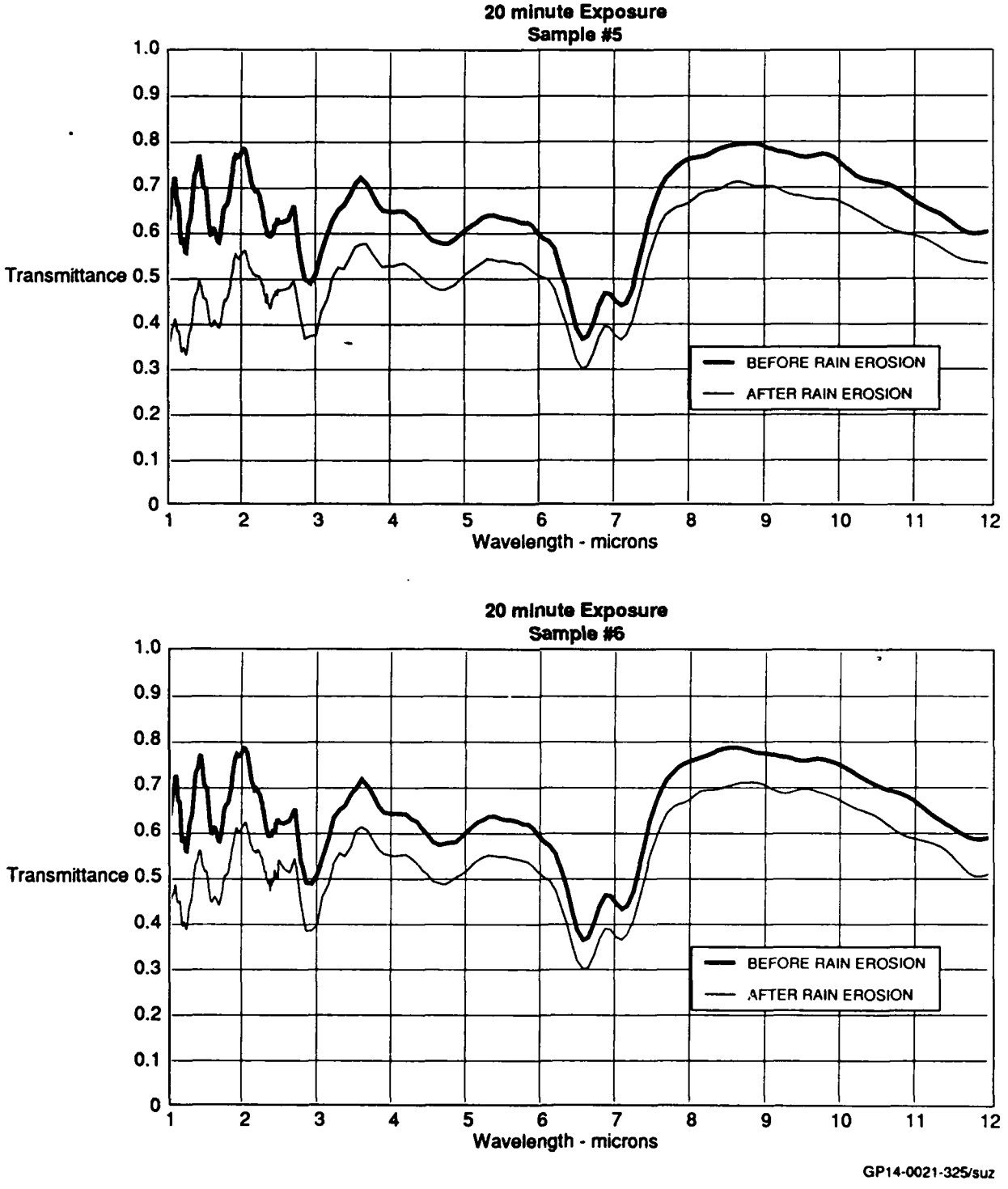

Figure C-7. (Continued) Change in Transmission Following Rain Erosion Exposure
ZnSe

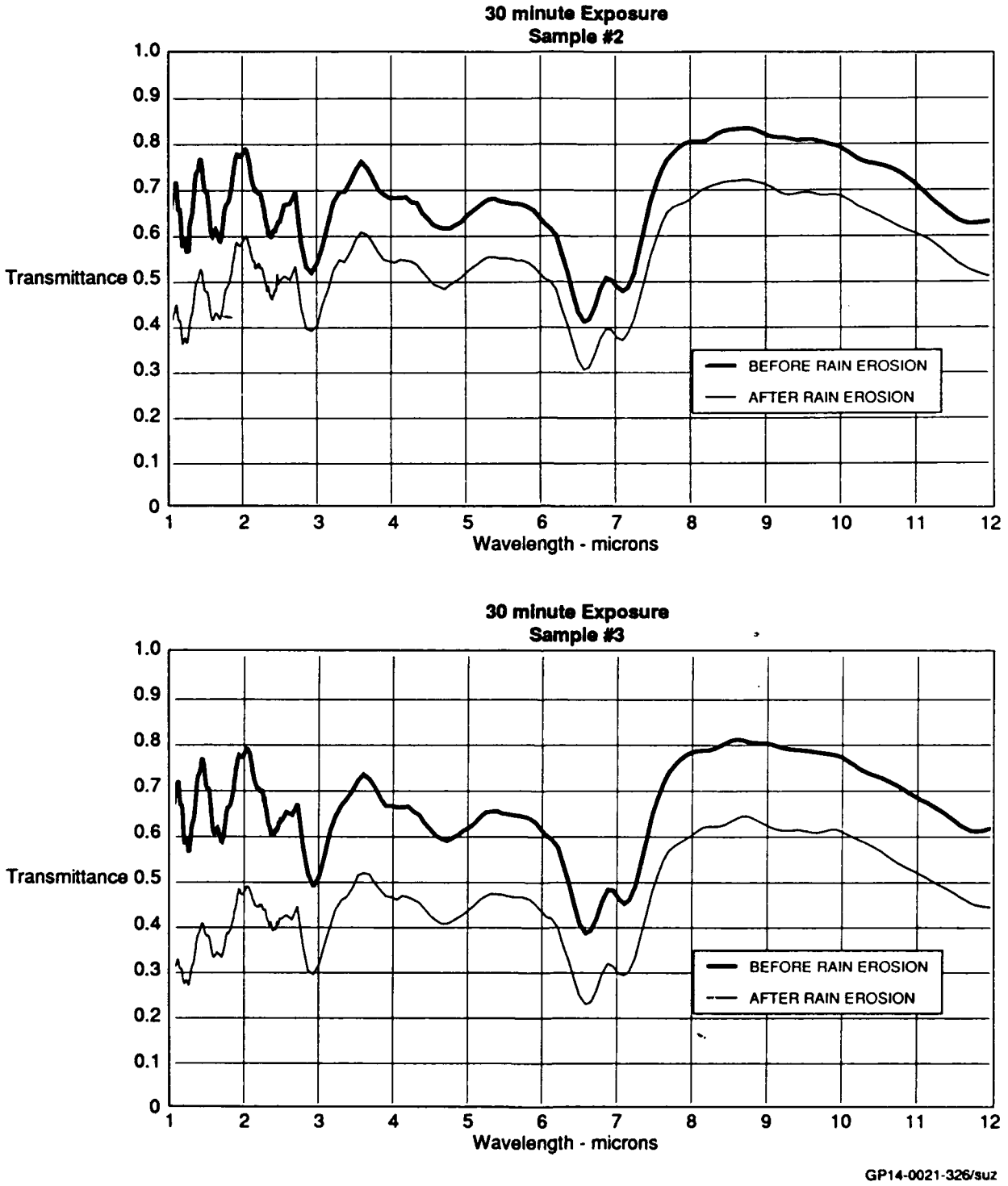

Figure C-7. (Concluded) Change in Transmission Following Rain Erosion Exposure
ZnSe